FINAL REPORT

Demonstration and Validation of a Fractured Rock Passive Flux Meter

ESTCP Project ER-200831

APRIL 2015

Kirk Hatfield
University of Florida

ESTCP

REPORT DOCUMENTATION PAGE

Form Approved
OMB No. 0704-0188

PLEASE DO NOT RETURN YOUR FORM TO THE ABOVE ORGANIZATION.

1. REPORT DATE *(DD-MM-YYYY)*	2. REPORT TYPE	3. DATES COVERED *(From - To)*
03-2015	Final Report	05-2008-03-2015

4. TITLE AND SUBTITLE
Demonstration and Validation of a Fractured Rock Passive Flux Meter

5a. CONTRACT NUMBER

5b. GRANT NUMBER

5c. PROGRAM ELEMENT NUMBER

6. AUTHOR(S)
Kirk Hatfield

5d. PROJECT NUMBER
ER-200831

5e. TASK NUMBER

5f. WORK UNIT NUMBER

7. PERFORMING ORGANIZATION NAME(S) AND ADDRESS(ES)
University of Florida
P.O. Box 116580, 365 Weil Hall
Gainesville, FL 32611

8. PERFORMING ORGANIZATION REPORT NUMBER
ER-200831

9. SPONSORING/MONITORING AGENCY NAME(S) AND ADDRESS(ES)
SERDP/ESTCP
4800 Mark Center Drive, Suite 17D08
Alexandria, VA 22350-3605

10. SPONSOR/MONITOR'S ACRONYM(S)
SERDP/ESTCP

11. SPONSOR/MONITOR'S REPORT NUMBER(S)

12. DISTRIBUTION/AVAILABILITY STATEMENT
Unlimited

13. SUPPLEMENTARY NOTES

14. ABSTRACT

The overall objective of this project was to demonstrate and validate a new closed-hole passive sensing technology for fractured media: the Fractured Rock Passive Fluxmeter (FRPFM). The FRPFM provides simultaneous measurement of (1) the presence of flowing fractures, (2) the location of active or flowing fractures; (3) active fracture orientation i.e., dip and azimuth; (4) direction of groundwater flow in each fracture; (5) cumulative magnitude of groundwater flux in each fracture; and (6) cumulative magnitude of contaminant flux in each fracture. Various technologies exist to measure (1), (2) and (3) above; however, the FRPFM is the only technology that also measures (4), (5) and (6).

15. SUBJECT TERMS

16. SECURITY CLASSIFICATION OF:			17. LIMITATION OF ABSTRACT	18. NUMBER OF PAGES	19a. NAME OF RESPONSIBLE PERSON
a. REPORT	b. ABSTRACT	c. THIS PAGE		194	Carmen Lebron
					19b. TELEPHONE NUMBER *(Include area code)* 352-392-9537

Reset

Table of Contents

Table of Contents i
List of Acronyms iv
List of Figures vi
List of Tables x
EXECUTIVE SUMMARY xi
1.0 INTRODUCTION 1
1.1 BACKGROUND 1
1.2 OBJECTIVE OF THE DEMONSTRATION 2
1.3 REGULATORY DRIVERS 2
2.0 TECHNOLOGY 2
2.1 TECHNOLOGY DESCRIPTION 3
2.2 TECHNOLOGY DEVELOPMENT 8
2.2.1. FRPFM FLOW and MASS TRANSPORT THEORY 9
2.2.2. TRANSPORT MODEL 11
2.2.3. FLUX ESTIMATION 14
2.2.4. MULTIPLE EQUIDISTANT PERPENDICULAR INTERSECTIONS 15
2.2.5. SINGLE NON-PERPENDICULAR INTERSECTION 16
2.3 ADVANTAGES AND LIMITATIONS OF THE TECHNOLOGY 19
3.0 PERFORMANCE OBJECTIVES 20
3.1 PERFORMANCE OBJECTIVE: DETECTION OF FLOWING FRACTURES . 20
3.1.1. DATA REQUIREMENTS 21
3.1.2. SUCCESS CRITERIA 21
3.2 PERFORMANCE OBJECTIVE: FRACTURE LOCATION 21
3.2.1. DATA REQUIREMENTS 21
3.2.2. SUCCESS CRITERIA 22
3.3 PERFORMANCE OBJECTIVE: FRACTURE ORIENTATION 22
3.3.1. DATA REQUIREMENTS 22
3.3.2. SUCCESS CRITERIA 22
3.4 PERFORMANCE OBJECTIVE: FRACTURE FLOW DIRECTION 22
3.4.1. DATA REQUIREMENTS 22
3.4.2. SUCCESS CRITERIA 23
3.5 PERFORMANCE OBJECTIVE: ACCURACY OF WATER FLUX MEASUREMENTS 23
3.5.1. DATA REQUIREMENTS 23
3.5.2. SUCCESS CRITERIA 23
3.6 PERFORMANCE OBJECTIVE: ACCURACY OF CONTAMINANT FLUX MEASUREMENTS 23
3.6.1. DATA REQUIREMENTS 23
3.6.2. SUCCESS CRITERIA 23
3.7 PERFORMANCE OBJECTIVE: EASE OF USE 24
3.7.1. DATA REQUIREMENTS 24
3.7.2. SUCCESS CRITERIA 24
3.8 PERFORMANCE OBJECTIVE: ACCEPTABILITY OF SAMPLE ANALYSIS 24
3.8.1. DATA REQUIREMENTS 24
3.8.2. SUCCESS CRITERIA 24
4.0 SITE DESCRIPTION 25
4.1 GUELPH TOOL SITE (GTS) 25

4.1.1 GTS: SITE LOCATION AND HISTORY 25
4.1.2 GTS: SITE GEOLOGY/HYDROLOGY 26
4.1.3 GTS: CONTAMINANT DISTRIBUTION 28
4.2 NAVAL AIR WARFARE CENTER (NAWC) 30
4.2.1 NAWC: SITE LOCATION AND HISTORY 30
4.2.2 NAWC: SITE GEOLOGY/HYDROLOGY 31
4.2.3 NAWC: CONTAMINANT DISTRIBUTION 31
5.0 TEST DESIGN 35
5.1 CONCEPTUAL EXPERIMENTAL DESIGN 35
5.2 BASELINE CHARACTERIZATION 35
5.2.1. GROUNDWATER LEVEL MEASUREMENTS 36
5.2.2. CONTAMINANT CONCENTRATION MEASUREMENTS 36
5.2.3. DISPOSAL OF INVESTIGATION-DERIVED WASTE (IDW) 36
5.3 LABORATORY STUDY RESULTS 36
5.3.1 LABORATORY EXPERIMENTAL PLAN 37
5.3.1.1 COMPONENT TESTING AND SELECTION 37
5.3.1.2 PROTOTYPE TESTING 38
5.3.1.3 FULL-SCALE INSTALLATION AND DEPLOYMENT TESTING 38
5.3.2 LABORATORY PROCEDURES AND APPARATUS 39
5.3.2.1 COMPONENT TESTING: SELECTION OF FABRIC AND VISUAL TRACER 39
5.3.2.2 COMPONENT TESTING: SELECTION OF SORBENT AND RESIDENT TRACERS 40
5.3.2.3 COMPONENT TESTING: TRACER ELUTION FUNCTIONS on AC-FELT 1300 48
5.3.2.4 PROTOTYPE TESTING: FRACTURE FLOW SIMULATOR 50
5.3.2.5 PROTOTYPE TESTING: AQUIFER BOX MODELS 52
5.3.2.6 INSTALLATION AND DEPLOYMENT TESTING (MOCK BOREHOLE) 53
5.3.3 LABORATORY SAMPLING PROCEDURES 54
5.3.4 LABORATORY RESULTS 56
5.3.4.1 COMPONENT TESTING AND SELECTION—PROTOTYPE DESIGN 56
5.3.4.2 PROTOTYPE TESTING 58
5.3.4.3 FULL-SCALE INSTALLATION AND DEPLOYMENT TESTING 80
5.4 DESIGN AND LAYOUT OF TECHNOLOGY COMPONENTS 81
5.4.1. FRPFM 81
5.4.2. BOREHOLE DILUTION TESTS 83
5.3.3. HIGH RESOLUTION TEMPERATURE PROFILES 84
5.5 FIELD TESTING 85
5.5.1. STARTUP 89
5.5.2. DIRECTIONAL FLOW SURVEY 89
5.5.3. BOREHOLE DILUTION TESTING 89
5.5.4. FRPFM DEPLOYMENT; RETRIEVAL, AND SAMPLING 89
5.5.5. DEMOBILIZATION 90
5.6 SAMPLING METHODS 90
5.7 SAMPLING RESULTS 93
6.0 PERFORMANCE ASSESSMENT 113
6.1 SUMMARY OF DATA TYPES AND PERFORMANCE OBJECTIVES 113
6.2 DATA ANALYSIS METHODS 114
6.3 FIELD DEMONSTRATION RESULTS 115
6.3.1. PERFORMANCE OBJECTIVE 1: IDENTIFICATION OF FLOWING FRACTURES 116
6.3.2. PERFORMANCE OBJECTIVE 2: FRACTURE LOCATION 116
6.3.3. PERFORMANCE OBJECTIVE 3: FRACTURE ORIENTATION 117
6.3.4. PERFORMANCE OBJECTIVE 4: FLOW DIRECTION 123
6.3.5. PERFORMANCE OBJECTIVE 5: ACCURACY OF WATER FLUX MEASUREMENTS 127

6.3.6. PERFORMANCE OBJECTIVE 6: ACCURACY OF CONTAMINANT FLUX MEASUREMENTS 127
7.0 COST ASSESSMENT 135
7.1 COST MODEL 135
7.2 COST DRIVERS 136
7.2.1. COST ELEMENT: Mobilization 136
7.2.2. COST ELEMENT: Baseline Characterization 136
7.2.3. COST ELEMENT: FRPFM 136
7.2.4. COST ELEMENT: Alternative Technologies 136
7.2.5. COST ELEMENT: Demobilization 136
7.3 COST ANALYSIS 137
8.0 IMPLEMENTATION ISSUES 142
8.1 Environmental Checklist 142
8.2 Other Regulatory Issues 142
8.3 End-User Issues 142
9.0 REFERENCES 143
APPENDICES 146
Appendix A: Points of Contact 146
Appendix B: Standard Operating Procedure for Analysis of Alcohol Tracers 147
Appendix C: Standard Operating Procedure for Analysis of Target Analytes in Groundwater Samples 152
Appendix D: Standard Operating Procedure for Extraction of Analytes from Flux Device Sorbents 156
Appendix E: Appendix E: Quality Assurance Project Plan (QAPP) 158

List of Acronyms

ACGIH	American Conference of Governmental Industrial Hygienists
ATV	acoustic televiewer
BHD	borehole dilution
CAR	corrective action report
CF	chloroform
CM	chloromethane
CVOCs	chlorinated volatile organic compounds
CV	coefficient of variation
DCE	cis-1,2-dichloroethene
DMP	2,4-dimethyl-3-pentanol
DNAPL	dense nonaqueous phase liquid
DO	dissolved oxygen
DoD	Department of Defense
EPA	Environmental Protection Agency
ESTCP	Environmental Security Technology Certification Program
FID	flame-ionization detector
FRPFM	Fractured Rock Passive Fluxmeter
FRTR	Federal Remediation Technology Roundtable
FTL	field team leader
GC	gas chromatography
HASP	health and safety plan
HPL	Hydrophysical Logging
HRTP	High resolution temperature profile
IDL	instrument detection limit
IDLH	immediately dangerous to life or health
IDW	investigation derived waste
MDL	minimum detection level
MeCl	methylene chloride
MLS	multilevel samplers
MS	matrix spike
MSD	matrix spike duplicate
MSDS	materials safety data sheets
NBS	national bureau of standards
NIOSH	National Institute for Occupational Safety and Health
NITS	National Institute of Standards and Testing
OSHA	Occupational Safety and Health Administration
OTV	optical televiewer
PCE	perchloroethylene
PEL	permissible exposure limit
PFM	Passive Fluxmeter
PPE	personal protective equipment
PSO	project safety officer
QAPP	quality assurance project plan

QA/QC	quality assurance/quality control
RCRA	Resource Conservation and Recovery Act
RPD	relative percent difference
RRF	relative response factors
RRT	relative retention times
SD	standard deviation
SOP	Standard operating procedure
SRM	Standard Reference Materials
SSO	site safety officer
TCE	trichloroethylene
TLV	threshold limit value
TVP	temperature vector probe
TWA	time weighted averages
VC	vinyl chloride
VOA	volatile organic acid

List of Figures

Figure 1. A profile view of an unscreened borehole containing a Fractured Rock PFM (FRPFM). 5
Figure 2. Horizontal cross-section of an FRPFM in an unscreened borehole. The FRPFM core is composed of an inner impermeable Inflatable Packer or Flexible liner, surrounded by a permeable layer of nonreactive mesh layer, surrounded by an internal permeable reactive sorbent layer (or fabric), and an external fracture flow visual indication layer. 5
Figure 3. FRPFM designed with an inflatable core and separate upper and lower end packers. The core is composed of an inner impermeable Inflatable Packer or Flexible liner, surrounded by a permeable layer of nonreactive mesh layer, surrounded by an internal permeable reactive sorbent layer (or fabric), and an external fracture flow visual indication layer. 6
Figure 4. (a) Flow domains Γ_1 (fracture plane) and Γ_2 (FRPFM surface) connected along circumference *ABCD* (example of perpendicular intersection). (b) Unrolled (flat) net of Γ_2. 9
Figure 5. (a) Example of solution for uniform two dimensional flow disturbed by a circular inhomogeneity. (b) Conformal map of uniform flow field in Γ_3 (top half) onto flow domain Γ_2 (for exemplary value of r_0 = 5 cm). Thick continuous lines are stream lines and thin dashed lines are potential lines. Green lines are isochrones, i.e., dye, tracer or contaminant fronts after different times of exposure (cumulative flux). 10
Figure 6. Results of Equations 8, 9 and 10 ($\Delta z/r_0$ thin continuous; $\Delta s/r_0$ thin dashed; $\Delta z \Delta s/r_0^2$ bold dashed; m_{out} bold continuous). 13
Figure 7. m_{out} as a function of τ for different sample strip widths w/r_0. Continuous lines from bottom up correspond to $w/r_0 = \{1, 2, 3, 4, \infty\}$. Dashed line is for $w/r_0 = 0.55$ from laboratory experiments. 14
Figure 8. α_m/α as a function of α for different values of d/r_0. 16
Figure 9. Fracture flow domain Γ_1 with elliptic flow domain Γ_3 (continuous) and circular flow domain from above (dashed). 17
Figure 10. Differences between the unrolled sorbent-fracture intersection lines in Γ_2 from cutting the sorbent (physical cosine shape; dashed) and conformal mapping by Equation 2 (continuous) for β = 15 and 45 degrees. 18
Figure 11. Stratigraphy underlying the Guelph Tool Site 27
Figure 12. Transects defining the general boundaries of the source zone and plume. 29
Figure 13. (a) Location of the former Naval Air Warfare Center (NAWC) site in West Trenton, NJ. (b) Plan view of NAWC site showing locations of pumping and monitoring wells. (Tiedeman et al, 2010). 32
Figure 14. The location of Site 1 and Site 3 TCE plumes interpreted at a depth of 100 feet below land surface at the Naval Air Warfare Center, West Trenton, NJ in May 2004 (Shapiro, 2008). 33
Figure 15. TCE concentrations in NAWC well 68BR. 34
Figure 16. Adsorption isotherm of resident alcohol tracers on AC Felt1300, FM 100 cloth, and Polyorgs. 43
Figure 17. Final Sorption Isotherms using AC Felt 1300. 46
Figure 18. Tracer extraction isotherms using AC Felt 1300 and methylene chloride as extraction solvent. 47
Figure 19. Resident tracer elution tests on AC-Felt 1300 showing relative tracer mass m_r remaining as function of cumulative pore volumes of water eluted. 48

Figure 20. Data from the linear portion of each resident tracer elution curve for AC-Felt 1300 eluted with water. Where relative residual tracer mass m_r is plotted against cumulative pore volumes of water eluted normalized to the tracer retardation factor *R* (after Hatfield et al. 2004). 49
Figure 21. Fracture Flow Simulator with FRPFM prototype deployed. 51
Figure 22. Aquifer box: screened-well high contrast flow simulator. 52
Figure 23. Aquifer box: screened-well high contrast flow simulator schematic showing dimensions of gravel and sand layers. 53
Figure 24. FRPFM Laboratory-Scale Prototype (Insert shows laboratory-scale prototype). 58
Figure 25. Schematic and image of laboratory-scale borehole dilution apparatus. 59
Figure 26. Dimensionless electrical conductivity of borehole water versus time for a borehole dilution test conducted in the Fracture Flow Simulator. 60
Figure 27. Measured fracture flows by borehole dilution versus actual fracture flows. 61
Figure 28. Simulated flow streamlines from the fracture flow simulator under open borehole conditions. 62
Figure 29. Results of numerical flow simulations showing variations in the flow convergence factor, α in the fracture simulator, as a function of fracture transmissivity. 63
Figure 30. FRPFM performance: Visual tracer results on the external FRPFM sock. 66
Figure 31. Measured cumulative water fluxes by FRPFM visible tracers versus controlled cumulative discharge in fracture simulator. 67
Figure 32. Measured cumulative water discharge by FRPFM alcohol tracers versus controlled cumulative discharge in the fracture simulator. 68
Figure 33. Measured cumulative contaminant discharge by FRPFM versus controlled cumulative contaminant discharge in the fracture simulator. 69
Figure 34. Results from a falling head permeameter test conducted on gravel used in the simulator. 71
Figure 35. Dimensionless electrical conductivity of well-screen water versus time for a borehole dilution test conducted in the gravel zone of Well-screen Flow Simulator. 72
Figure 36. FRPFM and borehole dilution measures for water flux in gravel layers. 77
Figure 37. FRPFM and borehole dilution measures for water flux in sand layers. 78
Figure 38. Schematic of FRPFM. 82
Figure 39. FRPFM for 4-inch diameter well with dimensions shown. Image a) shows the FRPFM with core extended out of the shield. Image B) shows the FRPFM in deployment and retrieval mode (withdrawn into the shield). 83
Figure 40. Field-scale borehole dilution apparatus for fractured rock boreholes. 84
Figure 41. (a) Image of temperature vector probe (TVP) with 4 thermistors and (b) schematic showing distribution of thermistors as viewed from below (Adapted from Pehme et al, 2014). . 85
Figure 42. Summary of flux measurements and visual results for Tests F, G, and H comparing vertical distribution of water flux (specific discharge), contaminant flux and presence of flowing fractures 103
Figure 43. Test J imagery of visual flow indications compared to ATV log at same depth. NOTE: Imagery is of FRPFM visual indication sock on uninflated device after deployment. In this form the visual features are mirror images of features in ATV/OTV logs. 104
Figure 44. Test K: (A) black and white image of visual features from a portion of the FRPFM sock. (B) Centroids of individual features referenced to the FRPFM accelerometer directional orientation. 105

Figure 45. Test K: (A) Black and white image of visual features from a portion of the FRPFM sock. (B) Visual features with fitted sine function traces, which are used to estimate fracture depth, azimuth and dip. 106
Figure 46. Test K: histograms of fracture depth, dip, orientation (azimuth) and centroid angles. Note: depth is the local depth along the 100-cm FRPFM interrogation zone. 107
Figure 47. Test O comparison of ATV, OTV, and FRPFM visual tracer with inferred flow direction. 108
Figure 48. Test O comparison of ATV, OTV, FRPFM visual tracer and FRPFM fluxes. 109
Figure 49. Test Q inferred general flow direction from faint visual features on FRPFM sock. 110
Figure 50. Test R Comparison of ATV/OTV with FRPFM visual indications of flowing circular feature intersecting two high-angle fractures. The FRPFM images were processed using multiple filters to enhance the circular feature and high angle fractures. Note: one side effect of image filtering was the enhanced appearance of weave pattern within the visual indication sock material. 111
Figure 51. Test R inferred general flow direction from visual features on FRPFM sock (Figure 50). 112
Figure 52. Test R vertical distribution of water and contaminant fluxes within FRPFM interrogation zone. 112
Figure 53. Comparison of results for data type 1A—identification of flowing fractures by HRTP and FRPFM visual tracers. 119
Figure 54. Summary of statistical analysis for data type 1A—identification of flowing fractures by HRTP and FRPFM visual tracers. 119
Figure 55. Comparison of results for data type 1B—identification of flowing fractures by HRTP and FRPFM alcohol tracers. 120
Figure 56. Summary of statistical analysis for data type 1B—identification of flowing fractures by HRTP and FRPFM alcohol tracers. 120
Figure 57. Comparison of results for data type 2A—fracture location by ATV/OTV and FRPFM visual tracers. 121
Figure 58. Summary of statistical analysis for data type 2A—fracture location by ATV/OTV and FRPFM visual tracers. 121
Figure 59. Comparison of results for data type 2B—fracture location by ATV/OTV and FRPFM visual tracers. 122
Figure 60. Summary of statistical analysis for data type 2B—fracture location by ATV/OTV and FRPFM visual tracers. 122
Figure 61. Flow directions referenced to true north. 125
Figure 62. Comparison of TVP thermal vector components against local pressure head stratification and horizontal gradients. (a) Time-Elevation-Head (TEH) section with direction, (b) passive temperature data, (c) horizontal thermal vector, (d) vertical thermal gradient, (e) local thermal vector, (f) direction of horizontal thermal vector, (g) inclination of total thermal vector off horizontal (Pehme et al., 2014). 126
Figure 63. Comparison of results for data type 5B—water flux by BHD and FRPFM alcohol tracers. 128
Figure 64. Summary of statistical analysis for data type 5B—water flux by BHD and FRPFM alcohol tracers. 128
Figure 65. Comparison of results for data type 6A—TCE flux by BHD and FRPFM. 129

Figure 66. Summary of statistical analysis for data type 6A—TCE flux by BHD and FRPFM. 129
Figure 67. Comparison of results for data type 6A—DCE flux by BHD and FRPFM. 130
Figure 68. Summary of statistical analysis for data type 6A—DCE flux by BHD and FRPFM. 130
Figure 69. Comparison of results for data type 6B—TCE flux average concentration by BHD and FRPFM. 132
Figure 70. Summary of statistical analysis for data type 6B—TCE flux average concentration by BHD and FRPFM. 132
Figure 71. Comparison of results for data type 6B—DCE flux average concentration by BHD and FRPFM. 133
Figure 72. Summary of statistical analysis for data type 6B—DCE flux average concentration by BHD and FRPFM. 133

List of Tables

Table 1. Performance Objectives. 20
Table 2. Candidate activated carbon fabrics. 41
Table 3. Chemical properties of tracers. 42
Table 4. Sorption coefficients and retardation factor values measured from batch tests. 42
Table 5. Water-based batch test result for uniform impregnated tracer distribution on AC felt 1300 44
Table 6. Acetone-based batch test result for uniform impregnated tracer distribution on AC felt 1300 45
Table 7. Tracer retardation factors R and sorption coefficients K_p to AC Felt 1300 estimated from tracer elution experiments. 49
Table 8. Model Parameters Used to Interpret FRPFM Measurements in the Fracture Simulator. 65
Table 9. Alcohol Tracer Partition Coefficients K_P and Retardation Factors R_{tra}. 65
Table 10. Model Parameters Used to Interpret FRPFM Measurements in high contrast flow zones. 76
Table 11. Comparison of Water Flux Measurement by Two Competing Technologies. 79
Table 12. Relative Measurement Differences between FRPFM and Borehole Dilution. 79
Table 13. Scheduled activities for FRPFM demonstration at the Guelph Tool Site 87
Table 14. Scheduled activities for FRPFM demonstration at the NAWC site 87
Table 15. Matrix of test results—provides general summary of data collected by FRPFM and comparative technology for all field tests. 88
Table 16. Total Number and Types of Samples to Be Collected 92
Table 17. Analytical Methods for Sample Analysis 92
Table 18. Matrix of flux results for comparative technologies (HRTP/TVP and BHD). 101
Table 19. Matrix of flux results for FRPFM technologies (visual tracer, alcohol tracer, and sorbent). 102
Table 20. Summary of data type comparisons for all technologies used to evaluate FRPFM performance. Each data type is referenced to the appropriate performance objective (Table 1). 114
Table 21. Summary of flow directions for all tests with comparative results. 125
Table 22. Summary of Quantitative Performance Objectives with Comparative Results 134
Table 23. FRPFM Deployment Cost. 138
Table 24. FRPFM Construction Cost. 139
Table 25. BHD Cost. 140
Table 26. HRTP/TVP Cost. 141

EXECUTIVE SUMMARY

Complex hydrogeologic conditions such as fractured and karst bedrock settings pose substantial economic and technical challenges both to the characterization and remediation of DNAPL source zones. The Army Environmental Center lists 34 installations where restoration may be technically impractical, even with a budget of $3 billion (approximately 50% of the Army's total projected environmental restoration budget). Of the 34 installations, 26 are underlain by complex fractured rock or karst aquifers.

To reduce the cost of characterization and remediation of fractured rock sites, it is critical to identify candidate sites for Monitored Natural Attenuation (MNA) and prioritize the remaining sites for remediation. To assist in this endeavor, cost-effective monitoring tools are needed that can be used in concert with existing borehole technologies to directly measure groundwater and contaminant flux in fractured rock. These flux measurements combined with data gathered from other available borehole technologies will bring the DoD much closer to estimating contaminant mass discharge from source zones and in turn expedite assessments of environmental risks and benefits associated with natural attenuation, source removal, or remediation at complex sites.

The overall objective of this project was to demonstrate and validate a new closed-hole passive sensing technology for fractured media: the Fractured Rock Passive Fluxmeter (FRPFM). The FRPFM provides simultaneous measurement of (1) the presence of flowing fractures, (2) the location of active or flowing fractures; (3) active fracture orientation i.e., dip and azimuth; (4) direction of groundwater flow in each fracture; (5) cumulative magnitude of groundwater flux in each fracture; and (6) cumulative magnitude of contaminant flux in each fracture. Various technologies exist to measure (1), (2) and (3) above; however, the FRPFM is the only technology that also measures (4), (5) and (6).

The FRPFM is designed with an inflatable core and separate upper and lower end packers. The core is simply a packer (or flexible inflatable liner) covered with an internal nonreactive layer of permeable mesh which is then wrapped in a permeable layer of material derived from activated carbon, ion exchange resin, or similar sorbent material impregnated with tracers, and then all of this is encased in a thin external permeable layer of cloth material impregnated with a visible dye. The core inflates separately from the two end packers to provide a mechanism for holding the one or more reactive fabrics against the face of the borehole and any fracture intersecting that borehole, while the end packers isolate the zone of interest from vertical hydraulic gradients within the borehole. As currently designed, the FRPFM provides high resolution measurements over a specified interrogation zone (typically 1 meter).

Deploying the FRPFM in a borehole and exposing it to flowing groundwater for duration t [T] gradually leaches visible dyes and tracers from the internal and external sorbent layers and produces residual dye and tracer distributions. Visual inspection of the external layer impregnated with a visible dye leads to estimates of the following for active or flowing fractures alone: (1) locations along the borehole; (2) number; (3) individual fracture orientations in terms of strike, dip, and orientation of dip (direction of falling dip, e.g., SW); (4) cumulative groundwater flux; and (5) groundwater flow direction. Fracture characteristics (1) through (3) can be obtained through existing borehole imaging technologies as long as those fractures possess apertures $\geq$1mm;

however, these commercially available technologies cannot distinguish active from inactive fractures or measure the magnitude or direction of fracture flow. Further analytical analysis of the FRPFM internal sorbent layer at indicated locations of active fractures yields: (1) additional estimates of cumulative groundwater flux in fractures; and (2) cumulative contaminant flux in those fractures. Thus, the in situ measurements of direction and magnitude of water and contaminant fluxes in active fractures are innovations given by the FRPFM alone.

Due to the high resolution nature of the FRPFM technology, its optimum application would be for characterizing targeted borehole depth intervals and not for screening conditions over an entire borehole. FRPFM prototypes tested in this project were used to interrogate 1 meter depth intervals in 4-inch and 6-inch fractured rock wells.

This report contains 9 chapters where theories pertinent to the FRPFM technology, demonstration/validation results from laboratory and field tests, and cost analyses with competitive technologies are presented. Chapter 1 presents the following specific project objectives:

1. demonstrate and validate an innovative technology for the direct in situ measurement of cumulative water and contaminant fluxes in fractured media,
2. formulate and demonstrate methodologies for interpreting contaminant discharge from point-wise measurements of cumulative contaminant flux in fractured rock, and
3. enable the technology to receive regulatory and end user acceptance.

Under the first objective, Chapter 2 presents pertinent fundamental theories on water flow and contaminant transport used to explain how the FRPFM functions and how laboratory and field measurements may be interpreted to estimate water and contaminant fluxes from fractures. Defined in Chapter 3 are 6 specific technology performance objectives (Table 20) and metrics established to evaluate and validate the FRPFM technology against competitive technologies. Performance goals and statistics were generated to compare FRPFM measures (contaminant and groundwater fluxes, flow direction, detection of active flowing fractures, fracture location and orientation) to those obtained from five different competing/comparative technologies: High Resolution Temperature Profiling (HRTP), Acoustic Televiewer (ATV), Optical Televiewer (OTV), Temperature Vector Probe (TVP), and Borehole Dilution (BHD). Field tests were conducted at two chlorinated solvent contaminated fractured rock sites described in Chapter 4. In Chapter 5 multiple laboratory tests are described and results are presented from a bench-scale fracture simulator and box aquifer. Also described are 16 separate field tests and their results. A total of 9 down-hole tests were executed in 4- and 6-inch rock wells at the Guelph Tool Site in Ontario Canada and another 7 tests were conducted in one 6-inch rock well located on the premises of the former Naval Air Warfare Center in West Trenton, New Jersey. Details of technology performance versus competing technologies appear in Chapter 6, where Table 22 lists the quantitative standards established for each performance objective and summarizes the field performance results. Based upon 16 field tests, the FRPFM achieved the standard in each of the 6 quantitative performance objectives (Table 22). Chapter 7 presents a cost assessment which demonstrates that the cost of FRPFM implementation is competitive with alternative technologies, none of which can provide the full suite of FRPFM capabilities. A key distinction however, is that FRPFM generate high resolution measures over a specified interval, and the FRPFM is best used

for characterizing targeted borehole depth intervals, not for screening conditions over an entire borehole. Chapter 8 addresses issues of implementation.

Under the second of the three project objectives, methodologies were formulated and demonstrated for interpreting contaminant discharge from point-wise measurements of cumulative contaminant flux in fractured rock. Those methods were published in a highly ranked peer-reviewed journal *Water Resources Research* (Acar et al. 2013).

Under the third project objective, Enviroflux Inc. assumed exclusive rights to commercialize the FRPFM technology (patented in 2008). At this time, Enviroflux Inc. is engaged in discussions to deploy FRPFMs for a major client of a large environmental firm. The U.S. Environmental Protection Agency (USEPA) has also shown interest in continued field testing and site selection is under way.

1.0 INTRODUCTION

1.1 BACKGROUND

Complex hydrogeologic conditions such as fractured and karst bedrock settings pose substantial economic and technical challenges both to the characterization and remediation of DNAPL source zones. The Army Environmental Center lists 34 installations where restoration may be technically impractical, even with a budget of $3 billion (approximately 50% of the Army's total projected environmental restoration budget). Of the 34 installations, 26 are underlain by complex fractured rock or karst aquifers.

The challenge of estimating cross-sectional discharge (integrated flux) in fractured media is quite different and perhaps much more difficult than granular media for various reasons. One of which is variations in fracture aperture between borehole (Novakowski et al. 2006), and another being some fractures are large and perhaps important hydraulically, while others are small and significant in the context of controlling plume structure. It is also important to keep in mind that contaminant flux in fractures can be approximated as the product of fracture flow and contaminant concentration. Some fractures can possess high contaminant concentrations but produce low fluxes because flow is negligible; whereas, in others concentrations can be low, but the fluxes high because flow is significant. Thus, it is not possible to identify fractures producing significant contaminant fluxes viewing concentration without flow and vice-versa. Finally, with respect to estimating contaminant discharge, it is pertinent to recognize the importance of fracture density. Small fractures, that individually produce low contaminant fluxes, can generate large contaminant discharges at the transect scale if fracture density is significant.

This report present results of a technology demonstration/validation study where cumulative or time-averaged water and contaminant fluxes were measured in fractured rock aquifers under ambient closed-hole conditions. Usually water and contaminant fluxes are estimated from observed contaminant concentrations in fractured rock boreholes and depth-average groundwater flows calculated or measured under open-hole conditions. This approach typically requires extensive aquifer characterization and costly flow and water quality monitoring in open boreholes. Hydrophysical logging, pulse flow meters (Model 40 GEOFLO), acoustic Doppler velocimeters, and colloidal borescopes are tools typically used that reveal much about fractured flows towards an open borehole (Wilson et al. 2001). Unfortunately, open borehole techniques are not likely to produce accurate estimates of ambient contaminant discharge for at least two reasons. First, open boreholes induce magnitude and directional changes in water and contaminant fluxes in fractures and between fractures that do not exist naturally as in the absence of a borehole. Hence, flows that do not occur under natural aquifer conditions are not likely to produce concentrations and depth-average discharges that represent ambient conditions. Second, water and contaminant fluxes vary significantly between fractures and over time; therefore, typical short-term or instantaneous measurements of flow and concentration do not generate representative long-term projections of flow, concentration, and contaminant discharge.

Closed-hole conditions are preferred for making ambient water and contaminant flux measurements. These conditions are closely approximated using FLUTe^{TM} and packers to isolate borehole sections (Cherry et al. 2007). These devices eliminate the exchange of water and

contaminant between fractures that occurs in open boreholes and in turn restore nature flows in fractures. FLUTe^{TM} have been used with high resolution temperature logging techniques to locate and rank active (flowing) fractures under closed-hole conditions. Beyond this study and to the best of our knowledge, individual fractured flows have not been measured under closed-hole conditions; however, isolated and depth-integrated fracture flows have been measured over isolated sections of a borehole using the point or borehole dilution method (Guitierrez et al. 1977; Xu et al. 1997; and Novakowski et al. 2006). Furthermore, direct measures of contaminant fluxes in fractures have not been reported. As a result, measurement and/or calculation of flux at the fracture scale are somewhat novel. Hence, published accounts of water or contaminant discharge estimated over fractured transects are almost non-existent (Acar et al. 2013; Plett 2006; and Novakowski et al. 2006).

1.2 OBJECTIVE OF THE DEMONSTRATION

The objective of this project was to demonstrate and validate the fractured rock passive flux meter (FRPFM) as new technology that measures the magnitudes and directions of cumulative water and contaminant fluxes in fractured rock aquifers. The specific project objectives were:

4. demonstrate and validate an innovative technology for the direct in situ measurement of cumulative water and contaminant fluxes in fractured media,
5. formulate and demonstrate methodologies for interpreting contaminant discharge from point-wise measurements of cumulative contaminant flux in fractured rock, and
6. enable the technology to receive regulatory and end user acceptance.

1.3 REGULATORY DRIVERS

To reduce the cost of characterization and remediation of fractured rock sites, it is critical to identify candidate sites for Monitored Natural Attenuation (MNA) and prioritize the remaining sites for remediation. To assist in this endeavor, cost-effective monitoring tools are needed that can be used in concert with existing borehole technologies to directly measure groundwater and contaminant flux in fractured rock. These flux measurements combined with data gathered from other available borehole technologies will bring the DoD much closer to estimating contaminant mass discharge from source zones and in turn expedite assessments of environmental risks and benefits associated with natural attenuation, source removal, or remediation at complex sites.

For fracture bedrock sites, a significant cost savings to DoD could be realized if certain sites were quantitatively found to pose little off-site risk due to natural attenuation. Based upon projected remediation costs of approximately $3 Billion per 34 difficult installations, it was estimated that approximately $2.3 Billion could be spent on 26 sites underlain by fractured rock and karst aquifers (SERDP and ESTCP Workshop, 2006). The greatest cost savings could be realized in less than five years, if FRPFM monitoring determined at any one site, natural attenuation was sufficient and active remediation could be avoided.

2.0 TECHNOLOGY

The technology demonstrated and validated in this project is a new closed-hole passive sensing technology for fractured media: the Fractured Rock Passive Fluxmeter (FRPFM). The FRPFM provides simultaneous measurement of (1) the presence of flowing fractures, (2) the location of

active or flowing fractures; (3) active fracture orientation i.e., dip and azimuth; (4) direction of groundwater flow in each fracture; (5) cumulative magnitude of groundwater flux in each fracture; and (6) cumulative magnitude of contaminant flux in each fracture. Various technologies exist to measure (1), (2) and (3) above; however, the FRPFM is the only technology that also measures (4), (5) and (6).

The FRPFM is essentially an inflatable packer or flute that holds one or more reactive fabrics against the wall of a borehole and to any water-filled fractures intersected by a borehole. These reactive fabrics are designed to intercept and retain target groundwater contaminants (i.e., TCE, DCE, VC); in addition, these fabric release non-toxic tracers, some of which visibly indicate active fracture location, orientation, and direction of fracture flow along a borehole, while others quantify cumulative groundwater discharge in these fractures.

Demonstration and validation studies were conducted at two sites where available field facilities permitted FRPFM testing in well-characterized rock wells and underlying fractured rock aquifers were contaminated with chlorinated solvents. Direct FRPFM measures of active fracture location, orientation, direction and magnitude of water and contaminant fluxes were compared to results generated using competing technologies (e.g., borehole imaging tools, high resolution temperature logging, and borehole dilution). The project demonstrated that the FRPFM was particularly cost-effective for fractured rock characterization and monitoring when used in concert with other borehole technologies (e.g., high resolution temperature logging). The project also demonstrated methods for interpreting water and contaminant discharge from a single well or transect of multiple boreholes (Acar et al. 2013).

2.1 TECHNOLOGY DESCRIPTION

Complex hydrogeologic conditions such as fractured bedrock and karst settings pose substantial challenges both to the characterization and remediation of DNAPL source zones. Cost-effective quantification of contaminant discharge is critical at complex sites in order to assess long term risk, evaluating remedial performance, and achieving regulatory compliance. For fracture bedrock sites, a significant cost savings to DoD can be realized if certain sites are quantitatively found to pose little off-site risk, or they do not require active remediation because contaminant mass discharge is low and can be attenuated by natural processes. Various open-hole technologies exist to locate fractures, measure fracture apertures, and determine fracture orientations in terms of strike, dip, and dip orientation (direction of falling dip, e.g., SW), and other technologies exist that measure fracture flows under open-hole conditions. Unfortunately, as stated above, open boreholes induce fracture flows which are not natural or ambient; consequently, open-borehole techniques are not likely to produce accurate estimates of ambient contaminant discharge. Monitoring tools that function in closed boreholes are needed to measure ambient water and contaminant flux in fractured rock. To be cost-effective in the field, these novel tools must generate complementary data to existing borehole technologies.

Technology Overview: The FRPFM constitutes a new closed-hole passive sensing technology for characterizing both water and contaminant fluxes in fractured rock systems. The sensor can be deployed at any depth provided that the unit is placed in a saturated flow system. The FRPFM functions like an inflatable (or mechanically expandable) packer or an impermeable flexible liner

that holds one or more reactive permeable fabrics against the wall of the borehole and to any water-filled fractures intersected by the borehole.

The FRPFM incorporates novel methods for measuring DNAPL and water fluxes in fractures, but also retains many of the field-tested concepts of the passive fluxmeter (PFM) developed under ESTCP project ER-0114 (Hatfield et al. 2004; Annable et al., 2005; and Klammler et al. 2007). For example, reactive fabrics function to intercept and retain target groundwater contaminants (i.e., TCE, DCE, VC) and release non-toxic resident tracers (e.g., visible dyes and branch alcohols). The original PFM was design for use in screened wells; however, installations in deep screened wells can be difficult. In addition, this original system was not designed to preclude the unwanted vertical exchange of flow between fractures in rock wells. Thus, a new passive fluxmeter design was needed that functions under closed-hole conditions in fractured rock wells and is easily installed in deep wells.

Figure 1 illustrates an idealized profile view of a fractured rock passive flux meter (FRPFM) intercepting fractures and matrix fluid flow over a given borehole depth. Figure 2 represents a plan view or horizontal cross-sectional view of the same FRPFM in a borehole. Both figures clearly show the device composed of an impermeable flexible liner (IFL), such as the commercially available technology sold under the brand name FLUTe^{TM} (Keller et al. 2007), and permeable reactive sorbent layers (or fabric) sandwiched between the IFL and the borehole circumference. The sorbent is a permeable fabric derived from activated carbon, ion exchange resin, etc. The IFL is made of a fluid impermeable flexible material typically available in a tube or sock design that is easily fitted into a borehole or equivalent aperture in a formation. Once inserted, it is inflated with a fluid to cause it to conform to the shape of the borehole. Hence, the FRPFM is essentially a sampling device with thin permeable layers of one or more removable sorbents attached to the outside surface of an IFL. Such a configuration allows the permeable sorbent layers to be pressed against the well screen or borehole wall when the fluxmeter is inserted and inflated. The sorptive layers passively intercept portions of both fracture and matrix flows in order to simultaneously measure local cumulative solute fluxes and groundwater fluxes. Because the IFL itself is impermeable, fracture flow does not enter the borehole, but is instead diverted around the IFL.

Figure 3 illustrates a second FRPFM system design, which is much shorter in length (~1-2 m) and easier to deploy over target depths. This system is designed with an inflatable core and separate upper and lower end packers. The core is simply a packer (or flexible inflatable liner) covered with an internal nonreactive layer of permeable mesh which is then wrapped in a permeable layer of material derived from activated carbon, ion exchange resin, or similar sorbent material, and then all of this is then encased in a thin external permeable layer of cloth material impregnated with a visible dye. The core inflates separately from the two end packers to provide a mechanism for sealing the core against the face of the borehole, while the end packers isolate the zone of interest from vertical gradients within the borehole. For this project, FRPFM testing was limited to system design illustrated in Figure 3.

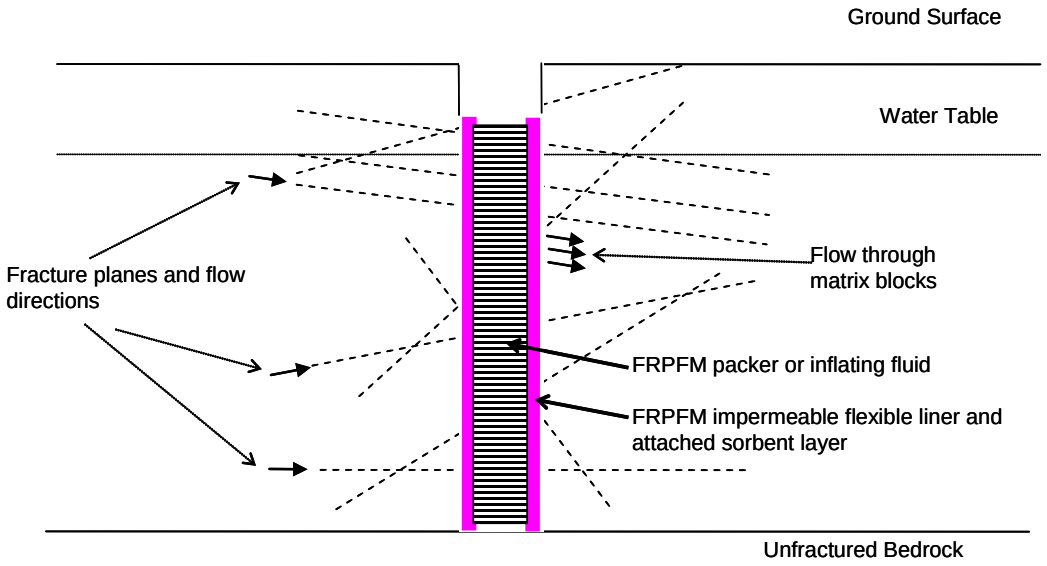

Figure 1. A profile view of an unscreened borehole containing a Fractured Rock PFM (FRPFM).

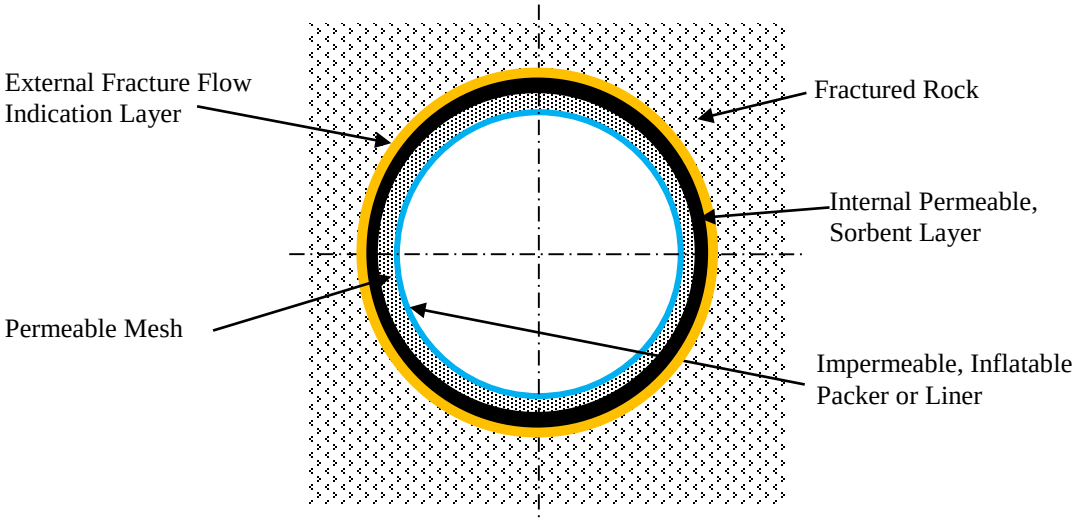

Figure 2. Horizontal cross-section of an FRPFM in an unscreened borehole. The FRPFM core is composed of an inner impermeable Inflatable Packer or Flexible liner, surrounded by a permeable layer of nonreactive mesh layer, surrounded by an internal permeable reactive sorbent layer (or fabric), and an external fracture flow visual indication layer.

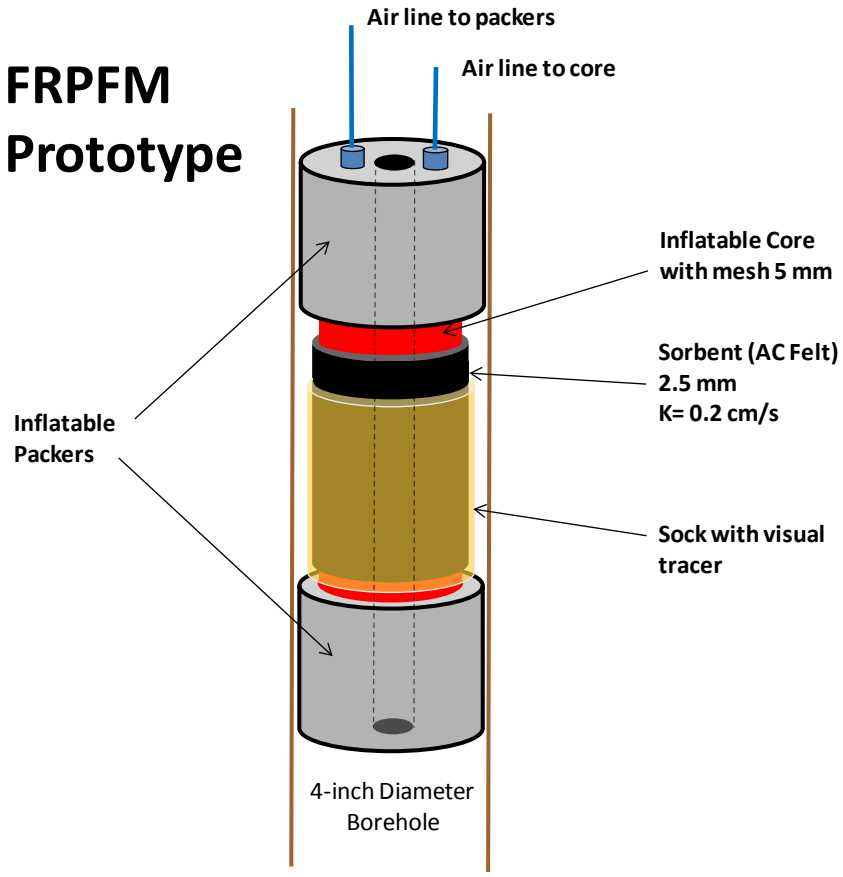

Figure 3. FRPFM designed with an inflatable core and separate upper and lower end packers. The core is composed of an inner impermeable Inflatable Packer or Flexible liner, surrounded by a permeable layer of nonreactive mesh layer, surrounded by an internal permeable reactive sorbent layer (or fabric), and an external fracture flow visual indication layer.

Exposing the FRPFM to flowing groundwater for duration t [T] gradually leaches the tracer from sorbent layers and produces residual tracer distributions. Visual inspection of the external fracture flow indication layer leads to estimates of the following for active or flowing fractures: (1) locations along the borehole; (2) number; (3) individual fracture orientations in terms of strike, dip, and orientation of dip (direction of falling dip, e.g., SW); (4) cumulative groundwater flux; and (5) groundwater flow direction. Fracture characteristics (1) through (3) can be obtained through existing borehole imaging technologies as long as those fractures possess apertures ≥1mm; however, these commercially available technologies cannot distinguish active from inactive fractures or measure the magnitude of fracture flow or flow direction. Further analytical analysis of the internal sorbent layer at indicated locations of active fractures yields: (1) additional estimates of cumulative groundwater flux in fractures; and (2) cumulative contaminant flux in fractures. Thus, the in situ measurements of direction and magnitude of water and contaminant fluxes in active fractures are **innovations** given by the FRPFM alone.

Field Implementation and Groundwater and Contaminant Flux Interpretation: The FRPFM will typically be deployed in deep fractured rock wells or in deep wells screened in fractured rock or unconsolidated materials. To achieve cost-efficiencies in characterizing rock wells, FRPFM deployments will likely follow after other characterization tools [e.g., high resolution temperature logging (Pehme et al. 2010 and 2014), contaminant profiling (Sterling et al., 2005), K-profiling or hydraulic conductivity profiling using a FLUTe^{TM} (Keller et al., 2007), etc.] have been used to locate contaminated active fractures and/or fractures believed to conduct the flows under closed-hole conditions. Following a specific deployment period in the rock well, the FRPFM is retrieved and the reactive fabrics removed from the unit for multiple analyses. First the external fracture flow indication fabric is inspected for evidence of visible tracer loss (indicating the location, orientation, and cumulative water flux of flowing fractures). The location of active fractures should compare well fracture locations predicted by high resolution temperature profiling in a FLUTe^{TM} (Pehme, 2007). Next the internal FRPFM sorbent fabric is extracted for retained contaminants and residual resident tracer(s) to generate estimates of cumulative contaminant fluxes and additional estimates of cumulative water fluxes.

Because the FRPFM provides data on descriptive fracture parameters including locations, strike, dip, and dip orientation. This information can be represented using classical hemispherical projections (e.g., Priest, 1985; Lisle and Leyshon, 2004), which is a standard tool for geologists and engineers. Fracture planes may be represented as great circles or poles of the normals to fracture planes and sets of similar fracture plane orientations may be defined. Furthermore, because FRPFMs generate measures of flux in fractures plane, hemispherical projections offer the possibility of simultaneously representing the directions of the groundwater (and contaminant) fluxes in each plane.

The visible tracers used on the FRPFM indicate the magnitude and the direction of groundwater flux in a fracture plane. However, a preferential orientation of fracture planes can introduce an apparent anisotropy in the flow domain, i.e., the directions of the hydraulic gradient and groundwater flow may differ. For this case standard vector algebra or hemispherical plots can be used to obtain the direction of the ambient hydraulic gradient from the local flow directions in two non-parallel fracture planes. Thus, a FRPFM transect of several boreholes will yield a matrix of local flux measurements, where hemispherical plots for each borehole location can be compared to assess geological continuity over the sampled transect and to identify fracture sets of similar orientation. After determining the direction of the hydraulic gradient and individual fracture orientations, measured local groundwater fluxes can be used to identify fractures of higher and lower conductivity. This conductivity information can be compared to data gathered by K-profiling (Keller et al., 2007). Assuming planar fractures and knowing both the locations of intersections within boreholes and fracture orientations, it may be possible to map intersections of factures common between boreholes.

Groundwater and Contaminant Discharges Interpretations: Quantifying water and contaminant mass discharges from a source area or at compliance boundaries in fracture rock is extremely complicated (Acar et al. 2013). However, discharge estimates and their associated estimation errors are critical to characterizing off-site risks and quantifying the effectiveness of active remediation and/or natural attenuation. Multiple complications evolve from spatial variations in

fracture characteristics and discontinuities in contaminant distribution (i.e., some fractures are contaminated and others not). To initiate a first-order interpretations of groundwater and contaminant discharges, local measurements of groundwater and contaminant fluxes from a borehole transect can be decomposed into their three spatial components and represented separately in transect contour plots. This representation contains information on location and magnitude ignored by hemispherical plots (described above) and allows for an investigation of local trends in the measurements (e.g., contaminant plume extension). For example, local groundwater and contaminant flux variability can be analyzed using standard geostatistical techniques (e.g., histogram). Spatial integration of each of flux components, appropriately weighted by facture densities, leads to respective spatial components of groundwater and contaminant discharges. If however, the monitoring network is regular (no preferential sampling pattern) local fluxes can be geometrically added, averaged (using local fracture densities as weights), and multiplied by the transect area to estimate transect discharge and indicate the magnitude and principal (effective) direction of groundwater flow and transport. Again, these discharge estimates are at best first-order approximations; but, they can prove useful in evaluating remediation performance, natural attenuation, and off-site risk. Furthermore, an analysis of errors can follow to examine estimation uncertainties. For example, one may consider uncertainties in the orientation of FRPFMs in the borehole, and to facilitate this analysis hemispherical projection methods exist.

Under the second project objective, multiple methods were published for estimating groundwater contaminant mass discharges and estimation uncertainties from point measures of FRPFM data gathered from one or more boreholes (Acar et al. 2013). These method use data on fracture orientations, fracture frequencies, groundwater flow directions, and water and contaminant fluxes were included in a generalized probabilistic framework. The utility and value of these methods and their water and contaminant mass discharge estimates are enhanced when used in concert with other borehole technologies. For example other logging methods used to target FRPFM deployments to limited sections of a borehole will reduce monitoring and characterization costs.

2.2 TECHNOLOGY DEVELOPMENT

The FRPFM is patented (Klammler et al. 2008) closed-hole passive sensor technology for characterizing water and contaminant mass fluxes in fractured media. This technology uses many of the field-tested concepts of the original PFM system developed under a previous ESTCP funding (ER0114). Each and every FRPFM component is available from commercial vendors. Packers can be constructed in-house or acquired from multiple manufactures (e.g., FLUTe^{TM} and Solinst LTD). Reactive fabrics such as polyacrylonitrile tissues, activated carbon cloth etc., can be ordered from various suppliers (e.g., Army-Technology; and Eco-tec-Inc.). Developed in the section that follows is flow and transport theory pertinent to understanding how the FRPFM functions in a fracture rock borehole. Presented are the derivations for the fundamental equations for estimating ambient cumulative water flux in fractured media using visible tracers and residual tracer masses. Also developed are equations for quantifying cumulative contaminant mass fluxes in fracture rock from contaminant mass intercepted and retained on the internal FRPFM sorbent. Appearing in Section 5.3 are results from FRPFM tests conducted in the laboratory and in Section 5.5 results from demonstration/validation tests conducted in the field.

2.2.1. FRPFM FLOW and MASS TRANSPORT THEORY

Figure 4a depicts the flow domain for a perpendicular intersection between the fracture plane and the FRPFM axis. It considers the fracture as a plane two dimensional flow domain Γ_1, which is geometrically and hydraulically coupled along a circumference *ABCD* to another two dimensional flow domain Γ_2 consisting of the curved cylindrical FRPFM surface (mesh plus compressed sorbent) of radius r_0 [L] and thickness $H << r_0$ [L]. Both the fracture and the FRPFM surface are, in fact, relatively thin (with respect to FRPFM diameter) and are idealized as homogeneous sheets of known effective transmissivities T_1 and T_2 [L^2/T] representing fracture aperture and FRPFM sorbent+mesh layer thickness multiplied by the respective hydraulic conductivities. Based on this, the FRPFM surface Γ_2 may be unrolled as shown in Figure 4b to obtain the flat rectangular net of the cylinder as the resulting flow domain. In other words, it is assumed that flow components in Γ_1, which are perpendicular to the fracture plane, and flow components in Γ_2, which are perpendicular to the borehole axis, are neglected. Shown in Figure 4 is also the coordinate system adopted with origin at the intersection point of borehole axis *z* and fracture plane (r,θ). $s = \theta r_0$ is a coordinate along *ABCD*, where $\theta = 0$ is aligned with the incident flow direction of the undisturbed (assumed uniform) fracture flux q_0. Note that q_0 is used in the dimensions of L^2/T, which is average fracture flow velocity times fracture aperture (or, equivalently, fracture flow per unit fracture length).

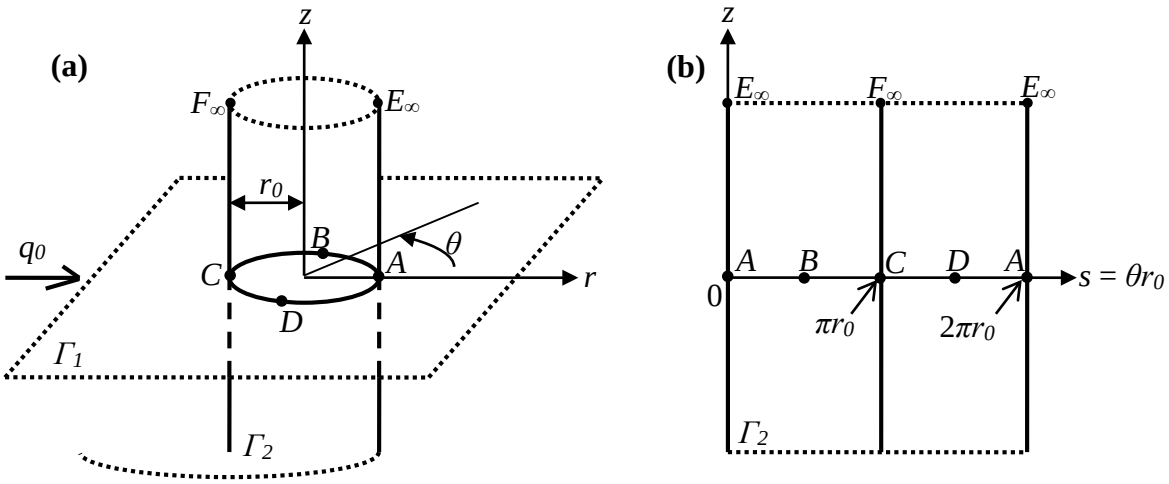

Figure 4. (a) Flow domains Γ_1 (fracture plane) and Γ_2 (FRPFM surface) connected along circumference *ABCD* (example of perpendicular intersection). (b) Unrolled (flat) net of Γ_2.

The hydraulic coupling of Γ_1 and Γ_2 is achieved by requiring continuity of flow as well as continuity of hydraulic head φ [L] across *ABCD*, while maintaining a uniform far field in Γ_1 (i.e., far from *ABCD*). An example of a well known solution in two dimensions (e.g., Strack, 1989; Klammler et al., 2007) for a circular inhomogeneity of contrasting conductivity disturbing an otherwise uniform flow field is depicted in Figure 5a (stream lines thick continuous; potential lines thin dashed). The fictitious (i.e., in the FRPFM problem non-existent) flow domain Γ_3 inside the circle *ABCD* in the fracture plane is of transmissivity $2T_2$, where the factor 2 stands for both sides of the sorbent (above and below the fracture). Independent of the transmissivity, however, Γ_3

contains a uniform flow field, which is of magnitude $q_1 = \alpha q_0$ [L^2/T], where α [-] is a flow convergence factor equal to (Klammler et al., 2007)

$$\alpha = \frac{2}{1+\frac{T_1}{2T_2}} \tag{1}$$

The hydraulic potentials used are $\Phi_1 = T_1\varphi$ in Γ_1 and $\Phi_3 = 2T_2\varphi$ in Γ_3 [both L^3/T], which results in the required discontinuity in potential across *ABCD* in order to preserve continuity of φ. The stream function Ψ [L^3/T] is the same in both flow domains and seen to be continuous everywhere.

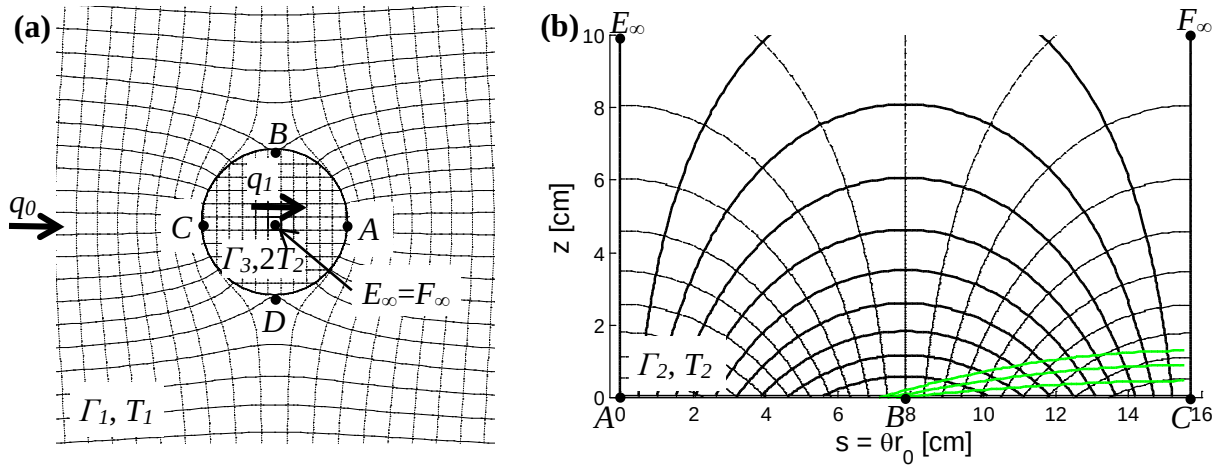

Figure 5. (a) Example of solution for uniform two dimensional flow disturbed by a circular inhomogeneity. (b) Conformal map of uniform flow field in Γ_3 (top half) onto flow domain Γ_2 (for exemplary value of r_0 = 5 cm). Thick continuous lines are stream lines and thin dashed lines are potential lines. Green lines are isochrones, i.e., dye, tracer or contaminant fronts after different times of exposure (cumulative flux).

We further define the complex coordinates $\zeta_3 = re^{i\theta}$ within Γ_3 and $\zeta_2 = s+iz$ within Γ_2. By the rules of conformal mapping (Betz, 1964; Strack, 1989) it is known that the logarithm maps the interior of a circle onto a half strip. Using adequate constants for shifting, scaling and rotation, ζ_2 and ζ_3 as depicted in Figure 5 can be related by

$$\zeta_2 = -ir_0 \ln\frac{\zeta_3}{r_0} = -ir_0\left(\ln\frac{r}{r_0} + i\theta\right) \tag{2}$$

where $i = (-1)^{1/2}$ is the imaginary unit. Splitting into real and imaginary parts gives

$$s = r_0\theta \tag{3}$$

$$z = r_0 \ln\frac{r_0}{r} \tag{4}$$

Note that Equation 3 maps the circumference *ABCD* from Figure 4a to its image in Figure 4b in the exact same way as if the cylindrical FRPFM surface was cut open along AE_∞ and rolled out flat. In more intuitive words, knowing the flow field in Figure 5b from applying Equation 2, it may be "cut out" of the piece of paper it is plotted on, rolled up as a cylinder and located on top of *ABCD* in Figure 5a instead of Γ_3 without affecting the flow field in Γ_1. This is because the geometric and hydraulic properties along *ABCD* in Γ_3 and along *ABCD* along the "rolled up" Γ_2 are identical (due to "conformal equivalence"). Since the flow field in Γ_3 is always uniform, independent of q_0, r_0 or T_2/T_1, it is also implied that the shape of the flow field in Figure 5b is not affected by these parameters. Due to symmetry with respect to *AC* and also between FRPFM sorbent above and below the fracture plane, Figure 5b as well as the following derivation (more specifically the choice of signs) limit attention to the flow field for segment *ABC* above the fracture. For the assumed direction of q_0, it is seen that flow enters across *BC* and leaves the sorbent across *AB*. AE_∞ and CF_∞ are stream lines acting like lateral no flow boundaries on Γ_2.

2.2.2. TRANSPORT MODEL

With other PFM models (e.g., Hatfield et al., 2004) it has been found appropriate to model tracer elution and contaminant sorption from/onto the sorbent material as (piecewise) linear, instantaneous and advection driven only (i.e., negligible diffusive transport). Although the exact transport behavior in the sorbent is directly affected by these assumptions, it is argued that the total amounts of tracer eluted and contaminant sorbed are relatively insensitive to deviations from the assumptions (e.g., diffusive transport does not matter as long as it is not across the sorbent aquifer interface). For purely advective transport in combination with linear and instantaneous sorption, the stream tube based method of Klammler et al. (2009) may be applied for particle travel time calculations, which takes advantage of Equation 2 and the uniform flow field in Γ_3. The fundamental idea is to integrate along the straight stream lines in Γ_3, while accounting for local scaling due to the conformal mapping process, rather than to integrate along curvilinear stream lines in Γ_2. This leads to a travel time $t = \frac{2HnR}{q_1}\int_{x_0}^{x_t}\left|\frac{d\zeta_2}{d\zeta_3}\right|^2 dx$, with $|d\zeta_2/d\zeta_3|^2 = r_0^2/(x^2+y^2)$ from Equation 2. By solving the integral, a dimensionless particle travel time

$$\tau = \frac{tq_1}{2HnRr_0} \tag{5}$$

may be expressed as

$$\tau = \frac{r_0}{y}\left(\arccos\frac{y}{r_0} + \arctan\frac{x_\tau}{y}\right) = \frac{r_0(\theta_0 - \theta_\tau)}{y} \tag{6}$$

where $x = r\cos\theta$ and $y = r\sin\theta$ are Cartesian coordinates in Γ_3; $x_0 = -(r_0^2-y^2)^{1/2}$ and θ_0 are the abscissa and angular coordinate of a tracer / contaminant particle at time $\tau = 0$ [T] on the up-gradient limit *BC* of Γ_3; x_τ and θ_τ are the abscissa and angular coordinate of the same particle at time $\tau > 0$; n [-] and R [-] are effective values of FRPFM layer (mesh plus compressed felt) porosity and tracer / contaminant retardation. The factor 2 in the denominator of Equation 5 accounts for the division of q_1 into two equal parts above and below the fracture intersection. Equation 6 may also be inverted to express $x_t(\tau,y)$, i.e., particle location in Γ_3 for a given stream line and travel time.

$$x_\tau = y\tan\left(\tau\frac{y}{r_0} - \arccos\frac{y}{r_0}\right) \tag{7}$$

Using $\zeta_3 = x+iy$ in Equation 2, resulting travel times or particle locations are mapped onto Γ_2, which results in the green isochrones in Figure 5b given as examples. Isochrones are lines of equal travel time and, under the assumptions made above, may be interpreted as particle fronts, which are pushed forward by water flow. In the case of initially present tracers / dye, the zone behind the front is cleared of all tracer / dye particles, while in the case of contaminants the opposite occurs (however, generally at different velocities due to different values of R). Experiments discussed later in this report will address the question of agreement between the isochrones in Figure 5b and the shape of the eluded dye marks observed in the laboratory and any agreement between the temporal evolution of the isochrones in Figure 5b with the experimentally observed behavior of increasing mark width near the up-gradient point C and barely any advance of mark tip near lateral point B. By letting y approach zero in Equation 6 and taking the limit, the respective coordinate of the tracer front in Γ_3 is found as $x_\tau = -r_0/(1 + \tau)$, which by Equation 4 gives a coordinate $z_0 = r_0\ln(1 + \tau)$ and a vertical dye mark width $\Delta z = 2z_0$ near point C of

$$\Delta z = 2r_0\ln(1+\tau) \tag{8}$$

From Equation 6 the time for a stream line at $y = y_{lim}$ to be empty of tracer is obtained by using $\theta_{lim} = \pi - \theta_0$ and, hence, $(\theta_0 - \theta_\tau) = 2\arccos(y_{lim}/r_0)$.

$$\tau = 2\frac{r_0}{y_{\lim}}\arccos\frac{y_{\lim}}{r_0} = \frac{\frac{\Delta s}{r_0} - \pi}{\sin\frac{\Delta s}{2r_0}} \tag{9}$$

The second equality in Equation 9 expresses τ in terms of the horizontal dye mark length $\Delta s = 2(r_0\pi - s_{lim})$ around the FRPFM circumference. Hereby, $s_{lim} = r_0\theta_{lim}$ by Equation 3, which denotes the coordinate of the tracer front on the abscissa of Figure 5b near point B and $y_{lim}/r_0 = \sin\theta_{lim}$ is used as a geometric relationship in Γ_3.

The area A [L^2] of the dye mark in Γ_2 may be found by integration in Γ_3 knowing that the local areal scaling factor between Γ_3 and Γ_2 is again $|d\zeta_2/d\zeta_3|^2 = r_0^2/(x^2+y^2)$. Introducing $m_{out} = A/r_0^2$ [-] as a relative measure of dye loss gives

$$m_{out} = 4\left(\int_0^{y_{\lim}}\int_{-\sqrt{r_0^2-y^2}}^{x_\tau}\frac{dxdy}{x^2+y^2} + \int_{y_{\lim}}^{r_0}\int_{-\sqrt{r_0^2-y^2}}^{\sqrt{r_0^2-y^2}}\frac{dxdy}{x^2+y^2}\right) \tag{10}$$

where the factor 4 accounts for symmetry between ABC and CDA in Figure 5a as well as for symmetry about the fracture plane (above and below). Note that Equation 10 is equivalently valid for invisible tracer loss, if $m_{out} = M_{out}/(C_t r_0^2)$ is used, where M_{out} [M] and C_t [M/L^2] are the tracer mass lost and initial tracer concentration per unit sorbent area, respectively. Using x_τ from Equation 7 the first double integral reduces to $\tau y_{lim}/r_0$, while the second double integral requires series

expansion to arrive at a rather lengthy approximate solution. As a consequence, Equation 10 is integrated numerically by dividing Γ_3 into a large number of grid points and summing $1/(x^2 + y^2)$ for all grid points behind the dye / tracer front. The results of this and Equations 8 and 9 are depicted in Figure 6. In practice, m_{out} for invisible tracers is determined by laboratory analysis for sample strips of the sorbent of finite width w [-], which is assumed to be centered about the fracture intersection. Knowing that a sampling strip corresponds to a ring in Γ_3 between radii $r_0 \exp[-w/(2r_0)]$ and r_0 (Equation 4) the numerical integration method applied above may be easily limited to grid points within the image of a given sampling strip in Γ_3. In this case, m_{out} is bounded by the size of the strip (initial amount of tracer on the strip), which is reflected by the leveling-off of the graphs shown in Figure 7 for different relative strip widths w/r_0. As long as $w > \Delta z$ tracer loss is entirely contained in the sampling strip and w does not affect m_{out}. However, choosing w very large may lead to a reduced sensitivity to the actual amount of tracer lost near the fracture. In contrast, small values of w correspond to the flat portions of the graphs in Figure 7, where m_{out} is rather insensitive to τ and, hence, cumulative flow $q_1 t$. The reason for this is that once the tracer front leaves the strip (i.e., $w < \Delta z$), an increasing portion of the additional tracer loss occurs outside the strip and is not perceived. Based on this, an optimal relative sample strip width is proposed as $w_{opt} \approx \Delta z$ [L]. Given a visually observed mark width Δz_{dye} of a dye of retardation R_{dye}, a respective value τ_{dye} may be found by inversion of Equation 8. By Equation 5 τ_{dye} may be converted to $\tau_{tra} = \tau_{dye} R_{dye}/R_{tra}$ for a tracer of retardation R_{tra} [-], which may again be used in Equation 8 to find w_{opt} for that tracer as

$$w_{opt} = 2r_o \ln\left\{1 + \frac{R_{dye}}{R_{tra}}\left[\exp\left(\frac{\Delta z_{dye}}{2r_0}\right) - 1\right]\right\} \tag{11}$$

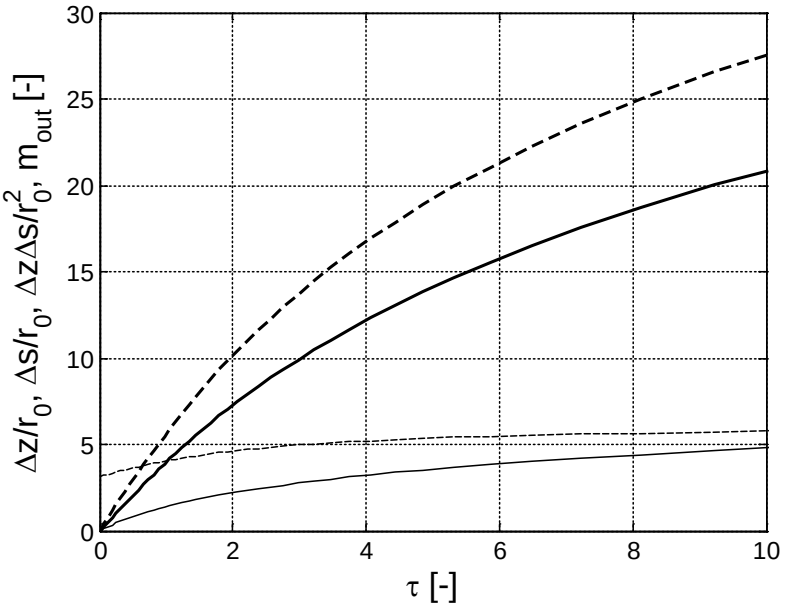

Figure 6. Results of Equations 8, 9 and 10 ($\Delta z/r_0$ thin continuous; $\Delta s/r_0$ thin dashed; $\Delta z \Delta s/r_0^2$ bold dashed; m_{out} bold continuous).

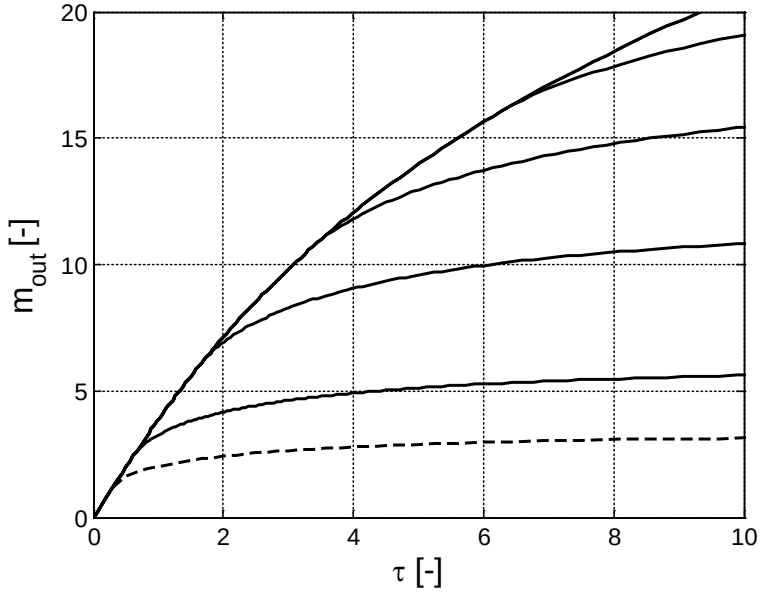

Figure 7. m_{out} as a function of τ for different sample strip widths w/r_0. Continuous lines from bottom up correspond to $w/r_0 = \{1, 2, 3, 4, \infty\}$. Dashed line is for $w/r_0 = 0.55$ from laboratory experiments.

2.2.3. FLUX ESTIMATION

Figures 6 and 7 provide the means for estimating τ by entering the charts with observed values of relative tracer loss or dye mark dimensions. Dye mark length Δs is seen to be a relatively insensitive to τ and, hence, not recommended for use. Dye mark width Δz or the product $\Delta s \Delta z$, however, may be easily measureable quantities in practice for a first visual ad-hoc estimation of τ. Once τ is known Equations 1 and 5 immediately yield an estimate of the undisturbed fracture flux q_0 as

$$q_0 = \frac{2HnR_{tra}r_0\tau}{\alpha t} \approx \frac{HnR_{tra}r_0 m_{out}}{2\alpha t} = \frac{HnR_{tra}w\pi(1-m_r)}{\alpha t} \tag{12}$$

where the approximation is valid for short times as long as $y_{lim} \approx r_0$, such that $m_{out} \approx 4\tau$ in Equation 10 (i.e., the portion of completely empty stream tubes is negligible) and $w \geq \Delta z$. The short time approximation is equivalent to using the tangent of all graphs in Figure 4 at the origin and it leads to an underestimation of q_0 of less than 10 % for $m_{out} < 7$. The final expression in Equation 12 uses the relative remaining tracer mass m_r [-] with respect to the initial tracer mass on the sampling strip, which is related to m_{out} by $m_r = 1 - m_{out}r_0^2/(2r_0\pi w)$. In situations, where the short time approximation is not appropriate any more, but the tracer front is still known to be within the sampling strip ($w > \Delta z$), the approximation

$$\tau \approx m_{out}\left(5.3e-4m_{out}^2 + 1.8e-4m_{out} + 0.25\right) \tag{13}$$

may be used as a visually indistinguishable alternative to the respective graph in Figure 6 (bold continuous). In practice, the condition $w > \Delta z$ may be verified by consecutively sampling strips away from the fracture intersection and observing no more tracer loss beyond a certain distance from the intersection (which would be approximately equal to $\Delta z/2$).

Figures 6 and 7 are also valid for the accumulation of target contaminants on the sorbent, if $m_{out} = M_c/(r_0^2 H n R_c C_c)$ is used, where M_c [M] is the mass of contaminant sorbed and the denominator represents the sorption potential for the contaminant on a sorbent of area r_0^2 (R_c [-] and C_c [M/L^3] denote the contaminant retardation factor and concentration in the pore water, respectively). Similarly, Equation 5 may be rewritten as $\tau = t\alpha J/(2HnR_c r_0 C_c)$, where $J = q_0 C_C$ [M/(LT)] is the undisturbed contaminant fracture flux (again defined as mass flow per unit fracture length or fracture width integrated flow). Obtaining τ from Figures 6, 7 or Equation 13 with an observed value of m_{out} for a specific contaminant allows for formulating the estimate $J = 2HnR_c r_0 C_c \tau/(\alpha t)$. However, the appropriate choice of a sorbent material should generally assure strong contaminant sorption ($R_c >> 1$). This translates into small values of τ and the validity of the short time approximation $m_{out} \approx 4\tau$ (no contaminant particle previously sorbed is again released from the sorbent). This results in a simplified estimate of

$$J = \frac{M_c}{2 r_0 \alpha t} \tag{14}$$

2.2.4. MULTIPLE EQUIDISTANT PERPENDICULAR INTERSECTIONS

In practice, more than a single fracture may intersect a FRPFM, which affects the flow fields inside the sorbent and the fractures. Here we consider the simplest case of a large number of perpendicular intersections of constant separation distance and of equal transmissivities T_1 exposed to a uniform gradient. Thus, the center plane between two fractures becomes a no-flow boundary in the sorbent flow domain Γ_2 of Figure 4b. Denoting the distance between neighboring fractures by d [L] this no-flow boundary corresponds to a horizontal line at $z = d/2$ in Figure 5b. By Equation 4 this translates into a circular no-flow boundary at $r = r_0/\exp[d/(2r_0)]$ in Γ_3 of Figure 5a. Using Klammler et al. (2007) this additional no-flow boundary may be accounted for by converting Γ_3 into a homogeneous flow domain (i.e., eliminating the no-flow boundary) of effective transmissivity T_{2m} given by

$$T_{2m} = T_2 \frac{\exp\left(\frac{d}{r_0}\right) - 1}{\exp\left(\frac{d}{r_0}\right) + 1} \tag{15}$$

which collapses to $T_{2m} = T_2$ for the single intersection case where $d/r_0 >> 1$. Thus, T_{2m} from Equation 15 may be used instead of T_2 in Equation 1 to obtain a generalized flow convergence factor α_m for multiple perpendicular fracture intersections of separation d as

$$\alpha_m = \frac{2}{1+\frac{T_1}{2T_{2m}}} \tag{16}$$

Other than the use of α_m instead of α in Equations 12 and 14, the short time approximations for estimating q_0 and J are not affected by d/r_0. The impact of d/r_0 on flow convergence in terms of the ratio α_m/α is illustrated by Figure 8. It may be seen that the impact of d/r_0 decreases with increasing flow convergence. For an intermediate value of $\alpha \approx 1$, for example, the reduction in flow convergence is less than 5 % for $d/r_0 > 3$.

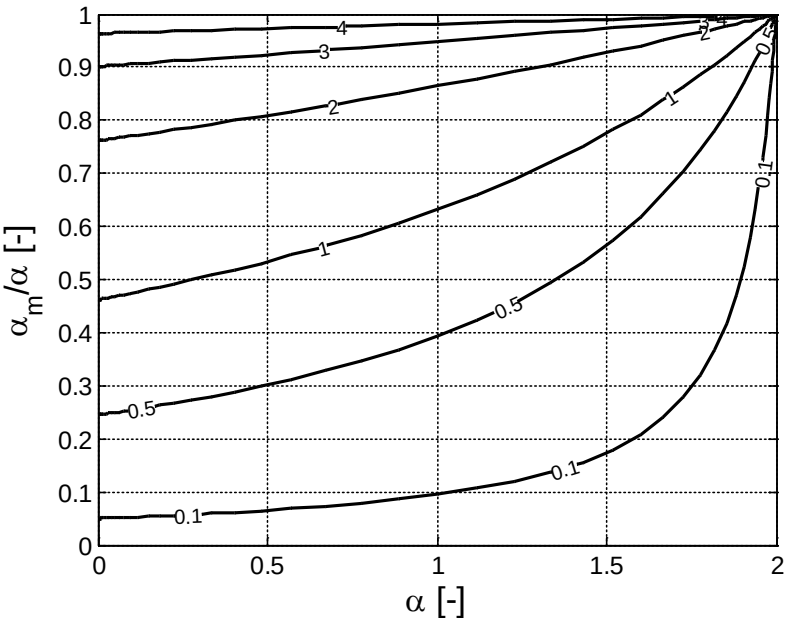

Figure 8. α_m/α as a function of α for different values of d/r_0..

2.2.5. SINGLE NON-PERPENDICULAR INTERSECTION

In general, the intersection angle β [-] between a fracture plane and a FRPFM axis is not perpendicular, i.e., $\beta > 0$. In such cases, the fracture intersects the sorbent along an ellipse of semi-major axis $a = r_0/\cos\beta$ [L] and semi-minor axis $b = r_0$ [L]. The intersection becomes a single period of a (co)sine shape of amplitude $c = r_0\tan\beta$ after unrolling. The loss of rotational symmetry prevailing at $\beta = 0$ further introduces the undisturbed fracture flow direction γ_0 [L] (defined here with respect to the orientation of the long axis; see Figure 9) as an additional variable. Given these complexities we investigate the usefulness of Equation 2 to generalize the results from above in an approximate way. For this purpose, similar to Figure 4a, the elliptical flow domain Γ_3 within the fracture is located as shown in Figure 8, where the offset parameter a_1 in x-direction is obtained from Equation 4 and imposing that the difference in z-coordinates between the images of points H and J in Γ_2 be equal to $2c$.

$$a_1 = \frac{2r_0}{\cos\beta\left[1+\exp\left(2\tan\beta\right)\right]} \tag{17}$$

The image of the (half) ellipse *HIJ* after mapping onto Γ_2 is graphically illustrated by the continuous lines in Figure 10 for two exemplary inclination angles of β = 15 and 45 degrees. For comparison, Figure 10 also contains dashed lines corresponding to the true (physical) cosine shape of the sorbent-fracture intersection after rolling the FRPFM sorbent out flat. Besides the overall shape, also the locations of points along the curves have to (approximately) coincide, as illustrated by the example of point *I*. While for $\beta = 0$ the result becomes identical to the exact mapping of Figure 5 ($a = a_1 = r_0$), the approximation for $\beta > 0$ is considered reasonable, in particular for the range $\beta \leq 45$ degrees shown. Consequently, the same (but now approximate) argument may be applied as with circular intersections, namely that the flow field in Γ_2, obtained from conformal mapping of a known flow field in Γ_3, may be "cut out" of the piece of paper it is plotted on, rolled up and located at an angle β along *HIJ* in Figure 8 instead of Γ_3 without disturbing the flow field in Γ_1.

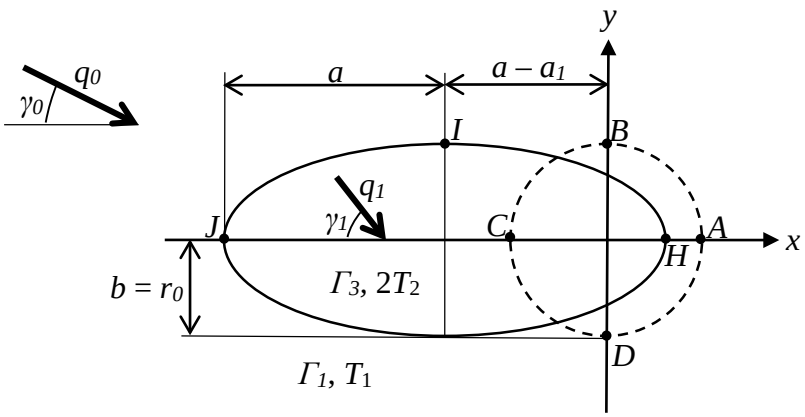

Figure 9. Fracture flow domain Γ_1 with elliptic flow domain Γ_3 (continuous) and circular flow domain from above (dashed).

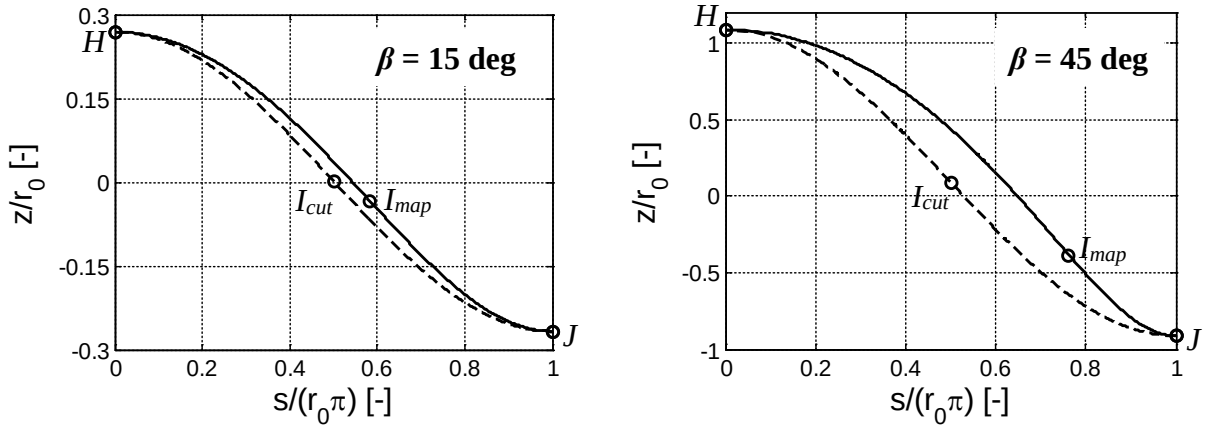

Figure 10. Differences between the unrolled sorbent-fracture intersection lines in Γ_2 from cutting the sorbent (physical cosine shape; dashed) and conformal mapping by Equation 2 (continuous) for β = 15 and 45 degrees.

The flow field inside the ellipse Γ_3 is known to be uniform of angle γ_1 [L], magnitude $q_1 = \alpha q_0$ and total flow Q [L^3/T] given by (Strack, 1989; Kacimov et al., 2011)

$$\gamma_1 = \arctan\left(\frac{1+\lambda\varepsilon}{1-\lambda\varepsilon}\tan\gamma_0\right) \tag{18}$$

$$\alpha = \frac{(1-\lambda)\cos\gamma_0}{(1-\lambda\varepsilon)\cos\gamma_1} \tag{19}$$

$$Q = 2q_0 a\cos\gamma_0 \frac{1-\lambda}{1-\lambda\varepsilon}\sqrt{\left[\frac{b(1-\lambda\varepsilon)}{a(1+\lambda\varepsilon)}\right]^2 + \tan^2\gamma_0} \tag{20}$$

where $\varepsilon = (a - b)/(a + b)$ and $\lambda = (T_1 - 2T_2)/(T_1 + 2T_2)$. For perpendicular intersections $\varepsilon = 0$, such that Equation 18 reduces to $\gamma_1 = \gamma_0$ and Equation 19 (as well as Equation 20 after division by $2q_0a$) collapses to Equation 1. With Equations 18 and 19, a numerical integration approach analogous to that of Equation 10 appears viable.

However, with perpendicular intersections we limit attention to the short time approximation, which is valid as long as the portion of Q not eluding any tracer is negligible. For the perpendicular case, the range of validity of this approximation was found to be quite large (less than 10 % error for $m_{out} < 7$). Under this premise, $m_{out} = Qt/(HnR_{tra}r_0^2)$, which correctly reduces to the short time approximation for circular intersetions ($m_{out} = 4\tau$) when combined with Equation 5 and $Q = 2r_0q_1$. Thus, Q may be directly estimated by

$$Q = \frac{m_{out} HnR_{tra} r_0^2}{t} \tag{21}$$

to find q_0 from Equation 20, where γ_0 is obtained from Equation 18, if γ_1 is inferred from the visual dye mark. Knowing also the mass M_c of a contaminant sorbed, the flux averaged contaminant concentration in the fracture $C_c = M_c/(Qt)$ leading to

$$J = \frac{q_0 M_c}{Qt} \tag{22}$$

By expressing q_0/Q from Equation 20 and using $\varepsilon = 0$ for a perpendicular intersection, Equation 22 reduces to Equation 14.

2.3 ADVANTAGES AND LIMITATIONS OF THE TECHNOLOGY

The FRPFM provides simultaneous measurement of 6 data types with regard to actively flowing fractures. (1) the presence of flowing fractures, (2) the location of active or flowing fractures; (3) active fracture orientation i.e., dip and azimuth; (4) direction of groundwater flow in each fracture; (5) cumulative magnitude of groundwater flux in each fracture; and (6) cumulative magnitude of contaminant flux in each fracture. Various technologies exist to measure (1), (2) and (3) above; however, the FRPFM is the only technology that also measures (4), (5) and (6).

Deploying the FRPFM in a borehole and exposing it to flowing groundwater for duration t [T] gradually leaches visible dyes and tracers from the internal and external sorbent layers and produces residual dye and tracer distributions. Visual inspection of the external layer impregnated with a visible dye leads to estimates of 5 types of information for actively flowing fractures: (1) locations along the borehole; (2) number; (3) individual fracture orientations in terms of strike, dip, and orientation of dip (direction of falling dip, e.g., SW); (4) cumulative groundwater flux; and (5) groundwater flow direction. Fracture characteristics (1) through (3) can be obtained through existing borehole imaging technologies as long as those fractures possess apertures $\geq$1mm; however, these commercially available technologies cannot distinguish active from inactive fractures or measure the magnitude or direction of fracture flow. Further analytical analysis of the FRPFM internal sorbent layer at indicated locations of active fractures yields: (1) additional estimates of cumulative groundwater flux in fractures; and (2) cumulative contaminant flux in those fractures. Thus, the in situ measurements of direction and magnitude of water and contaminant fluxes in active fractures are innovations given by the FRPFM alone.

As currently designed, the FRPFM provides high resolution measurements over a specified interrogation zone (typically 1 meter). Due to the high resolution nature of the FRPFM technology, its optimum application would be for characterizing targeted borehole depth intervals and not for screening conditions over an entire borehole. FRPFM prototypes tested in this project were used to interrogate 1 meter depth intervals in 4-inch and 6-inch fractured rock wells.

3.0 PERFORMANCE OBJECTIVES

Performance objectives are a critical component of any demonstration plan, as they provide the basis for evaluating the performance and costs of an innovative technology. Meeting these performance objectives is essential for successful demonstration and validation of the FRPFM.

Table 1 lists the Performance Objectives evaluated during field demonstration of the FRPFM. With regards to the quantitative performance objectives, it is understood that future field application of the technology is contingent upon rigorous statistical comparison of FRPFM measures (e.g., solute and groundwater fluxes, flow direction, active fracture location and orientation) to those obtained using conventional/comparative technologies. Thus, as part of this demonstration, statistics are presented and comparisons made between FRPFM measures for each qualitative performance objective and those obtained by alternative fracture rock technologies.

Table 1. Performance Objectives.

Performance Objective		Data Requirements	Success Criteria
Quantitative Performance Objectives			
1	Detection of Flowing Fractures	Measures from visible and non-visible FRPFM tracers and comparative technologies	Detect presence of flowing fractures within +/- 10%
2	Fracture location (depth)	Measures from visible and non-visible FRPFM tracers and comparative technologies	Detect fracture location (depth) within +/- 10%
3	Fracture orientation	Visible dye measures and measures from comparative technology	Measurement validation to within *+/- 15%*
4	Fracture Flow Direction	Visible dye measures and measures from competing technology	Measurement validation to within *+/- 25%*
5	Accuracy of water flux measurements	Measures from FRPFM and comparative technologies	Measurement validation to within *+/- 25%*
6	Accuracy of contaminant flux measurements	Measures from FRPFM and comparative technologies	Measurement validation to within *+/- 25%*
Qualitative Performance Objectives			
7	Ease of use	Operator acceptance	Field technicians able to effectively take measurements
8	Acceptability of sample analysis	Sample analysis evaluated by external lab	Environmental laboratory acceptance

The FRPFM provides measures of discrete fracture properties (e.g., dip and azimuth) and flux only at the surface of the borehole and not beyond. That is, the FRPFM does not provide measures of fracture properties and fluxes between boreholes; however, estimates for these properties can be obtained using geostatistical models and FRPFM data (Acar et al, 2013).

3.1 PERFORMANCE OBJECTIVE: DETECTION OF FLOWING FRACTURES

The ability to identify active flowing fractures under closed-hole conditions is a critical tool for characterization of fractured rock wells. The effectiveness of the FRPFM to identify active fractures using visible and non-visible tracers depends on the magnitude of flow occurring in these

fractures. Laboratory studies suggest effective flow detection was achieved for flows as low as 10 cm/d.

3.1.1. DATA REQUIREMENTS

FRPFM identification of active flowing fractures is compared to active flow zones identified using high resolution temperature profiles (HRTP) (Pehme et al., 2010), a closed-hole technique executed in an impermeable flexible liner (e.g., a FLUTe^{TM}). The effectiveness of the FRPFM to identify active flowing fractures is based upon analysis of two data comparisons. Data type 1A compares the identification of flowing fractures by HRTP and FRPFM visual tracers. While data type 1B compares the identification of flowing fractures by HRTP and FRPFM alcohol tracers. Quantitative comparison for identification of flowing fractures is based upon the depth at which flow is quantified by each technology. It should be noted that quantitative statistical comparisons can only be made for cases where both technologies identified active flow. Due to the higher resolution of detection by FRPFM visual tracers and alcohol tracers within the interrogation zone, there are instances where FRPFM indications of flow did not have matching HRTP identified flow. But, all FRPFM target zones are initially selected based upon HRTP screening for flow.

3.1.2. SUCCESS CRITERIA

Comparative analyses were performed to determine if FRPFM measurements were statistically different from field measurements produced by a competing technology (Bland and Altman, 1986). This objective was considered met if the FRPFM was capable of detecting the presence of active flowing fractures within ±10cm (within 10% over 1 meter interrogation zone).

3.2 PERFORMANCE OBJECTIVE: FRACTURE LOCATION

An important clarification between performance objective 1 (detection of flowing fractures) and performance objective 2 (fracture location) is the capability of the technologies compared. For performance objective 1, each technology compared (HRTP and FRPFM) is capable of identifying flowing fractures, and as such is a measure of how accurately each technology identifies flow. Whereas, for performance objective 2, FRPFM locations are compared to ATV and OTV locations, which are acoustic and optical measures of the borehole rock face with no indication of flow. As such performance objective 2 is a comparison of the apparent location (depth) of features regardless of flow. An important distinction and subsequent benefit is that comparison of these technologies allows for identification of which ATV/OTV features are actively flowing based upon FRPFM measures.

3.2.1. DATA REQUIREMENTS

The effectiveness of the FRPFM to locate flowing fractures is based upon analysis of two data comparisons. Data type 2A compares the depth of fractures identified by ATV/OTV and FRPFM visual tracers. While data type 2B compares the depth of fractures identified by ATV/OTV and FRPFM alcohol tracers. It should be noted that quantitative statistical comparisons could only be made for cases where both technologies identified fractures. Due to the higher resolution of fracture detection by FRPFM visual tracers and alcohol tracers within the interrogation zone, there were instances where FRPFM-identified fractures did not have matching ATV/OTV fractures.

3.2.2. SUCCESS CRITERIA

Comparative analyses were performed to determine if FRPFM measurements were statistically different from field measurements produced by ATV/OTV (Bland and Altman, 1986). The objective was considered met when compared to ATV/OTV if the FRPFM was capable of detecting the location of fractures within ±10cm (within 10% over 1 meter).

3.3 PERFORMANCE OBJECTIVE: FRACTURE ORIENTATION

Evaluation of performance objective 3 is based upon comparison of fracture orientation determined from ATV/OTV logs and FRPFM visual tracers. Two components of fracture orientation (azimuth and dip) are quantitatively compared.

3.3.1. DATA REQUIREMENTS

Data requirements include direct measures of fracture orientations using open-hole optical borehole imaging tools ATV/OTV (Wilson et al. 2001) and direct measures of flowing fracture orientations using visible tracer from reactive FRPFM fabrics. Quantitative comparison for fracture orientation is based upon the apparent shape of features identified by each technology. It should be noted that quantitative comparisons can only be made for cases where both technologies identified fractures. Due to the higher resolution of FRPFM visual tracers within the interrogation zone, there were multiple instances where the FRPFM identified flowing fractures that did not have matching ATV/OTV fractures.

3.3.2. SUCCESS CRITERIA

Comparative analyses were performed to determine if FRPFM measurements were statistically different from field measurements produced by ATV/OTV (Bland and Altman, 1986). The objective was considered met if FRPFM measured fracture orientations were within 15% of corresponding measures obtained from ATV/OTV.

3.4 PERFORMANCE OBJECTIVE: FRACTURE FLOW DIRECTION

Evaluation of performance objective 4 is based upon comparison of flow direction estimated by TVP (Pehme et al., 2014) and FRPFM visual tracers. All flow direction comparisons are based upon reference to true north. It is important to note that for fractured rock systems the hydraulic gradients and corresponding flow directions are both spatially and temporally variable, which makes high resolution measurement of flow direction considerably challenging. It follows that the quantitative comparison of flow direction estimates is strongly influenced by the relative location and time of observation. The only way to guarantee a truly consistent comparison between two alternate technologies is for the observations to be made at the exact same location and time, which is typically not possible within a borehole.

3.4.1. DATA REQUIREMENTS

Data requirements include measures of flow direction using TVP (Pehme, et al 2014) and measures of flow direction indicated by visible tracers on FRPFM fabric. Pehme et al. (2014) addresses the spatial and temporal variation of flow measurements using TVP. FRPFM high resolution

directional measures are based upon visual indication of discrete fracture flows within the FRPFM 1-meter interrogation zone, and as such will experience at least as much if not more spatial variation in flow direction when compared to TVP.

3.4.2. SUCCESS CRITERIA

Comparative analyses were performed to determine if FRPFM measurements were statistically different from field measurements produced by TVP (Bland and Altman, 1986). The objective was considered met if FRPFM measured flow direction within 25% of corresponding measures obtained from TVP.

3.5 PERFORMANCE OBJECTIVE: ACCURACY OF WATER FLUX MEASUREMENTS

Evaluation of performance objective 5 is based upon two data comparisons. Data type 5A compares water flux values from BHD to those determined from FRPFM visual tracers. While data type 5B compares water flux values from BHD to those determined from FRPFM alcohol tracers.

3.5.1. DATA REQUIREMENTS

FRPFM measures of water and contaminant fluxes were compared to measured/calculated fluxes from borehole dilution (BHD) tests performed over the same 1-meter interrogation zone.

3.5.2. SUCCESS CRITERIA

Comparative analyses were performed to determine if FRPFM measurements were statistically different from field measurements produced by BHD (Bland and Altman, 1986). The performance objective was considered met if FRPFM measurements were within 25% of measures obtained from BHD.

3.6 PERFORMANCE OBJECTIVE: ACCURACY OF CONTAMINANT FLUX MEASUREMENTS

Evaluation of performance objective 6 is based upon two data comparisons. Data type 6A compares contaminant flux values from BHD to those determined from FRPFM. While data type 6B compares contaminant flux average concentrations from BHD to those determined from FRPFM.

3.6.1. DATA REQUIREMENTS

FRPFM measures of water and contaminant fluxes were compared to measured/calculated fluxes gathered from borehole dilution (BHD) tests.

3.6.2. SUCCESS CRITERIA

Comparative analyses were performed to determine if FRPFM measurements were statistically different from field measurements produced by BHD (Bland and Altman, 1986). The performance

objective was considered met if FRPFM measurements were within 25% of measures obtained from BHD.

3.7 PERFORMANCE OBJECTIVE: EASE OF USE

Qualitative approaches were used to characterize the FRPFM technology in term of ‘ease of use’.

3.7.1. DATA REQUIREMENTS

Data evaluated measured operator’s acceptance of the technology. Data requirements include comments on the ‘ease of use’ and ‘required level of training’ in the context of competing technologies. General assessments were made concerning the quality and resolution of data generated. System reliability were evaluated (e.g., number of deployments that fail). Advantages and disadvantages of the FRPFM were reported for consideration by the potential users of the technology.

3.7.2. SUCCESS CRITERIA

The objectives was considered met if Field technicians were able to effectively take measurements given a reasonable level of training.

3.8 PERFORMANCE OBJECTIVE: ACCEPTABILITY OF SAMPLE ANALYSIS

Qualitative approaches were used to characterize the FRPFM technology in terms of ‘acceptability of sample analysis’.

3.8.1. DATA REQUIREMENTS

Data requirements included sample analysis evaluated by an external lab

3.8.2. SUCCESS CRITERIA

The objectives were considered met if samples received environmental laboratory acceptance.

4.0 SITE DESCRIPTION

Over the duration of this project a total of 18 FRPFM deployments were performed at two sites: the Guelph Tool Site (GTS) in Ontario, Canada and the former Naval Air Warfare Center (NAWC) in West Trenton, New Jersey both sites had previously existing networks of well characterized fractured frock wells.

4.1 GUELPH TOOL SITE (GTS)

4.1.1 GTS: SITE LOCATION AND HISTORY

Guelph Tool Inc. is an automotive parts manufacturing company in the City of Guelph. Since 1986, Guelph Tool Inc. has owned the GTS or the land overlying the known and expected TCE contamination in the underlying dolostone aquifer. The GTS is situated near two municipal water-supply wells owned by the City of Guelph (population 110,000). These two wells have not operated since TCE contamination was found in them and the dolostone aquifer over a decade ago.

The criteria and requirements used in selecting the Guelph Tool Inc. site (GTS) were the following:

a. It has an excellent existing infrastructure to support the demonstration,
b. The site is well-characterized,
c. The site has several well-characterized shallow boreholes in fracture rock of high bulk conductivity,
d. Rock fractures range from medium (<1 mm) to large apertures (>1 mm),
e. The site has chlorinated solvent contamination, and
f. The site has natural-gradient flow conditions.

The GTS is located ~1 mile from the G360 Centre for Applied Groundwater Research at the University of Guelph in Guelph, Ontario. Dr. Parker (one of project PI's) is the director of G360. G360's proximity to the GTS ensured that sufficient infrastructure existed to support the demonstration of the fractured rock passive fluxmeter (FRPFM). Guelph Tool Inc. owns nearly all of the land overlying the known and expected contamination. Dr. Parker initiated research at GTS in 2004 with the approval of the Ontario Ministry of the Environment and the City of Guelph and the support of Guelph Tool Inc. to drill multiple wells.

Multiple rock wells have been drilled in the fractured dolostone underlying the site. The depth of the boreholes is quite shallow because the water table and potentiometric surfaces are close to ground surface (<8m); these conditions served to maximize the likelihood of a successful FRPFM demonstration. Several wells had been visually and hydraulically characterized at 1.5 m depth intervals. The bulk hydraulic conductivity of the dolostone is high. The contaminant of concern is TCE which currently migrates under natural gradient conditions (i.e., no pumping). The demonstration efforts at GTS generated the first direct field measures of both water and TCE fluxes in fracture rock under ambient conditions.

The GTS provided challenges for measuring low fluxes in fractures which are visually undetectable (apertures <1mm) to large (aperture >1 mm). The site's proximity to G360 and on-site infrastructure enabled the research team to demonstrate detailed characterization of fracture

flux variations in multiple well-characterized boreholes. In addition, Dr. Parker's group performed high resolution temperature profiling which enabled the team to demonstrate that the FRPFM detects flow in fractures that are not detectable using optical or acoustic techniques.

4.1.2 GTS: SITE GEOLOGY/HYDROLOGY

4.1.2.1 GTS: SURFICIAL GEOLOGY

The GTS is located within the physiographic region defined as the Guelph Drumlin Field. It comprises an area of approximately 829 square kilometres, and is centered around the City of Guelph. The overburden in the area consists predominantly of till which is regionally on the order of 10 m thick. However, data collected within the GTS indicates that the overburden thickness is as little as 5 m in some places.

4.1.2.2 GTS: BEDROCK

The bedrock in the Guelph area corresponds to Paleozoic sedimentary rocks of Middle Silurian age. In the vicinity of the GTS, these are the dolostones of the Guelph Formation which are underlain by dolostones of the Amabel Formation (see Figure 11 for the stratigraphy underlying the GTS).

Typically, the Guelph Formation consists of buff brown, fine and medium crystalline dolostone which emits a distinct petroliferous odour when broken. The upper part of the strata is weathered and brownish, and forms beds from 5 cm to more than 1.2 m thick. The Guelph Formation was deposited under sub tidal and biothermal conditions. The thickness of the Guelph Formation is approximately 30 m.

The Amabel Formation shows considerable variation, and is subdivided into numerous members which are not always present. Generally, the Amabel Formation is a thick succession of fossiliferous dolomite, commonly light grey, bluish grey and buff, fine to coarsely crystalline, in places porous, and deposited in beds from 0.6 to 1.2 m thick. The thickness of the Amabel Formation is approximately 60 m at GTS. In the vicinity of GTS, the combined thickness of the Guelph and Amabel Formations is approximately 90 m.

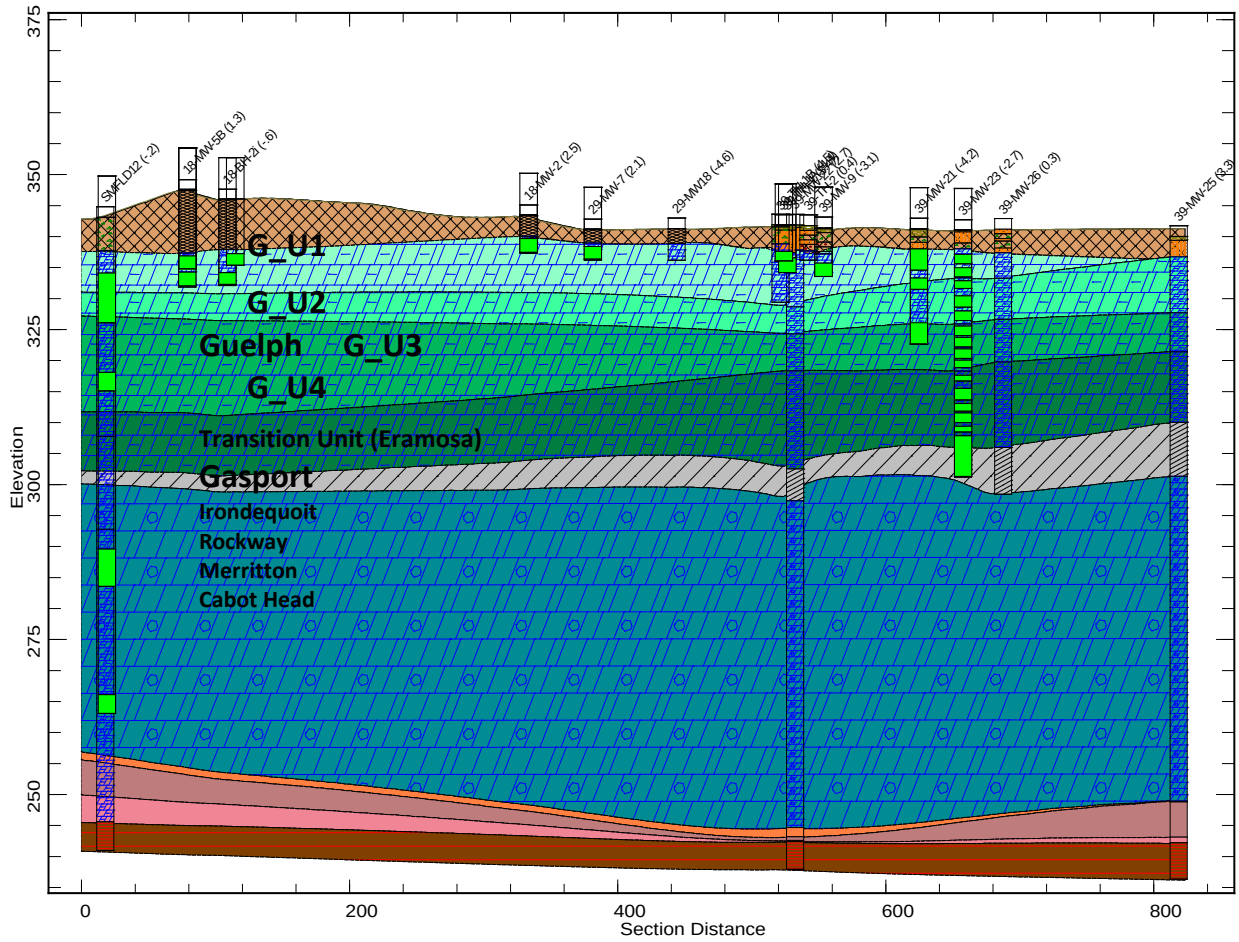

Figure 11. Stratigraphy underlying the Guelph Tool Site.

The regional fracture pattern of the sedimentary rock in the Guelph area is relatively unknown; however, major rivers, creeks, and one buried bedrock channel are all aligned northeast to southwest. In addition, segments of major river channels run in north to south directions. The above noted observations would indicate that the major trends in vertical to subvertical fracturing are either aligned northeast to southwest, or north to south.

4.1.2.3 GTS: HYDROLOGY

The four principal hydrostratigraphic units that have been interpreted at the GTS include:

1. Overburden Aquifer - generally consists of sand and gravel deposits of limited extent, suitable only for domestic purposes.
2. Overburden Aquitard - areally and vertically extensive silty till deposits which separate the overburden aquifer (where it exists) from the bedrock aquifer.
3. Bedrock Aquifer - consists of the dolostone bedrock of the Guelph and Amabel Formations (traditionally referred to as the Guelph Amabel Aquifer).
4. Bedrock Aquitard - the Reynales Formation of the Clinton Group underlies the Amabel Formation and is considered to regionally function as an aquitard based on the presence of shale interbeds within the unit.

The focus of the following discussion is on the Guelph Amabel (Bedrock) aquifer, as it is the principal aquifer in the area.

4.1.2.4 GTS: GROUNDWATER FLOW

Flow within the bedrock is expected to be predominantly to the south and east, based on limited water level data. The permeability of the Guelph Amabel aquifer is due primarily to the chemical dissolution of dolostone along fractures and bedding planes. The permeability is variable due to the large differences in opening sizes and patterns caused by fracturing. Due to weathering processes, the upper 5 m of the aquifer is generally the most permeable.

Regional groundwater discharge zones include surface water bodies such as the Eramosa and Speed Rivers. City of Guelph municipal wells tend to be located in discharge areas. Recharge zones tend to be areas located on topographic highs that have relatively thin overburden layers. A major regional recharge zone is the Arkell Springs Grounds, located approximated 10 km southeast of the GTS. The GTS is not located within any major regional discharge or recharge zones.

4.1.3 GTS: CONTAMINANT DISTRIBUTION

The contamination at the GTS occurs in a small area and at shallow depths and offers opportunities for examining the internal source zone and plume characteristics in great detail. Transects defining the general boundaries of the source zone and plume are illustrated in Figure 12.

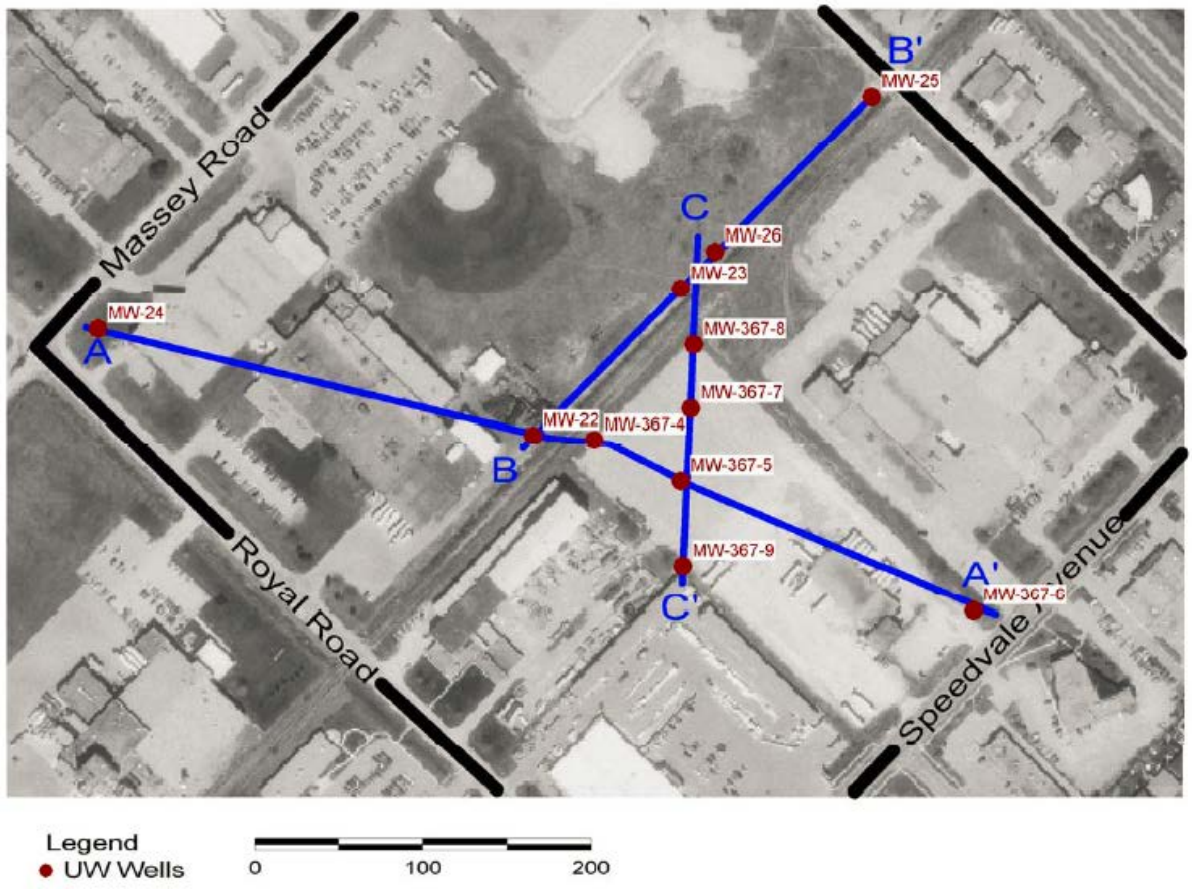

Figure 12. Transects defining the general boundaries of the source zone and plume.

4.2 NAVAL AIR WARFARE CENTER (NAWC)

4.2.1 NAWC: SITE LOCATION AND HISTORY

NAWC is a 60 acre facility located in West Trenton, NJ. The NAWC served as a Naval testing facility for aircraft jet engines from the 1950's to 1994. During its operation, TCE was used for its properties of heat exchange in testing aircraft engines under various conditions of temperature and pressure. The handling and disposal of TCE at the site resulted in two source areas of TCE contamination; identified as Site 1 and Site 3. Site 1 was the area where TCE was stored and handled, and where TCE was spilled or leaked onto the ground. Site 1 was also the location of a network of above-ground TCE pipelines and waste lines that lead to the barometric well; and the West Ditch where TCE-laden wastewater was disposed. Site 3 consists of a former wastewater lagoon, which was a sludge disposal area and received waste water containing dissolved TCE (Shapiro, 2008).

In 1994, the Navy moved the testing of aircraft engines from the NAWC to other facilities and started the process of decommissioning the site. The site was officially closed in 1998 and has been subsequently transferred for private development. In the vicinity of Site 1, the soil was excavated to remove residual TCE and the area was graded with fine gravel. Monitoring wells in the underlying bedrock showed the presence of high concentrations of dissolved TCE.

Pumping from bedrock wells has been ongoing at the site since 1995 to remove and treat contaminated groundwater and limit the migration of TCE and degradation products. Currently there are 8 pumping wells. Not all of these wells are operated simultaneously, and in general, the combined pumping rate of the wells ranges from 39 to 56 gallons per minute (gpm) [Shapiro, 2008].

Currently, the site and its buildings are vacant awaiting decisions on redevelopment by the owner. The current owner has performed limited demolition of the existing buildings; however, the Navy retains the responsibility for the environmental cleanup of the site, including the right of access for the operations associated with monitoring and remediation.

The NAWC site has been the focus of several studies including the current SERDP project ER1555 (Shapiro, 2008). The focus of this study is to compare the effectiveness of pump-and-treat, natural attenuation, and enhanced biodegradation as competitive remediation solutions to chlorinated ethene-contaminated fractured rock.

The criteria and requirements used in selecting Former Naval Air Warfare Center (NAWC) site were the following:

a. The site has an excellent existing infrastructure to support the demonstration,
b. The site is well-characterized,
c. There are several well-characterized shallow boreholes in fracture rock of very low to high bulk conductivity,
d. Rock fractures range from nonexistent to large apertures (>1 mm),
e. There exists fractured rock data on fracture frequency and fracture length distributions gathered from an exposed outcrop,
f. The site has ongoing SERDP supported activities that can be leveraged,

g. The site has chlorinated solvent contamination, and
h. The site has induced-gradient flow conditions.

The NAWC site provided the challenges of demonstrating the FRPFM in fractured bedded mudstones under induced hydraulic conditions (active pumping). All tests were performed in well 68BR where there are multiple zones of TCE and DCE transport. Some zones are dominated by high convective flows while deeper zones experience lower flows. All FRPFM tests were conducted over zones previously tested by the USGS using competing technologies. The on-site infrastructure and the activities of project ER1555 were leveraged to provide support for FRPFM demonstration. The existence of the ongoing site activity maximized the likelihood of a successful demonstration.

4.2.2 NAWC: SITE GEOLOGY/HYDROLOGY

The NAWC site (Figure 13) lies on the bedded, fractured sedimentary rocks of the Newark Basin. Soil and weathered rock cover the site to a depth of approximately 15 ft. The water table varies from 5 to 15 feet below land surface over the site. The underlying competent rocks are primarily mudstones and sandstones of the Lockatong and Stockton Formations. The formations generally dip from 20 to 50 degrees toward the NNW, and are separated from each other by a near-vertical fault zone (Shapiro, 2008).

Based on data gathered from approximately 100 wells in the soil, weathered rock, and the underlying competent bedrock at the NAWC site, the underlying rocks north of the fault are within the Lockatong Formation, which is composed of four facies – a basal red massive mudstone, a black carbon-rich mudstone, a laminated dark-gray mudstone, and an upper massive light-gray to red mudstone.

Of the four facies, the carbon-rich mudstones are fissile and extensively fractured, and provide permeable pathways for the movement of groundwater and contaminants. Laminated dark-gray mudstones are less prone to fracturing than the black carbon-rich mudstones, but still can form water-bearing zones in the shallow bedrock. Light gray to red mudstones typically behave as semi-confining units. Stratabound, subvertical fractures are observed in the rock, and are likely to transmit fluid and solutes, but are much less permeable than the fractures parallel to bedding (Shapiro, 2008).

4.2.3 NAWC: CONTAMINANT DISTRIBUTION

Concentrations of TCE, DCE, and VC have been detected to depths of approximately 200 ft. Because DCE and VC were not independently used at the NAWC, the presence of DCE and VC implies the presence of microbial degradation of TCE to its daughter products. Coring in the bedrock during the first year of activities under SERDP project ER-1555 detected the presence of free-phase TCE and groundwater at concentrations as high as about 100,000 µg /L. Samples from rock cores collected showed that the upper part of the bedrock (approximately the top 10 meters of bedrock) has uniform, high concentrations of TCE in the pore fluid of the rock matrix. At greater depths in bedrock, however, TCE concentrations in the pore fluid of the rock matrix are highest near the bedding plane parting fractures. Due to the high concentrations of TCE in fractures, dissolved-phase TCE, DCE, and VC have diffused from fractures into the primary porosity of the

sedimentary rock. Because the permeability of the intact rock is many orders of magnitude less than the permeability of the fractures, groundwater in the primary porosity of the rock is not readily accessible to groundwater flow, and diffusion is the primary process controlling the migration of TCE from the intact rock back into the permeable fractures. The back-diffusion is believed to be responsible for the persistently high concentrations of TCE, DCE, and VC detected at the pumping wells at the NAWC. Interpreted concentration contours define the general boundaries of source zones and plumes are illustrated in Figure 14 (Shapiro, 2008).

One of the most highly characterized wells at NAWC is monitoring well 68BR. Figure 15 summarizes the vertical distribution of TCE concentrations as reported by Shapiro, 2008.

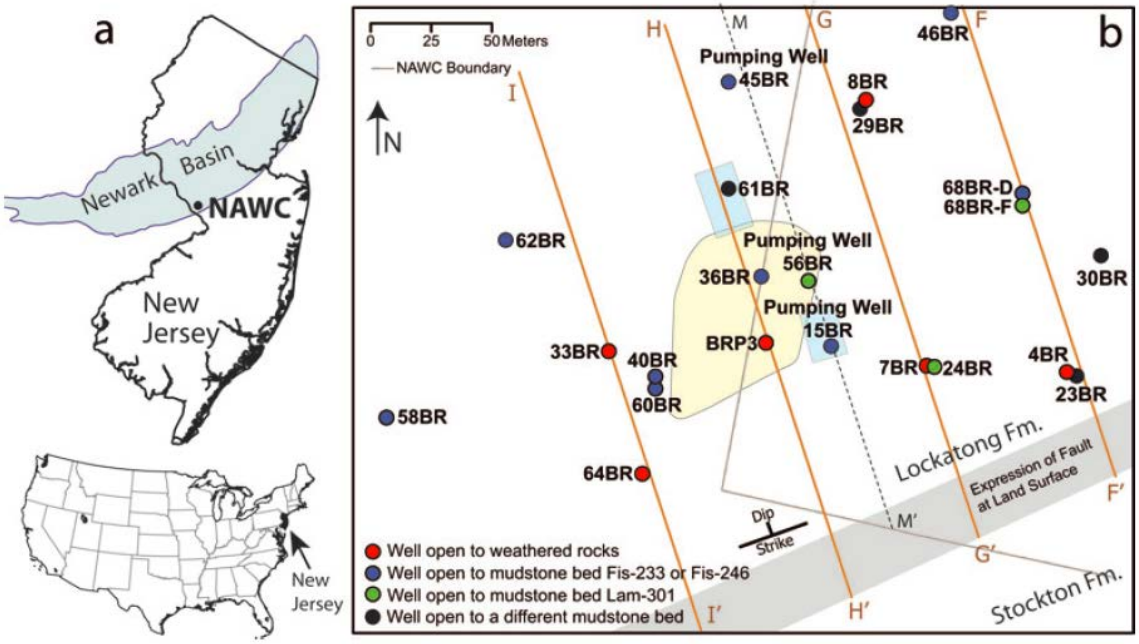

Figure 13. (a) Location of the former Naval Air Warfare Center (NAWC) site in West Trenton, NJ. (b) Plan view of NAWC site showing locations of pumping and monitoring wells. (Tiedeman et al, 2010).

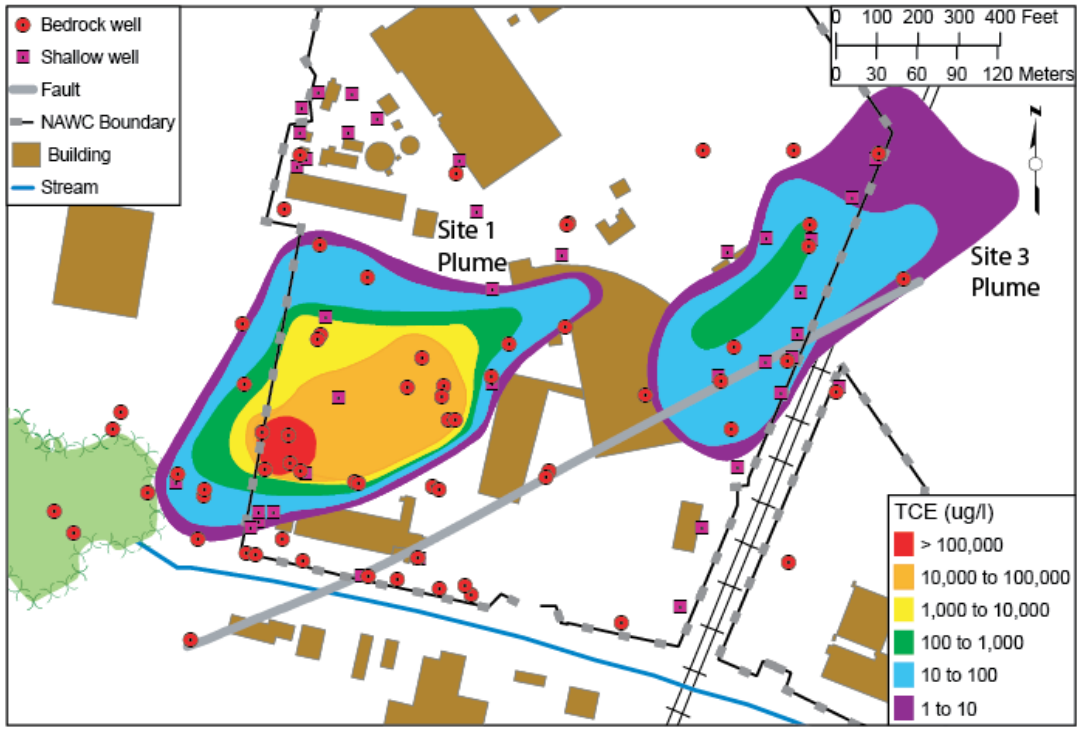

Figure 14. The location of Site 1 and Site 3 TCE plumes interpreted at a depth of 100 feet below land surface at the Naval Air Warfare Center, West Trenton, NJ in May 2004 (Shapiro, 2008).

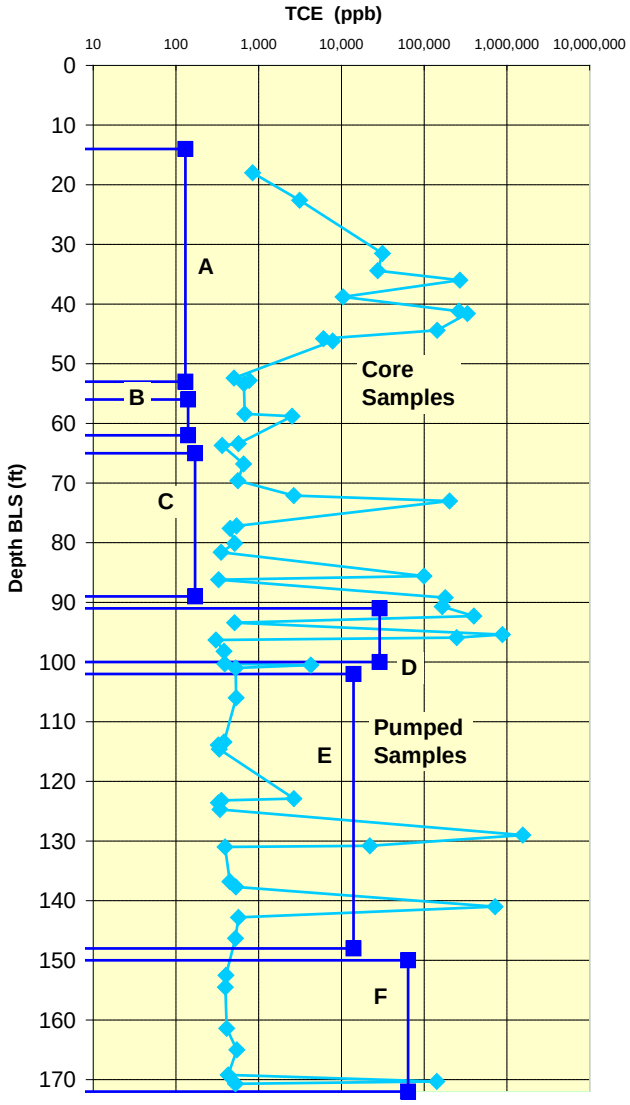

Figure 15. TCE concentrations in NAWC well 68BR.
Bulk concentration of TCE from samples of rock core taken from monitoring well 68BR as a function of depth are shown in comparison to the concentrations of TCE from water samples collected from the 6 monitoring intervals in 68BR (A, B, C, D, E, F). (Shapiro, 2008).

5.0 TEST DESIGN

5.1 CONCEPTUAL EXPERIMENTAL DESIGN

In this demonstration the FRPFM was tested under ambient and induced flow conditions in well-characterized boreholes in both fractured mudstone and dolostone. Repeated flux measurements were taken over regular depth intervals for comparison to competing technologies. Borehole dilution (BHD) tests were conducted over the same depth intervals for validation of flux measurements. To know in advance at what depth intervals to conduct FRPFM testing, selected boreholes were characterized based upon the extent to which data existed on:

1) location and orientation of visible fractures;
2) location of flowing fractures under ambient conditions; and,
3) fractured rock transmissivity at a regular 0.3 to 1.5m depth interval.

Thus, the experimental design involved testing the FRPFM performance over multiple 1.0 m intervals using existing characterization data to guide testing and in addition generate new data from the use of competitive technologies. Given the estimated locations of flowing fractures from high resolution temperature profiling, it was feasible to directly assess FRPFM performance under ambient conditions with respect to:

1) Detecting the location of flowing fractures using visible tracers (compared to detection by high resolution temperature profiling);
2) Measuring active fracture orientation using visible tracers (compared to optical detection methods);
3) Measuring water flux at discrete intervals (compared to borehole dilution tests);
4) Measuring TCE and DCE fluxes at discrete intervals (compared to calculated fluxes from TCE and DCE concentrations and measured water flux by borehole dilution tests); and,
5) Measuring active fracture flow direction as indicated by the elution of a visible tracer at locations of active fractures (compared to high resolution temperature profiling measurements).

The fundamental virtue of this basic field demonstration design was the repetitive testing of the FRPFM against competing technologies in one or more well-characterized boreholes in a fractured mudstone and dolostone, thus producing data that can be subjected to rigorous statistical analysis.

5.2 BASELINE CHARACTERIZATION

It is prudent to anticipate that the FRPFM will typically be deployed in deep fractured rock wells or in deep wells screened in fractured rock or unconsolidated materials. To achieve cost-efficiencies in characterizing rock wells, FRPFM deployments will likely follow after other characterization tools [e.g., high resolution temperature logging (Pehme et al. 2007), contaminant profiling (Sterling et al., 2005), hydrophysical logging (Wilson et al. 2001), K-profiling or hydraulic conductivity profiling using a FLUTe$_{TM}$ (Keller et al., 2007), etc.] have been used to locate contaminated fractures and/or fractures believed to conduct flows under closed-hole

conditions. Thus, if the FRPFM demonstration were being conducted on a new borehole, baseline characterization would include the following:

1) Measuring groundwater levels;
2) Measuring contaminant concentrations;
3) Conducting high resolution temperature logging in a FLUTeTM (closed hole conditions) to detect locations of flow fractures;
4) Conducting a down hole optical survey of visible fractures;
5) Analyzing rock cores for fractures or zones of contamination; and possibly,
6) Conducting targeted straddle packer tests Fracture hydraulic conductivity or hydraulic conductivity profiling using a FLUTeTM (Keller et al., 2007).

Because baseline characterization activities 3-6 were previously completed at both the Guelph Tool and NAWC sites in multiple wells, measurement of water levels and contaminant concentrations were the two characterizations that were necessary prior to and during FRPFM field testing.

5.2.1. GROUNDWATER LEVEL MEASUREMENTS

In this demonstration the FRPFM was tested under natural gradient and pumping conditions in multiple well-characterized boreholes in fractured dolostone and mudstone. Groundwater levels were measured in each test borehole and in three to four nearby wells before and after testing the FRPFM. The intent was to monitor for potential changes in head gradients produced by transient hydrologic conditions (e.g., rainfall events and pumping).

5.2.2. CONTAMINANT CONCENTRATION MEASUREMENTS

Multiple groundwater samples were collected from each test well for analysis of TCE and DCE concentrations. These samples were collected immediately before FRPFM testing began. The intent was to assess ambient depth-average TCE and DCE concentrations under open-hole conditions and over isolated depth intervals.

5.2.3. DISPOSAL OF INVESTIGATION-DERIVED WASTE (IDW)

It is estimated that the demonstration produced 7 kg of IDW; 4 kg of spent activated carbon felt waste, 1 kg of spent cotton socks, and 2 kg of plastic mesh. The University of Guelph/Florida/USGS disposed of all waste.

5.3 LABORATORY STUDY RESULTS

This section provides a detailed description of laboratory testing that was conducted in order to address the performance objectives outlined in Section 3.0. The intent of this phase of work was to select 1) resident tracers and sorbent appropriate for the target contaminants and fracture flow conditions, 2) an appropriate visual tracer (dye) and fabric for visual indication of flowing fractures; and 3) to perform initial prototype design and deployment testing to prepare for field-scale testing.

5.3.1 LABORATORY EXPERIMENTAL PLAN

The laboratory experimental plan consisted of three distinct stages of work:

1. Component testing and selection (sorbents and tracers)
2. Prototype testing (fracture flow simulator and aquifer box)
3. Full-scale installation and deployment testing (mock borehole)

Each stage of lab work had multiple tasks, and portions of each stage were performed in parallel to determine the best individual device components for specific purposes (i.e.. the best combination of dyes and fabric to provide visual indication of flowing fracture, and the best combination of sorbents and resident tracers for measuring water flow/flux within fractures). Once tested, the individual components were assembled for prototype testing using two different physical flow simulators (fracture flow simulator and large three-dimensional aquifer box). The flow tests were used to evaluate FRPFM performance under controlled flow conditions, and to compare results from competing open- and closed-hole technologies. A third and final stage of lab testing was performed in a full-scale mock borehole (4-inch diameter PVC casing 36 feet deep) to simulate field deployment conditions in order to assess field-scale installation issues and develop optimal installation procedures in preparation for field tests. Between each stage of testing the FRPFM prototype was modified and scaled-up to prepare for field testing.

5.3.1.1 COMPONENT TESTING AND SELECTION

The objective of this task was to identify a range of sorptive media and tracers to be used both independently or in combination to 1) provide a visual indication of the presence of flowing fractures (including direction and orientation) and 2) measure target surrogate contaminant and water flux within the flowing fractures. Multiple conceptual models for FRPFM were initially considered in order to provide the capability of visualizing flowing fractures while simultaneously allowing for the measurement of water and surrogate contaminant mass flux within the fractures. Ideally, the system would be constructed of one sorbent that allows for use of visual tracers (fracture flow visualization), resident alcohol tracers (water flux), and sorption of target contaminants (contaminant flux). But, research and testing of currently existing sorbent materials indicated that the ideal sorbent was not readily available (i.e. sorbents that provided good visual indication did not perform well with resident tracers and target contaminants – and sorbents that performed well with resident tracers and target contaminants did not provide good visual indication of flow). Without an ideal one sorbent system, the most appropriate conceptual model was to construct the device using a two layer design. The outer layer (or sock) is made from an elastic fabric which is used to provide a visual indication of flow through the device, and the inner layer is composed of a sorbent material that readily sorbs and elutes resident tracers while capturing target contaminants (Figure 3).

Batch sorption tests were performed in parallel for both tracer/sorbent systems (visual tracers and resident alcohol tracers). Visual tracer performance was evaluated qualitatively by visual inspection (under both visible and UV light), while resident tracer performance was evaluated quantitatively by chemical analysis. Evaluation of both tracer/sorbent systems also included flow-through test components.

As noted above, component testing and selection consisted of two primary tasks which were performed in parallel with the objectives outlined below.

Selection of visual tracer and outer fabric layer: considered numerous fabrics and visual tracers (food grade dyes) which in combination had to demonstrate

- Good dye/fabric interaction and performance to provide visual indication of water flow through the device. Dye had to uniformly stain the fabric, while also demonstrating a site-specific visual change once exposed to flow.
- Fabric had to be elastic in order to expand and contract with inflatable core without tearing or deforming.
- Fabric had to have relatively high permeability with respect to inner sorbent in order to allow for flow through the device and avoid flow bypassing.

Selection of resident tracers and inner sorbent layer: considered numerous sorbent materials (fabrics, felts, papers) and potential resident tracers (branched alcohols) which in combination had to demonstrate

- High fabric permeability to allow for flow through device
- Good sorption capacity for tracers on fabric
- Adequate tracer elution during aqueous flow in order to provide accurate measure of water flux
- High extraction efficiency of tracers from fabric for proper analysis
- Good sorption and extraction efficiency of target contaminant with selected fabric

In addition to initial batch tests, multiple series of flow through tests were performed for both visual tracer and resident tracer selection in order to evaluate performance of selected components during aqueous flow conditions. Details of all testing procedures are provided in section 5.3.2.

5.3.1.2 PROTOTYPE TESTING

The primary objective of this task was to evaluate FRPFM prototype performance under controlled laboratory conditions. The secondary objective of this task was to assess the performance of competing technologies (including borehole dilution tests) for characterizing flow in fractured systems. Tests were performed in two separate flow simulators: a planar single fracture flow simulator and a large-scale three-dimensional aquifer box with layered high contrast flow zones. The objective of these tests was to compare results and develop a collaborative standard operating procedure incorporating the most appropriate tools for accurately characterizing flow and contaminant flux in fractured rock systems. Details of all prototype testing procedures are provided in section 5.3.2.

5.3.1.3 FULL-SCALE INSTALLATION AND DEPLOYMENT TESTING

Installation and deployment of FRPM is more challenging than that of standard PFM due to both the increased complexity of the device and because deployments will often be performed in exposed-rock open boreholes rather than screened wells, which increases the likelihood of the device getting caught on exposed rock and possibly lodged down hole. For this reason, the

objective of this task was to develop and test procedures for deployment of the FRPFM at realistic field depths in both screened wells and open boreholes. Tests for this objective were performed in two separate systems: a large-scale aquifer box and a full-scale mock borehole. Various strategies for deploying the device were investigated in order to establish the optimal procedure for installing and successfully recovering the FRPFM.

5.3.2 LABORATORY PROCEDURES AND APPARATUS

The following sections provide a discussion of the laboratory procedures and apparatus that were used to achieve the objectives discussed in section 5.3.1.

5.3.2.1 COMPONENT TESTING: SELECTION OF FABRIC AND VISUAL TRACER

Initial research efforts for this project focused on testing visible tracers (dyes) and reactive-fabric (sorbent) systems for the purpose of providing a visual indication of flowing fractures. The need for visualizing flowing fractures was threefold: first, as an overall project objective it was necessary in order to identify where flowing fractures exist within a borehole; second, to estimate the cumulative water fluxes from visible tracers, and third due to the relative scale of the fractures with respect to the device itself, it was a functional objective in order to determine where to actually sample the device to analyze for resident tracer loss and accumulation of target contaminants in order to estimate water flux and contaminant mass flux respectively. The later task, identifying where to sample the device, is extremely critical and requires a higher degree of resolution.

Visual Tracers (Dyes)

Numerous nontoxic, food-grade dyes were considered as candidate visible tracers including allura red (FD&C Red #40 and closely related FD&C Yellow #6), scarlet green (FD&C Red #4), and tartrazine (FD&C Yellow #5 and closely related Orange B), blueberries, beets, purple grape juice, tea, and turmeric. Two synthetic dyes were also tested, diammonium salt (Acid Blue 9) and sulforhodamine B (Acid Red 52) that are fluorescent tracers and are used readily in groundwater studies.

Fabrics

Initial tests with natural and synthetic fabrics were performed with wool, cotton, lycra, fleece, felt, two different cotton/spandex blends (94/6 and 97/3 as percent) and a nylon/spandex blend. Wool and cotton were selected natural fabrics because both are readily available and were easily stained with most dyes. The cotton/spandex and nylon/spandex blends were chosen because of their elasticity, which is an additional benefit when considering attachment of the material to inflatable packers for deployment. Important attributes of these fabrics that were considered were dye fastness, durability, thickness, hydraulic conductivity and commercial availability.

Flow through dye tests

To test the performance of each dye/fabric combination under aqueous flow conditions, a flow-through test apparatus was constructed by cutting two concentric 5-cm diameter holes in the center of two acrylic sheets. The acrylic sheets were bolted together, and the fabric swatches were placed flat between them, allowing for water to pass through only the 5-cm diameter opening. Water-saturated, dyed swatches were fastened between the acrylic sheets and exposed

to a stream of water centered on the 5-cm hole. A standard volume of 5 gallons (3.8 liters) of water was run through each swatch for a consistent duration to see which dyes and fabrics performed the best. This test allowed for demonstration of the fastness of the dyes to the fabrics and observation of any color change under both visible and UV light.

5.3.2.2 COMPONENT TESTING: SELECTION OF SORBENT AND RESIDENT TRACERS

Laboratory batch experiments were performed to determine the sorption affinity, elution characteristics, and solvent extraction efficiency for candidate tracers and sorbents. Sorption and desorption isotherms were developed in order to assess the effectiveness of each candidate sorbent and tracer combination. Sorption and extraction efficiencies for target contaminants were also evaluated.

Preliminary batch experiments were performed with 10 candidate activated carbon fabrics using a suite of five alcohol tracers to test sorbent (fabric) affinity for each of the tracers. The alcohol tracers used were, Methanol (methyl alcohol), Ethanol (ethyl alcohol), IPA (isopropanol), TBA (tert-butyl alcohol), and 2,4-DMP (2,4-dimethyl-3-pentanol). The activated carbon fabrics tested were provided by multiple manufacturers and had a range of material thickness and available activated carbon content. Descriptions of each fabric tested are provided in Table 2. For convenience, the labels listed in the table for each fabric are used throughout this report in lieu of their commercial name.

Table 2. Candidate activated carbon fabrics.

	Fabric Type	Commercial Name	Label
A	Felt	Polyorgs Activated Carbon Fabric	Polyorgs
B	Felt	Nirvana Activated Carbon Blanket	Nirvana
C	Felt	AmeriAsia BET 1000 felt	AC Felt 1000
D	Felt	AmeriAsia BET 1300 felt	AC Felt 1300
E	Felt	AmeriAsia BET 1500 felt	AC Felt 1500
F	Cloth	Calgon Carbon Zorflex cloth FM 10	FM 10
G	Cloth	Calgon Carbon Zorflex cloth FM 100	FM 100
H	Cloth	AmeriAsia MY-QW-011, BET 1000 cloth	BET 1000
I	Cloth	AmeriAsia MY-QW-013, BET 1300 cloth	BET 1300
J	Cloth	AmeriAsia MY-QW-015, BET 1500 cloth	BET 1500

Tests indicated favorable results with all fabrics except fabric B. With the most favorable performance being fabrics C - J based upon the isotherms for IPA, TBA and 2,4-DMP. These fabrics were used for additional testing for selection of the best material. During preliminary tests, the isotherms for methanol and ethanol showed little promise in all cases; as a result, these tracers were no longer considered. As sorption is typically proportional to molecular weight, it was decided to replace methanol and ethanol with longer chain alcohols (i.e. higher molecular weights: such as 1-hexanol, 1-heptanol, 2-octanol, 2-ethy-l-hexanol, and 1-octanol).

Batch sorption test procedure.

Based upon results from the preliminary round of batch tests, the three fabrics exhibiting the best performance (AC-felt 1300, FM-100, and Polyorgs) were selected for more detailed testing with a suite of 8 tracers. The second round of sorption tests were conducted with higher detail (more analytical points were considered for higher resolution isotherms) to determine sorption

coefficients between resident tracers and fabrics. Tracers used in the second round of testing are listed in table 3 with relevant chemical properties.

Table 3. Chemical properties of tracers.

Chemical property of tracers

	Formula	MW	Density	mp	bp	Solubility
		(g/mol)	(g/cm3)			(mg/L)
1-propanol	C3H8O	60	0.803	-126.5	97.1	250538
2-butanol	C4H10O	74.12	0.808	-114.7	94	150000
1-butanol	C4H10O	74.12	0.809	-89.5	117.7	79421
3-pentanol	C5H12O	88.15	0.809	-63.68	115.3	54353
1-pentanol	C5H12O	88.15	0.814	-77.6	137.9	22658
2,4 Dimethyl 3 pentanol	C7H16O	116.2	0.829	-70	139	7002
1-hexanol	C6H14O	102.2	0.819	-52	156	6300
1-heptanol	C7H16O	116.2	0.819	-34.6	175.8	1800

For batch sorption tests, tracer concentrations ranged from 600 to 800 mg/L. Tracer solution was prepared in 3L of water and transferred in 30ml aliquots to 40 ml EPA vials with Teflon-lined screw caps. Next, varying amounts of sorbent were added to each vial. The vials were rotated for 48 hrs and the equilibrated samples were analyzed using a gas chromatograph (GC) with flame ionization detector (FID). Resulting sorption isotherms for select tracers and sorbents are shown Figure 14. Illustrated in Figure 15 are the final sorption isotherms for all tracers on AC Felt 1300. Sorption coefficients from correlation of adsorbed tracer amount (mg and g felt) and equilibrium concentration (mg/L) were determined and shown in Table 4.

The bulk density and porosity of AC Felt 1300 used for retardation factor estimation were 0.075 (g/cm3) and 0.92, respectively.

Table 4. Sorption coefficients and retardation factor values measured from batch tests.

Estimated Sorption Coefficients (Kd)

	2-BUTANOL	1-BUTANOL	3-PENTANOL	1-PENTANOL	24DMP	1-HEXANOL	1-HEPTANOL
	(mg/g)/(mg/L)	(mg/g)/(mg/L)	(mg/g)/(mg/L)	(mg/g)/(mg/L)	(mg/g)/(mg/L)	(mg/g)/(mg/L)	(mg/g)/(mg/L)
Felt 1300	0.064	0.157	0.3	0.77	4	5	48
FM100	0.04	0.11	0.19	0.52	2.7	4	40
Plyorgs	0.03	0.08	0.15	0.36	1.1	2.9	34

Estimated Retardation Factor

	2-BUTANOL	1-BUTANOL	3-PENTANOL	1-PENTANOL	24DMP	1-HEXANOL	1-HEPTANOL
Felt 1300	6	14	25	64	327	409	3918

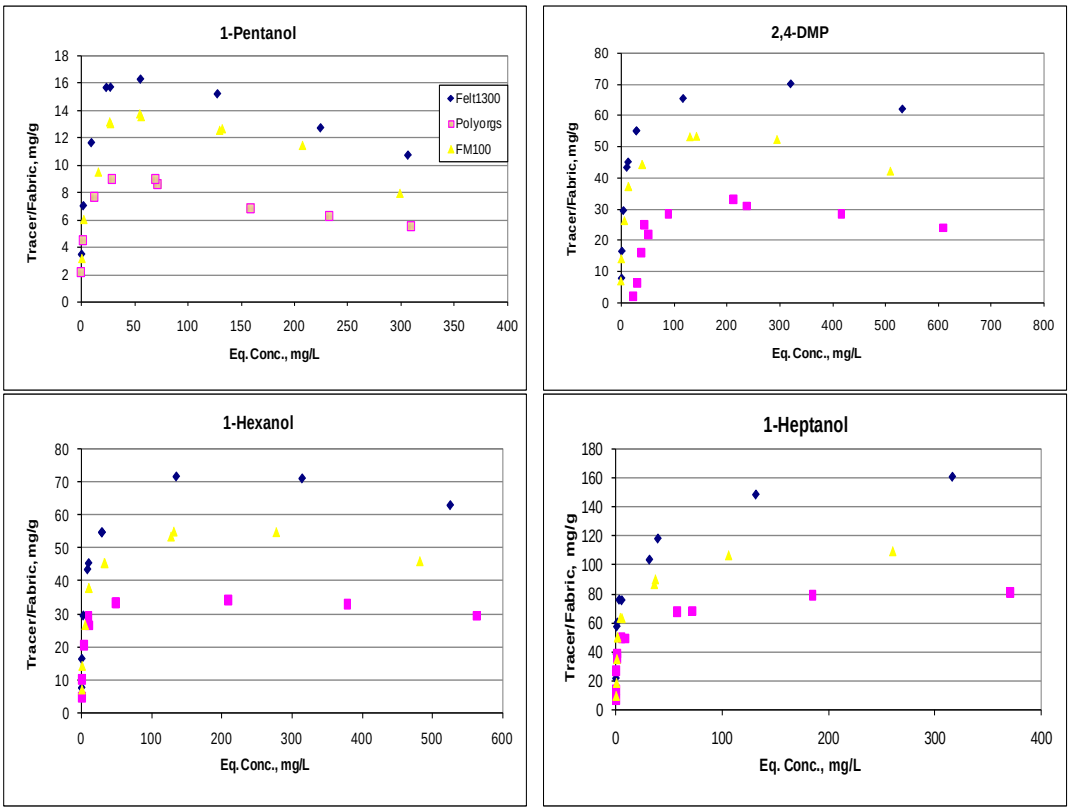

Figure 16. Adsorption isotherm of resident alcohol tracers on AC Felt1300, FM 100 cloth, and Polyorgs.

Procedure for generating a uniform tracer distribution on sorbent material.
Based upon performance evaluated with detailed batch sorption tests, the fabric selected for application with FRPFM was activated carbon felt (AC Felt 1300). Once the sorbent was selected, the next critical step to provide for proper performance of the device was to establish a method for consistently generating a uniform tracer distribution on the sorbent material. This was done by testing multiple tracer application methods and subsequent sampling of sorbent to determine the distribution of tracers on the felt. Two of the methods tested are outlined here: water based preparation and acetone based preparation. For both techniques, tracer concentrations ranged from 600 to 800 mg/L. For water based preparation tracers were prepared in 16 liter of water in a 20 liter jug, and for acetone based preparation tracers were prepared with 1.7 L of acetone in a 2 L glass bottle. For both cases approximately 13 g (about 60cm x 13 cm) of AC Felt 1300 were added in to each container and each container was rotated using a drum rotator for 48 hrs. After rotating, the tracer impregnated AC felt from each container was sampled as follows:

1. For AC felt prepared in water, the water-wet felt was drained for 1 min and cut into 6 pieces. Then each piece was put in a 125-ml glass bottle with 90 ml of methylene chloride solvent. The bottles were rotated for 48 hrs and then solvent was analyzed for tracer extraction.
2. For AC felt prepared in acetone, the acetone-wet felt was cut to 6 pieces of felt (each piece with 7.5 cm length). Each piece of acetone-wet felt was put on a stainless rack and placed in a laboratory exhaust hood for 30 min to let acetone volatilize off from the felt. After acetone drying process was complete, each piece of felt was put in a 125-ml glass bottle with 90 ml of methylene chloride solvent. The bottles were rotated for 48 hrs and then solvent was analyzed for tracer extraction.

The extraction samples were collected in 2-ml glass chromatography vials and analyzed using a gas chromatograph (GC) with FID. The results are shown in Table 5 and 6 and Figure 16.

Table 5. Water-based batch test result for uniform impregnated tracer distribution on AC felt 1300.

	1-propanol	**2-butanol**	**1-butanol**	**3-pentanol**	**1-pentanol**	**2,4DMP**	**1-hexanol**	**1-heptanol**
	(mg/L)/g felt	(mg/L)/g felt	(mg/L)/g felt	(mg/L)/g felt	(mg/L)/g felt	(mg/L)/g felt	(mg/L)/g felt	(mg/L)/g felt
1	0.2	0.4	0.7	1.2	4.4	52.5	49.2	237.4
2	0.2	0.4	0.7	1.3	4.8	57.6	54.8	261.1
3	0.1	0.3	0.7	1.2	4.5	52.6	49.4	235.2
4	0.2	0.3	0.7	1.3	4.5	52.3	49.3	236.2
5	0.2		0.7	1.3	4.5	53.0	50.1	237.1
6	0.2		0.7	1.2	4.4	51.5	48.3	230.5
avg	0.2	0.4	0.7	1.3	4.5	53.3	50.2	239.6
stv	0.0	0.0	0.0	0.0	0.2	2.2	2.3	10.8

Table 6. Acetone-based batch test result for uniform impregnated tracer distribution on AC felt 1300.

	1-propanol	2-butanol	1-butanol	3-pentanol	1-pentanol	2,4DMP	1-hexanol	1-heptanol
	(mg/L)/g felt	(mg/L)/g felt	(mg/L)/g felt	(mg/L)/g felt	(mg/L)/g felt	(mg/L)/g felt	(mg/L)/g felt	(mg/L)/g felt
1	47.6	64.8	79.8	85.4	92.7	73.1	73.6	81.5
2	45.8	61.9	77.5	82.3	90.6	70.7	71.2	75.0
3	46.5	64.5	82.2	87.9	98.6	76.9	80.4	86.9
4	44.3	61.7	77.4	83.7	92.4	72.5	73.2	79.8
5	44.4	61.6	77.3	83.3	90.8	72.4	72.3	83.1
6	45.3	61.7	77.4	82.8	91.1	71.7	72.6	77.0
avg	45.6	62.7	78.6	84.2	92.7	72.9	73.9	80.6
stv	1.3	1.5	2.0	2.1	3.0	2.1	3.3	4.3

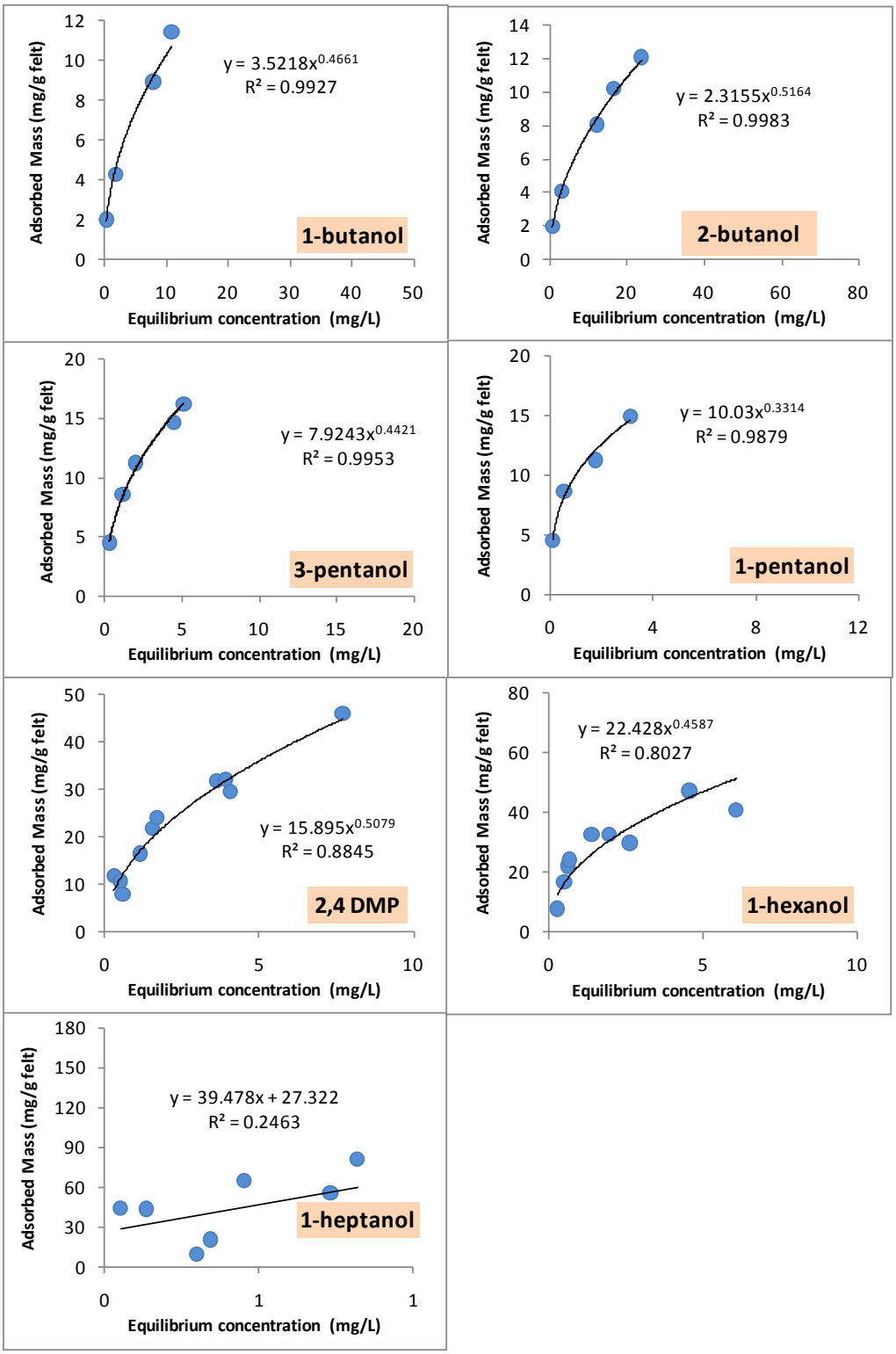

Figure 17. Final Sorption Isotherms using AC Felt 1300.

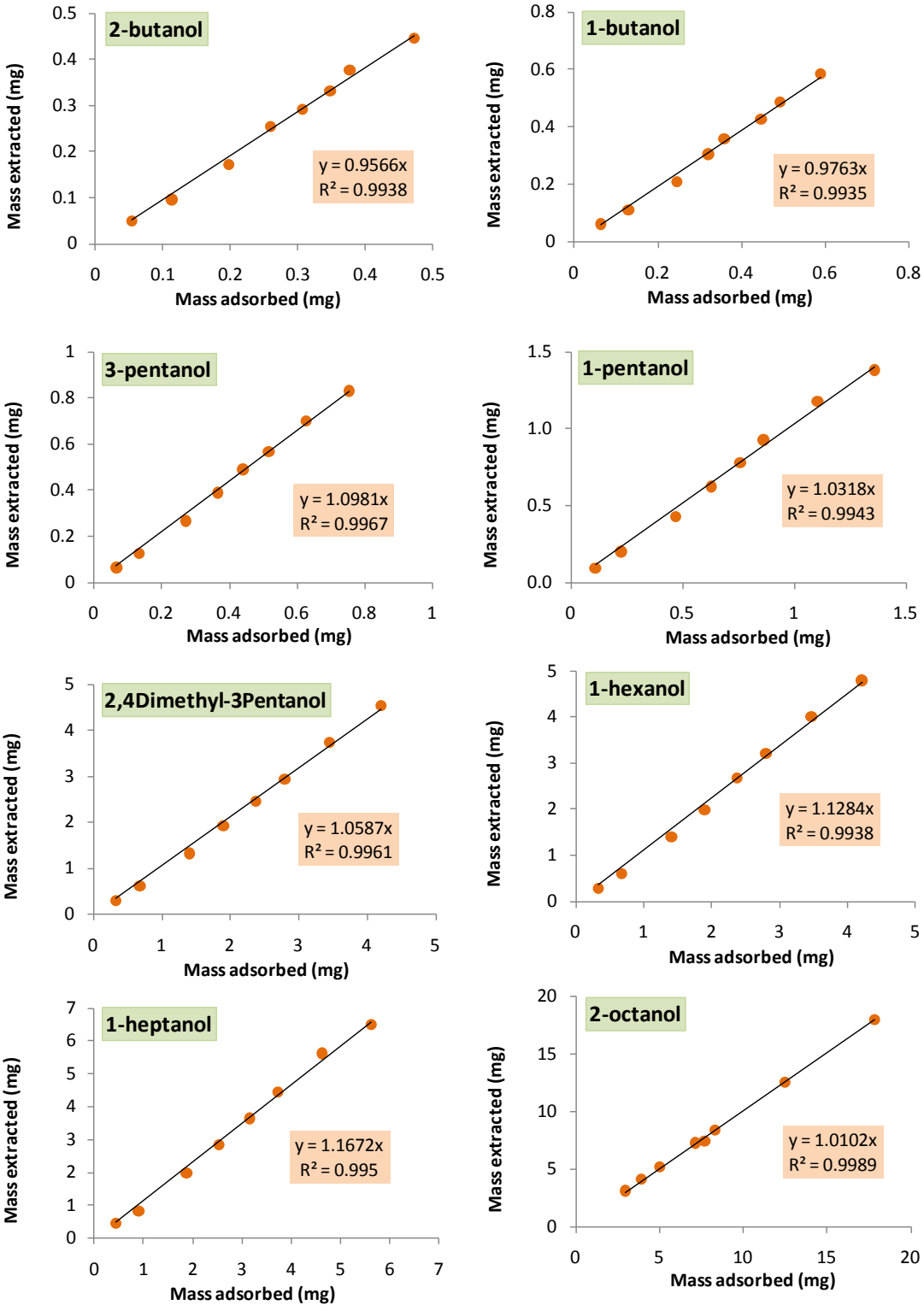

Figure 18. Tracer extraction isotherms using AC Felt 1300 and methylene chloride as extraction solvent.

5.3.2.3 COMPONENT TESTING: TRACER ELUTION FUNCTIONS on AC-FELT 1300

Flow-through column experiments were conducted with AC-Felt 1300 to characterize the elution behavior of resident tracers as a function of cumulative water flow. Elutions are shown Figures 17 and 18. Columns with 1.5 cm I.D. and 5 cm long were wet-packed with the eight tracers preloaded on AC-Felt 1300. The packed columns were then flushed with steady water flow at 0.5–2.5ml/min to effect tracer elution. After a specific period of water flow, the AC-Felt was removed from the column and carefully extracted as describe above to quantify the mass of all resident tracers remaining, m_r. Results from these elution tests are shown in Figure 17. The retardation factor *R* of each tracer for the AC-Felt 1300 was estimated from the slope of the linear portion of each tracer elution function (Hatfield et al. 2004). Those R values and resultant sorption coefficients for AC appear in Table 7. Figure 18 illustrates the linear portion of each elution function used to estimate a tracer retardation factor.

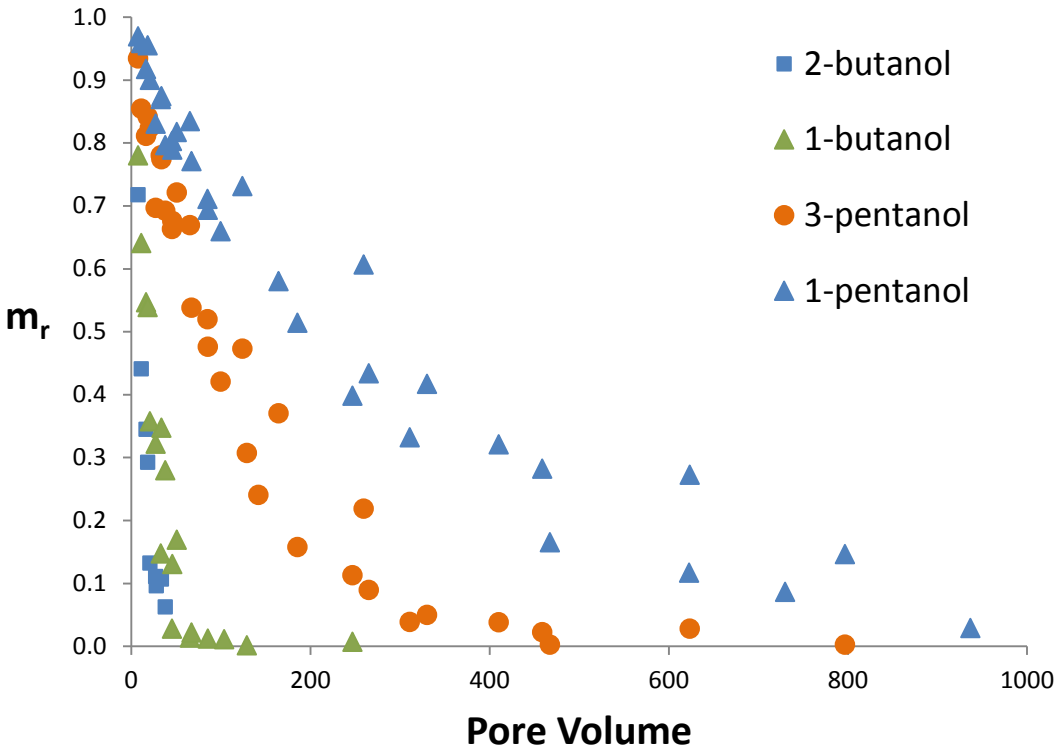

Figure 19. Resident tracer elution tests on AC-Felt 1300 showing relative tracer mass m_r remaining as function of cumulative pore volumes of water eluted.

Table 7. Tracer retardation factors R and sorption coefficients K_p to AC Felt 1300 estimated from tracer elution experiments.

	Tracers			
	2-butanol	1-butanol	3-pentanol	1-pentanol
R	24	37	175	433
K_p (cm^3/g) Carbon	282	503	2134	5300

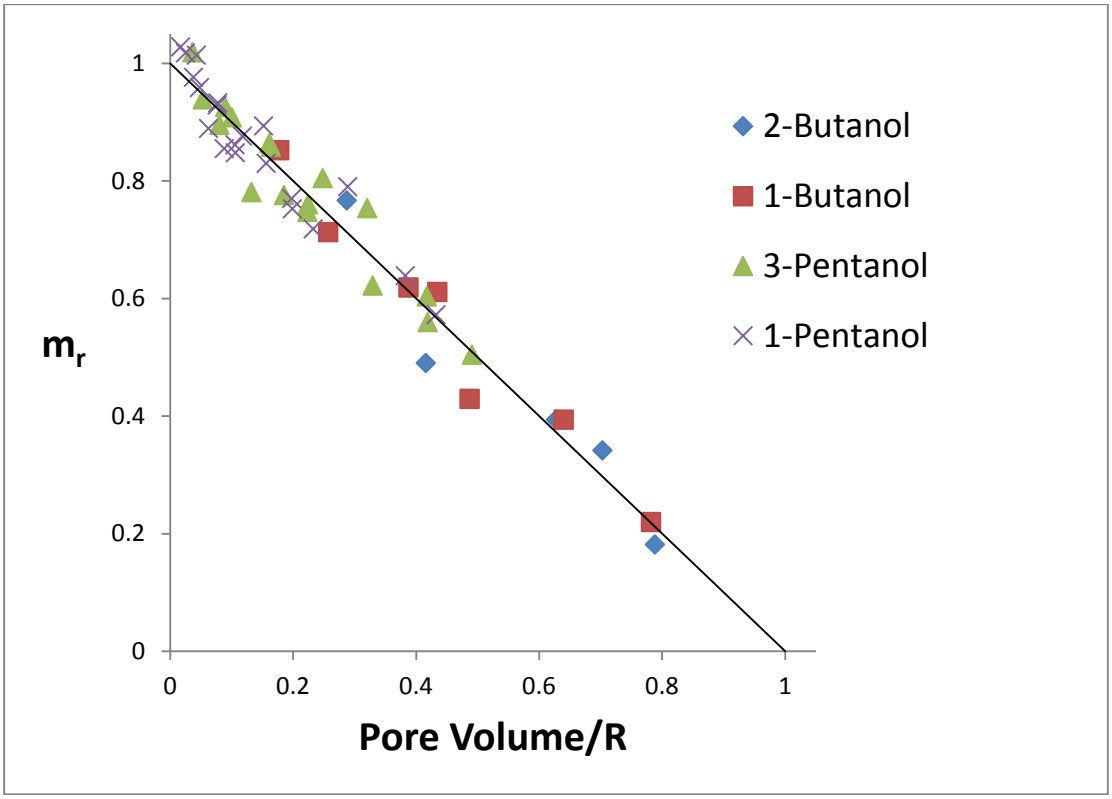

Figure 20. Data from the linear portion of each resident tracer elution curve for AC-Felt 1300 eluted with water. Where relative residual tracer mass m_r is plotted against cumulative pore volumes of water eluted normalized to the tracer retardation factor R (after Hatfield et al. 2004).

5.3.2.4 PROTOTYPE TESTING: FRACTURE FLOW SIMULATOR

Multiple fracture flow simulators were constructed for laboratory-scale testing of the FRPFM. The fracture simulators were constructed using clear PVC pipe with 4-inch (10.16 cm) inside diameter and ½ inch thick acrylic sheets. The simulators were constructed so that the PVC pipes are aligned with 4-inch diameter holes centered on each sheet. In order to maintain a flush fracture interface between sheets, the pipes do not pass completely through the acrylic sheets rather they are sealed into place in circular recessions that penetrate ½ of the sheet thickness (¼ inch). The bottom PVC pipe and acrylic sheet were anchored to a free standing base and there was an inlet port at the base of the PVC pipe to allow for the water level within the device to be adjusted as needed. The top acrylic sheet was fastened on top of the bottom sheet so that the PVC pipes were aligned and the sheets were separated using incompressible rubber spacers to maintain a uniform distance (fracture aperture) between the sheets. The completed system simulates a borehole intersecting a horizontal planar fracture. The outer perimeter of the fracture plane was sealed using a compressible rubber gasket. There was one inlet and one outlet port located on the bottom sheet of acrylic in order to establish flow along the longitudinal length (53 cm) of the plane. Both the inlet (up gradient) and effluent (down gradient) ports were connected to a channel etched into the inner face of the acrylic creating a specified head boundary at either end of the flow system. A Marriotte (aspirator) bottle was connected to the influent line and in order to maintain constant atmospheric pressure at the up gradient (influent) port. Flow through the system was controlled by adjusting the elevation of the effluent end of the down gradient tube relative to the Marriotte bottle, creating a change in head across the system and inducing flow proportional to the resulting hydraulic gradient. The Marriotte bottle was filled with source solution consisting of surrogate contaminant (2-octanol) in aqueous solution. The laboratory configuration is shown in Figure 19. Tests discussed in this report were performed using a horizontal fracture orientation with an aperture of 0.5 mm (500 μm) and planar dimensions of 26 cm by 53 cm. Testing in the fracture simulator was used to meet objectives of Section 5.3.1.

Fracture Dimensions:

- Horizontal orientation
- Aperture = 500 μm
- Width = 26 cm
- Length = 53 cm
- Conductivity ~0.7 cm/s

Borehole:

- Diameter 10.16 cm

Figure 21. Fracture Flow Simulator with FRPFM prototype deployed.

5.3.2.5 PROTOTYPE TESTING: AQUIFER BOX MODELS

A large scale aquifer box model was used for laboratory-scale testing of the FRPFM in full size 4-inch (10.16 cm) diameter wells installed in high contrast flow zones meant to simulate fractured media and karst systems (Figures 20 and 21). The aquifer box model was used to evaluate the performance of full-scale prototypes including all components of field deployment (deployment mechanisms, sorbents, visual tracers (dyes), and alcohol tracers) under controlled flow conditions. The system allowed for repetitive testing and validation of FRPFM performance along with the ability to compare FRPFM results with existing borehole technologies such as borehole dilution, and standard PFM (using granular activated carbon). Testing in the aquifer box was used to meet objectives of Section 5.3.1.

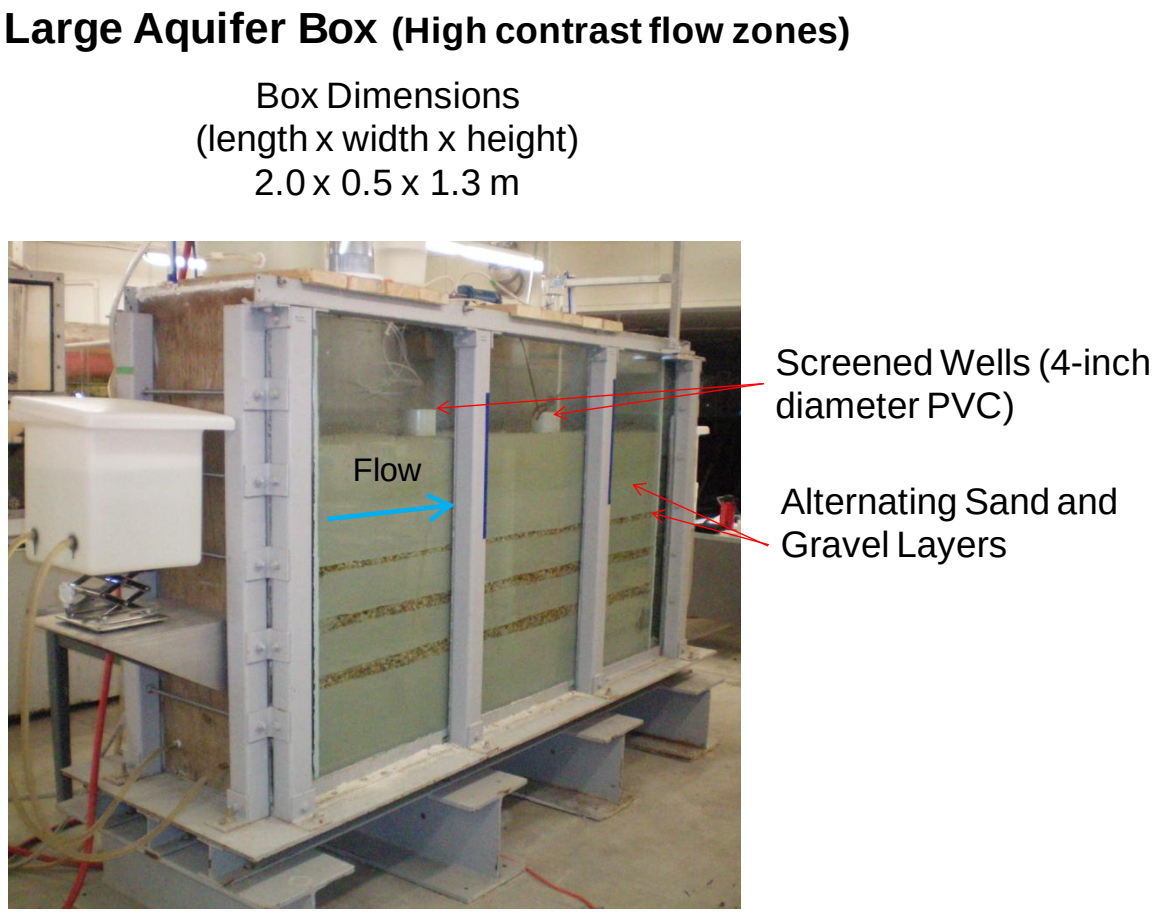

Figure 22. Aquifer box: screened-well high contrast flow simulator.

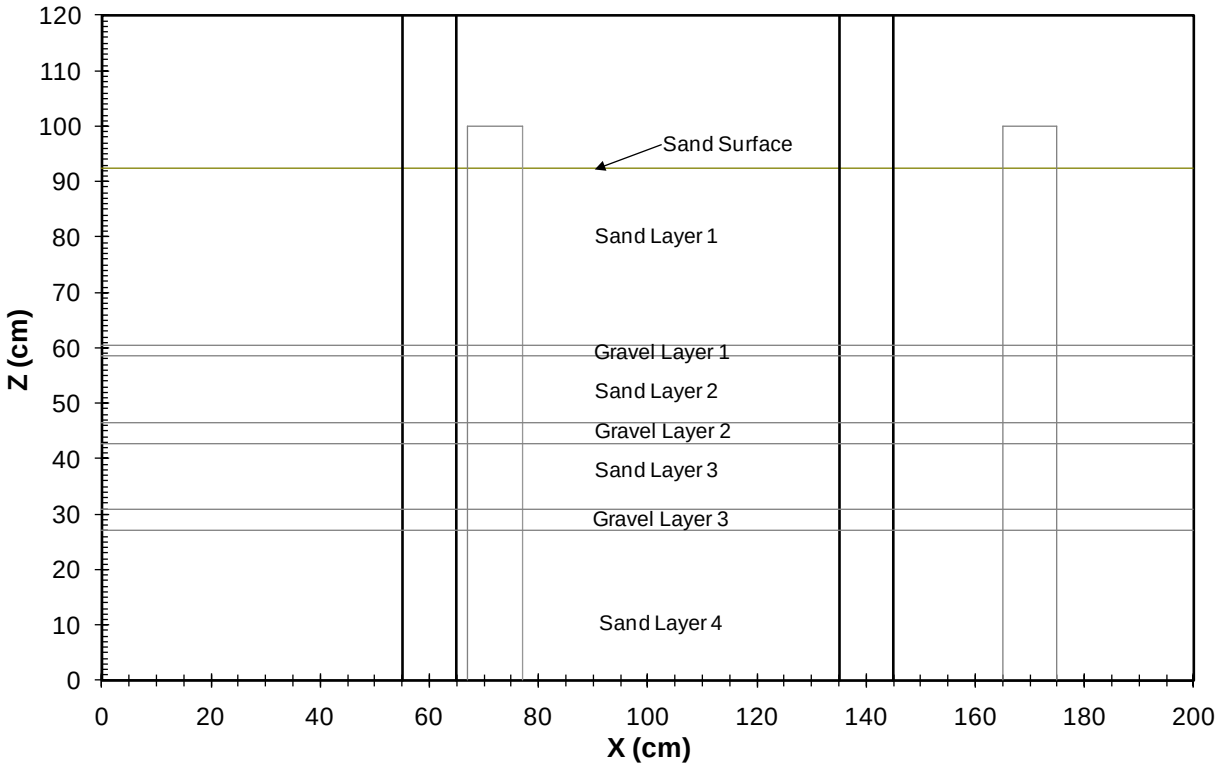

Figure 23. Aquifer box: screened-well high contrast flow simulator schematic showing dimensions of gravel and sand layers.

5.3.2.6 INSTALLATION AND DEPLOYMENT TESTING (MOCK BOREHOLE)

A full-scale mock borehole (4-inch diameter PVC casing – 36 feet deep) was constructed in the University of Florida Coastal Engineering Laboratory explicitly for the purpose of testing FRPFM prototype. The mock borehole was used to simulate field deployment conditions in order to assess field-scale installation issues in preparation for field demonstration. The apparatus allowed for convenient, repetitive testing of alternative FRPFM prototypes and various deployment strategies.

The borehole was constructed above ground using schedule 40 PVC pipe with a lower 5-foot section made of clear pipe. Access to the top of the borehole is provided by an existing three-story catwalk within the Coastal Engineering Laboratory. The clear PVC section is set at eye level on the main floor of the laboratory which allows for observation of device operation while submerged at realistic field depths and provides for close inspection of possible mechanical issues during deployment such as faulty packer inflation and fabric/sorbent tearing or gathering

which could not be readily observed, and subsequently corrected, in the field. This apparatus was used for objectives of section 5.3.1.

5.3.3 LABORATORY SAMPLING PROCEDURES

The objective of the laboratory experiments was to determine the optimal design and necessary deployment strategies for effective field-scale application of the technology. As such, one objective of the laboratory experiments was to determine the sampling plan that will result in sufficient data to validate the technology performance under real-world conditions and allow regulatory agencies and managers to evaluate the innovative technology. Laboratory test results were designed to assist with optimal sampling strategies that will take into account spatial and temporal variations in order to ensure a thorough evaluation. The following subsection outlines the sampling procedures for laboratory studies, which will be adapted for application at the field scale.

Sample Collection. Two types of samples were collected during this study, simulated groundwater samples (from aquifer box observation wells), and sorbent samples from FRPFM. Sampling methods and sample handling procedures are briefly described here and discussed in more detail in Appendices B-D.

Water samples were collected in EPA VOA vials with zero headspace. Samples were analyzed for target contaminants (such as TCE and DCE).

Sorbent samples were collected from the extracted FRPFM. Regular intervals of the FRPFM sorbent were segmented and transferred to 40-ml VOA vials containing an extraction fluid such as isobutanol or methylene chloride. Approximately 20 grams of sorbent were extracted with 20 ml of solvent.

Sample Analysis. All samples were analyzed at laboratories at the University of Florida. Volatile organics, including alcohol tracers, were analyzed by direct liquid injection on Gas Chromatographs. Details of analytical methods are provided in Appendix B-D. Detection limits are approximately 1 mg/L. Headspace analysis was used in the event that low concentrations were encountered. Detection limits for HS is approximately 50 ug/L

Experimental Controls. The fracture flow simulator and box aquifer experiments were designed to provide known contaminant fluxes for subsequent comparisons to flux meter measurements.

Data Quality Parameters. Data quality was maintained and checked throughout the project. Details on approaches for maintaining data quality are provided in the QA/QC plan in Appendix E.

Calibration Procedures, Quality Control Checks, and Corrective Action. Initial and continuing calibration procedures for analytical instrumentation, quality control checks, and corrective actions are required to maintain reproducible experiments. These procedures are fully described in the QA/QC plan in Appendix E.

Data Quality Indicators. Simple regression analysis was used to assess the quality of data collected at any single location. However, more sophisticated techniques of spatial analysis will be performed with data collected to assess the spatial mean and variance of contaminant and water fluxes evaluated over transects or within a plume.

5.3.4 LABORATORY RESULTS

The discussion of results is presented to correspond with the sequence of project objectives as listed in section 5.3.1 (Laboratory Plan) and the relevant experimental apparatus and procedures are detailed in section 5.3.2 (Laboratory Apparatus and Procedures).

5.3.4.1 COMPONENT TESTING AND SELECTION—PROTOTYPE DESIGN

Visual Tracer Results

Test results indicated that there were two dye/fabric systems that provided good visual indication of flowing fractures. For purely visual indication, the best combination of dye and fabric was turmeric on 94/6 cotton/spandex blend fabric. The dye was vibrant and visible to the naked eye on the fabric, and when the proper staining method was used a uniform distribution of color could be readily achieved. When exposed to flow, there was a noticeable change in color within the zone exposed to flow that was not observed in the zones that were unexposed. Although this system provided the most vibrant visual result, the permeability of the fabric was very low (with respect to the inner sorbent) which could reduce flow through the device.

For optimal performance regarding the detection of flowing fractures and the quantification of water and contaminant flux, the best dye/fabric system was turmeric on nylon/spandex blend. This was because the nylon/spandex blend had a much higher permeability than the 94/6 cotton/spandex fabric and the inner sorbent. Visual indication of flow was not nearly as vibrant as the cotton/spandex fabric, but it was sufficient for device application.

For both cases, color change was evident under both visible and UV light, but it was far more distinct when viewed under black light (UV spectrum). Multiple conditions affect dye performance including pH, temperature, and overall water chemistry.

Thus, for high resolution visual indication of flowing fractures, the choice was turmeric on 94/6 cotton spandex fabric. For visual detection of active fractures and the measurement of water and contaminant mass flux, the best option was turmeric on nylon/spandex blend fabric.

Prototype Design

Based upon results of component testing and the evaluation of various conceptual models for device deployment, the final prototype constructed using an inflatable core assembled with upper and lower end packers and designed smaller than the borehole diameter so that it could move freely up and down inside the borehole past potentially sharp edges of fractures intersecting a rock hole (critical for moving to field deployments). The core with two reactive fabric layers provides the mechanism for sealing the sorbent against the face of the borehole, while the end packers isolate the zone of interest from vertical gradients within the borehole. The core inflates separately from the two end packers.

The outer layer of the FRPFM core consisted of an elastic fabric (nylon/spandex blend) pre-treated with a water soluble visual dye which was used to provide a visual indication of flow through the device. To prepare the visual dyed fabric (5700 cm^2), 60 ml of Turmeric was simmered in two liters of water for 1-2hrs and then allowed to cool. The dissolved dye was then

transferred to a reservoir containing the fabric. The reservoir was slowly agitated for 12 hrs before the dyed fabric material was removed, drained, and used to construct the FRPFM.

The inner layer of sorbent material was Activated Carbon Felt 1300 (source information), that was 0.25 cm thick and had a respective porosity and dry bulk density of 0.92 and 0.075 g/cm3. 1-butanol, 2-butanol, 1-pentanol, 3-pentanol, 2,4-dimethyl-3-pentanol, 1-hexanol, 1-octanol, and 1-heptanol served as resident tracers pre-equilibrated on the AC felt. Pre-equilibration involved the use of acetone spiked the eight tracers. Two pieces of AC felt (each 30cm by 15.5 cm) were placed in a 2 liter glass jar with 1.7 liter of acetone tracer solution. The jar was slowly shaken over 48 hours to generate a uniform tracer distribution on the AC-felt. The acetone-wet felt was placed on a stainless screen rack in a laboratory exhaust hood for 1hour to promote acetone volatilization. After drying, the felt was used for FRPFM assembly.

The FRPFM assembly and installation involved the following steps: First, the inflatable core packer was wrapped with nylon mesh (Poly-Net™ Protective Netting, HDPE, Cole Parmer) to a thickness of 0.5 cm. The mesh had a porosity of 0.81 and was highly permeable. Its purpose was to facilitate flow through the thin visible dye layer and the AC felt sorbent of 0.25 cm thickness. Next, the two pieces of tracer preloaded AC felt were wetted with solute/tracer free water and carefully placed and wrapped over the mesh layer. Prior to assembly, an AC Felt sample (approximate 1 cm length and 15.5 cm width) was collected to quantify the initial concentrations of each resident tracer. The final assembly procedure was to emplace the Turmeric dyed sewn elastic fabric socks (nylon/spandex) blend, 30cm long and 22cm circumference) over the AC Felt layer. The porosity and felt carbon density of the combined felt+mesh layer were respectively 0.83 and 0.028 g/cm^3.

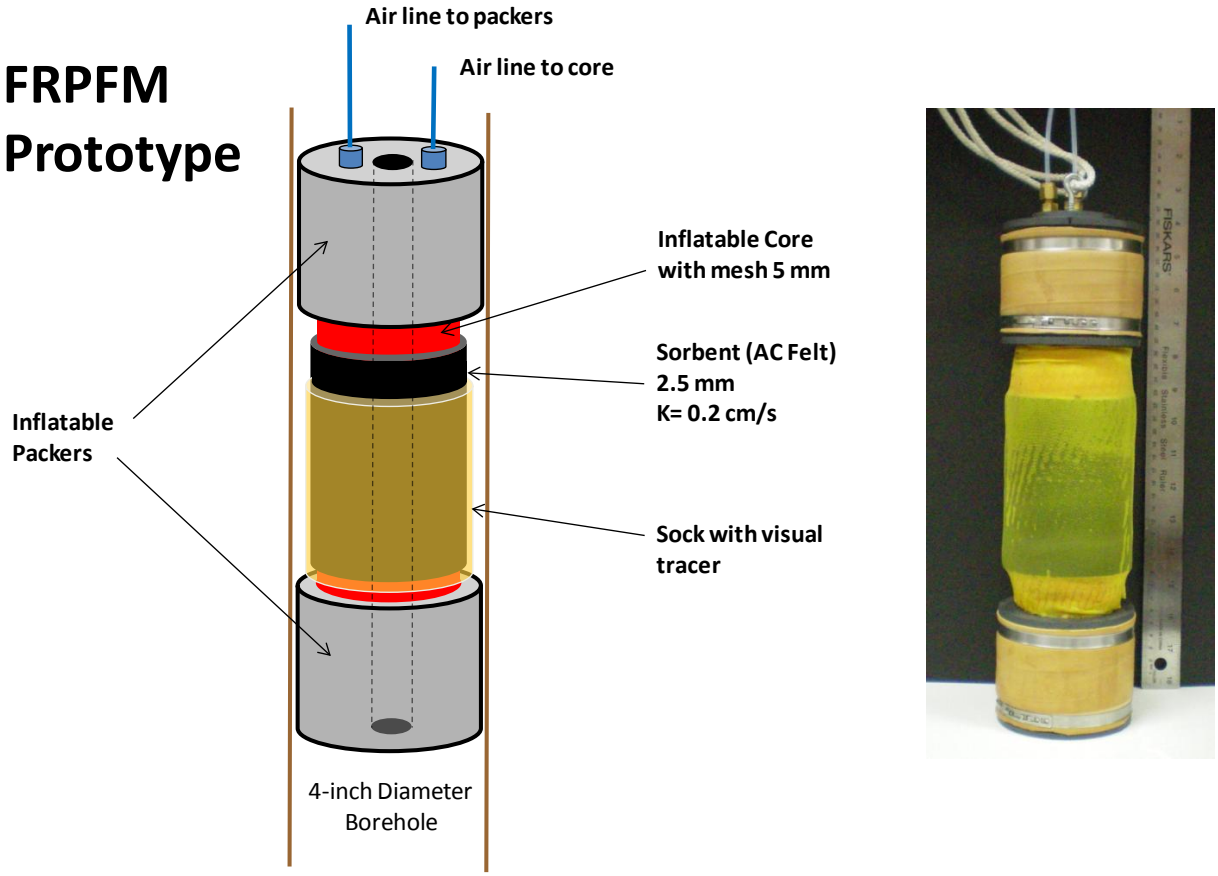

Figure 24. FRPFM Laboratory-Scale Prototype (Insert shows laboratory-scale prototype).

5.3.4.2 PROTOTYPE TESTING

Experiments in the Fracture Flow Simulator

The initial stage of lab-scale prototype testing was performed in the fracture flow simulator as outlined in section 5.3.2.4. In order to accurately evaluate FRPFM performance it was necessary to characterize flow conditions within the fracture simulator.

Hydraulics of the Fracture Flow Simulator: Hydraulic characterization of the simulator was conducted using three methods: 1) borehole dilution to compare flows in the fracture to flows in an open borehole intersecting the fracture; 2) a simple gradient experiment to measure fracture transmissivity under steady flow conditions; and 3) modeling to confirm the observed flow convergence under open borehole conditions and the observed fracture transmissivity under steady flow conditions.

Multiple borehole dilution tests were conducted under a range of controlled fracture flow conditions ranging from 3.2 to 15.8 m/d in a fracture of 0.05 cm aperture. The test involves packing off a section of borehole intersected by a fracture and measuring the fracture flow within the isolated section of borehole. The laboratory-scale borehole dilution apparatus is shown in figure 23. Fracture flow is interpreted from a change in the electrical conductivity of water in the borehole as water from the fracture displaces water originally in the borehole water. The test works if water from the fracture has a significantly different electrical conductivity than water originally in the borehole.

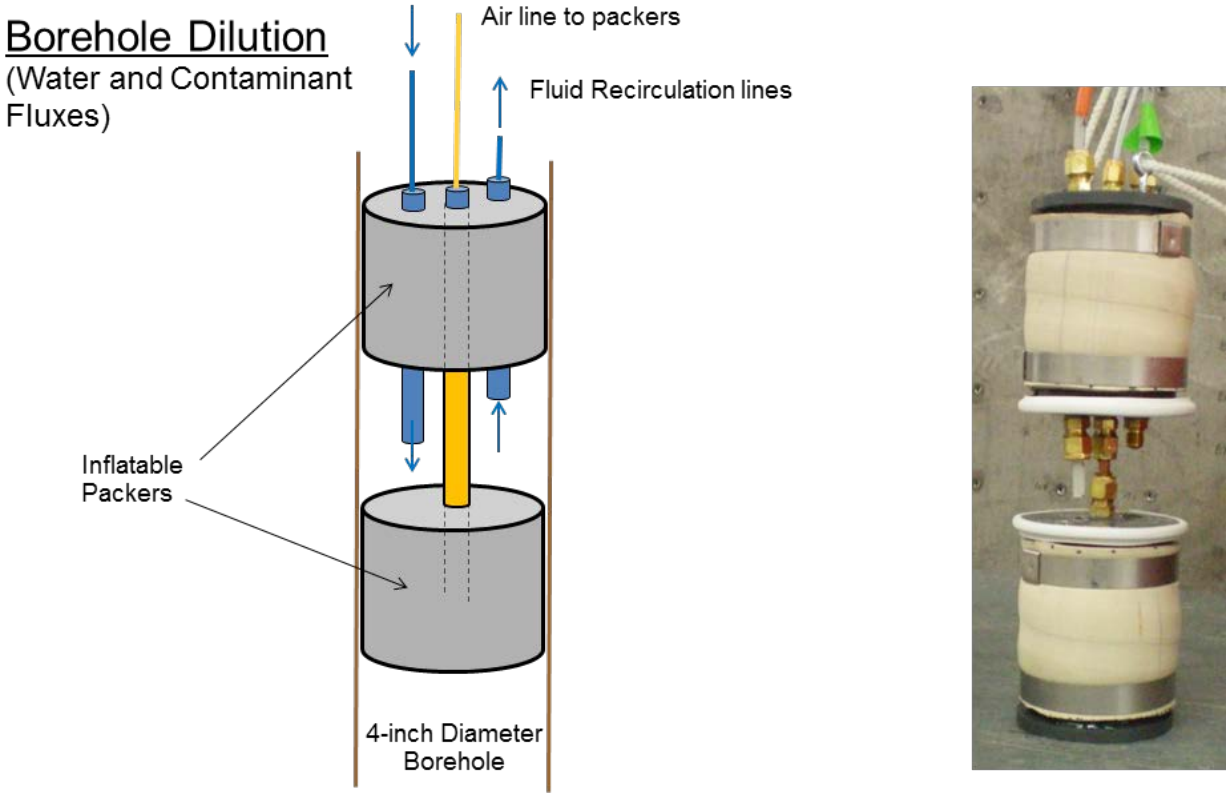

Figure 25. Schematic and image of laboratory-scale borehole dilution apparatus.

The Borehole dilution test is conducted under steady fracture flow conditions using a conductivity meter to measure transient changes in borehole water conductivity. The test begins with a pulse exchange of a salt solution with ambient borehole water to produce instantaneous increase in borehole salinity; because the storage volume of fractures is very small, a new technique was developed that introduces the salt solution with no net change in the volume of water originally in the borehole. This technique precludes the introduction of salt into the fracture which would complicate the interpretation of results. Below are typical results of observed conductivity changes with respect to time.

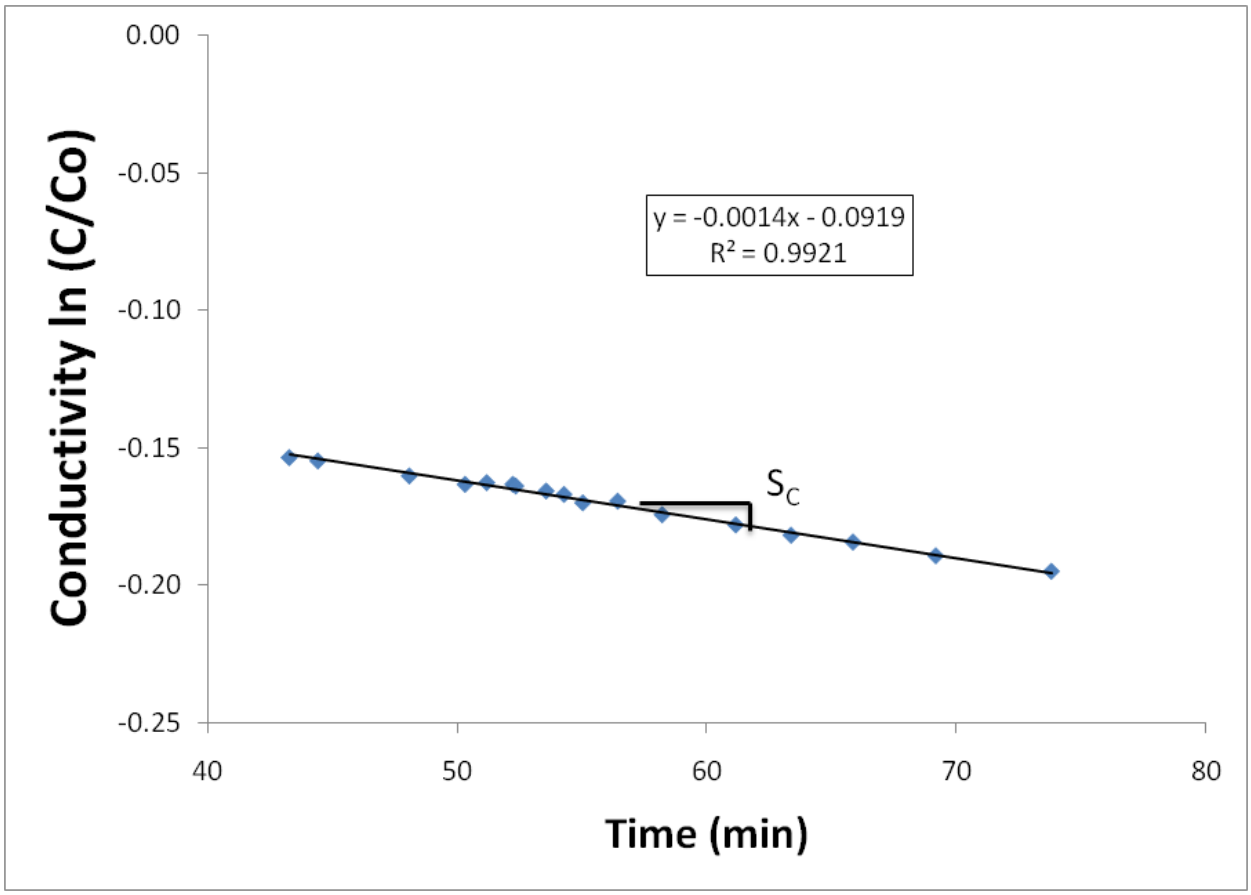

Figure 26. Dimensionless electrical conductivity of borehole water versus time for a borehole dilution test conducted in the Fracture Flow Simulator.

To interpret fracture flows from a borehole dilution test, the following relationships are required:

$$Ln\left(\frac{C}{C_O}\right) = S_C t \tag{23}$$

and

$$q_0 = \frac{S_C \forall_{BHD}}{\alpha 2r_0} \tag{24}$$

where C_O is the initial electrical conductivity of the borehole water at the initial time of monitoring; C is the electrical conductivity of borehole water at all subsequent times; S_C is the ratio of fracture flow into the borehole to the borehole dilution instrument mixing volume (including volume of water between packers, volume of tubing, etc.), [1/T]; t is time, [T]; q_0 is the flow per unit fracture length, [L^2/T]; $\forall_{BHD}$ is the mixing volume of the borehole dilution

instrument, [L^3]; α is a flow convergence factor or the ratio of flow measured by the borehole dilution test to ambient fracture flow, [-]; and r_0 is the borehole radius, [L]. The value of parameter S_C is obtained from the slope of the borehole dilution curve (See Figure 24).

In theory, $\alpha \to \alpha_\infty = 2$ when the lateral extend of the fracture flow field is large compared to the dimensions of the borehole. In our case, the borehole dilution tests produces values of α ranging from 1.72 - 1.76. This is illustrate in Figure 25, where fracture flows measured by borehole dilution are plotted against true flows and the best fit slope of that plot is 1.76. The apparent reduction in α is a consequence of the limited physical dimensions of the simulator. Figure 25 also suggests measured fracture water flux by borehole dilution can be quite accurate.

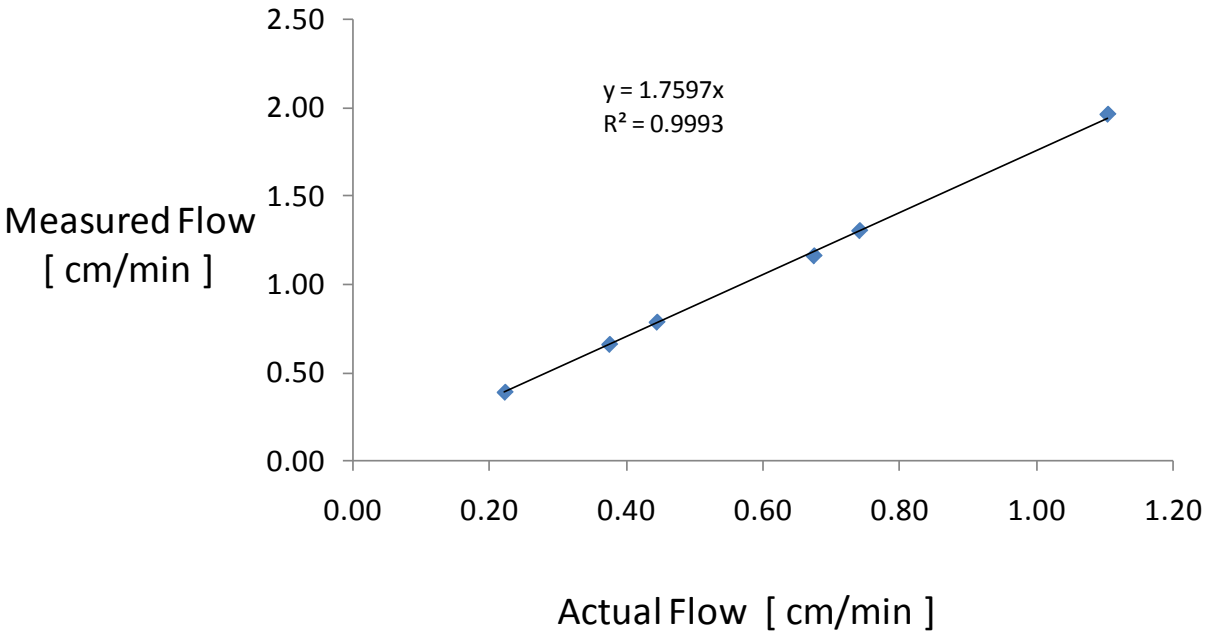

Figure 27. Measured fracture flows by borehole dilution versus actual fracture flows.

To further investigate the experimental artifact resulting from the finite dimension of the simulator, a series of numerical flow simulations were conducted using MODFLOW for a quarter of the fracture flow domain (53 cm in flow direction and 26 cm across) with a cell resolution of 130 x 265. The diameter of the borehole in the fracture simulation is 10.16 cm, and its Transmissivity T_1 for these simulations was varied through the following values: 0.01, 0.1, 0.2, 0.5, 1, 2, 5, 10, 100 and 1000. The fracture Transmissivity T_0 was maintained as 1. Simulated fractured flow streamlines are illustrated from a single simulation in Figure 26.

Simulation results in terms of α are represented by the black circles in the Figure 27. The maximum assumed value for T_1 = 1000 produces an α = 1.766, which is smaller than the

theoretical value of 2 from the convergence equation for an infinite flow domain ($\alpha_\infty = 2/(1+T_1/T_2)$). α_∞ is shown as the continuous line and the relative difference α_∞/α by the red circles, which reflect the fact that the nearby boundaries reduce both flow divergence around ($\alpha_\infty/\alpha < 1$ for $T_2/T_1 < 1$) and flow convergence towards ($\alpha_\infty/\alpha > 1$ for $T_2/T_1 > 1$) the well. Maximum differences are approximately 15 % and the similar shape of the relative error to the α_∞-graph itself suggests an approximation $\alpha \approx \alpha_\infty \alpha_c$, where $\alpha_c = A + B/(1+T_1/T_2)$. This is a vertically scaled and shifted version of α_∞. By imposing $\alpha = 1$ for $T_2/T_1 = 1$ and $\alpha = 1.766$ for $T_2/T_1 = \infty$ we get $A = 1.117$ and $B = -0.234$, with which we can write a corrected α-equation valid for the boundary conditions of the laboratory fracture simulator as

$$\alpha = \frac{2.234}{1+\frac{T_1}{T_2}} - \frac{0.468}{\left(1+\frac{T_1}{T_2}\right)^2} \qquad (25)$$

This is represented by the black stars and the relative approximation error by the red stars. In the case of a rock PFM installed we can calculate its effective T_2 (from felt/mesh transmissivity) and use this equation.

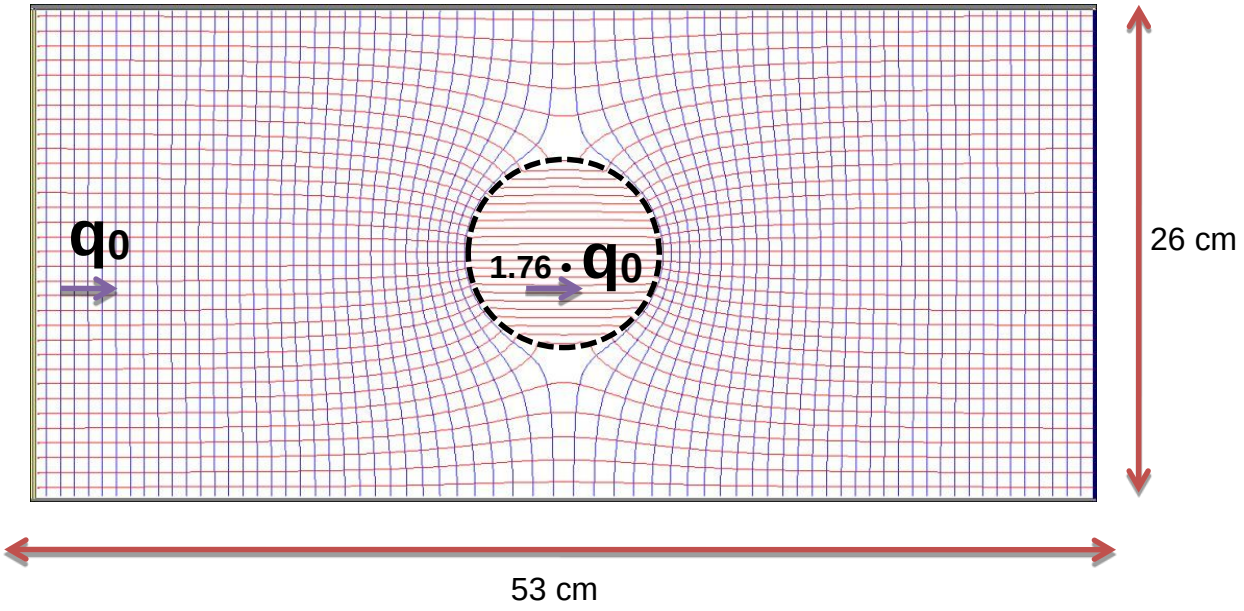

Figure 28. Simulated flow streamlines from the fracture flow simulator under open borehole conditions.

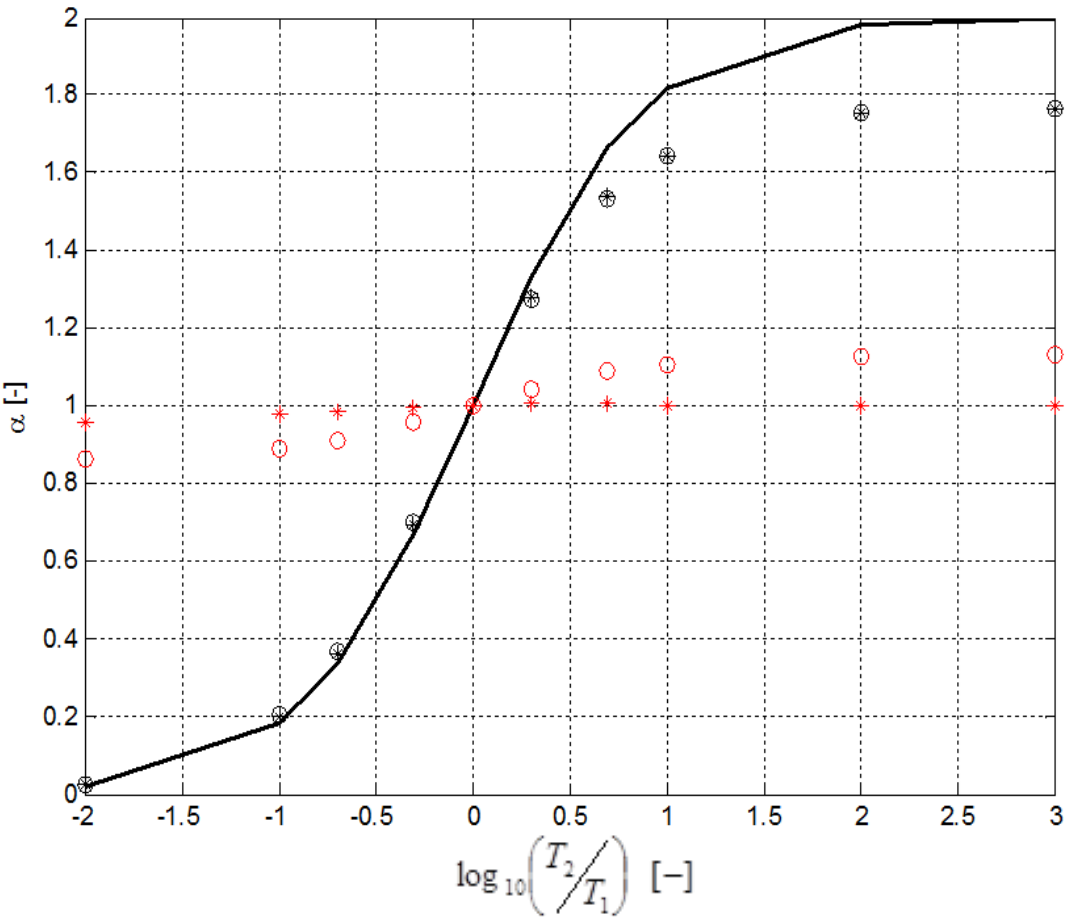

Figure 29. Results of numerical flow simulations showing variations in the flow convergence factor, α in the fracture simulator, as a function of fracture transmissivity.

Steady flow tests were also conducted to measure the transmissivity of the fracture in the laboratory fracture simulator. These tests were conducted with a packer inflated in the borehole to isolate the fracture from the borehole. For three different flow rates, the drop in energy head across the simulator was measured. From these flow experiments and Darcy's law, the estimated fracture transmissivity was 0.49 m^2/d; this estimate is low, because the inflated packer used to isolate the borehole from this fracture represented an obstacle to flow (for an open borehole it would be the opposite). To demonstrate this, numerical flow simulations were again conducted, using same physical dimensions as the laboratory fracture simulator. These simulations produced a ratio of 1.13 between fracture discharges for a uniform fracture (no hole) and a fracture with a packer. Hence, the estimated fracture hydraulic conductivity should be 13 % larger or 0.55 m^2/d.

FRPFM Measurements of Water and Contaminant Fluxes in the Fracture Simulator: Once flow within the fracture simulator was characterized using borehole dilution tests, the lab-scale FRPFM prototype was used to measure water and contaminant fluxes using experimental procedures outlined in section 4.2.4.

Equations for interpreting water and contaminant fluxes in fractures from FRPFMs:
To interpret fracture flows from alcohol resident tracers lost from the FRPFM's AC Felt, equation is (12) used:

$$q_0 = \frac{HnR_{tra} w\pi(1-m_r)}{\alpha t} \qquad (12)$$

where q_0 is the flow per unit length of fracture, [L^2/T]; t is the duration to FRPFM installation in the borehole, [T]; H is the thickness of the combined felt+mesh layer, [L]; n is the effective void volume of the combine felt-mesh layer 0.83, [-]; R_{tra} is the effective retardation factor for the resident tracer on the felt-mesh layer, [-]; w is the width of the sorptive felt sample in the direction of the long axis of the FRPFM, [L]; m_r is the relative mass of resident tracer remaining on the FRPFM felt after time *t*, [-]; and α the fracture flow convergence factor, which is normally estimated using Equation (1), but for the fracture flow simulator is calculated using Equation (25), [-]. The tracer alcohol tracer retardation factor is obtained from

$$R_{tra} = 1 + \frac{\rho_C K_P}{n} \qquad (26)$$

where K_P is the tracer partition coefficient for the activated-carbon-felt-water system listed in Table 8., [l/Kg]; and ρ_C is activated carbon density of the felt-mesh layer when the FRPFM is deployed 0.028 g/cm^3, [M/L^3].

To interpret fracture flows from visible tracers, Equations (5) and (8) are combined to give:

$$q_0 = \frac{HnR_{dye}\Delta Z}{\alpha t} \qquad (27)$$

where ΔZ is maximum thickness a trace visible on the turmeric dyed fabric layer which was produced by water flowing from the fracture and into FRPFM, and in the process eluting turmeric dye from the external nylon/spandex sock, [L]. R_{dye} is the retardation factor of the turmeric dye on the nylon/spandex blend, [-].

In addition to groundwater flow, it is of interest to know the contaminant flux in the fracture which is given from Equation (13):

$$J = \frac{M_C}{\alpha 2r_0 t} \qquad (13)$$

where J is the contaminant mass flux per unit fracture length, [M/L]; and M_C is the mass of contaminant intercepted from fracture and captured on the sorptive felt, [M]. Values of

parameter used in the above equations to describe FRPFM measurements in the laboratory appear in Table 7 and Table 8.

Table 8. Model Parameters Used to Interpret FRPFM Measurements in the Fracture Simulator.

Parameter	Value
n	0.83
α	0.28
r_0	5.08 cm
T_1	0.55 m^2/d
T_2	0.082 m^2/d
w	0.5 cm
H	0.66 cm
R_{dye}	330

Table 9. Alcohol Tracer Partition Coefficients K_P and Retardation Factors R_{tra}.

	Alcohol Tracers			
	2-butanol	1-butanol	3-pentanol	1-pentanol
K_P [cm^3/g]	282	503	2134	5300
R_{tra}	11	16	74	182

Results—Visual Tracer Performance: Turmeric was used as a visible tracer to provide indications active fracture location, orientation and flow direction. Figure 28 below presents photographs of active fracture traces captured as discolorations on the external nylon/spandex blend sock of the FRPFM. The discoloration appears on the up-gradient side of the FRPFM indicating the direction of flow. In addition, the location and orientation of discoloration corresponds to the location and the orientation of the active fracture. In Figure 29 a comparison is show between water flux estimated using the visual tracer elution pattern on nylon/spandex blend sock and Equation (29).

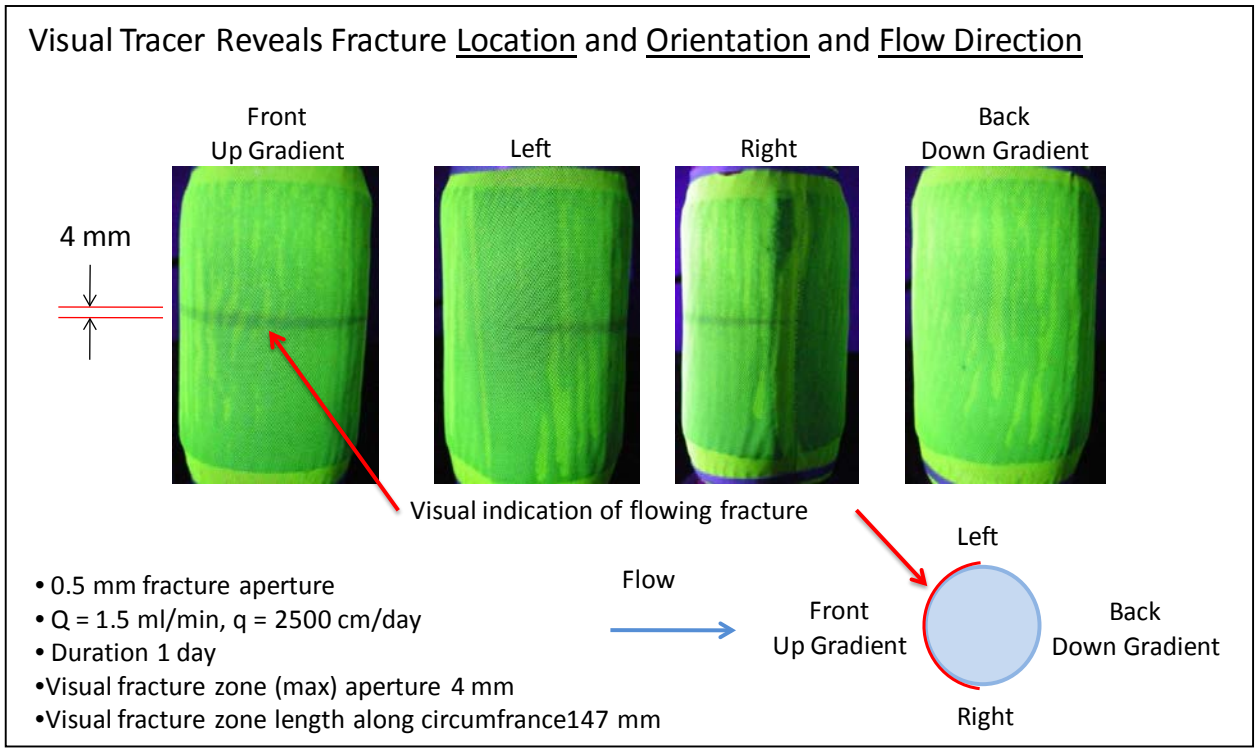

Figure 30. FRPFM performance: Visual tracer results on the external FRPFM sock.

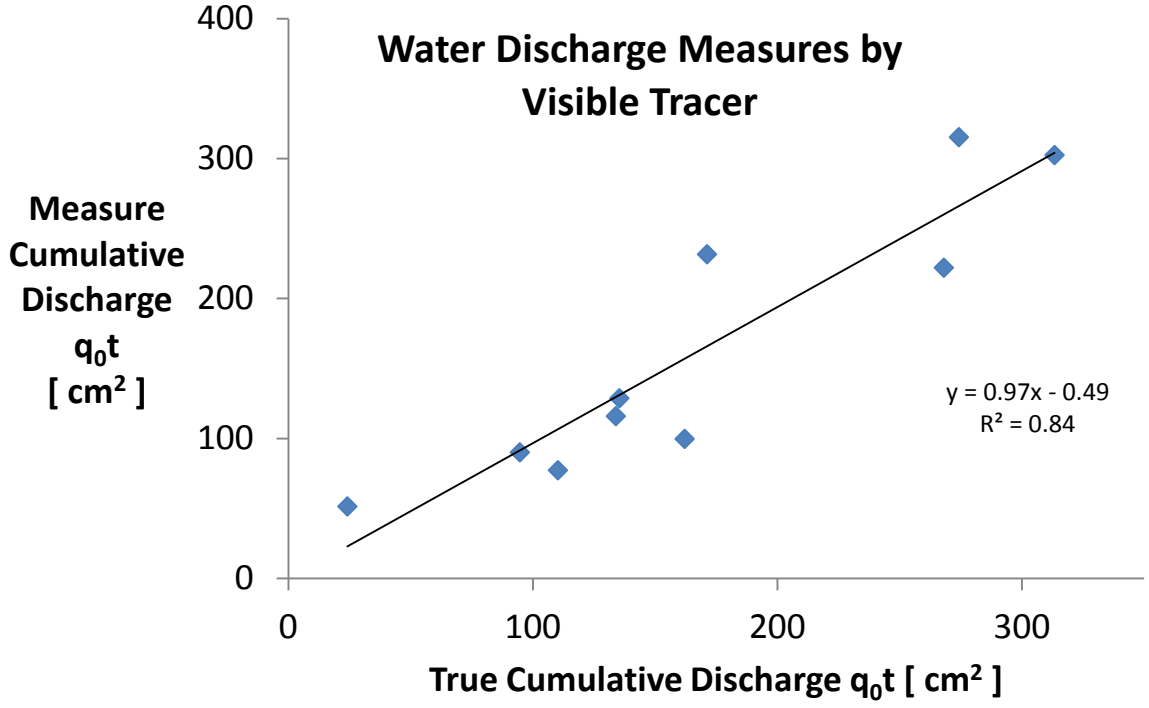

Figure 31. Measured cumulative water fluxes by FRPFM visible tracers versus controlled cumulative discharge in fracture simulator.

Results—FRPFM Measures of Water and Contaminant Fluxes: FRPFM test results are illustrated in Figures 30 and 31 for respective measurements of cumulative water and contaminant fluxes in the fracture simulator. The average relative error on measured contaminant fluxes was -2 ± 16%. And for water fluxes, the average relative measurement error was 2 ± 25%. The convergence factor α giving the minimum biased estimate of both water and contaminant fluxes was 0.28. Based upon this estimate of α and the above estimate of 0.55 m^2/d for the fracture transmissivity, T_1; the felt-mesh transmissivity, T_2 was estimated to be 0.82 m^2/d. This value for T_2 is used for FRPFM field applications.

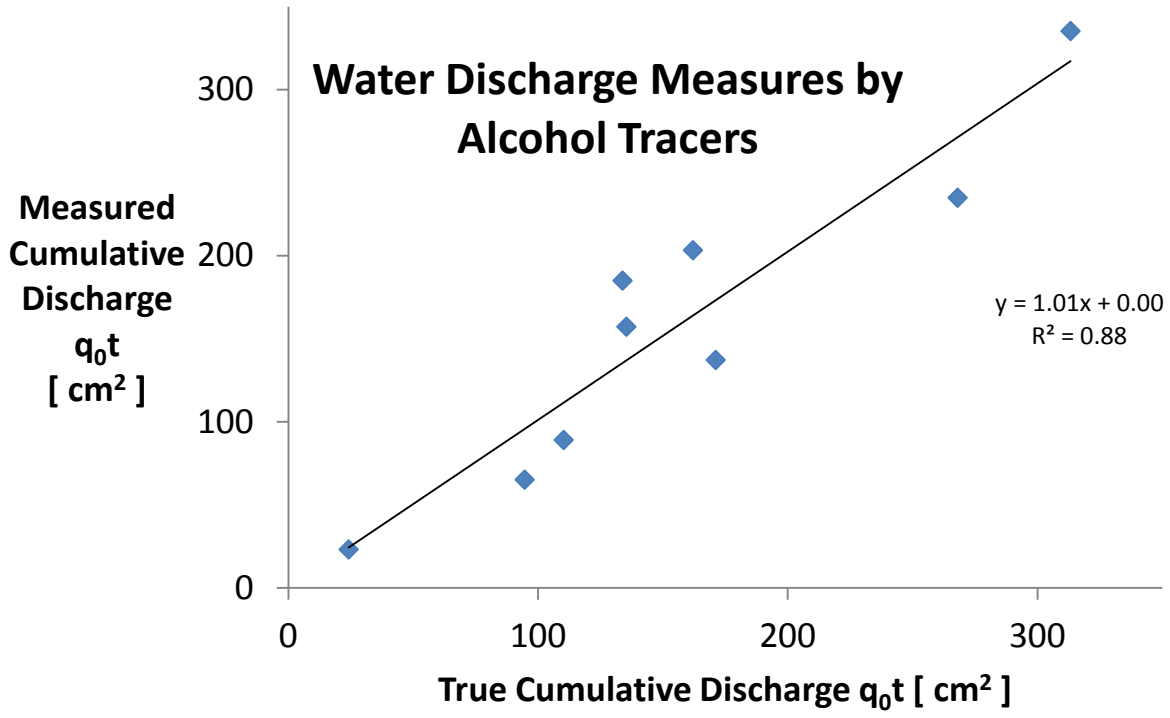

Figure 32. Measured cumulative water discharge by FRPFM alcohol tracers versus controlled cumulative discharge in the fracture simulator.

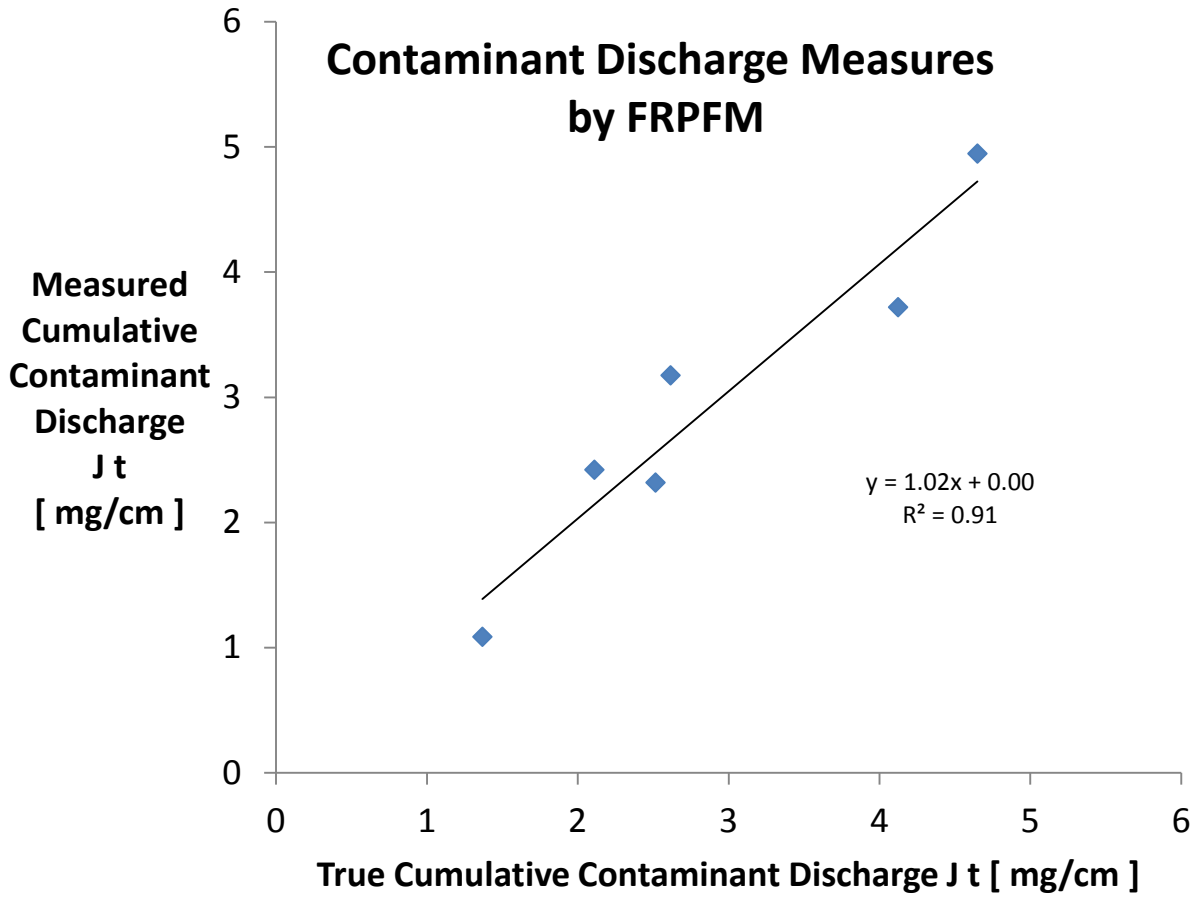

Figure 33. Measured cumulative contaminant discharge by FRPFM versus controlled cumulative contaminant discharge in the fracture simulator.

Experiments in the screened-well high-contrast flow simulator

The new FRPFM is designed to function in screened-wells as well as in rock wells. This section of the report presents theory for application of the FRPFM in screened-wells and includes laboratory test results from experiments performed in a pilot-scale screened-well flow simulator configured to simulate high contrast flow zones as outlined in section 4.2.5.

Hydraulics of the Screened-well Flow Simulator: Hydraulic characterization of all components of the simulator was conducted to facilitate the interpretation FRPFM results. The components of interest include the hydraulic conductivity of the sand and gravel flow layers as well as well screen permeability. Three methods of characterization were used: 1) simple falling-head permeameter tests to measure the hydraulic conductivities of gravel and sand materials; 2) porous media flow modeling coupled with multiple borehole dilution tests; and 3) down-hole testing using hydrophysical logging. For the latter two methods, a flow rate of 2,954 cm^3/min was maintained in the simulator under a hydraulic gradient of 0.0182.

Under the first hydraulic characterization method, simple falling-head permeameter experiments were conducted to measure the hydraulic conductivities of gravel and sand materials under steady flow conditions. The relevant equation is:

$$Ln\left(\frac{h}{h_O}\right) = \frac{-K}{L_m}t \qquad (28)$$

where h_0 the initial head, [L]; h is the hydraulic head at time t, [L]; L_m is the thickness of the porous medium tested, [L]; K is the hydraulic conductivity, [L/T]; and t is time, [T]. The thickness of samples tested was $L_m = 30\,cm$. Figure 32 is a plot of test results for gravel. Measured hydraulic conductivities for gravel and sand were 3376 m/d and 30 m/d respectively. Using these measured conductivities, the width of simulator (50 cm), the measured thicknesses of sand and gravel layers (77.75 cm of sand and 9.35 of cm gravel), and the above stated gradient, the total discharge though the simulator was calculated and found to be 27% less than the measured discharge. This finding was not unexpected. The falling-head permeameter tends to generate measures that are somewhat more representative of vertical hydraulic conductivity which are typically lower than the horizontal conductivity that governs flow through the simulator.

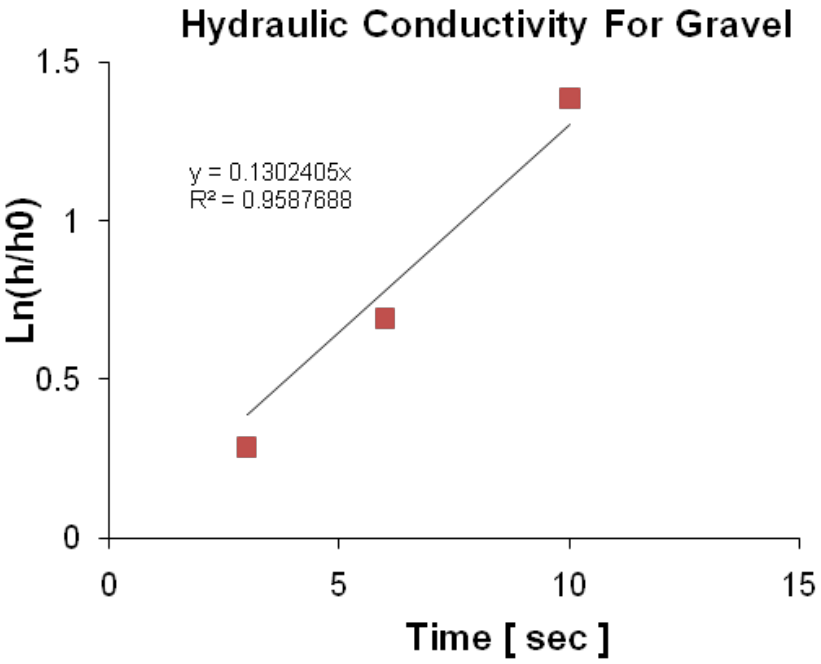

Figure 34. Results from a falling head permeameter test conducted on gravel used in the simulator.

Hydraulic characterization of the flow simulator under the second approach requires a coupled Darcy-Borehole Dilution and Model (CBDM). This hybrid model generates estimates the effective flow convergence in the screened-well (α_w) of the simulator from which sand and gravel hydraulic conductivities can be estimated that are consistent with observed flows from multiple borehole dilution tests conducted over isolated intervals of the well.
A Borehole dilution test is typically conducted over an isolated depth interval and under steady flow conditions using a conductivity meter to measure transient changes in well-screen water electrical conductivity. The test begins with a pulse exchange of a salt solution with ambient well water to produce instantaneous increase in well water salinity. Because the storage volume within the isolated section of the well-screen is very small, a new technique was developed that introduces the salt solution with no net change in the volume of water originally in the well screen. This technique precludes the introduction of salt into the model aquifer which would complicate the interpretation of results. Flow is interpreted from a change in the measured electrical conductivity of water in the isolated section of screened well. The change occurs as water from the granular porous media displaces saline water in the well. The test works if water from the model-aquifer (or true aquifer) has a significantly different electrical conductivity than water originally in the well screen.

Multiple borehole dilution tests were conducted in the simulator, under a constant hydraulic gradient of 0.01823 which produced a steady depth-average specific discharge of 9.8 m/d. Each borehole dilution test involved packing off a section of well-screen intersecting layers of gravel or sand and measuring flow within the isolated section of the well-screen. Presented below (Figure 33) are typical results gathered from the gravel zone which show observed conductivity changes with respect to time.

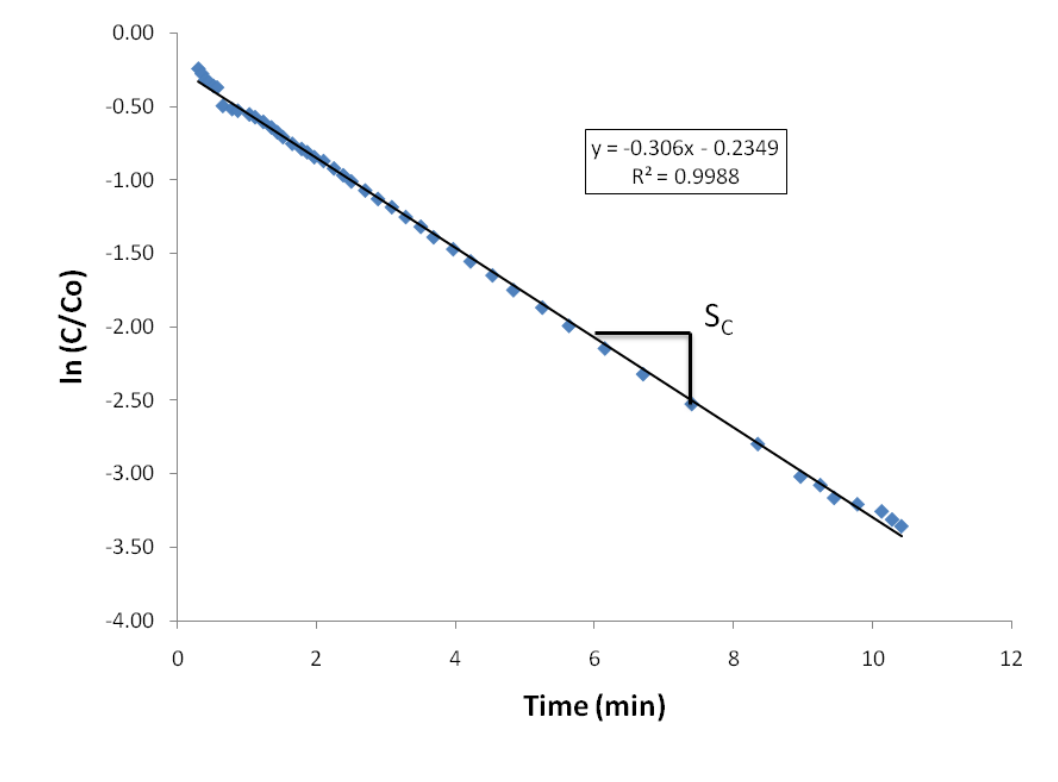

Figure 35. Dimensionless electrical conductivity of well-screen water versus time for a borehole dilution test conducted in the gravel zone of Well-screen Flow Simulator.

To interpret groundwater flows from a borehole dilution test conducted over an isolated section of well-screen, the following relationships are required:

$$Ln\left(\frac{C}{C_O}\right) = S_C t \tag{29}$$

and

$$q_{SW} = \frac{S_C \forall_{BHD}}{D_{WS} L_w} \tag{30}$$

and

$$q = K\varphi = \frac{q_{SW}}{\alpha} \tag{31}$$

where C_O is the initial electrical conductivity of the borehole water at the initial time of monitoring; C is the electrical conductivity of borehole water at all subsequent times; S_C is the ratio of ambient groundwater flow into the borehole to the mixing volume of the borehole dilution instrument (including volume of water between packers, volume of tubing, etc.), [1/T]; q_{SW} is the specific discharge through a cross section of well screen, [L/T]; $\forall_{BHD}$ is the mixing volume of the borehole dilution instrument, [L^3] or 597.5 cm^3; D_{WS} is the inside well screen diameter, [L] or 10.16 cm; L_w length of isolated section of well screen where flows are being measured, [L] 6 cm; α is a flow convergence factor or the ratio of flow measured by the borehole dilution test to the ambient aquifer specific discharge, [-]; K is the hydraulic conductivity of the porous media, [L/T]; φ is the hydraulic gradient in the simulator or 0.0182; and q is the ambient aquifer specific discharge, [L/T]. The value of parameter S_C is obtained from the slope of the borehole dilution curve (See above Figure 33).

In an open screened well with no filter pack, the appropriate equation for determining α_w is the following (Hatfield et al. 2004):

$$\alpha_w = \frac{4}{\left(1+\frac{k_0}{k_S}\right)+\left(1-\frac{k_0}{k_S}\right)\cdot\left(\frac{r_I}{r_O}\right)^2} \tag{32}$$

where k_S is the well screen hydraulic conductivity, [L/T]; k_O is the aquifer conductivity, [L/T]; r_O is the outside radius of the well screen, [L]; and r_I is the inside radius of the well screen, [L]. In an open screened well; however, the screen permeability tends to be less than the contiguous aquifer media such that it constrains flow. Klammler et al. (2007) suggest the screen hydraulic conductivity can be estimated from: $k_S \cong \Gamma f_0 k_0$, where $\Gamma = 2$; and f_0 is the fraction screen open area, [-]. Thus, the above equation can then be simplified to:

$$\alpha_w = \frac{8 f_0}{(2 f_0 + 1)+(2 f_0 - 1)\cdot\left(\frac{r_I}{r_O}\right)^2} \tag{33}$$

For the well-screen used in the simulator, f_0 equals 0.0457. Using the above equation, the convergence factor α_w was estimated to be 0.98.

Using an independent approach, the effective convergence factor α_e can be estimated for the simulator using data on simulator components and borehole dilution test data. For this approach, the CBDM is used:

$$\alpha_e = \frac{\forall_{BHD} W_S}{Q D_{WS} L_w}\left(b_g S_{C\_g} + b_s S_{C\_s}\right) \qquad (34)$$

in which Q is the total flow through the simulator, [L^3/T]: 2954 cm^3/min; W_S is the width of the simulator, [L]: 50 cm; b_g is the total thickness of all gravel layers, [L]: 9.35 cm; b_s is the total thickness of all sand layers, [L]: 77.75 cm; S_{C_g} is the average slope of the borehole dilution electrical conductivity elution curves generated from gravel layers, [1/T]: 0.341 min^{-1} ; and S_{C_s} is the average slope of the borehole dilution electrical conductivity elution curves generated from sand layers, [1/T]: 0.009 min^{-1} . From the CBDM, the effective α_e was 0.95, which corresponds to a screen open area of 4.3%. Under ideal condition $\alpha_e = \alpha_w$ their close correspondence hear appears to support the theory presented in Klammler et al. (2007).

Assuming α_e is the best estimate of the actual converge the convergence factor for an open well, α_w, it was then feasible to use the above equations to estimate the *in situ* conductivities of sand and gravel layers at those location where borehole dilution tests were conducted. For gravel layers 2 and 3 the corresponding estimated conductivities were 4006 m/d and 4789 m/d. Borehole dilution tests from sand layers 3 and 4 produced respective conductivity estimates of 98 m/d and 40 m/d. Average conductivities of all measurements were 4398 m/d for gravel and 69.5 m/d for sand. Using these averages, measured thickness of sand and gravel layers, and the above stated gradient, it can be shown the calculated discharge must match the measured discharge through the simulator.

Down-hole hydrophysical logging was used as method to independently identify the location/transition of high contrast flow zones. RAS Inc., performed hydrophysical logging (HPL) within the aquifer box wells using the same flow conditions for which borehole dilution and FRPFM tests were performed. HPL provided accurate estimates of the location of high contrast flow zones which compared well with FRPFM suggesting HPL could be useful for identifying zones of interest for FRPFM deployment.

FRPFM Measurements of Water and Contaminant Fluxes in the Screened-well Flow Simulator

Equations for interpreting water and contaminant fluxes in screened wells from FRPFMs:
To interpret groundwater flows from resident tracers lost from the FRPFM deployed in a screened well, the following equation is used:

$$q_{0S} = \frac{1.67\, n\, R_{tra} r_1 \left(1 - m_r\right)}{\alpha\, t} \qquad (36)$$

where. q_0 is the specific discharge, [L/T]; and all parameters have been previously define.

In addition to groundwater flow, it is of interest to know the contaminant flux in the aquifer J, [M/L^2/T]. This is calculated from the mass of contaminant captured by the FRPFM sorbent:

$$J_S = \frac{1.67 M_C}{\alpha\, 2 r_1 w t} \qquad (37)$$

from which all parameters have been previously define.

The flow convergence factor α is given from an equation presented by Klammler et al. (2007.

$$\alpha = \frac{4}{\left(1+\frac{k_0}{k_S}\right)\cdot\left(1+\frac{k_S}{k_1}\right)+\left(\frac{r_1}{r_S}\right)^2\cdot\left(1-\frac{k_0}{k_S}\right)\cdot\left(1-\frac{k_S}{k_1}\right)-\left(\frac{r_2}{r_1}\right)^2\cdot\left(1+\frac{k_0}{k_S}\right)\cdot\left(1-\frac{k_S}{k_1}\right)-\left(\frac{r_2}{r_S}\right)\left(1-\frac{k_0}{k_S}\right)\cdot\left(1+\frac{k_s}{k_1}\right)} \qquad (38)$$

where k_S is the well screen hydraulic conductivity which varies as described above if the contiguous media is sand or gravel, [L/T]; k_0 is the aquifer hydraulic conductivity (sand or gravel), [L/T]; k_1, the effective hydraulic conductivity of the felt-mesh, [L/T]; r_S, the outside radius of the well screen, [L]; r_1, the inside radius of the screened well, [L]; and r_2 is the inside radius of the felt-mesh layer. The value of α must be known to assess the ambient groundwater flux q_{0S}. In general, prior estimates of hydraulic conductivity parameters k_0 and k_1 are needed. Values of parameter used in the above equations to describe FRPFM measurements in the laboratory appear in Table 9 and Table 10.

Table 10. Model Parameters Used to Interpret FRPFM Measurements in high contrast flow zones.

Parameter	Mean Value
α_{gravel}	0.025
α_{sand}	0.465
r_S	5.72
r_1	5.08 cm
r_2	4.42 cm
L_W	6.0 cm
w	1.0 cm
$k_{0\ gravel}$	4398 m/d
$k_{0\ sand}$	69.5 m/d
k_{fm}	12.4 m/d.
k_S Sand layer	6.0 m/d
k_S Gravel layer	402 m/d
$\forall_{BHD}$	597.5 cm^3

Results:

FRPFM test results are illustrated in the Figures 34 and 35 for respective measurements of water fluxes in gravel and sand layers. In addition, these figures indicate (with an arrow) fluxes measured by borehole dilution (BHD). Mean fluxes and measurement standard deviations are given for both the FRPFM and borehole dilution in Table 11. Relative differences in measurements given by both technologies for different sand and gravel layers are listed in Table 12. In general, relative differences in water flux measurements given by the two technologies ranged from -7% to 38% but average 7%. The standard deviation on those relative differences were also of the same order. Results suggests the two technologies produce comparable water flux measurements in the laboratory.

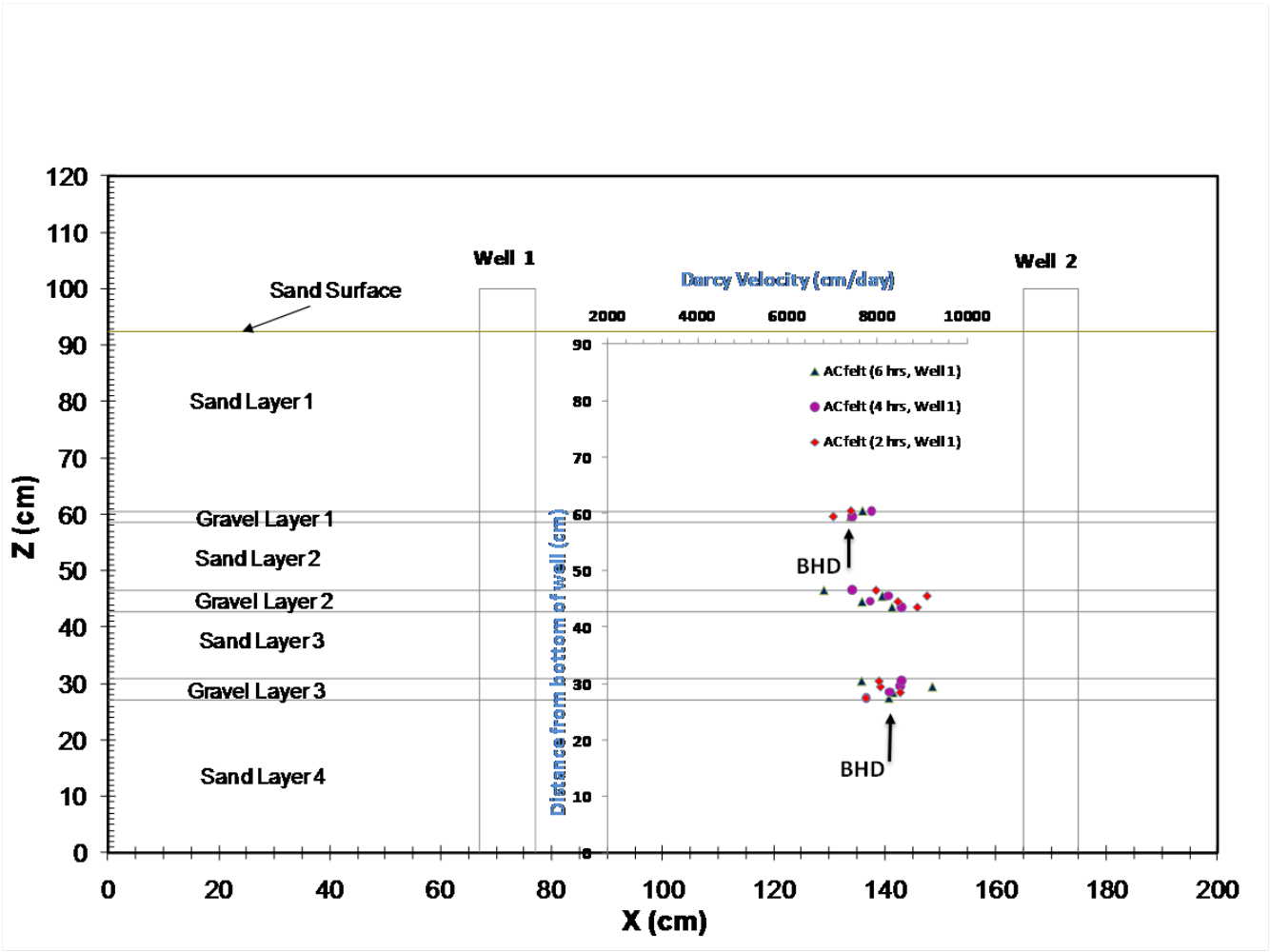

Figure 36. FRPFM and borehole dilution measures for water flux in gravel layers. Symbols indicate FRPFM measured water fluxes in gravel zones of the laboratory screened-well flow simulator. The horizontal displacement of the black arrows indicates the magnitude of the measured water flux by BHD in gravel layers 1 and 3.

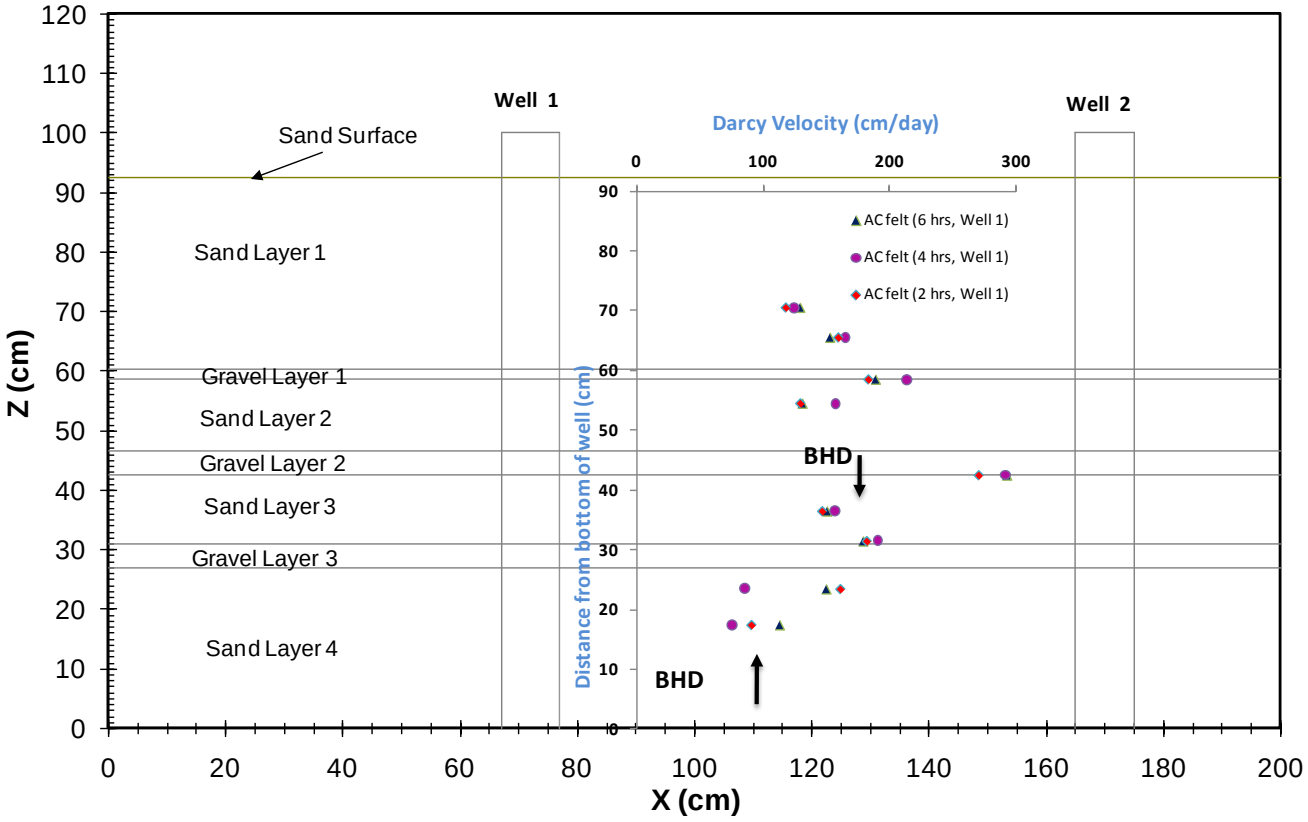

Figure 37. FRPFM and borehole dilution measures for water flux in sand layers. Symbols indicate FRPFM measured water fluxes in sand zones of the laboratory screened-well flow simulator. The horizontal displacement of the black arrows indicates the magnitude of the measured water flux by BHD in sand layers 3 and 4.

Table 11. Comparison of Water Flux Measurement by Two Competing Technologies.

Layer	FRPFM		Borehole Dilution	
	Mean Flux [cm/d]	Standard deviation [cm/d]	Mean Flux [cm/d]	Standard deviation [cm/d]
Gravel Layer 1	7469	287	7302	165
Gravel Layer 3	8243	440	8731	226
Sand Layer 3	167	18	178	-
Sand Layer 4	113	36	73	-

Table 12. Relative Measurement Differences between FRPFM and Borehole Dilution.

Layer	Mean Measurement Difference %	Standard Deviation of Measurement Difference %
Gravel Layer 1	2.2	3.9
Gravel Layer 3	-7.0	4.0
Sand Layer 3	-6.8	11.0
Sand Layer 4	38.4	29.3

5.3.4.3 FULL-SCALE INSTALLATION AND DEPLOYMENT TESTING

The final series of laboratory tests included full-scale experiments to evaluate alternative deployment strategies as outlined in section 4.2.6. As part of this process one objective was to develop a protective shield for the FRPFM. The shield was designed to serve two purposes: 1) to keep FRPFM components from getting caught on exposed rock and possibly lodged down hole and 2) to minimize the loss of resident tracers during insertion and retrieval. The shield was constructed using a 6-foot length of thin-walled stainless steel pipe with a dedicated shield-packer attached to the top of the stainless steel pipe.

The deployment procedure consists of inserting the FRPFM into the base of the shield and inflating the FRPFM packers to hold the device securely in place within the shield. The shielded device is then inserted into a well and lowered to the desired depth. Once at depth, the shield-packer is inflated to hold the shield in place and the FRPFM packers are deflated allowing gravity to draw the FRPFM down out of the sheath. Once in place the FRPFM core and packers are inflated and the device is deployed—flux measurement is initiated. To retrieve the FRPFM, the core and packers are deflated, the device is drawn back up into the protective shield, and the FRPFM packers are re-inflated to secure the device. The entire assembly is then retrieved from the well. Once at land surface, the FRPFM packers are deflated to release the device from the shield for sampling as outlined in section 4.3.

5.4 DESIGN AND LAYOUT OF TECHNOLOGY COMPONENTS

Field demonstration of the FRPFM required three major sets of equipment, the FRPFM, a custom designed device built for conducting modified borehole dilution (BHD) tests over an isolated interrogation interval that matches the 1-meter FRPFM interrogation interval, and high resolution temperature profiling (HRTP) equipment with temperature vector probe (TVP).

5.4.1. FRPFM

The FRPFM interrogates an isolated 1-meter section of the rock hole with the intent of providing high resolution evaluation of the location and orientation of active flowing fractures, water and contaminant fluxes in those fractures, and the direction of fracture flow. Figures 36 and 37 provide a schematic and images of the FRPFM as tested in the field. Major instrument components include three inflatable packers, a common air line to the terminal packer, and another airline to the central packer. In addition, there is an expandable plastic mesh material that covers the inflatable central core (a long small diameter packer), the core mesh is wrapped with an activated carbon felt sorbent equilibrated with non-toxic alcohols tracers. Finally, there is an external cotton sock with visible tracers extruded onto the central core.

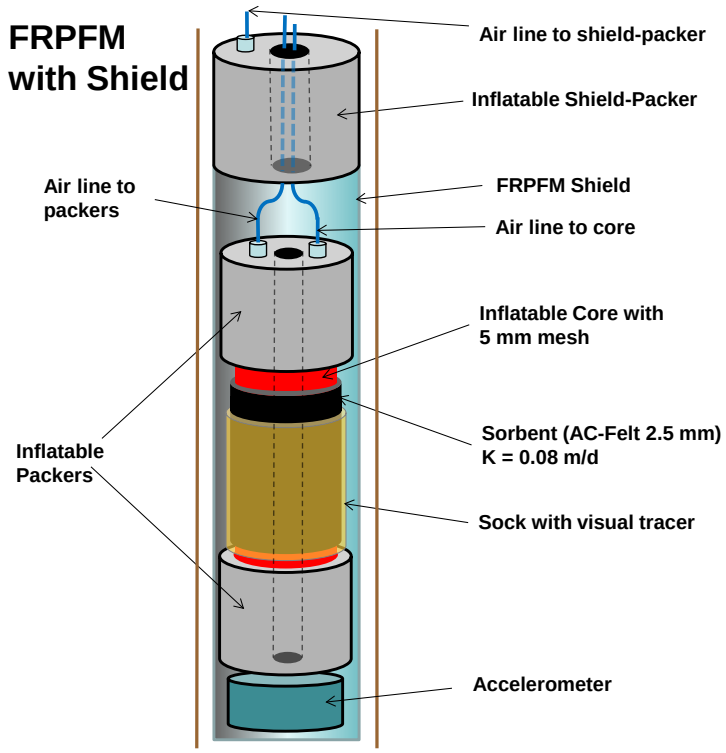

Figure 38. Schematic of FRPFM.

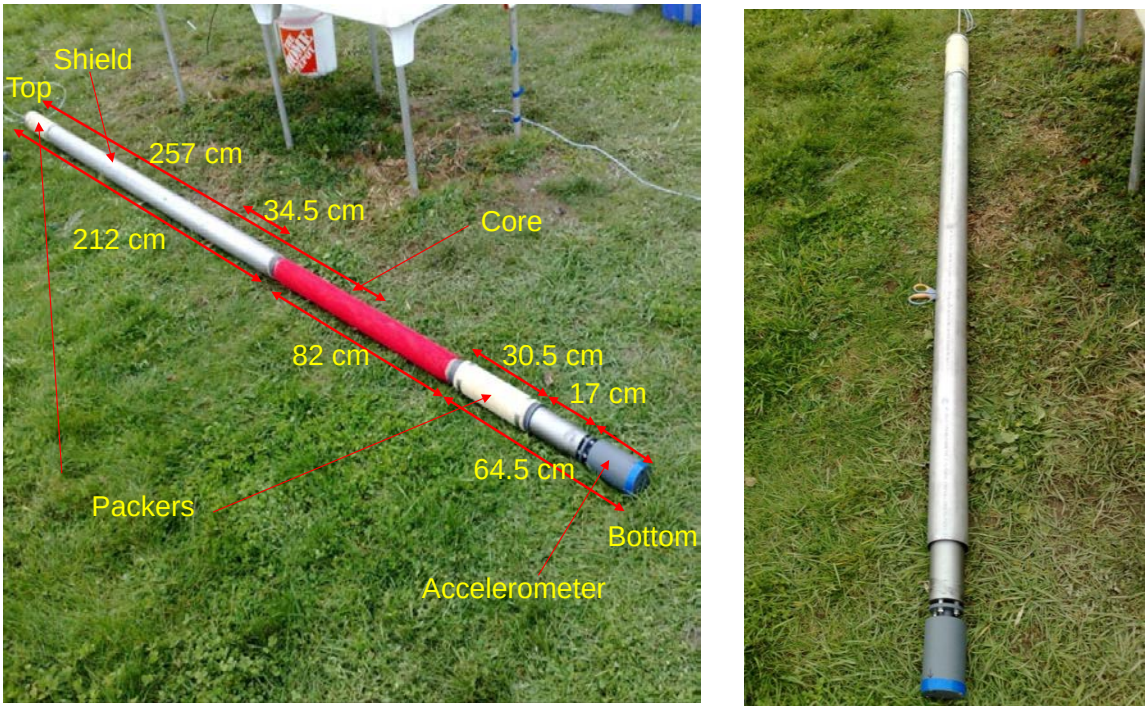

Figure 39. FRPFM for 4-inch diameter well with dimensions shown. Image a) shows the FRPFM with core extended out of the shield. Image B) shows the FRPFM in deployment and retrieval mode (withdrawn into the shield).

5.4.2. BOREHOLE DILUTION TESTS

Borehole dilution tests were used to measure water fluxes over isolated sections of the rock hole (Guitierrez et al. 1977; Xu et al. 1997; and Novakowski et al. 2006). During borehole dilution tests, water samples were collected over the isolated section of rock hole and analyzed for target contaminants. The contaminant concentrations were used to calculate contaminant flux. Figure 38 shows the field-scale borehole dilution apparatus that was designed and custom built for comparative testing with the FRPFM. Major instrument components "in the well" include two inflatable packers, an air line to the packers, a submersible pump and fluid recirculation lines. Above, ground there is a recirculation manifold, a source of compressed nitrogen (or air) for inflating packers, an in-line electrical conductivity meter, a mixing chamber and sampling port.

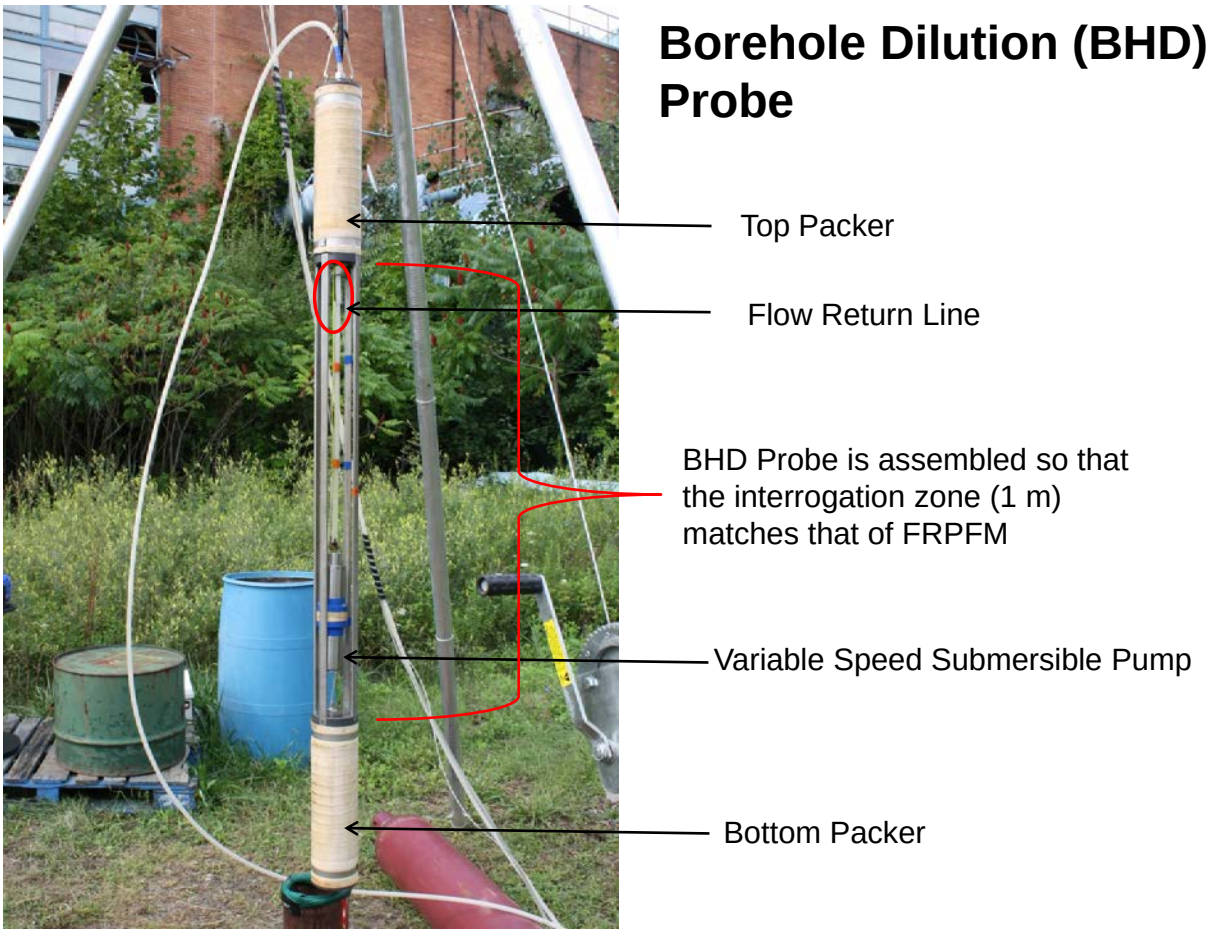

Figure 40. Field-scale borehole dilution apparatus for fractured rock boreholes.

5.3.3. HIGH RESOLUTION TEMPERATURE PROFILES

Recent developments have led to revitalization of the use of temperature logging for characterizing flow through fractured rock. The sealing of boreholes using water-filled, flexible impermeable liners prevents vertical cross connection between fractures intersecting the hole and establishes a static water column with a temperature stratification that mimics that in the surrounding formation (Pehme et al, 2014). Measurement of the temperature profile of the lined-hole, water column provides a tool for identifying fractures with active flow under ambient groundwater conditions (without cross connecting flow along the borehole). Detection of flow in fractures is improved with the use of a heater to create thermal disequilibrium in the active line source (ALS) technique and eliminate normal depth limitations in the process.

HRTP methods (Pehme et al, 2010) provide indication of actively flowing fractures while TVP (Pehme et al, 2014) provides indication of flow direction. An image of the TVP probe along with a schematic of the thermistor distribution are provided in figure 41. The results from HRTP and TVP measurements were used for comparison to FRPFM measures for the location (depth) of active flowing fractures and the inferred direction of groundwater flow.

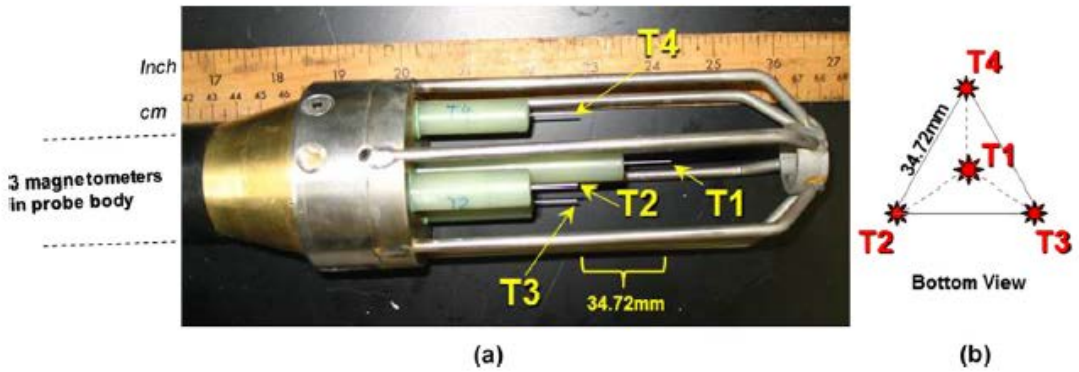

Figure 41. (a) Image of temperature vector probe (TVP) with 4 thermistors and (b) schematic showing distribution of thermistors as viewed from below (Adapted from Pehme et al, 2014).

5.5 FIELD TESTING

Over the duration of the project 22 FRPFM deployments and 35 modified borehole dilution tests were performed at two sites: the Guelph Tool Site (GTS) in Ontario, Canada and the former Naval Air Warfare Center (NAWC) in West Trenton, New Jersey both of which had previously existing networks of well characterized fractured frock wells. The field demonstration tests were performed in a sequential fashion, progressively testing individual components of the FRPFM technology while incrementally incorporating newer components and evaluating field deployment challenges in order to determine optimal deployment mechanisms and strategies. Gantt charts showing the schedule of field activities performed at GTS and NAWC are provided in Tables 13 and 14 respectively.

In parallel with laboratory testing and development, during 2008 and 2009, collaborators at the University of Guelph performed directional flow surveys at the Guelph Tool site and provided high resolution temperature profiles for all potential wells. Then the initial 4 FRPFM field deployments were performed with the primary intent of evaluating the challenges of field-scale deployment. These early tests only incorporated the visual tracer component of the FRPFM technology suite. These early field tests experienced limited success with visual tracers on a cotton visual indication sock. Visual indication of potential fractures were observed and confirmed with acoustic and optical televiewer (ATV and OTV). More importantly, these tests provided invaluable information with regard to deployment mechanisms that were directly implemented in the design of the next stage of FRPFM field prototypes tested in 2010.

All field tests with quantifiable results are summarized in the matrix of results (table 15) which provides a general outline of all data collected by FRPFM and comparative technologies. As mentioned above, the initial four field deployments were used to evaluate field-scale deployment challenges and are not included in table 15. There were also two tests performed to completion (Tests E and M) that are not listed in the table. These tests did not provide quantifiable results due to vandalism and damaged equipment. As such, there are 16 tests listed in the table that

provide comparison between FRPFM and three comparative technologies—acoustic and optical televiewer (ATV/OTV), high resolution temperature profiles with temperature vector probe (HRTP/TVP), and borehole dilution tests (BHD).

During 2010 five FRPFM field deployments were performed at the Guelph Tool site. The target zones for FRPFM interrogation were determined based upon pre-existing geophysics data (ATV/OTV) and closed-hole HRTP/TVP profiles used to indicate the presence of flow within the borehole. The first FRPFM test of 2010 incorporated two components of the FRPFM technology suite: 1) internal alcohol tracers on a new sorbent media (activated carbon felt) that was selected specifically for fracture rock applications based upon extensive laboratory testing and 2) improved visual tracer sock now composed of a nylon-spandex blend (again specifically selected for fracture rock applications based upon extensive laboratory testing). The internal tracers provide a direct measure of volumetric water flux (specific discharge) through the FRPFM, while the visual tracer provides indication of the presence, spatial distribution, and orientation of flowing fractures along with the direction of groundwater flow and an independent measure of water flux. Subsequent field tests during 2010 incrementally added new components to each subsequent FRPFM field prototype. Tests were performed incorporating a stainless steel shield used to encapsulate the FRPFM during downward deployment and upward retrieval within the borehole. The shield serves two purposes: 1) it physically protects the integrity of the visual tracer sock and underlying activated carbon felt by preventing contact with fracture rock face of borehole and 2) it precludes internal tracer loss due to vertical flow of water through the device during deployment and retrieval. The final phase of testing during 2010 incorporated an accelerometer on the base of the FRPFM assembly in order to record the orientation of the device with regard to magnetic north during deployment. This allows for evaluation of the direction of flow within the FRPFM interrogation zone. With the inclusion of the accelerometer, the complete suite of FRPFM technologies had been assembled and tested at the field scale.

During 2011 three FRPFM field deployments were performed along with three modified borehole dilution tests at Guelph Tool site. The intent for this phase of testing was to evaluate the FRPFM capabilities for quantifying contaminant flux, and to validate the FRPFM values for water flux and contaminant flux with independent measures obtained using modified borehole dilution tests.

During 2012 field demonstration efforts were expanded to include tests running in parallel at both the Guelph Tool site and the NAWC site in New Jersey. A total of 5 FRPFM deployments were performed, along with one FRPFM push-pull test and 16 borehole dilution tests.

The final phase of field testing was performed during 2013 at the NAWC site. A total of 5 FRPFM deployments were performed along with 16 modified borehole dilution tests.

The outcome of the combined results from all of the field tests is to demonstrate that the FRPFM provides direct, high-resolution, simultaneous measure of 6 data types with regard to actively flowing fractures. The data type correspond to the quantitative performance objectives outlined in Table 1: 1) detection of flowing fractures, 2) fracture location (depth), 3) fracture orientation, 4) fracture flow direction, 5) groundwater flux (specific discharge), and 6) contaminant mass flux.

Table 13. Scheduled activities for FRPFM demonstration at the Guelph Tool Site

Field Testing: Guelph Tool Site					
Activity	Year 2008-2012				
	2008	2009	2010	2011	2012
Startup	x				
Directional Flow Survey (HRTP/TVP)	x	x			
FRPFM deployment, extraction, and sampling	x	x	x	x	x
Borehole Dilution Testing			x	x	x
Demobilization					x

Table 14. Scheduled activities for FRPFM demonstration at the NAWC site

Field Testing: NAWC		
Activity	Year 2012-2013	
	2012	2013
Startup—mobilization	x	
Directional Flow Survey (HRTP/TVP)	x	
FRPFM deployment, extraction, and sampling	x	x
Borehole Dilution Testing	x	x
Demobilization		x

Table 15. Matrix of test results—provides general summary of data collected by FRPFM and comparative technology for all field tests.

		Comparative Technology							FRPFM						
	Test	ATV/OTV		HRTP		BHD			Visual Tracer				Alcohol Tracer	FRPFM Sorbent	
		Fracture Depth	Fracture Orient	Fracture Flow Depth	Flow Direction	Specific Discharge	Contaminant Flux	Contaminant Flux conc	Fracture Depth	Fracture Orient	Specific Discharge	Flow Direction	Specific Discharge	Contaminant Flux	Contaminant Flux conc
Guelph	A	x	x	x	x	NA	NA	NA	x	x	x	NA	x	NA	NA
	B	x	x	x	x	NA	NA	NA	x	x	x	x	x	NA	NA
	C	x	x	x	x	NA	NA	NA	NA	NA	x	NA	x	NA	NA
	D	x	x	x	x	NA	NA	NA	x	x	x	x	x	NA	NA
	F	x	x	x	x	NA	NA	NA	x	x	x	x	NA	NA	NA
	G	x	x	x	x	NA	NA	NA	x	x	x	x	x	x	x
	H	x	x	x	x	NA	NA	NA	NA	NA	NA	NA	x	x	x
	I	x	x	x	x	x	x	x	NA	NA	NA	NA	x	x	x
	L	x	x	x	x	x	x	x	NA	NA	NA	NA	x	x	x
NAWC	J	x	x	x	x	x	x	x	x	x	x	x	x	x	x
	K	x	x	x	x	x	x	x	x	x	x	x	x	x	x
	N	x	x	x	x	x	x	x	x	x	NA	NA	x	x	x
	O	x	x	x	x	x	x	x	x	x	x	x	x	x	x
	P	x	x	x	x	x	NA	NA	x	x	NA	NA	x	x	x
	Q	x	x	x	x	x	NA	NA	x	x	NA	NA	x	x	x
	R	x	x	x	x	x	x	x	x	x	NA	x	x	x	x

x--Quantifiabe results
NA--Not Available

5.5.1. STARTUP

Because much of the desired baseline characterization data existed for all of the test wells; the primary start up activity, included a thorough review of existing data and the measurement of water levels and contaminant concentrations prior to FRPFM field testing. Groundwater levels were measured in each test borehole and in nearby wells before and after testing the FRPFM at each depth interval. The intent was to monitor potential changes in head and gradients produced by changes in local hydrologic conditions (e.g., rainfall events) during the field demonstration period. In addition, contaminant concentrations were evaluated in each test well prior to FRPFM testing in order to assess ambient depth-average contaminant concentrations.

5.5.2. DIRECTIONAL FLOW SURVEY

One of the principal investigators, University of Guelph, used high resolution temperature profiling (HRTP) (Pehme et al, 2010) to identify active flowing fractures along with a temperature vector probe (TVP) (Pehme et al, 2014) to measure the direction of fracture flow over isolated sections of the borehole. These tools provide a vertical distribution of horizontal groundwater flow direction throughout the entire length of lined borehole. It typically takes three days to survey all the fractures within a well. The directional flow survey was conducted in its entirety before FRPFM deployment began and portions of the results are presented in Pehme et al, 2014.

5.5.3. BOREHOLE DILUTION TESTING

Borehole dilution tests were conducted to measure water and contaminant fluxes over the same isolated sections of the rock hole interrogated by the FRPFM. These tests were conducted immediately before and/or after the FRPFM were deployed. A submersible pump is used to circulate water from an isolated borehole test section through an above-ground recirculation manifold that incorporates an in-line electrical conductivity meter, along with a mixing chamber and sampling port. Changes in electrical conductivity were monitored continuously to quantify water fluxes. Water samples were collected over the same isolated section of rock hole during each borehole dilution test and analyzed for target contaminants. Measured contaminant concentrations were used to calculate contaminant flux. Depending on flow conditions, borehole dilution tests took anywhere between 4 hours to 7 days.

5.5.4. FRPFM DEPLOYMENT; RETRIEVAL, AND SAMPLING

Based on high-resolution temperature logs for all wells, FRPFM were deployed strategically to measure fluxes in zones with expected active fractures. Each FRPFM deployment interrogated a 1.0-m depth interval. Depending on flow conditions, FRPFM deployments ranged from 18 hours to 30 days.

At the end of each deployment period, the FRPFM was extracted for visual inspection, imaging, documentation, and sampling. Visual inspection of the external FRPFM fabric under UV light

provides evidence of visible tracer loss that indicates active fracture locations, orientations, and directions of flow. Pictures were taken to document the location of active tracers, their orientation, and direction of fracture flow. Locations of active fractures and direction of flow are then compared to fracture locations indicated by HRTP (Pehme et al, 2010). Fracture orientation are compared to available optical and acoustic surveys, and flow direction is compared to TVP results (Pehme et al, 2014) and previous published measures for each site.

Once the external visible tracer data were recorded, the FRPFM sorbent fabric was removed and sampled and preserved as described in section 5.6. The samples were shipped on ice to the University of Florida and/or the University of Guelph for analysis. Sample analysis produces measures of residual alcohol tracer masses and the intercepted TCE (and DCE) mass from each fracture. Tracer masses are used to quantify cumulative fracture flows in accordance with equation (12). TCE mass intercepted from fractures is used with equation (14) to quantify contaminant fluxes.

5.5.5. DEMOBILIZATION

It is estimated that the demonstration produced 7 kg of IDW; 4 kg of spent activated carbon felt waste, 1 kg of spent cotton socks, and 2 kg of plastic mesh. The University of Guelph/Florida/USGS disposed of all waste. No equipment was left on site and no wells were decommissioned.

5.6 SAMPLING METHODS

The objective of the sampling plan for this study was to acquire sufficient data to validate FRPFM technology performance in the field and allow regulatory agencies and managers to evaluate the innovative nature of the technology. Because the FRPFM provides time integrated measures of both water and contaminant fluxes, temporal variations in flux are not a concern. However, spatial variations in flux can be significant. The visible tracers used on the FRPFM provide an indication of where sorbent sampling is needed to quantify water and contaminant fluxes in active fractures. Using visual tracer results to inform sorbent sampling allows for proper evaluation of spatial variations in both water and contaminant fluxes.

Sample Collection. Two types of samples were collected during this study, ground water samples and sorbent samples from FRPFM. Tables 16 and 17 respectively provide details on the number and type of samples collected and analytical methods of analysis. Sampling methods and sample handling procedures are briefly described here and discussed in more detail in Appendices B-D.

Water samples were collected in EPA VOA vials with zero headspace. Samples were drawn from tested rock wells before FRPFM testing and they were collected periodically during borehole dilution tests. The contaminant concentrations measured during the borehole dilution tests were used with borehole dilution flow data to calculate contaminant flux and flux average concentrations over isolated depth intervals. Samples were analyzed for target contaminants (TCE and DCE).

Sorbent samples were collected from the extracted FRPFM from a depth interval typically 30-40 times the fracture aperture. Regular intervals of the FRPFM sorbent were segmented and transferred to 40-ml VOA vials containing an extraction fluid such as isobutanol. Approximately 20 grams of sorbent were extracted with 20 ml of solvent.

Sample Analysis. All samples were analyzed at laboratories at the University of Florida and/or University of Guelph. Volatile organics, including alcohol tracers, were analyzed by direct liquid injection on Gas Chromatographs. Details of analytical methods are provided in Appendix B-D. Detection limits are approximately 1 mg/L. Headspace analysis (HS) is used in the event that low concentrations are encountered. Detection limits for HS is approximately 50 ug/L

Data Quality Parameters. Data quality was maintained and checked throughout the project. Details on approaches for maintaining data quality are provided in the QA/QC plan in Appendix E.

Quality Assurance Sampling. A description of the quality assurance (QA) samples that were collected, such as field duplicates, equipment blanks, trip blanks, and field blanks are provided in the QA/QC plan in Appendix E.

Calibration Procedures, Quality Control Checks, and Corrective Action. Initial and continuing calibration procedures for analytical instrumentation, quality control checks, and corrective actions are required to maintain reproducible experiments. These procedures are fully described in the QA/QC plan in Appendix E.

Data Quality Indicators. Simple regression analysis was used to assess the quality of data collected at any single well. However, more sophisticated techniques of spatial analysis were performed with data collected to assess the spatial mean and variance of contaminant and water fluxes evaluated over transects or within a plume.

Table 16. Total Number and Types of Samples to Be Collected

Component	Matrix	Number of Samples	Analyte	Location
Pre-demonstration sampling	Groundwater	5	TCE	One from each rock well.
Technology performance sampling	AC Sorbent	20 or 4 per active fracture	TCE Alcohol tracers: 2-butanol 1-butanol 3-pentanol 1-pentanol 2,4dimethyl pentanol 1-hexanol 1-octanol	At 5 active fracture locations 4 samples taken
	Groundwater	20 or 4 per Borehole dilutions test	TCE	At 5 active fracture locations 4 samples taken

Table 17. Analytical Methods for Sample Analysis

Matrix	Analyte	Method	Container	Preservative[1]	Holding Time
Groundwater	TCE	Appendices B-D	EPA VOA Vials	None	14 days
AC sorbent	Alcohol tracers: 2-butanol 1-butanol 3-pentanol 1-pentanol 2,4dimethyl pentanol 1-hexanol 1-octanol	Appendices B-D	EPA VOA Vials	Isobutyl Alcohol	14 days
AC sorbent	TCE	Appendices B-D A	EPA VOA Vials	Isobutyl Alcohol	14 days

5.7 SAMPLING RESULTS

During 2010 five FRPFM field deployments were performed at the Guelph Tool site (Tests A, B, C, D, and E). The target zones for FRPFM interrogation were determined based upon pre-existing geophysics data and closed-hole high resolution temperature profiles used to indicate the presence of flow within the borehole. The objectives of these early tests were to 1) test the capability of the FRPFM to identify flowing features within fractured rock systems and 2) provide estimates for flow direction. It should be noted that the deployment depth for all tests is referenced to the center of the 1-meter FRPFM interrogation zone. As such, there is 0.5 m (1.64 ft) of interrogation above and below the listed deployment depth.

The first FRPFM test (Test A) was performed in well MW-26 with deployment duration of 4 days at a depth of 13.30 m-bgs (43.64 ft-bgs). This phase of field tests incorporated two components of the FRPFM technology suite: 1) internal alcohol tracers on a new sorbent media (activated carbon felt) that was selected specifically for fractured rock applications based upon extensive laboratory testing and 2) improved visual tracer sock now composed of a nylon-spandex blend (again specifically selected for fracture rock applications based upon extensive laboratory testing). The elution of internal tracers provide a direct measure of volumetric water flux (specific discharge) through the FRPFM, while the visual tracer provides indication of the presence, spatial distribution, and orientation of flowing fractures along with the direction of groundwater flow and an independent measure of water flux. When the initial FRPFM prototype was retrieved, imaged, and sampled there were faint visual indications of a three potential flowing vertical and diagonal fractures with centroids at 13.29, 13.35 and 13.41 m-bgs. ATV-OTV logs indicated horizontal features at 13.43 and 13.72 m-bgs, and HRTP had indicated flow at 13.3 m-bgs. Analysis of the FRPFM internal alcohol tracers indicated a flow per unit width of 60 cm^2/day, while evaluation of the apparent aperture and length of the individual visual dye features indicated a flow per unit width of 76 cm^2/day. There was no quantifiable contaminant flux at this depth. Flux data for all tests are summarized in Tables 18 and 19. Table 18 summarizes results for comparative technologies (HRTP/TVP and BHD) while table 19 summarizes results for FRPFM technologies (visual tracers, alcohol tracers and sorbent).

Subsequent field tests during 2010 incrementally added new components to each FRPFM field prototype that was deployed. The next component that was incorporated was an accelerometer on the base of the FRPFM assembly in order to record the orientation of the device with regard to magnetic north during deployment. This allows for evaluation of the direction of flow within the FRPFM interrogation zone. Test B was the first phase of testing that incorporated the accelerometer and was performed in well MW-26 with deployment duration of 4 days at a depth of 13.40 m-bgs (43.96 ft-bgs). When the FRPFM was retrieved, imaged, and sampled there were visual indications of two vertical flowing features. The upper feature was 21 cm long with a centroid at 13.23 m-bgs (43.41 ft-bgs) and an apparent aperture of 0.33 cm, while the lower feature was 10 cm long with a centroid at 13.92 m-bgs (45.67 ft-bgs) and an apparent aperture of 0.93 cm. The location of the upper feature corresponded with a potential vertical fracture noted in the acoustic televiewer data log possibly connecting two apparent horizontal fractures. FRPFM alcohol tracers indicated an average flow per unit width of 56 cm^2/day while evaluation of visual dye features indicated an average flow per unit width of 49 cm^2/day (table 19). There was no quantifiable contaminant flux at this depth. Both of the visual features were on the same face of the FRPFM and were essentially collinear at approximately 106^o from north (with a

reported accuracy of 0.5 to 2.0 degrees root mean squared error for the accelerometer). As discussed in section 5.3.4, the visual features on the FRPFM sock indicate where flow has entered the device. As such, the inferred flow direction is offset by 180^o, and the estimated groundwater flow direction within the FRPFM interrogation zone during Test B was 286^o (W).

Test C was the first test performed that incorporated a stainless steel shield that was designed to encapsulate the FRPFM during deployment and retrieval within the borehole. The shield serves two purposes: 1) it physically protects the integrity of the visual tracer sock and underlying activated carbon felt by preventing contact with the fracture rock face of the borehole and 2) it precludes internal tracer loss due to vertical flow of water through the device during deployment and retrieval. Test C was performed in the highly weathered upper portion of MW26 with deployment duration of 5 days at a depth of 6.48 m-bgs (21.25 ft-bgs). The rock in this zone is unconsolidated with large voids and sharp edges. Preliminary FRPFM tests during 2009 in this zone had experienced both packer and visual sock failure due to contact with the sharp rock face. Once the shield was incorporated for Test C, FRPFM deployment, retrieval, and sampling all went well with no complications. Imagery of the visual indication sock showed significant washout on one face of the FRPFM with little to no dye remaining in the active flow zone. But, above and below the flow zone there was still tracer visible on the sock and more importantly, on the back (down gradient) side of the FRPFM there was still visual tracer present on the sock. All of these conditions correspond with expected results previously validated using the large scale aquifer box with high contrast flow zones at the University of Florida Coastal Laboratory (as discussed in section 5.3.4). Based upon analysis of internal alcohol tracers, the specific discharge within the washout zone was 33 cm/day (table 19). There was no quantifiable contaminant flux at this depth. Test B and C were performed in parallel with two separate FRPFM prototypes. The prototype used for test C did not incorporate an accelerometer and as such the flow direction was not estimated.

Test D was performed in well MW25 with a deployment duration of 5 days at a depth of 7.93 m-bgs (26 ft-bgs). When retrieved there were visual indications of three vertical flowing features with centroids located at 7.63 m-bgs (25.05 ft-bgs), 7.88 m-bgs (25.85 ft-bgs), and 8.04 m-bgs (22.39 ft-bgs). The upper feature was 20 cm long with an apparent aperture of 0.17 cm, the middle feature was 4.5 cm long with an apparent aperture of 0.05 cm, and the bottom feature was 10 cm long with an apparent aperture of 0.35 cm. FRPFM alcohol tracers indicated an average flow per unit width of 10.8 cm^2/day while evaluation of visual dye features indicated an average flow per unit width of 8.3 cm^2/day (table 19). There was no quantifiable contaminant flux at this depth. The three centroids of the visual features were located at 35.6^o, 66.3^o and 84.4^o from north with inferred flow directions of 215.6^o, 246.3^o, and 264.4^o respectively. As such, the estimated general direction of groundwater flow within the FRPFM interrogation zone during Test D was 242^o (SW).

Test E was run to completion, and the FRPFM was successfully retrieved. However, it was determined that the packer assembly had developed a leak during the deployment and the interrogation zone had not been vertically sealed for the duration of the test compromising the FRPFM results. As such, no data is reported but the test E designation is still recorded for continuity of discussion.

During 2011 three FRPFM field deployments were completed. The intent for this phase of testing was to evaluate the FRPFM capabilities for quantifying contaminant flux. A new well was selected for this phase of testing (MW-367-8) as it was anticipated to be along the periphery of the longitudinal axis of the contaminant plume.

Test F was performed in well MW-367-8 with a deployment duration of 10 days at a depth of 10.32 m-bgs (33.86 ft-bgs). When retrieved there were visual indications of 56 discrete horizontal flowing features distributed along the device (Figure 42). Evaluation of the visual features indicated a flow per unit width of 101 cm^2/day corresponding to a specific discharge of 1.28 cm/day over the interrogation zone (table 19). Unfortunately, all samples of the FRPFM sorbent were destroyed during shipping from Canada to the US and no analytical analysis of flux was possible. Evaluation of the location of centroids for each of the discrete horizontal features was used to estimate an average groundwater flow direction of 177^o (S) (Table 19).

Test G was performed in well MW-367-8 at the same depth as test F (10.32 m-bgs) with a deployment duration of 7 days. When retrieved, imagery indicated significant vertical washout of visual tracers at both the top and bottom of the interrogation zone. It was confirmed that the packers had maintained pressured for the duration of the test and the interrogation zone had been sealed. However, there was significant rainfall prior to and during the test. The visual dye washout zones were all predominantly on the same face of the FRPFM corresponding to an inferred groundwater flow direction of 184^o (S). FRPFM alcohol tracers indicated a flow per unit width of 834 cm^2/day with a specific discharge of 10.3 cm/day over the interrogation zone (table 19 and figure 42). Analysis of the FRPFM sorbent indicated a TCE mass flux of 1,514 µg/m^2/day with flux averaged TCE concentration of 16.5 µg/L (table 19 and figure 42).

Test H was performed in well MW-367-8 with the deployment depth shifted down 0.1 m to 10.42 m-bgs (34.19 ft-bgs) to avoid a large fracture that had been intercepted by the upper shield packer during tests F and G. Although the packer had not failed during tests F and G, it had shown significant signs of fatigue after test G. The packer was replaced and a deployment was attempted at the same depth (10.32 m-bgs), but the packer ruptured almost immediately. The packer was again replaced and again ruptured during another attempted deployment at 10.32 m-bgs. It was then that the decision was made to shift the deployment depth down by 0.1 m to 10.42 m-bgs (34.19 ft-bgs). At this depth the FRPFM packers held pressure, and maintained integrity for a deployment duration of 4 days. The 4-day duration was selected due to the relatively high fluxes that had been observed during test G. However, when the FRPFM was retrieved there were minimal visual indications of flow. FRPFM alcohol tracers indicated a flow per unit width of 123 cm^2/day with a specific discharge of 1.5 cm/day over the interrogation zone (table 19 and figure 42). Analysis of the FRPFM sorbent indicated a TCE mass flux of 172 µg/m^2/day with flux averaged TCE concentration of 11.2 µg/L (table 19 and figure 42).

Figure 42 summarizes results for tests F, G and H comparing the vertical distribution of water flux (specific discharge) from FRPFM alcohol tracers, contaminant flux from FRPFM sorbent, and FRPFM visual indication of flowing fractures. There was an order of magnitude increase in water and contaminant flux during test G, which can likely be attributed to significant rainfall prior to and during test G.

During 2012 field demonstration efforts were expanded to include tests running in parallel at both GTS and the NAWC site in New Jersey. A total of 5 FRPFM deployments were performed (two at GTS and three at NAWC), along with one FRPFM push-pull test and 16 borehole dilution tests. The intent of this phase of testing was to evaluate all components of the FRPFM technology suite. The conditions between the two test sites provide a drastic contrast for FRPFM testing. The Guelph site has relatively low aqueous contaminant concentrations (mean flux average TCE concentration = 8.15 µ/L) and experiences relatively low ambient groundwater velocities. NAWC is an active pump and treat site with induced gradient conditions (higher groundwater velocities) and significantly higher contaminant concentrations (mean flux average TCE concentration = 3,319 µ/L).

At GTS all final tests were performed in a newly selected well (MW-367-9) which was expected to be along the primary longitudinal axis of the contaminant plume resulting in higher contaminant concentrations. The selection of MW-367-9 presented a new challenge, as all previous FRPFM wells had been 4-inch diameter. MW-367-9 is a 6-inch diameter well, requiring construction of new larger diameter FRPFM prototypes. Two new 6-inch FRPFM prototypes were constructed, one for GTS and one for NAWC.

Test I was performed at GTS in MW-367-9. Prior to deployment a series of low flow sampling and borehole dilution (BHD) tests were performed to select a target FRPFM deployment depth with both quantifiable flow and contaminant flux. The results indicated that there was only one zone that had consistently quantifiable contaminant concentrations (both TCE and DCE) and a target deployment depth of 27.73 m-bgs (90.99 ft-bgs) was selected within this zone. At this depth, BHD results indicated a specific discharge of 0.44 cm/day with TCE and DCE mass flux values of 9.5 $\mu g/m^2$/day and 9.9 $\mu g/m^2$/day respectively (Table 18) within the 1-meter interrogation zone. As mentioned previously, the BHD probe was constructed to interrogate a 1-meter zone identical to that of the FRPFM. Following BHD tests, FRPFM Test I was completed with a deployment duration of 39 days at the target depth of 27.73 m-bgs. The 39-day duration was selected due to the low specific discharge values observed during BHD testing. When retrieved, imagery showed little to no visual indications of flow. FRPFM alcohol tracers indicated a specific discharge of 0.4 cm/day over the interrogation zone (table 19). Analysis of the FRPFM sorbent indicated TCE and DCE mass flux values of 16.1 $\mu g/m^2$/day and 18.0 $\mu g/m^2$/day respectively (table 19).

Note: Test L was performed in parallel with test J and K, with test L at GTS and tests J and K at NAWC. For continuity of discussion Test L is discussed next before Tests J and K.

Test L was the final test performed at GTS and was also performed in in MW-367-9 at the same deployment depth as Test I. Prior to deployment another borehole dilution (BHD) test was performed for comparison to and validation of FRPFM flux measurements. BHD results indicated a specific discharge of 0.91 cm/day with TCE and DCE mass flux values of 19.4 $\mu g/m^2$/day and 20.6 $\mu g/m^2$/day respectively (Table 18). FRPFM Test L was then completed with a deployment duration of 32 days at the target depth of 27.73 m-bgs. When retrieved, imagery again showed little to no change in visual tracers (similar to Test I). FRPFM alcohol tracers indicated a specific discharge of 0.9 cm/day over the interrogation zone (table 19). Analysis of

the FRPFM sorbent indicated TCE and DCE mass flux values of 8.5 µg/m^2/day and 13.6 µg/m^2/day respectively (table 19).

All tests at NAWC were performed in a well characterized 6-inch diameter well (68-BR). Prior to FRPFM deployment by the University of Florida, the University of Guelph with assistance from USGS and FLUTe completed ATV/OTV logs of the open hole along with a transmissivity log and HRTP/TVP profiles of the lined hole (closed-hole conditions). The HRTP/TVP results were used to identify five target zones with active flow for potential investigation with FRPFM. The University of Florida then performed a series of low flow sampling and borehole dilution tests to evaluate each of the five HRTP/TVP-identified target zone for quantifiable flow and contaminant flux.

Test J was the first FRPFM test performed at the NAWC site in West Trenton, NJ. Based upon HRTP/TVP logs and BHD results a target depth of 95 ft-bgs was selected for FRPFM deployment. BHD results at this depth had indicated a specific discharge of 2.9 cm/day over the interrogation zone with TCE and DCE mass flux values of 116,870 µg/m^2/day and 48,343 µg/m^2/day respectively (Table 18). Test J was performed with a deployment duration of 9 days at a depth of 95 ft-bgs. When retrieved there were visual indications of 56 discrete horizontal flowing features distributed along the device. The most striking of these features was a large diagonal feature at the bottom of the FRPFM interrogation zone that appeared to correspond precisely with USGS ATV logs at this depth (Figure 43). As discussed in section 5.3.4, visual features on the FRPFM sock indicate where flow has entered the device. As such, the inferred flow direction is offset by 180^o. For the case of the visual features shown in Figure 43, flow enters along the eastern face of the FRPFM and exits along the western face. Based upon the location of centroids for all visual features, referenced to the FRPFM accelerometer directional orientation, the inferred general flow direction for Test J was 245^o (WSW). Evaluation of the visual features indicated a specific discharge of 2.1 cm/day over the interrogation zone (table 19). FRPFM alcohol tracers indicated an average specific discharge of 2.5 cm/day over the interrogation zone (table 19). Analysis of the FRPFM sorbent indicated TCE and DCE mass flux values of 105,116 µg/m^2/day and 57,116 µg/m^2/day respectively (table 19).

Test K was performed at NAWC in well 68BR with a deployment duration of 18 hours at a depth of 96.64 ft-bgs. The short deployment duration was selected due to relatively high discharges observed during BHD tests at this depth. BHD results indicated a specific discharge of 21.6 cm/day over the interrogation zone with TCE and DCE mass flux values of 171,720 µg/m^2/day and 86,832 µg/m^2/day respectively (Table 18). When retrieved there were visual indications of 80 discrete horizontal flowing features distributed along the device. As part of Test K, improved image analysis techniques were incorporated in order to better evaluate visual features on the FRPFM sock. As part of the new protocol, the FRPFM sock was returned to the laboratory, cut open and lain flat for image processing. Figure 44 shows a black and white image of a portion of the FRPFM sock with centroids for each individual feature referenced to the FRPFM accelerometer directional orientation. The inferred general flow direction for Test K was 248^o (WSW). Evaluation of the visual features indicated a specific discharge of 24 cm/day over the interrogation zone (table 19). FRPFM alcohol tracers indicated a specific discharge of 21.6 cm/day over the interrogation zone (table 19). Analysis of the FRPFM sorbent indicated TCE and DCE mass flux values of 161,646 µg/m^2/day and 83,503 µg/m^2/day respectively (table 19).

Test M was performed to completion at NAWC but the results were compromised by vandalism and theft of equipment maintained at land surface during deployment. The FRPFM packers were damaged as a result, but the FRPFM prototype was recovered and repaired. There are no results available for report.

The final phase of field testing was performed during 2013 at the NAWC site. A total of 5 FRPFM deployments were performed (Tests N-R) along with 16 modified borehole dilution tests. Tests N-Q were performed sequentially within zone D of 68BR (Figure 15), which is known to be a zone with higher flow and contaminant concentrations based upon previous studies by USGS (Shapiro, 2008; Tiedeman et al, 2010; and Lacombe, 2011). The initial depth of 95.12 ft-bgs within this zone was selected as a priority target based upon HRTP/TVP data collected by the University of Guelph that confirmed quantifiable flow at this depth. Test R was performed within zone F of 68BR (Figure 15) which also was expected to be a zone with quantifiable flow and contaminant concentrations based upon previous studies (Shapiro, 2008; Tiedeman et al, 2010; and Lacombe, 2011) HRTP/TVP measurements indicated flow at a target depth of 133 ft-bgs within zone F.

Because NAWC is an active pump and treat site, the flow conditions can be altered through use of the pump and treat extraction wells. Previously published work by the USGS demonstrated the benefit of such tests (Tiedeman et al, 2010). Results of the Tiedeman et al, 2010 study indicated a direct hydraulic connection between zones D and F in monitoring well 68BR (Figure 15) and extraction well 15BR. Well locations are provided in Figure 13.

Tests N and O were performed at the same deployment depth (95.12 ft-bgs) but with different pumping conditions at extraction well 15BR. The objective was to evaluate how the FRPFM performed under varied flow conditions. Test N was performed with a deployment duration of 8 days and a reduced extraction rate of 6.4 GPM at 15BR. This was the minimum rate at which 15BR could be operated while still maintaining permitted contaminant extraction levels at the pump and treat boundary. BHD tests under these conditions indicated a specific discharge of 3.2 cm/day over the interrogation zone, with TCE and DCE mass flux values of 40,545 $\mu g/m^2$/day and 24,486 $\mu g/m^2$/day respectively (Table 18). When the FRPFM was retrieved there were minimal to no visual indications of flow. FRPFM alcohol tracers indicated a specific discharge of 3.2 cm/day over the interrogation zone (table 19). Analysis of the FRPFM sorbent indicated TCE and DCE mass flux values of 50,091 $\mu g/m^2$/day and 27,558 $\mu g/m^2$/day respectively (table 19).

Test O was performed with a deployment duration of 6 days and increased extraction rate of 13.7 GPM at 15BR. This is the typical extraction rate maintained at 15BR during regular operation of the pump and treat system. BHD tests under these conditions indicated only a slight increase in specific discharge to 3.4 cm/day over the interrogation zone when compared to Test N. TCE and DCE mass flux values also showed slight increases to 42,712 $\mu g/m^2$/day and 25,795 $\mu g/m^2$/day respectively (Table 18). In stark contrast to Test N however, when the FRPFM was retrieved there were visual indications of 68 discrete flowing features (Figures 47 and 48). Evaluation of the visual features indicated a specific discharge of 5.5 cm/day over the interrogation zone (table 19). FRPFM alcohol tracers indicated a specific discharge of 3.8 cm/day over the interrogation

zone (table 19). Analysis of the FRPFM sorbent indicated TCE and DCE mass flux values of 148,849 µg/m^2/day and 55,647 µg/m^2/day respectively (table 19).

Test O provides a complete demonstration of the full FRPFM technology suite with the results summarized in Figures 47 and 48. The FRPFM visual tracer sock provides a high-resolution distribution of the location and orientation of actively flowing fractures within the interrogation zone, which are compared to ATV and OTV images in figure 47. The centroids of the visual features were used with the FRPFM accelerometer orientation to estimate a general groundwater flow direction of 199^o (SSW) figure 47. The vertical distribution of FRPFM water and contaminant fluxes are also compared to ATV, OTV and FRPFM visual features in figure 48. It can be seen that there are considerable variations in specific discharge and TCE flux within the interrogation zone, and the FRPFM data collected allows for evaluation of the relative contribution to flow and contaminant flux on a per feature basis. More in depth analysis and comparison of results is provided in section 6.3.

Tests P and Q were performed with same extraction rate as Test O (13.7 GPM at 15BR), with Test P overlapping the upper half of the interrogation zone of Test O, and Test Q overlapping the lower half of the interrogation zone of Test O. The intent was to evaluate how results vary based upon placement of the FRPFM within a larger zone of interest.

Test P was performed with a deployment duration of 7 days at a deployment depth of 93.62 ft-bgs. BHD tests indicated a specific discharge of 3.8 cm/day over the interrogation zone, with TCE and DCE mass flux values of 147,524 µg/m^2/day and 48,679 µg/m^2/day respectively (Table 18). When the FRPFM was retrieved there extremely faint variations in visual tracers, but no conclusive visual indications of flow. FRPFM alcohol tracers indicated a specific discharge of 3.3 cm/day over the interrogation zone (table 19). Analysis of the FRPFM sorbent indicated TCE and DCE mass flux values of 144,475 µg/m^2/day and 52,865 µg/m^2/day respectively (table 19).

Test Q was performed with a deployment duration of 8 days at a depth of 96.62 ft-bgs. BHD tests indicated a specific discharge of 2.3 cm/day over the interrogation zone, with TCE and DCE mass flux values of 155,791 µg/m^2/day and 40,803 µg/m^2/day respectively (Table 18). When the FRPFM was retrieved there were faint visual indications of two discrete features along the same horizontal arc on the FRPFM at approximately 96.15 ft-bgs. The inferred flow direction from the faint visual features was ESE (113 ^{o}) (figure 49). FRPFM alcohol tracers indicated a specific discharge of 2.1 cm/day over the interrogation zone (table 19). Analysis of the FRPFM sorbent indicated TCE and DCE mass flux values of 145,523 µg/m^2/day and 51,888 µg/m^2/day respectively (table 19).

Test R was the final FRPFM deployment and was performed 68BR at a depth of 133.62 ft-bgs. The pump and treat extraction rates were maintained similar to Tests O, P and Q (13.7 GPM at 15BR). BHD results indicated a specific discharge of 1.3 cm/day over the interrogation zone with TCE and DCE mass flux values of 28,473 µg/m^2/day and 6,680 µg/m^2/day respectively (Table 18). Based upon the lower BHD specific discharge, a longer FRPFM deployment duration (15 days) was selected. When retrieved there were faint but distinct visual indications of a circular feature (centroid at 134.75 ft-bgs) intersected by two high-angle fractures. Figure 50

provides a comparison of ATV/OTV images with FRPFM visual indications of the flowing circular feature and two high-angle fractures. The FRPFM images were processed using multiple filters to enhance the circular and high angle features. One negative side effect of image filtering was enhanced appearance of the weave pattern within the visual indication sock material which could provide a false positive for flowing fractures when seen by an untrained observer. Evaluation of the visual features with the FRPFM accelerometer orientation provided a general groundwater flow direction of 288^{o} (WNW) figures 50 and 51. FRPFM alcohol tracers indicated a specific discharge of 1.0 cm/day over the interrogation zone (table 19). Analysis of the FRPFM sorbent indicated TCE and DCE mass flux values of 23,279 µg/m^2/day and 33,072 µg/m^2/day respectively (figure 52 and table 19).

Discussion of analysis methods and comparison of results is provided in section 6.

Table 18. Matrix of flux results for comparative technologies (HRTP/TVP and BHD).

					Comparative Technology								
					HRTP/TVP	BHD							
	Test	Well ID	Deployment Depth (m-bgs)	Deployment Depth (ft-bgs)	Flow Direction	Specific Discharge (cm/day)	Flow per unit width (cm^2/day)	TCE Flux (ug/m^2/day)	DCE Flux (ug/m^2/day)	TCE mass discharge per length of fracture (ug/m/day)	DCE mass discharge per length of fracture (ug/m/day)	TCE flux-average concentration (ug/L)	DCE flux-average concentration (ug/L)
Guelph	A	MW-26	13.30	43.64	SSE	NA	NA	NA	NA	NA	NA	NA	NA
	B	MW-26	13.40	43.96	SSE	NA	NA	NA	NA	NA	NA	NA	NA
	C	MW-26	6.48	21.25	SSE	NA	NA	NA	NA	NA	NA	NA	NA
	D	MW-25	7.93	26.00	SSE	NA	NA	NA	NA	NA	NA	NA	NA
	F	MW-367-8	10.32	33.86	SSE	NA	NA	NA	NA	NA	NA	NA	NA
	G	MW-367-8	10.32	33.86	SSE	NA	NA	NA	NA	NA	NA	NA	NA
	H	MW-367-8	10.42	34.19	SSE	NA	NA	106.2	NA	NA	NA	11.805	NA
	I	MW-367-9	27.73	90.99	SSE	0.44	47.5	9.5	9.944	10.3	10.8	2.16	2.26
	L	MW-367-9	27.73	90.99	SSE	0.91	93.7	19.656	20.566	21	22.2	2.16	2.26
NAWC	J	68-BR	28.96	95.00	WNW	2.9	292	116,870	48,343	116,870	48,343	4,030	1,667
	K	68-BR	29.46	96.64	WNW	NA	NA	NA	NA	171,720	86,832	795	402
	N	68-BR	28.99	95.12	WNW	3.2	318	38,400	23,968	40,545	24,486	1,200	749
	O	68-BR	28.99	95.12	WNW	3.4	318	148,802	63,086	40,576	24,505	4,442	1,883
	P	68-BR	28.53	93.62	WNW	3.8	NA	147,524	48,679	NA	NA	4,610	1,521
	Q	68-BR	29.45	96.62	WNW	2.3	NA	155,791	40,803	NA	NA	8,200	2,148
	R	68-BR	40.73	133.62	WSW	1.3	NA	69,634	43,773	NA	NA	5,483	3,447

x--Quantifiabe results
NA--Not Available

Table 19. Matrix of flux results for FRPFM technologies (visual tracer, alcohol tracer, and sorbent).

					FRPFM											
					Visual Tracer			Alcohol Tracer		FRPFM Sorbent					
	Test	Well ID	Deployment Depth (m-bgs)	Deployment Depth (ft-bgs)	Specific Discharge (cm/day)	Flow per unit width (cm^2/day)	Flow Direction	Specific Discharge (cm/day)	Flow per unit width (cm^2/day)	TCE Flux (ug/m^2/day)	DCE Flux (ug/m^2/day)	TCE mass discharge per length of fracture (ug/m/day)	DCE mass discharge per length of fracture (ug/m/day)	TCE flux-average concentration (ug/L)	DCE flux-average concentration (ug/L)
Guelph	A	MW-26	13.30	43.64	NA	76	NA	NA	60	NA	NA	NA	NA	NA	NA
	B	MW-26	13.40	43.96	NA	49	W (286o)	NA	56	NA	NA	NA	NA	NA	NA
	C	MW-26	6.48	21.25	NA	NA	NA	33	NA	NA	NA	NA	NA	NA	NA
	D	MW-25	7.93	26.00	NA	8.3	SW (242o)	NA	10.8	NA	NA	NA	NA	NA	NA
	F	MW-367-8	10.32	33.86	1.28	101	S (177o)	NA	NA	NA	NA	NA	NA	NA	NA
	G	MW-367-8	10.32	33.86	NA	NA	S (184o)	10.3	1432	1514	NA	1378	NA	16.5	NA
	H	MW-367-8	10.42	34.19	NA	NA	NA	1.5	123	172	NA	137	NA	11.2	NA
	I	MW-367-9	27.73	90.99	NA	NA	NA	0.4	41	16.1	18.0	16.6	18.5	4	4.5
	L	MW-367-9	27.73	90.99	NA	NA	NA	0.9	92	8.5	13.6	8.7	14.0	0.9	1.4
NAWC	J	68-BR	28.96	95.00	2.1	206	WSW (245o)	2.5	252	105,116	57,116	105,116	57,116	4,179	2,287
	K	68-BR	29.46	96.64	24	2,400	WSW (248o)	21.6	2,159	161,646	83,503	161,646	83,503	751	386
	N	68-BR	28.99	95.12	NA	NA	NA	3.2	323	50,091	27,558	50,091	27,558	1,466	807
	O	68-BR	28.99	95.12	3.9	390	SSW (199o)	3.8	360	148,849	55,647	141,407	52,865	3,771	1,410
	P	68-BR	28.53	93.62	NA	NA	NA	3.3	317	144,475	52,865	137,251	50,222	4,247	1,554
	Q	68-BR	29.45	96.62	NA	NA	ESE (113o)	2.1	199	145,523	51,888	138,247	49,293	6,639	2,367
	R	68-BR	40.73	133.62	NA	NA	WNW (288o)	1.0	98	23,279	33,072	22,115	31,418	2,182	3,100

x--Quantifiabe results
NA--Not Available

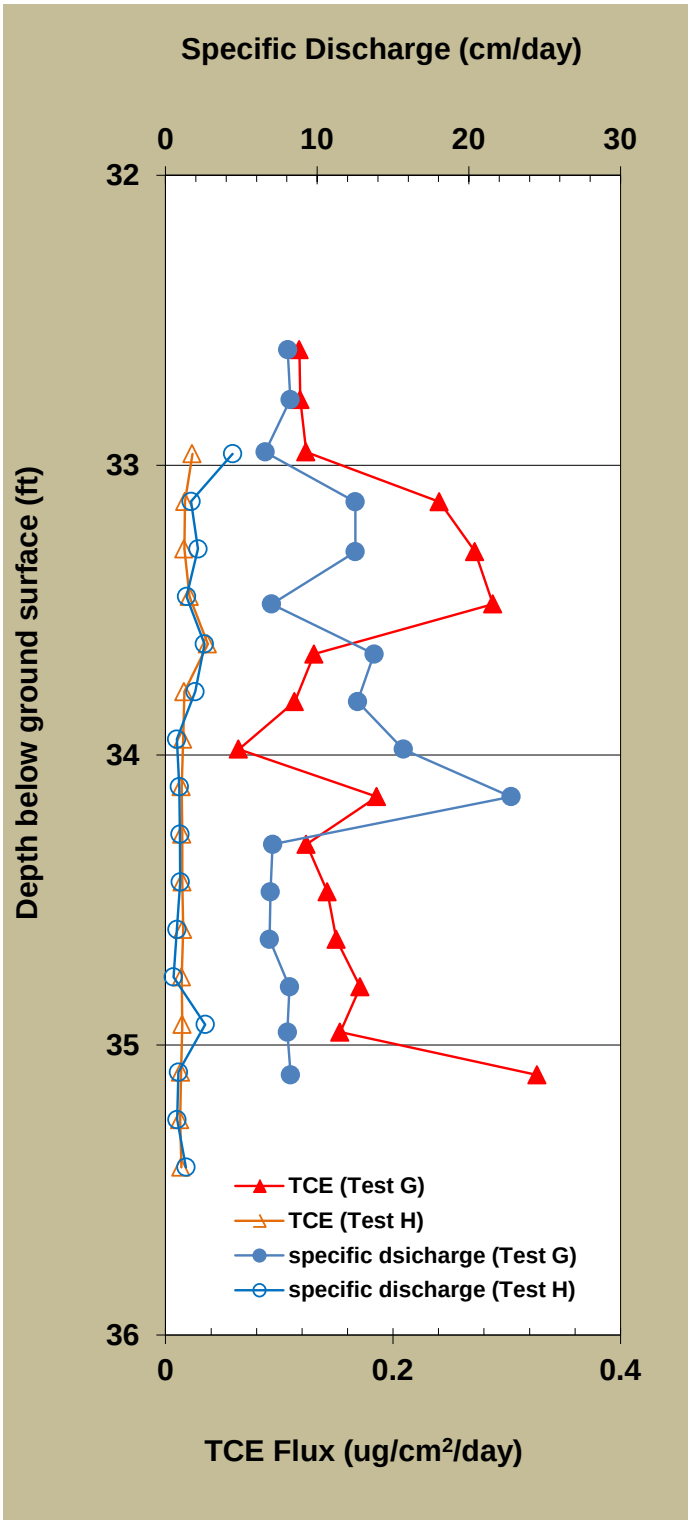

UV image of visual dye sock from Test F

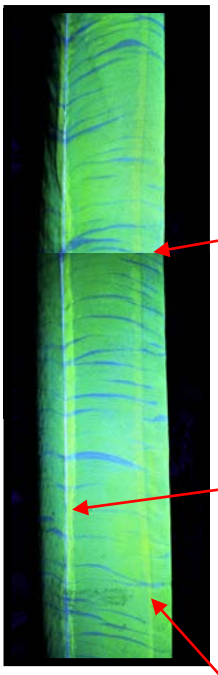

Image overlap

Sock seam

AC-felt (sorbent) overlap beneath visual sock.

Note: Image is of uninflated FRPFM after retrieval with width (diameter) = 3.2 inches. When deployed, the device was inflated with a diameter of 3.8 inches. As such, the visual features in the image have exaggerated curvature with respect to actual conditions.

Figure 42. Summary of flux measurements and visual results for Tests F, G, and H comparing vertical distribution of water flux (specific discharge), contaminant flux and presence of flowing fractures.

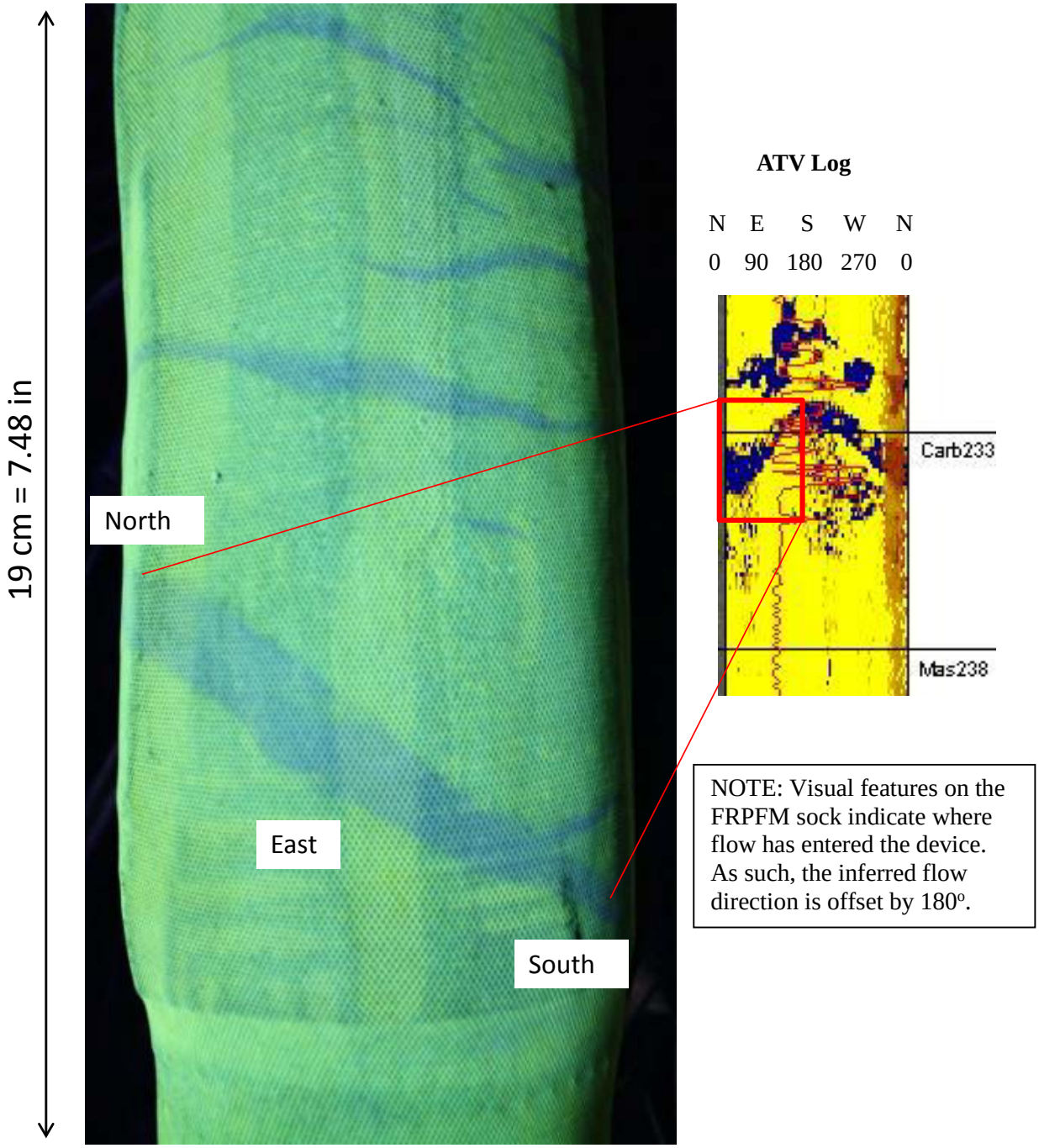

Figure 43. Test J imagery of visual flow indications compared to ATV log at same depth. NOTE: Imagery is of FRPFM visual indication sock on uninflated device after deployment. In this form the visual features are mirror images of features in ATV/OTV logs.

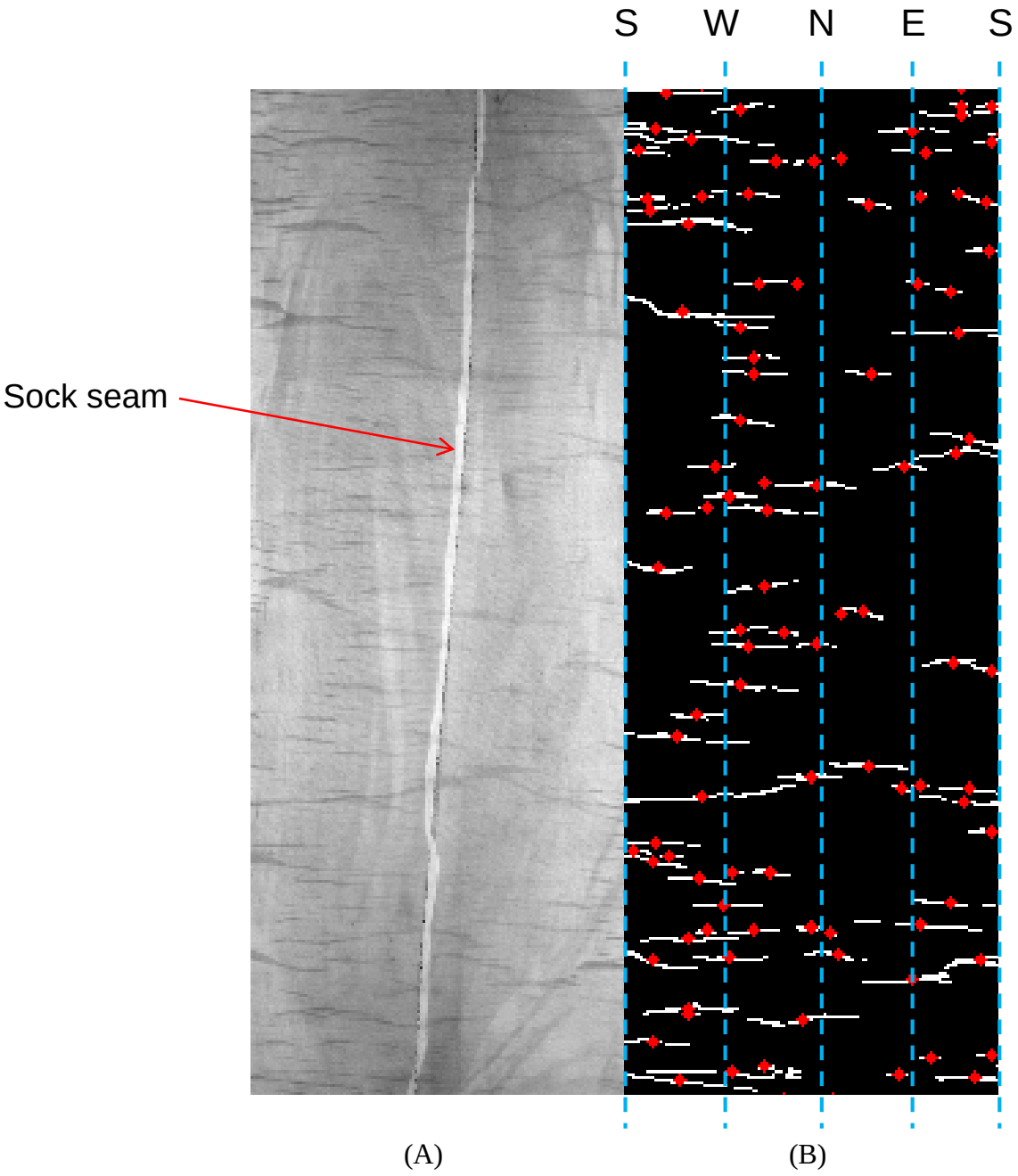

Figure 44. Test K: (A) black and white image of visual features from a portion of the FRPFM sock. (B) Centroids of individual features referenced to the FRPFM accelerometer directional orientation.

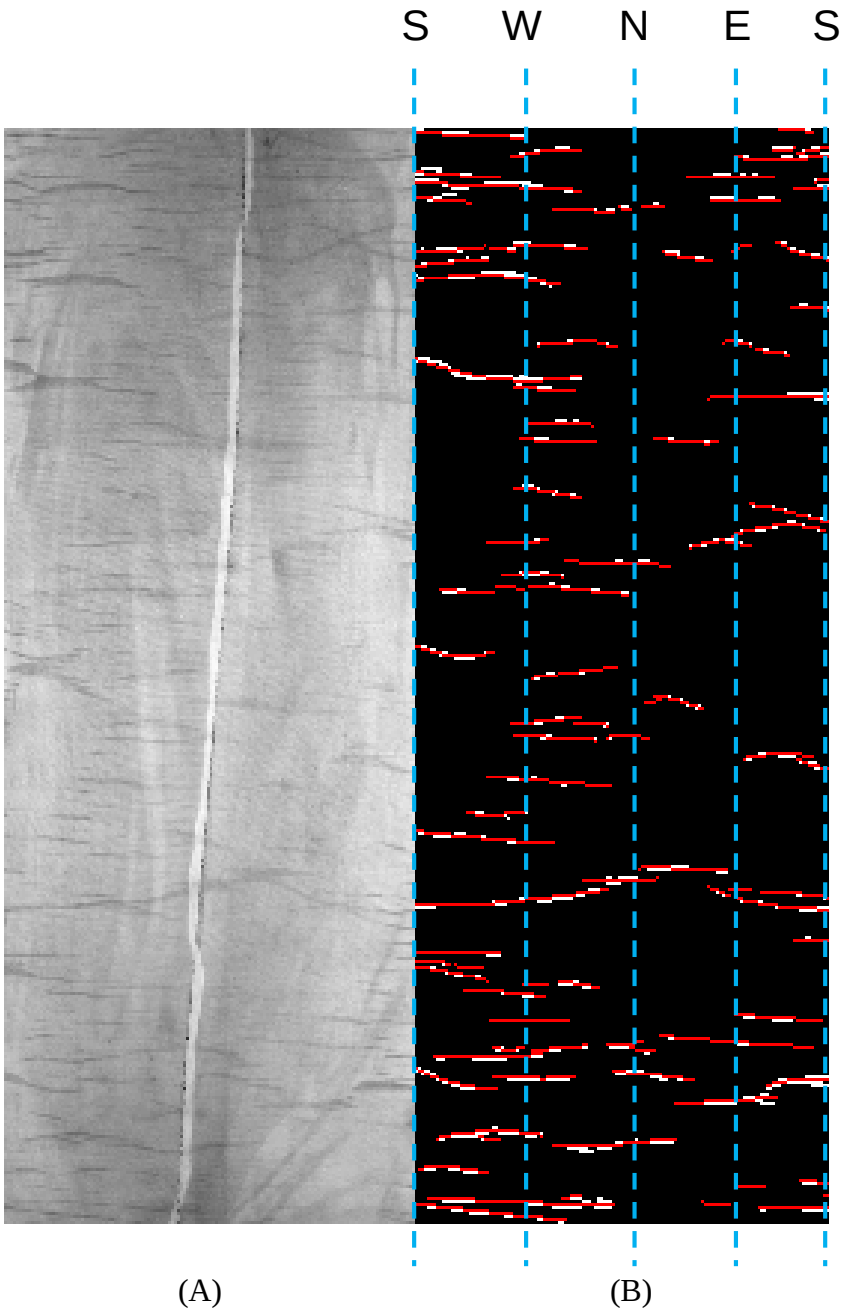

Figure 45. Test K: (A) Black and white image of visual features from a portion of the FRPFM sock. (B) Visual features with fitted sine function traces, which are used to estimate fracture depth, azimuth and dip.

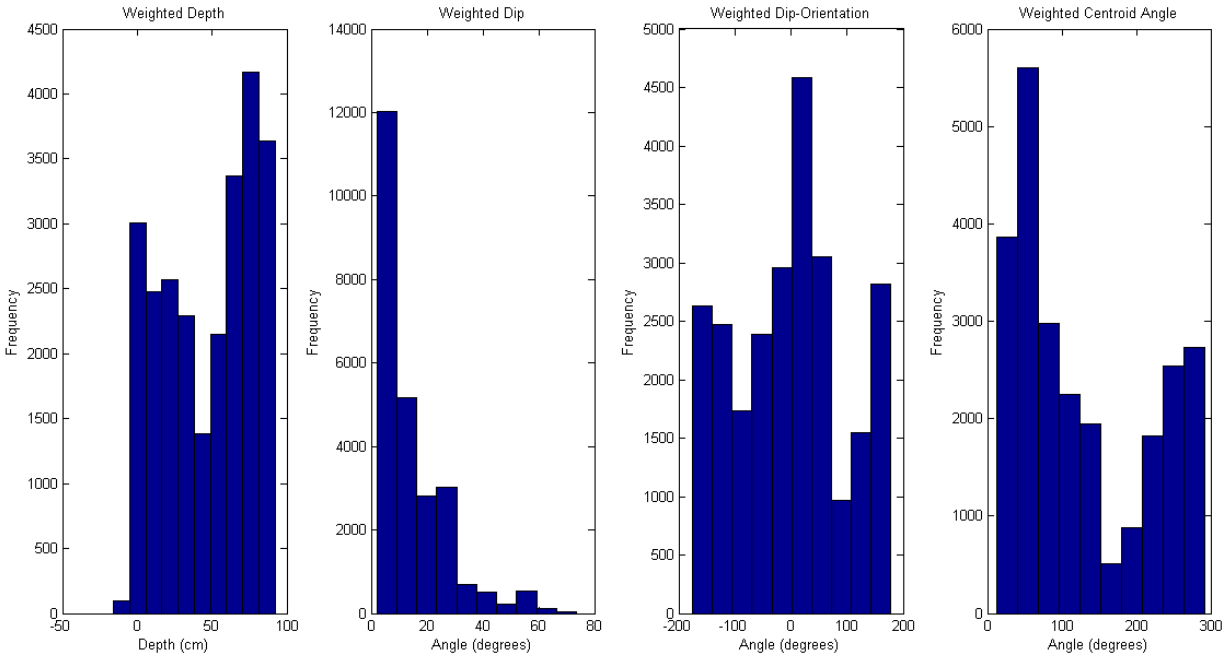

Figure 46. Test K: histograms of fracture depth, dip, orientation (azimuth) and centroid angles. Note: depth is the local depth along the 100-cm FRPFM interrogation zone.

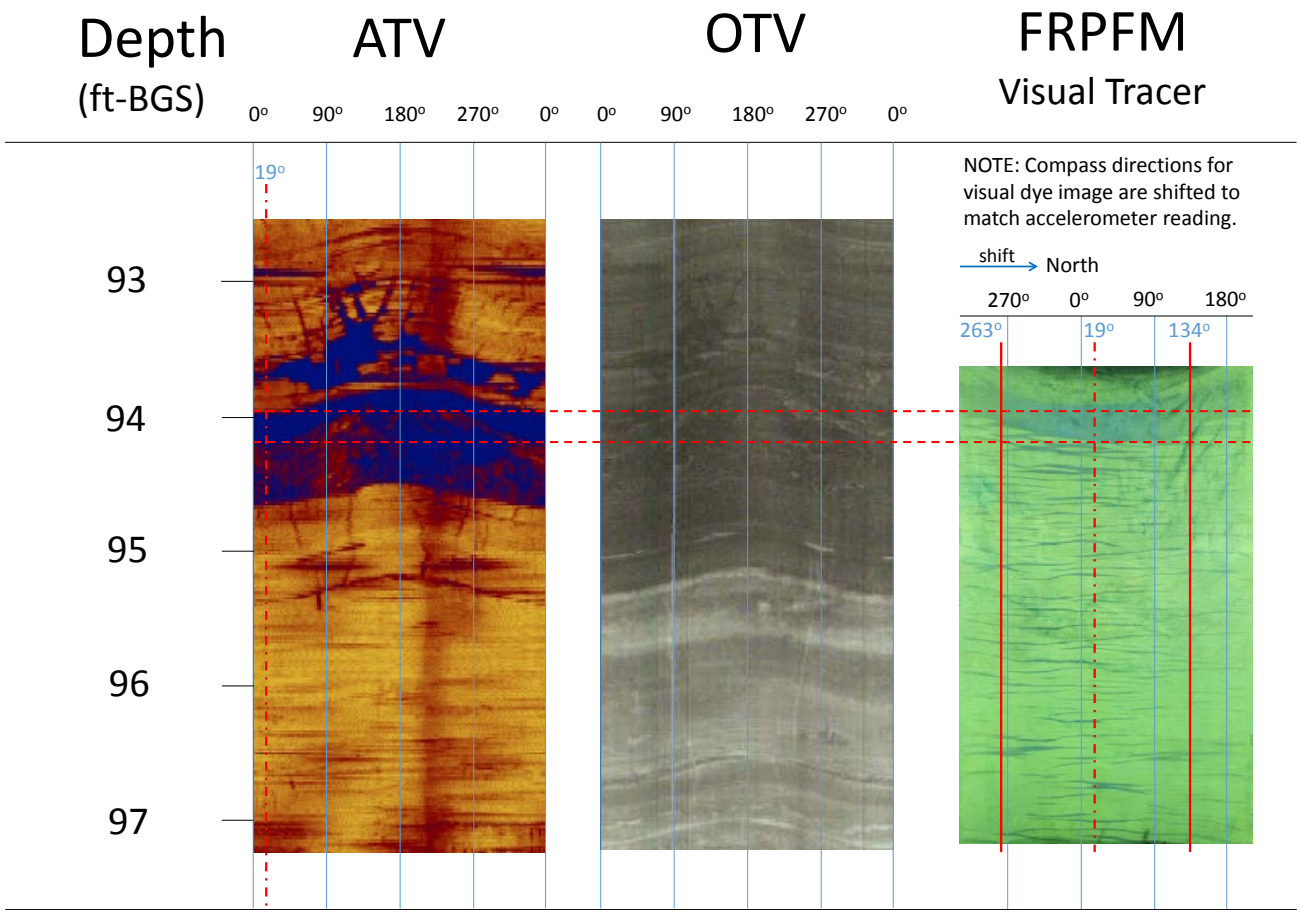

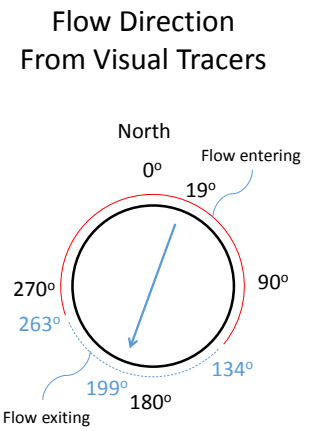

Visual traces indicate where flow enters the FRPFM—flow direction is offset by 180 degrees

General Flow Direction = 199º = (SSW)

Figure 47. Test O comparison of ATV, OTV, and FRPFM visual tracer with inferred flow direction.

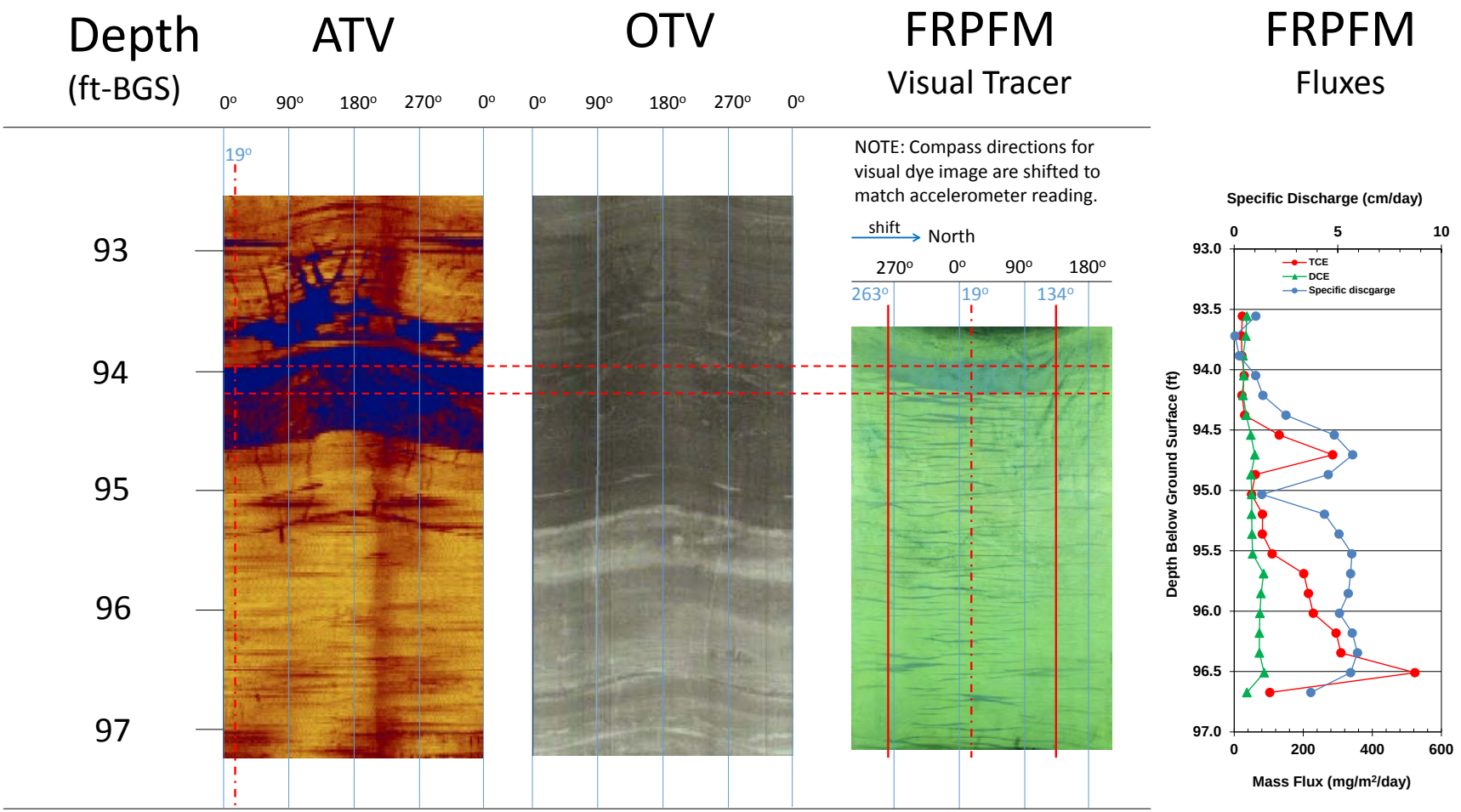

Figure 48. Test O comparison of ATV, OTV, FRPFM visual tracer and FRPFM fluxes.

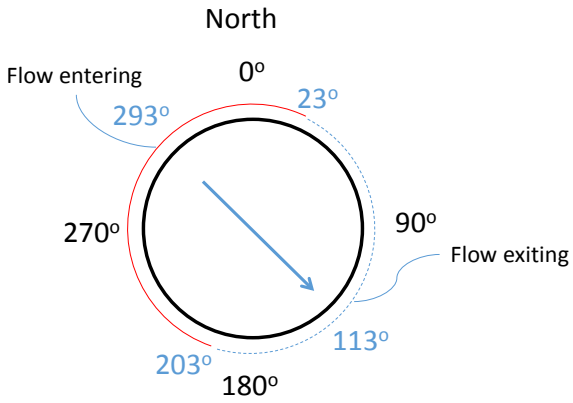

Visual traces indicate where flow enters the FRPFM—flow direction is offset by 180 degrees

General Direction of Flow = 113° = (ESE)

Figure 49. Test Q inferred general flow direction from faint visual features on FRPFM sock.

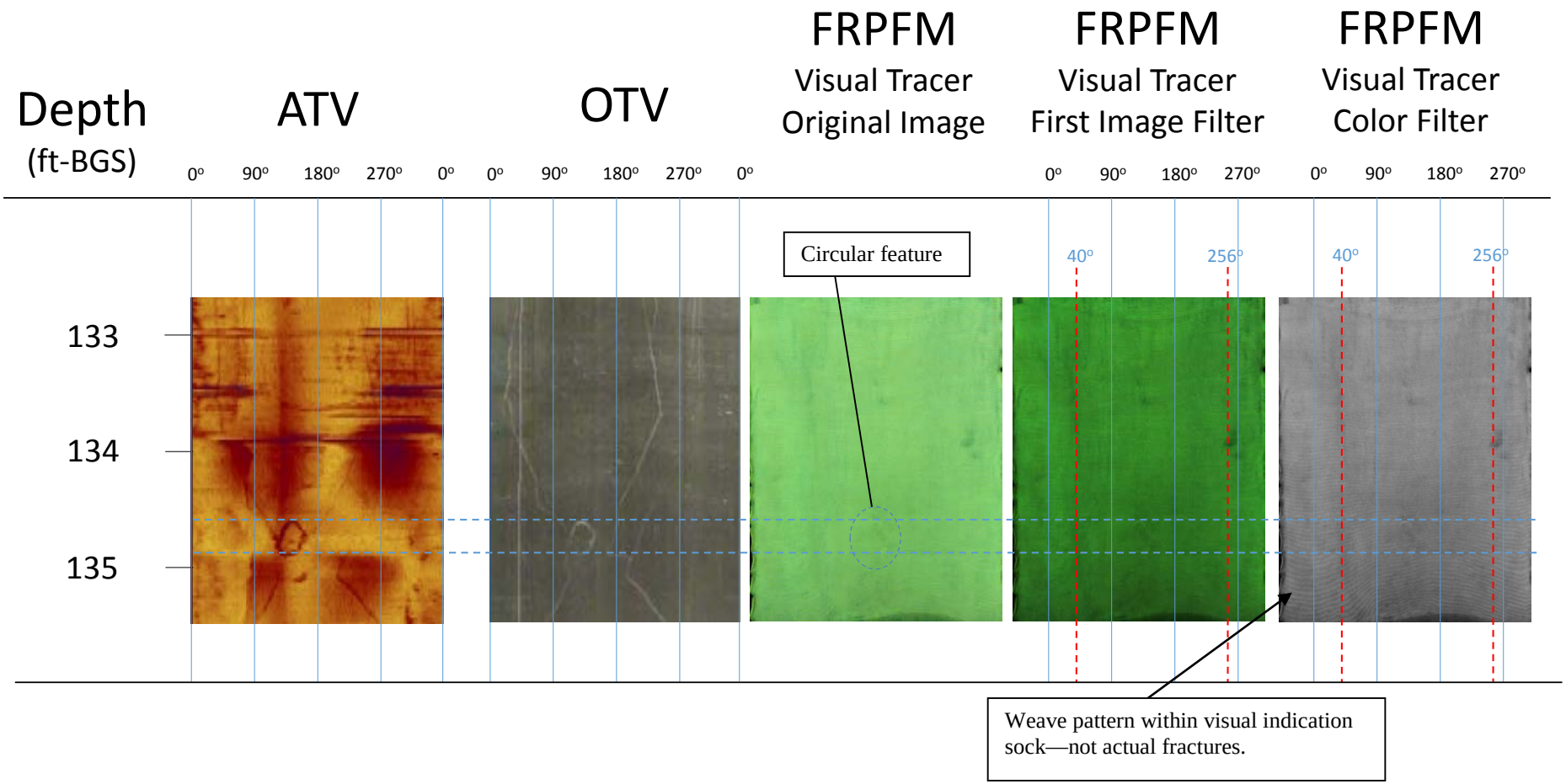

Figure 50. Test R Comparison of ATV/OTV with FRPFM visual indications of flowing circular feature intersecting two high-angle fractures. The FRPFM images were processed using multiple filters to enhance the circular feature and high angle fractures. Note: one side effect of image filtering was the enhanced appearance of weave pattern within the visual indication sock material.

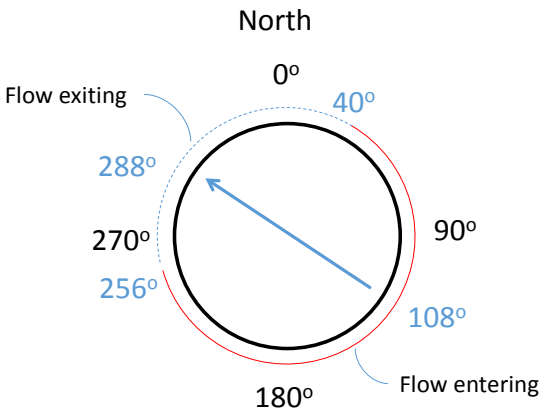

Visual traces indicate where flow enters the FRPFM—flow direction is offset by 180 degrees

General Direction of Flow = 288º = (WNW)

Figure 51. Test R inferred general flow direction from visual features on FRPFM sock (Figure 50).

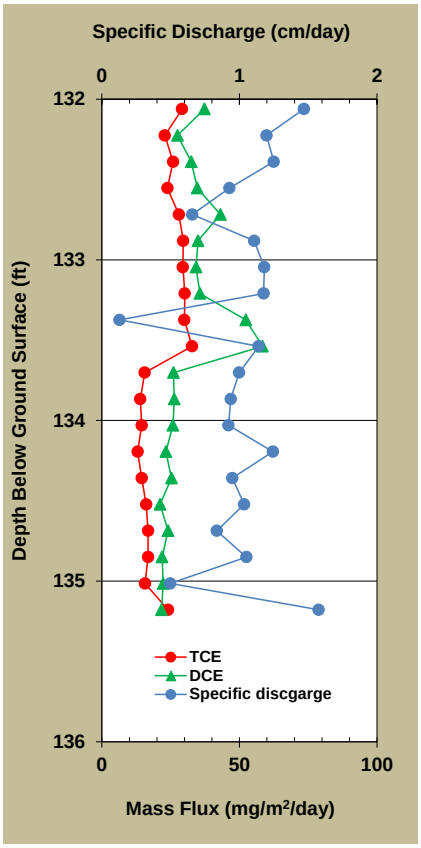

Figure 52. Test R vertical distribution of water and contaminant fluxes within FRPFM interrogation zone.

6.0 PERFORMANCE ASSESSMENT

6.1 SUMMARY OF DATA TYPES AND PERFORMANCE OBJECTIVES

The FRPFM provides independent measures of 6 data types with regard to actively flowing fractures. Data types correspond to the quantitative performance objectives outlined in Table 1: 1) detection of flowing fractures, 2) fracture location (depth), 3) fracture orientation, 4) fracture flow direction, 5) groundwater flux (specific discharge), and 6) contaminant mass flux.

It is important to note that the FRPFM technology suite provides redundancy for data types 1, 2, and 5 as they are each simultaneously and independently measured by two different technology components of the FRPFM—the visual tracer and the alcohol tracers. Imagery of the visual indication sock provides high resolution measures for data types 1, 2, and 5. The alcohol tracers also provide measures of data types 1, 2, and 5 with the resolution of these measures defined by the size of the sampling interval of the FRPFM sorbent—smaller samples with higher frequency provide higher resolution.

Data type 3 and 4 are determined through evaluation of a visual tracer. Evaluation of the individual features provides information relative to fracture orientation (e.g. azimuth and dip), while referencing centroids for all individual features to magnetic north (based upon FRPFM accelerometer directional orientation) provides flow direction information.

Data types 5 and 6 are obtained independently from the elution of internal alcohol tracers from and the sorption of contaminant mass to the FRPFM sorbent. It should be noted that the ratio of FRPFM measures of contaminant mass flux and groundwater flux can be used to estimate flux average contaminant concentrations, which can be compared to current and previous measures of aqueous contaminant concentrations obtained from standard groundwater sampling and comparative technologies.

When including the functional redundancy for data types 1, 2, 5 and 6 as discussed above, the FRPFM effectively provides independent measures of 10 data types as outlined in Table 20. The data type IDs listed in Table 20 were established to indicate which quantitative performance objective each data type corresponds to. These 10 data types are the basis for discussion of results, as each data type is evaluated through comparisons of FRPFM results to measures from at least one other competing technology. These comparisons are then used to evaluate FRPFM performance.

Table 20. Summary of data type comparisons for all technologies used to evaluate FRPFM performance. Each data type is referenced to the appropriate performance objective (Table 1).

Data Type ID	Comparative Technologies		Performance Objective	
	Tech 1	Tech 2		
1A	HRTP	FRPFM Visual tracer	1	Detection of flowing fracture
1B	HRTP	FRPFM Alcohol tracers	1	Detection of flowing fracture
2A	ATV/OTV	FRPFM Visual tracer	2	Fracture location (depth)
2B	ATV/OTV	FRPFM Alcohol tracers	2	Fracture location (depth)
3	ATV/OTV	FRPFM Visual tracer	3	Fracture orientation
4	TVP	FRPFM Visual tracer	4	Fracture flow direction
5A	BHD	FRPFM Visual tracer	5	Water flux
5B	BHD	FRPFM Alcohol tracers	5	Water flux
6A	BHD	FRPFM sorbent	6	Contaminant flux
6B	BHD	FRPFM sorbent	6	Contaminant flux average concentration

6.2 DATA ANALYSIS METHODS

With regards to quantitative performance objectives, it is understood that future field application of this technology is contingent upon rigorous statistical comparison of FRPFM measures (e.g., solute and groundwater fluxes, flow direction, active fracture location and orientation) to those obtained using conventional/competitive technologies. For this purpose, classic regression analyses are conducted, but these are not sufficient on their own. To augment analysis, statistical methods from Bland and Altman (1986) were applied. These methods are briefly described in the following paragraphs.

When comparing two technologies or methods (e.g., A and B) for measuring a parameter of interest (i.e., groundwater flux), Bland and Altman (1986) recommend first plotting the difference $\Delta = a - b$ between measurements of the same parameter given by two methods against their mean $(a+b)/2$; where a and b are actual measurements of same parameter using methods A and B respectively. The plot allows one to investigate lack of agreement between methods A and B and to investigate any possible relationship between the measurement error and the mean of the two measurements (which is the best estimate of the unknown true value). Sometimes, the distribution measurement errors vary proportionately with the mean (as with log normally distributed random variables like concentration).

Assuming no relation between the difference (Δ) and the mean, the lack of agreement between methods or the bias is estimated from the mean difference ($\bar{\Delta}$) and the standard deviation of the differences (S). If differences are normally distributed (Gaussian), 95% of differences will lie between these limits of agreement:

$$\bar{\Delta} \pm 1.96 \bullet s$$

If the distribution of difference is not normal but skewed, other methods exist for determining asymmetric confidence intervals (Willink 2005).

Because the above limits of agreement are estimates for the population, standard errors and confidence intervals are used to assess the precision of the above estimated limits of agreement. Again, assuming normality the standard error (s_E) of the mean difference ($\bar{\Delta}$) is:

$$s_E = \sqrt{s^2/n}$$

where *n* is the number of samples. For the limits of agreement, the standard error (s_{EL}) of $\bar{\Delta} - 1.96 \bullet s$ and $\bar{\Delta} - 1.96 \bullet s$ is approximately:

$$s_{EL} = \sqrt{3s^2/n}$$

Confidence intervals (e.g. the 95% confidence interval) are calculated using an appropriate value of *t* (e.g. for α =0.05) obtained from t-distribution tables and assuming n -1 degrees of freedom. The confidence interval on the mean difference is:

$$\bar{\Delta} \pm t \bullet s_E$$

Whereas confidence intervals on the lower and upper limit of agreement are:

$$\bar{\Delta} - 1.97s \pm t \bullet s_E$$

$$\bar{\Delta} + 1.97s \pm t \bullet s_E$$

Since true water and contaminant flux cannot be known for most fractured flow systems, an alternative means of assessing performance is measurement agreement to a competing technology (Bland and Altman, 1986). The above approach is used to assess FRPFM performance with comparative technologies for each of the data type outlined in Table 20 based upon the quantitative performance objectives appearing in Table 1.

6.3 FIELD DEMONSTRATION RESULTS

In this section, the statistical analysis methods presented in section 6.2 are used to evaluate quantitative results for all field tests summarized in section 5.7. The discussion of results is organized based upon the performance objectives (Table 1) and corresponding quantitative data types (Table 20) used to evaluate each objective.

6.3.1. PERFORMANCE OBJECTIVE 1: IDENTIFICATION OF FLOWING FRACTURES

Evaluation of performance objective 1 is based upon analysis of two data type comparisons (Table 20). Data type 1A compares the identification of flowing fractures by HRTP and FRPFM visual tracers. While data type 1B compares the identification of flowing fractures by HRTP and FRPFM alcohol tracers. Quantitative comparison for identification of flowing fractures is based upon the depth at which flow was quantified by each technology. It should be noted that quantitative statistical comparisons can only be made for cases where both technologies identified active flow. Due to the higher resolution of detection by FRPFM visual tracers and alcohol tracers within the 1-meter interrogation zone, there were multiple instances where FRPFM indications of flow did not have a matching HRTP identified flow. But, all FRPFM target zones were initially selected based upon HRTP screening for flow.

For data type 1A there were 59 discrete flowing fractures identified by both HRTP and FRPFM visual tracers across all tests (A-R). The identified flow depths for both technologies are compared in figure 53. Statistical analysis of the results is summarized in figure 54 which compares the average depth of flow for each technology to the difference between measured depths. The mean difference is -0.24 ft with a standard error of 0.11 ft and limits of agreement between 0.78 and -1.26 ft corresponding to a 95% confidence interval (Bland and Altman, 1986). Results indicate good agreement between the two technologies with an average percent difference of -0.40% and the FRPFM estimating flow depths on average 0.24 ft (2.9 inches) higher than HRTP.

For data type 1B there were 26 discrete flowing fractures identified by both HRTP and FRPFM visual tracers across all tests (A-R). The identified flow depths for both technologies are compared in figure 55. Statistical analysis of results is summarized in figure 56 which compares the average depth of flow for each technology to the difference between measured depths. The mean difference is -0.14 ft with a standard error of 0.14 ft and limits of agreement between 0.69 and -0.96 ft corresponding to a 95% confidence interval (Bland and Altman, 1986). Results indicate good agreement between the two technologies with an average percent difference of -0.42% and the FRPFM estimating flow depths on average 0.14 ft (1.7 inches) higher than HRTP.

6.3.2. PERFORMANCE OBJECTIVE 2: FRACTURE LOCATION

Evaluation of performance objective 2 is based upon analysis of two data type comparisons (Table 20). Data type 2A compares the depth of fractures identified by ATV/OTV and FRPFM visual tracers. While data type 2B compares the depth of fractures identified by ATV/OTV and FRPFM alcohol tracers. An important clarification between data type 1 (identification of flowing fractures) and data type 2 (fracture location) is the capabilities of the technologies compared. For data type 1, each technology compared is capable of identifying flowing fractures, and as such is a measure of how accurately each technology identifies flow. Whereas, for data type 2, ATV and OTV are acoustic and optical measures of the borehole rock face with no indication of flow, and as such data type 2 is a comparison of the apparent location (depth) of features regardless of flow. An important distinction and benefit is that comparison of results for data type 2 allows for identification of which ATV/OTV features are actively flowing based upon FRPFM measures.

Evaluation of data type 2 consistently demonstrated that the FRPFM provides results at much higher resolution than existing optical and acoustic technologies (ATV/OTV); quantitative comparisons ATV/OTV for each field test typically indicated between 2 to 11 discrete fractures over the FRPFM interrogation interval, while the FRPFM typically identified from 3 to 63 discrete flowing fractures. Lab tests showed that the FRPFM is capable of identifying flowing fractures with aperture of 0.5 mm (Figure 28), which is below the detection limit of existing acoustic and optical devices.

Quantitative comparisons for fracture location are based upon fracture centroid depths identified by each technology. It should be noted that quantitative statistical comparisons can only be made for cases where both technologies identified fractures. Due to the higher resolution of FRPFM visual tracers and alcohol tracers within the 1-meter interrogation zone, there were multiple instances where FRPFM indications of flow did not have a matching ATV/OTV identified fracture.

For data type 2A there were 59 discrete fractures identified by both ATV/OTV and FRPFM visual tracers across all tests (A-R). The identified depths for both technologies are compared in figure 57. Statistical analysis of the results is summarized in figure 58 which compares the average fracture depth for each technology to the difference between measured depths. The mean difference is -0.0046 ft with a standard error of 0.04 ft and limits of agreement between 0.34 and -0.35 ft corresponding to a 95% confidence interval (Bland and Altman, 1986). Results indicate good agreement between the two technologies with an average percent difference of 0.01% and the FRPFM estimating flow depths on average 0.0046 ft (0.05 inches) higher than ATV/OTV.

For data type 2B there were 53 discrete flowing fractures identified by both ATV/OTV and FRPFM alcohol tracers across all tests (A-R). The identified flow depths for both technologies are compared in figure 59. Statistical analysis of the results is summarized in figure 60 which compares the average fracture depth for each technology to the difference between measured depths. The mean difference is 0.0042 ft with a standard error of 0.02 ft and limits of agreement between 0.17 and -0.16 ft corresponding to a 95% confidence interval (Bland and Altman, 1986). Results indicate good agreement between the two technologies with an average percent difference of 0.04% and the FRPFM estimating flow depths on average 0.0042 ft (0.05 inches) lower than ATV/OTV.

6.3.3. PERFORMANCE OBJECTIVE 3: FRACTURE ORIENTATION

Evaluation of performance objective 3 is based upon analysis of one data type comparison (Table 20). Data type 3 compares fracture orientation determined from ATV/OTV logs and FRPFM visual tracers. Two components of fracture orientation (azimuth and dip) are compared.

Quantitative comparison for fracture orientation is based upon the apparent shape of features identified by each technology. It should be noted that quantitative comparisons can only be made for cases where both technologies identified fractures. Due to the higher resolution of FRPFM visual tracers within the 1-meter interrogation zone, there were multiple instances where the FRPFM identified flowing fractures that did not have matching ATV/OTV fractures. An additional constraint for comparison is that ATV/OTV evaluation of azimuth and dip is usually

only determined for significant fractures intersecting a major portion of the borehole perimeter. This further reduces the number of fractures for one to one comparison of fracture orientation. In order to provide the most consistent comparison possible, Test O was selected for detailed analysis of FRPFM visual tracer features using the same methods typically applied to ATV/OTV logs. Test O was selected because it provides a complete demonstration of the full suite of FRPFM technologies.

Using data from Test O as the basis for data type 3 comparisons, there were 10 discrete flowing fractures identified by both ATV/OTV and FRPFM visual tracers that were consistently evaluated using typical ATV/OTV procedures. For fracture azimuth, the mean difference was 37.27 degrees with a standard error of 12.01 degrees. For fracture dip, the mean difference was 19.13 degrees with a standard error of 6.91 degrees. Results indicate good agreement between the two technologies with average percent differences of 3.34% and 1.92% respectively and the FRPFM estimating fracture azimuth and dip lower than ATV/OTV by an average 19.13 degrees and 6.91 degrees respectively.

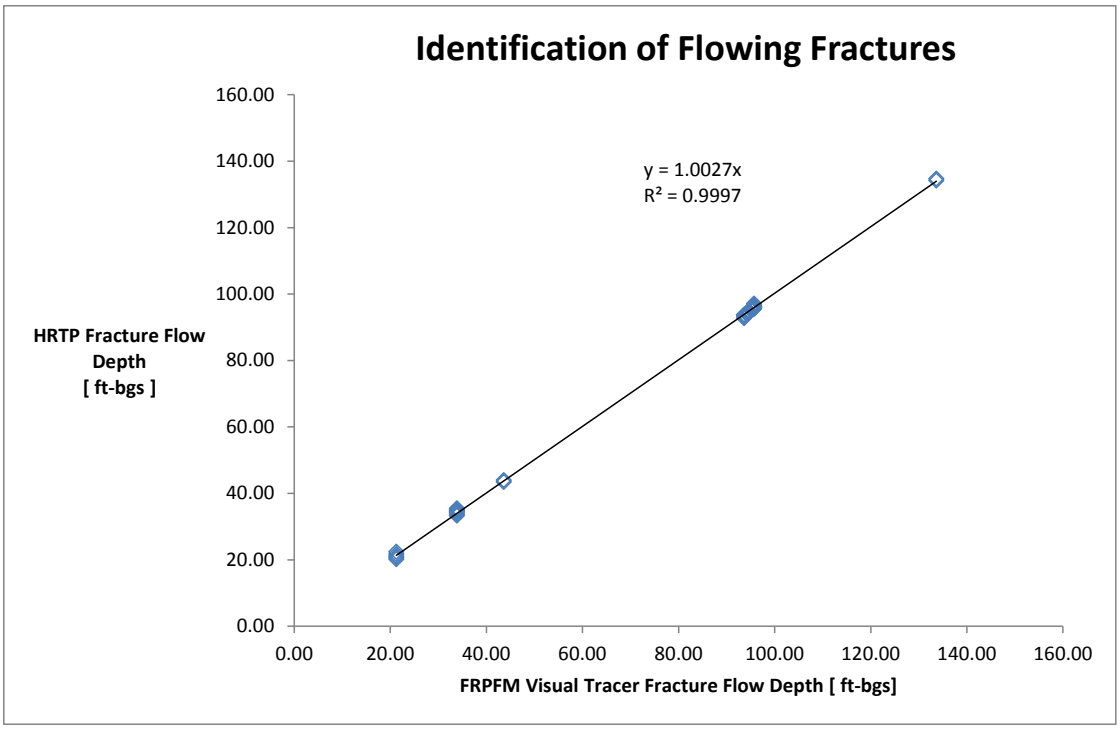

Figure 53. Comparison of results for data type 1A—identification of flowing fractures by HRTP and FRPFM visual tracers.

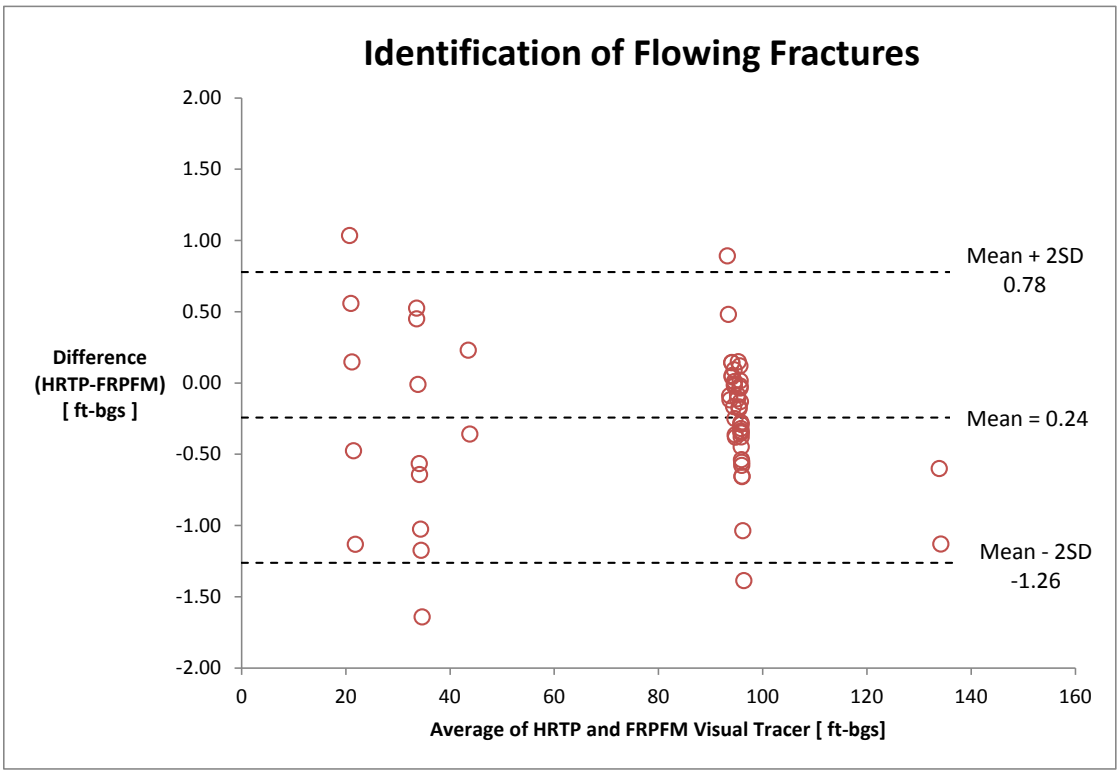

Figure 54. Summary of statistical analysis for data type 1A—identification of flowing fractures by HRTP and FRPFM visual tracers.

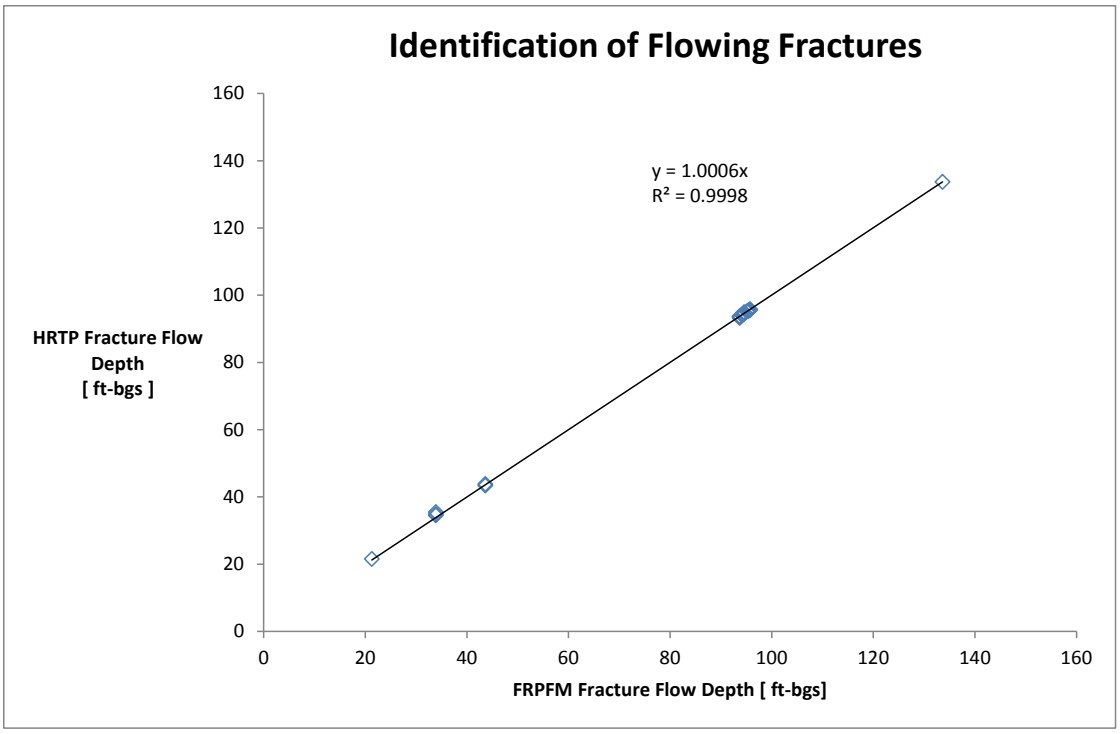

Figure 55. Comparison of results for data type 1B—identification of flowing fractures by HRTP and FRPFM alcohol tracers.

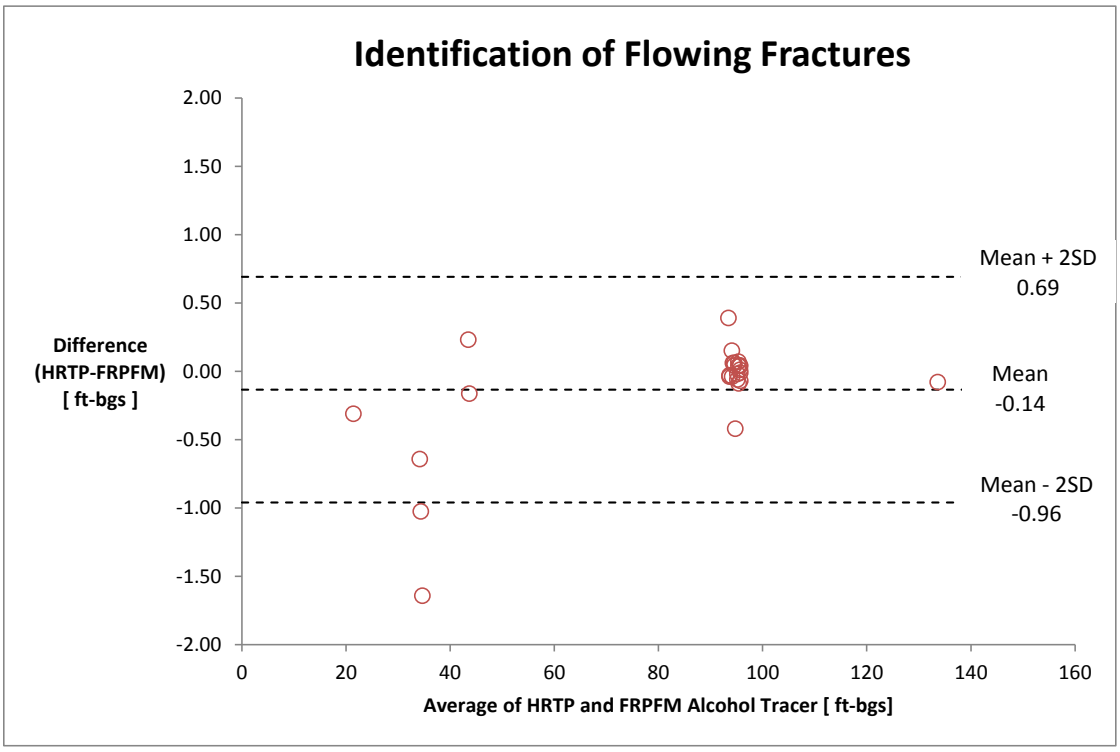

Figure 56. Summary of statistical analysis for data type 1B—identification of flowing fractures by HRTP and FRPFM alcohol tracers.

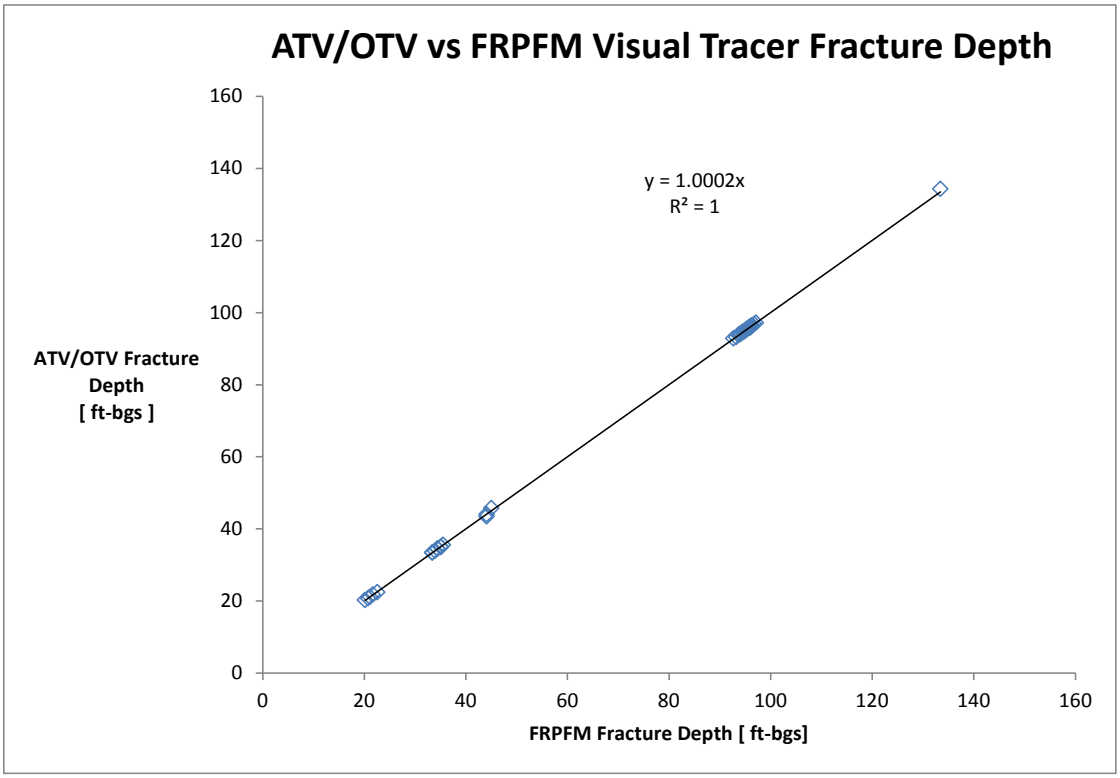

Figure 57. Comparison of results for data type 2A—fracture location by ATV/OTV and FRPFM visual tracers.

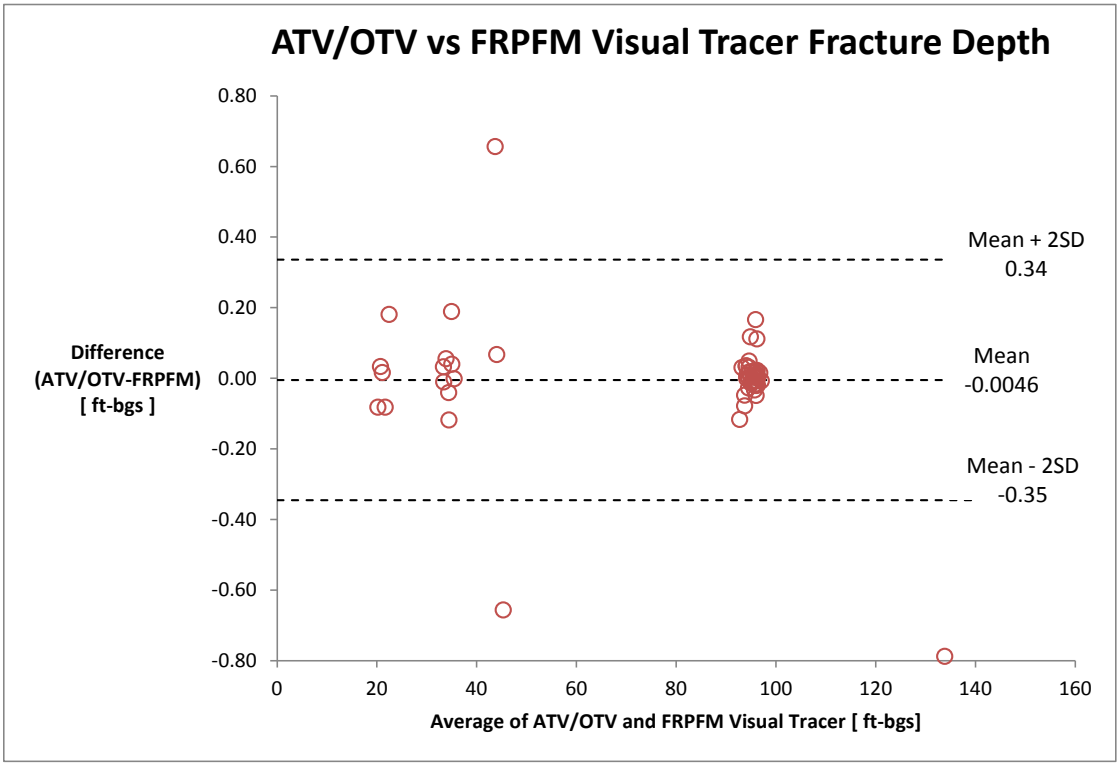

Figure 58. Summary of statistical analysis for data type 2A—fracture location by ATV/OTV and FRPFM visual tracers.

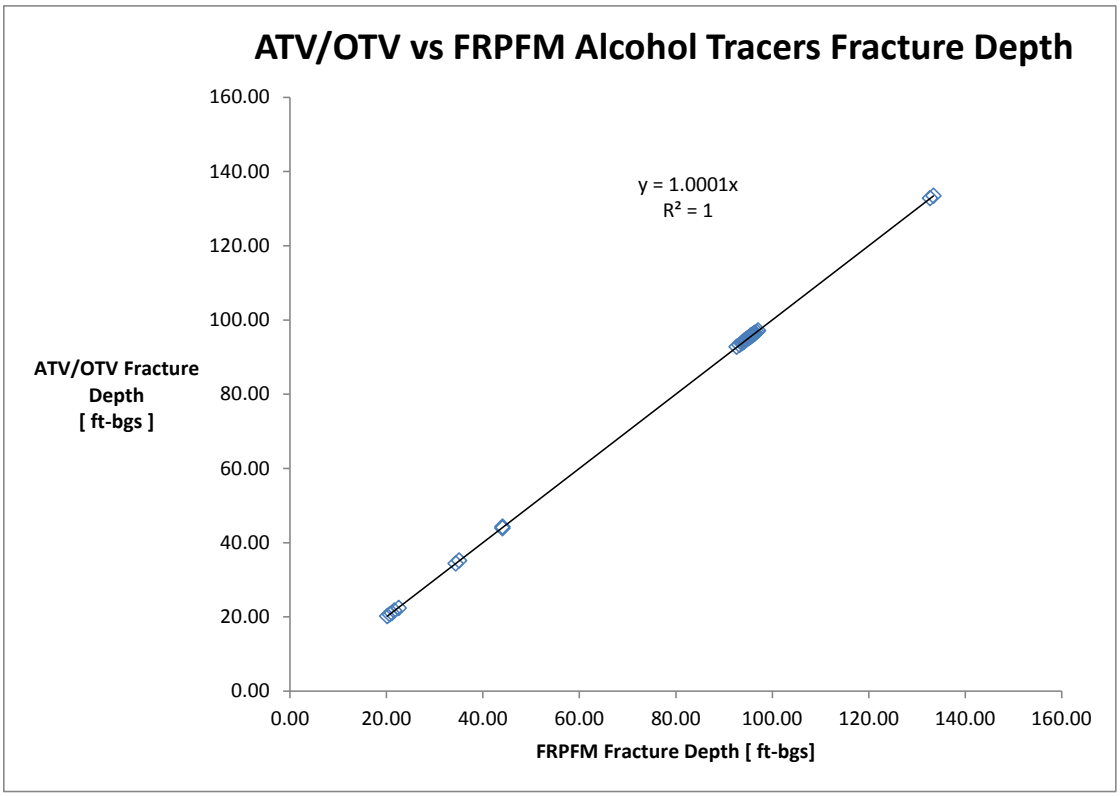

Figure 59. Comparison of results for data type 2B—fracture location by ATV/OTV and FRPFM visual tracers.

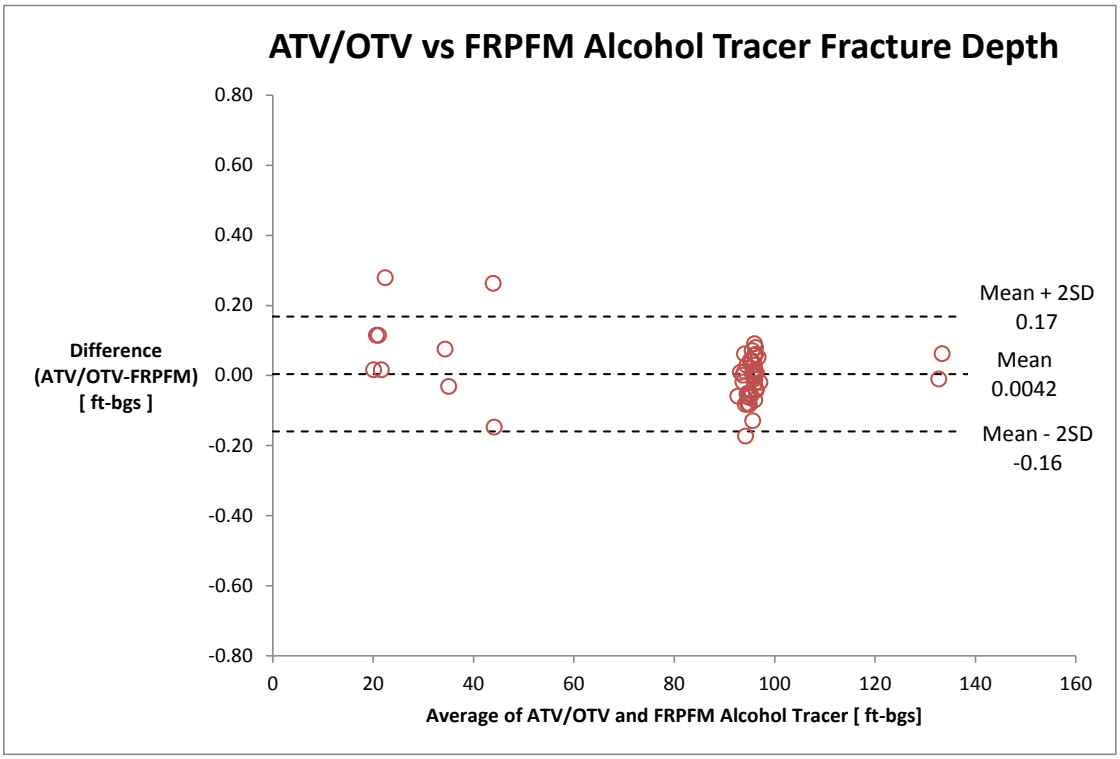

Figure 60. Summary of statistical analysis for data type 2B—fracture location by ATV/OTV and FRPFM visual tracers.

6.3.4. PERFORMANCE OBJECTIVE 4: FLOW DIRECTION

Evaluation of performance objective 4 is based upon analysis of one data type comparison (Table 20). Data type 4 compares flow direction estimated by TVP and FRPFM visual tracers. All flow direction comparisons are based upon reference to true north as summarized in figure 61. It is important to note that for fractured rock systems the hydraulic gradients and corresponding flow directions are both spatially and temporally variable, which makes high resolution measurement of flow direction considerably challenging. It follows that the quantitative comparison of flow direction estimates is strongly influenced by the relative location and time of observation. The only way to guarantee a truly consistent comparison between two alternate technologies is for the observations to be made at the exact same location and time, which is typically not possible within a borehole.

Pehme et al. (2014) addresses the spatial and temporal variation of flow measurements using TVP for the Guelph Tool Site. Figure 62 summarizes TVP data collected at GTS with column f providing a vertical (spatial) distribution of the horizontal thermal vector relative to true north. It can be seen that between elevations 320-330 masl the general horizontal direction SE, but there is observable spatial variation within this zone, and considerable variation in overlying and underling zones.

FRPFM high resolution directional measures are based upon visual indication of discrete fracture flows within the FRPFM 1-meter interrogation zone, and as such will experience at least as much if not more spatial variation in flow direction when compared to TVP.

Bearing in mind the considerable spatial and temporal variations in fracture flow direction, comparisons of general flow direction based upon TVP and FRPFM technologies are summarized in Table 21. FRPFM directional measures can only be obtained when sufficient visual features are present on the visual indication sock—as such flow direction estimates were only possible for the 9 Tests included in Table 21 with an average percent difference of 19.13%. It is important to note that for Tests B, D, and G the flowing features identified by FRPFM were vertical not horizontal which may affect how their flow contribution is interpreted when compared to TVP.

For GTS the overall general flow direction was estimated as SSE using TVP (Pehme et al., 2014). For FRPFM Test B (deployment elevation 327.41 masl) the inferred flow direction over the 1-meter interrogation zone was W which corresponds to scatter present in the TVP distribution at that depth. For FRPFM Test D (deployment elevation 331.94 masl) the inferred flow direction over the 1-meter interrogation zone was SW which corresponds to a strong line of scatter present in the TVP distribution at that depth. For FRPFM Tests F and G (deployment elevation 331.6 masl) the inferred flow direction over the 1-meter interrogation zone was S which corresponds well to a scatter cluster in the TVP distribution at that depth and is reasonably close to the TVP general flow direction.

For NAWC the issues of spatial and temporal variation were more pronounced due to the active pump and treat activities on site. As mentioned previously, it is not possible to deploy both TVP and FRPFM at the same time, which means that a truly consistent comparison is not possible. Due to logistics of mobilization and running tests in parallel on two sites, all ATV/OTV logging

and any procedures requiring a FLUTe liner were performed prior to FRPFM testing. HRTP/TVP was performed at NAWC in June, 2012 with FRPFM tests commencing in July of 2012 and running through November 2013.

For FRPFM Test J (deployment 95 ft-bgs) the inferred flow direction over the 1-meter interrogation zone was WSW which compares reasonably well with the TVP direction of WNW at this depth. A likely contributor to the slight difference in measured flow direction was that the pump and treat plant underwent a carbon exchange during the same period as HRTP/TVP testing. During carbon exchange the protocol on site is to reduce the pumping rate at extraction well 15BR which is located SW of FRPFM well 68BR (Figure 13) while maintaining extraction rates at all other wells on site. With extraction rates reduced at 15BR the next closest well is 29BR located NW of FRPFM well 68BR (Figure 13).

For FRPFM Test K (deployment 96.64 ft-bgs) the inferred flow direction over the 1-meter interrogation zone was WSW which compares reasonably well with the TVP direction of WNW at this depth when taking into account the onsite pumping conditions as discussed above. For FRPFM Test O (deployment 95.12 ft-bgs) the inferred flow direction over the 1-meter interrogation zone was SSW while TVP indicated a direction of WNW at this depth. A key note here is that temporal variations are likely more significant for Tests O, Q, and R flow direction comparisons as the FRPFM tests and TVP log were performed more than a year apart. During this period the distribution of extraction rates for pump and treat wells were altered as a new contractor took over operation of the pump and treat facility onsite. Extraction well 15BR was maintained as the well with highest extraction rate, but additional extraction wells were brought online. For FRPFM Test Q there were only faint visual indications of two discrete features along the same horizontal arc on the FRPFM at approximately 96.15 ft-bgs. The inferred flow direction from the faint visual features was ESE while TVP indicated a direction of WNW at this depth. Test R was the final FRPFM test performed at a deployment depth of 133.62 ft-bgs. The visual results were the most unique of all tests performed with faint but distinct visual indications of a circular feature (centroid at 134.75 ft-bgs) intersected by two high-angle fractures (Figure 50). Evaluation of the visual features inicates a general groundwater flow direction of WNW figures 50 and 51 which compares well with the TVP direction of WSW at this location.

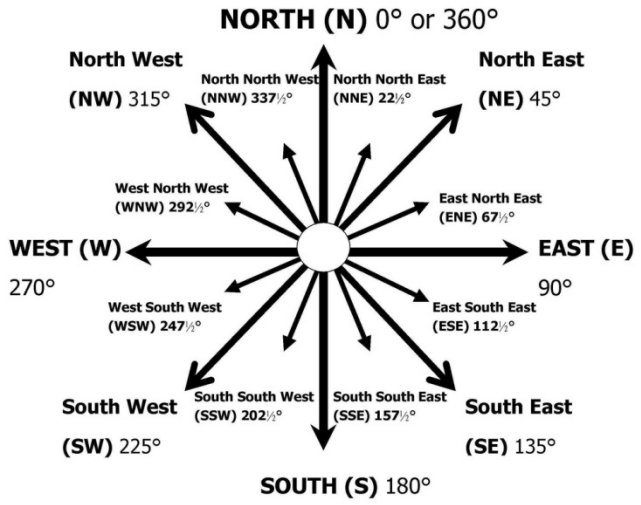

Figure 61. Flow directions referenced to true north.

Table 21. Summary of flow directions for all tests with comparative results.

	Test	HRTP/TVP Flow Direction	FRPFM Flow Direction
GTS	B	SSE (135°)	W (286°)
	D	SSE (135°)	SW (242°)
	F	SSE (135°)	S (177°)
	G	SSE (135°)	S (184°)
NAWC	J	WNW (299°)	WSW (245°)
	K	WNW (339°)	WSW (248°)
	O	WNW (313.5°)	SSW (199°)
	Q	WNW (339°)	ESE (113°)
	R	WSW (232°)	WNW (288°)

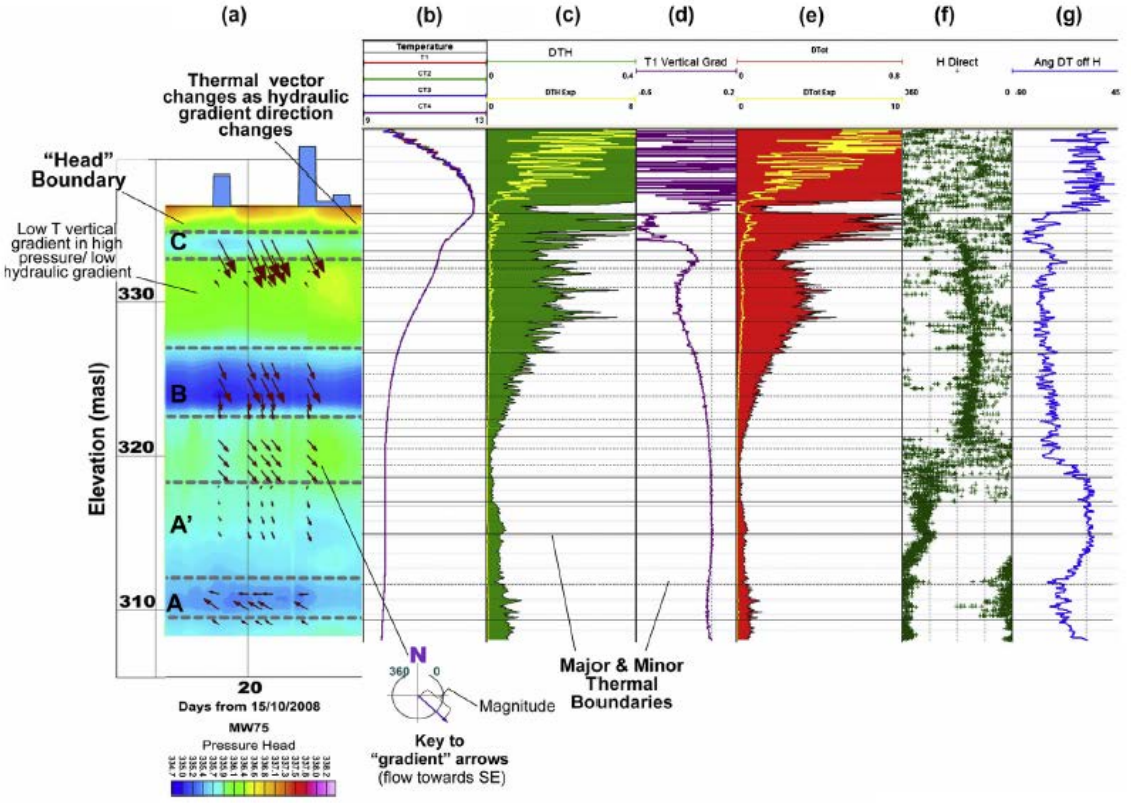

Figure 62. Comparison of TVP thermal vector components against local pressure head stratification and horizontal gradients. (a) Time-Elevation-Head (TEH) section with direction, (b) passive temperature data, (c) horizontal thermal vector, (d) vertical thermal gradient, (e) local thermal vector, (f) direction of horizontal thermal vector, (g) inclination of total thermal vector off horizontal (Pehme et al., 2014).

6.3.5. PERFORMANCE OBJECTIVE 5: ACCURACY OF WATER FLUX MEASUREMENTS

Evaluation of performance objective 5 is based upon analysis of two data type comparisons (Table 20). Data type 5A compares water flux values from BHD to those determined from FRPFM visual tracers. While data type 5B compares water flux values from BHD to those determined from FRPFM alcohol tracers.

For data type 5A there were two tests that produced measures for water flux (specific discharge) by both BHD and FRPFM visual tracers (Tests J and O). Using the methods of Bland and Altman (1986) the mean difference is 0.125 cm/day with a standard error of 1.17 cm/day and limits of agreement between 2.03 and -1.78 cm/day corresponding to a 95% confidence interval. Results indicate good agreement between the two technologies with an average percent difference of 8.41% and the FRPFM visual tracers estimating water fluxes on average 0.125 cm/day lower than BHD.

For data type 5B there were eight tests that produced measures for water flux (specific discharge) by both BHD and FRPFM alcohol tracers (Tests I, J, L and N-R). The measured water flux values for both technologies are compared in figure 63. Statistical analysis of the results is summarized in figure 64 which compares the average water flux for each technology to the difference between measured fluxes. The mean difference is 0.11 cm/day with a standard error of 0.17 cm/day and limits of agreement between 0.67 and -0.46 cm/day corresponding to a 95% confidence interval (Bland and Altman, 1986). Results indicate good agreement between the two technologies with an average percent difference of 6.70% and the FRPFM alcohol tracers estimating water fluxes on average 0.11 cm/day less than BHD.

6.3.6. PERFORMANCE OBJECTIVE 6: ACCURACY OF CONTAMINANT FLUX MEASUREMENTS

Evaluation of performance objective 6 is based upon analysis of two data type comparisons (Table 20). Data type 6A compares contaminant flux values from BHD to those determined from FRPFM. While data type 6B compares contaminant flux average concentrations from BHD to those determined from FRPFM. Two contaminants were measured at both sites, TCE and DCE.

For data type 6A there were 9 tests that produced measures for TCE flux by both BHD and FRPFM (Tests H, I, J, L, and N-R) and 8 tests that produced measures for DCE flux by both BHD and FRPFM (Tests I, J, L and N-R). The measured TCE and DCE flux values for both technologies are compared in figures 65 and 67 respectively. Statistical analysis of the results is summarized in figures 66 and 68 which compare the average contaminant flux for each technology to the difference between measured fluxes. The mean difference for TCE flux is 6,625 $\mu g/m^2$/day (6.6 mg/m^2/day) with a standard error of 9,450 $\mu g/m^2$/day (9.45 mg/m^2/day) and limits of agreement between 39,361 and -26,111 $\mu g/m^2$/day (39 to -26 mg/m^2/day) corresponding to a 95% confidence interval (Bland and Altman, 1986). Results indicate good agreement between the two technologies with the FRPFM estimating TCE fluxes on average 6,625 $\mu g/m^2$/day (6.6 mg/m^2/day) lower than BHD.

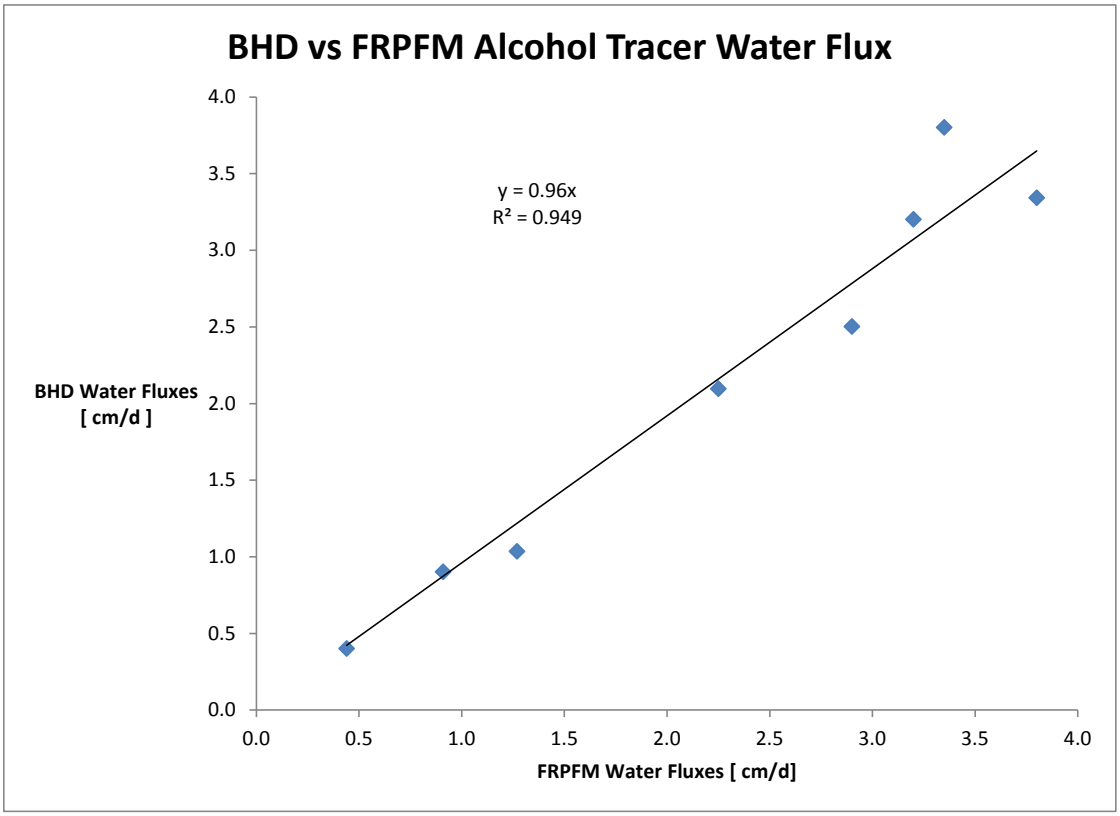

Figure 63. Comparison of results for data type 5B—water flux by BHD and FRPFM alcohol tracers.

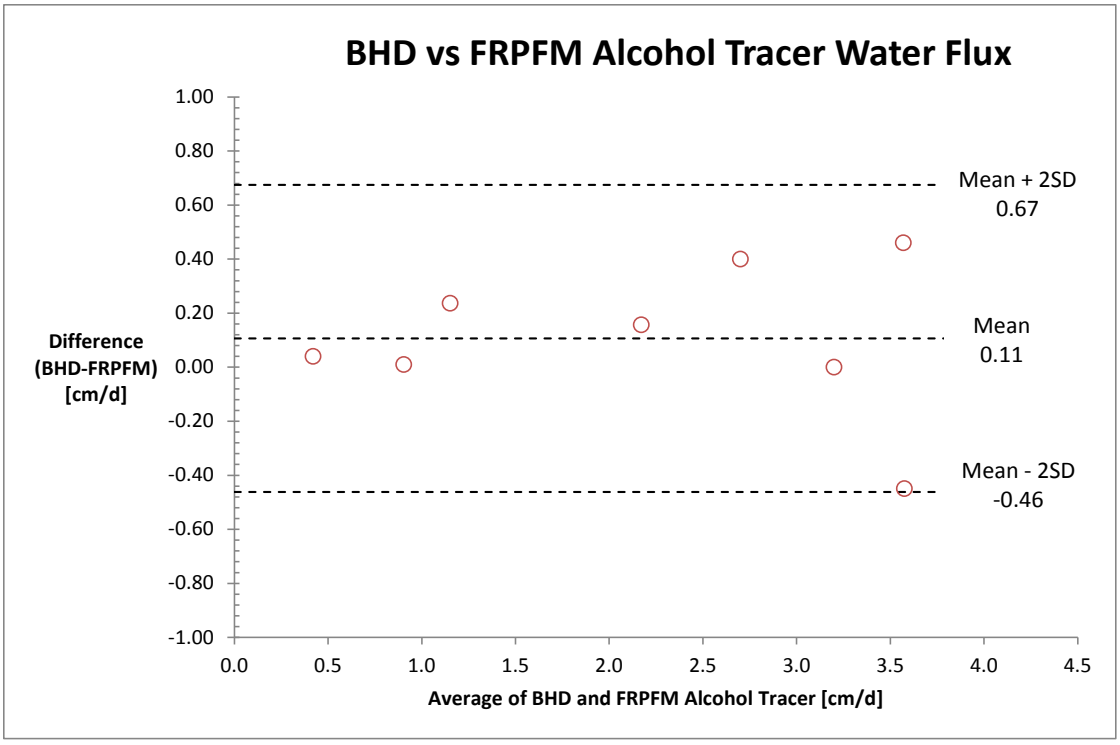

Figure 64. Summary of statistical analysis for data type 5B—water flux by BHD and FRPFM alcohol tracers.

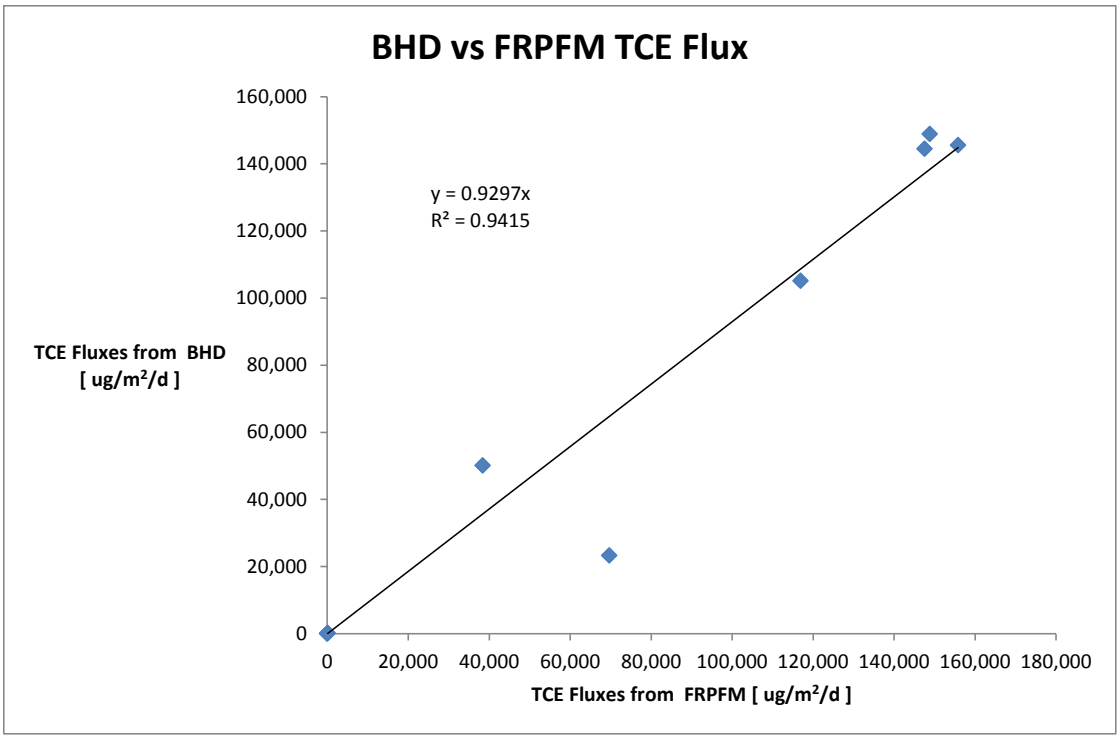

Figure 65. Comparison of results for data type 6A—TCE flux by BHD and FRPFM.

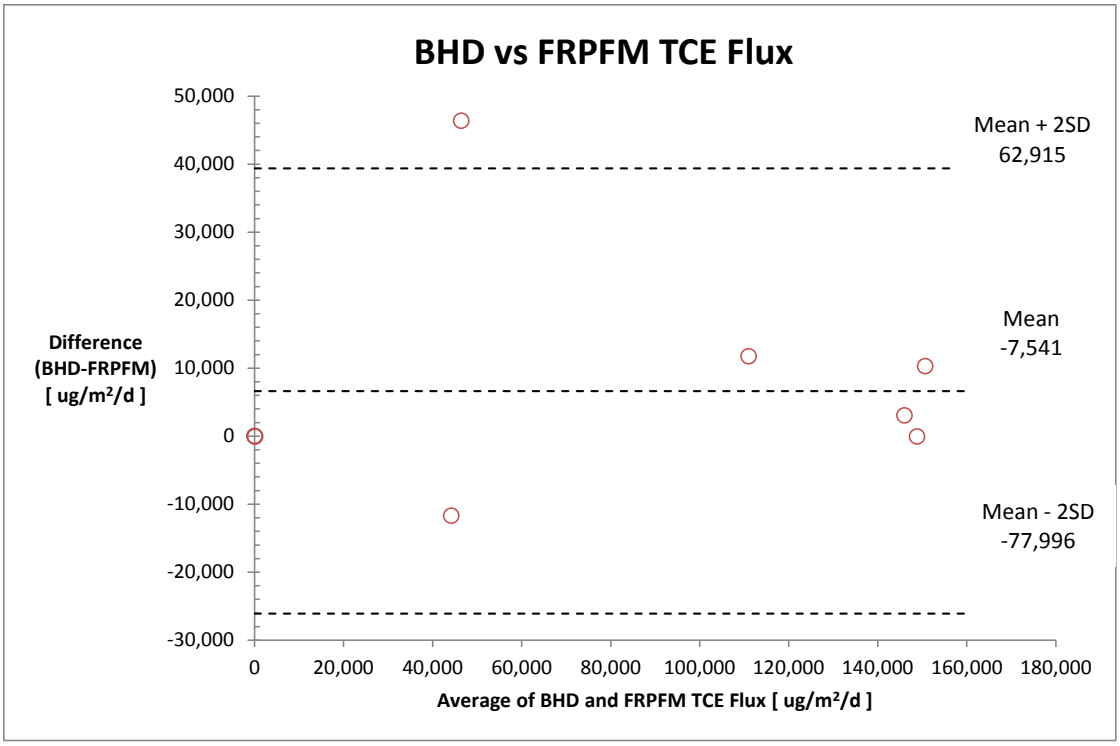

Figure 66. Summary of statistical analysis for data type 6A—TCE flux by BHD and FRPFM.

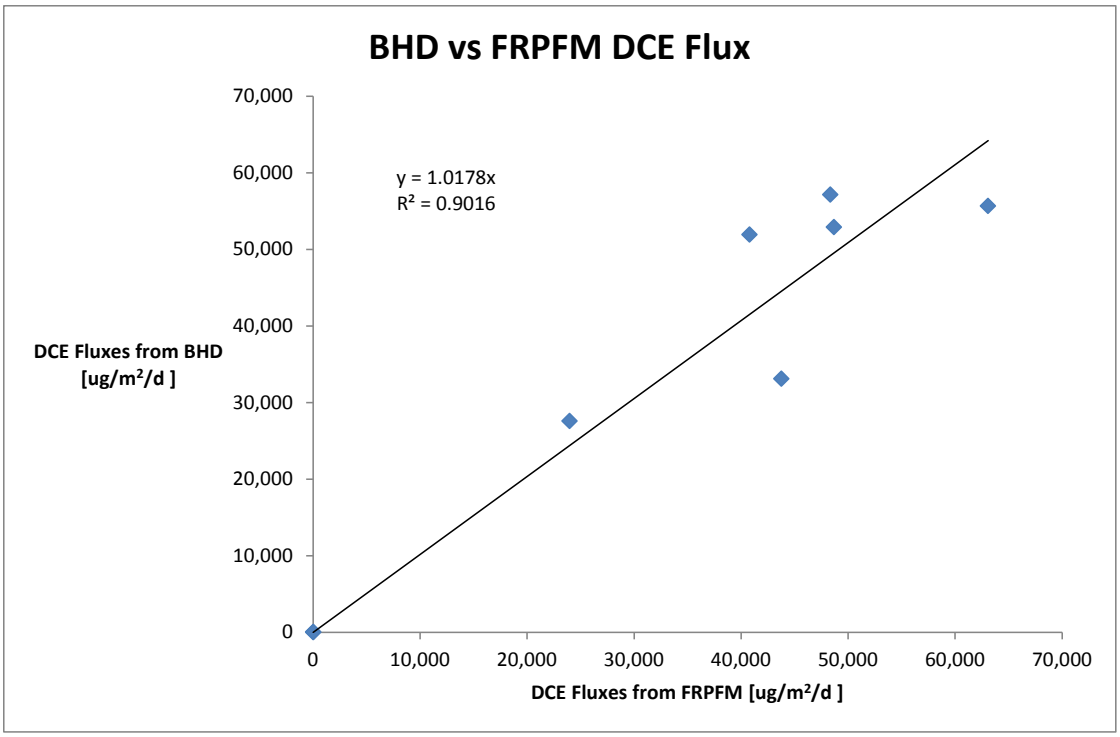

Figure 67. Comparison of results for data type 6A—DCE flux by BHD and FRPFM.

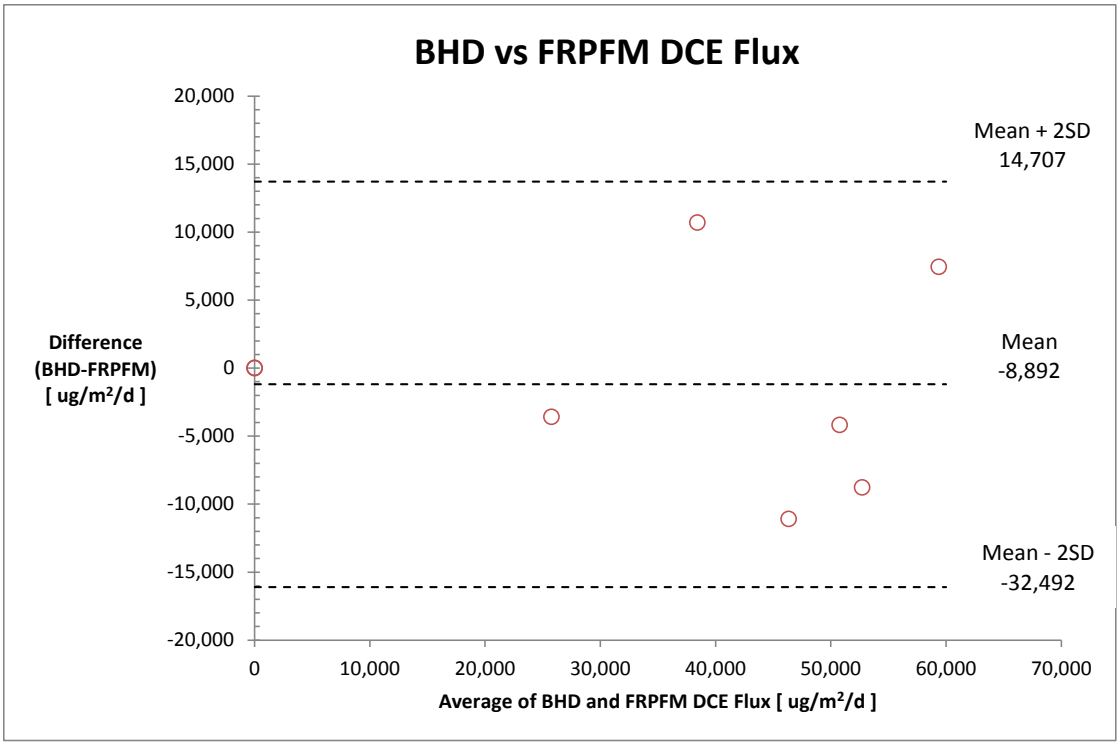

Figure 68. Summary of statistical analysis for data type 6A—DCE flux by BHD and FRPFM.

The mean difference for DCE flux is -1,187 µg/m^2/day (-1.2 mg/m^2/day) with a standard error of 4,564 µg/m^2/day (4.6 mg/m^2/day) and limits of agreement between 13,719 and -16,093 µg/m^2/day (13.7 to -16.1 mg/m^2/day) corresponding to a 95% confidence interval (Bland and Altman, 1986). Results indicate good agreement between the two technologies with the FRPFM estimating DCE fluxes on average 1,187 µg/m^2/day (1.2 mg/m^2/day) higher than BHD. The average percent difference between BHD and FRPFM measurements for both TCE and DCE flux is 2.0%.

For data type 6B there were 10 tests that produced measures for TCE flux average concentration by both BHD and FRPFM (Tests H-L and N-R) and 9 tests that produced measures for DCE flux average concentration by both BHD and FRPFM (Tests I-L and N-R). The measured TCE and DCE flux average concentration values for both technologies are compared in figures 69 and 71 respectively. Statistical analysis of the results is summarized in figures 70 and 72 which compare the mean flux average concentration for each technology to the difference between measured values. The mean difference for TCE flux average concentration is 552.65 µg/L (0.55 mg/L) with a standard error of 604.40 µg/L (0.60 mg/L) and limits of agreement between 2,760 and -1,654 µg/L (2.76 to -1.65 mg/L) corresponding to a 95% confidence interval (Bland and Altman, 1986). Results indicate good agreement between the two technologies with the FRPFM estimating TCE fluxes on average 552.65 µg/L (0.55 mg/L) lower than BHD.

The mean difference for DCE flux average concentration is -10.42 µg/L (-0.01 mg/L) with a standard error of 180.51 µg/L (0.18 mg/L) and limits of agreement between 615 and -636 µg/L (0.615 to -0.636 mg/L) corresponding to a 95% confidence interval (Bland and Altman, 1986). Results indicate good agreement between the two technologies with the FRPFM estimating DCE fluxes on average 10.42 µg/L (0.01 mg/L) higher than BHD. The average percent difference between BHD and FRPFM for both TCE and DCE flux average concentration is 6.07%.

Evaluation of the quantitative performance objectives based upon average percent difference (Table 22) establishes good agreement between FRPFM measures and those provided by alternative technologies. The results demonstrate that the FRPFM provides accurate, independent and simultaneous measure of 6 data types: 1) detection of flowing fractures, 2) fracture location (depth), 3) fracture orientation, 4) fracture flow direction, 5) groundwater flux (specific discharge), and 6) contaminant mass flux. There is no other current technology that can currently measure all of these simultaneously.

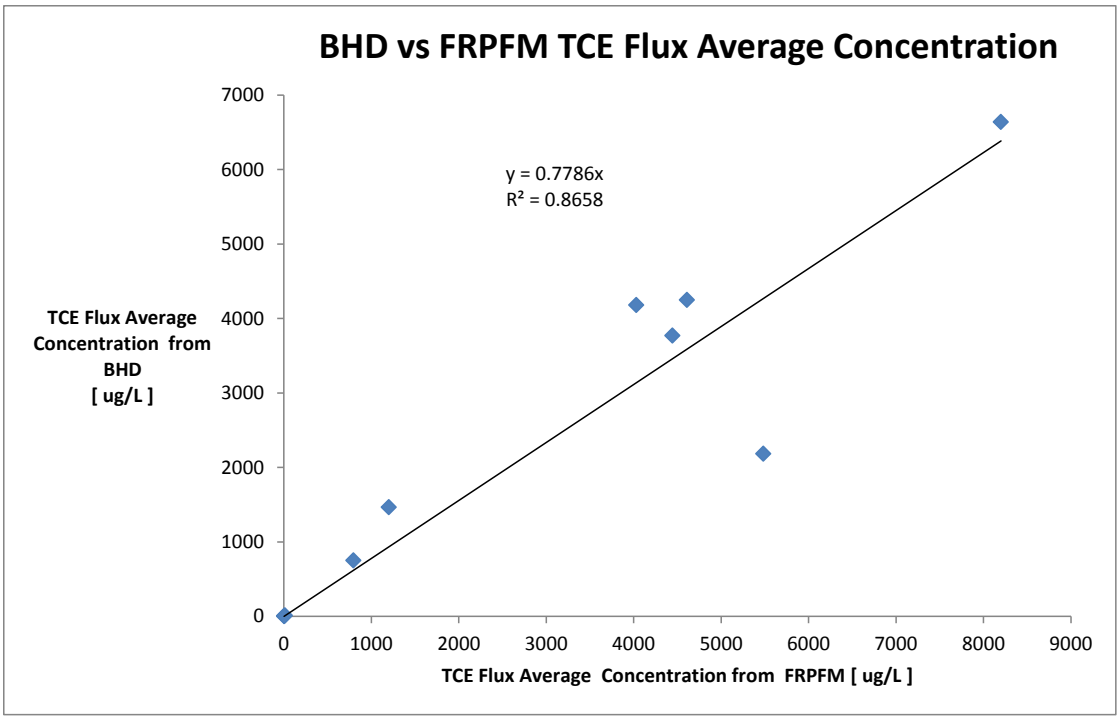

Figure 69. Comparison of results for data type 6B—TCE flux average concentration by BHD and FRPFM.

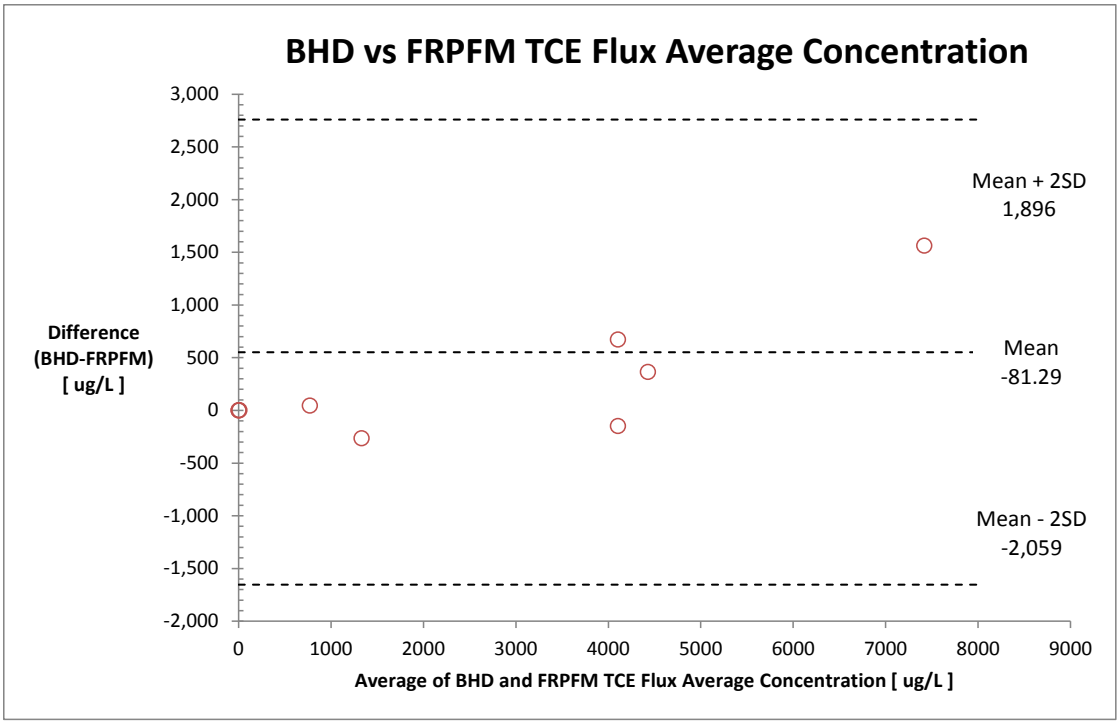

Figure 70. Summary of statistical analysis for data type 6B—TCE flux average concentration by BHD and FRPFM.

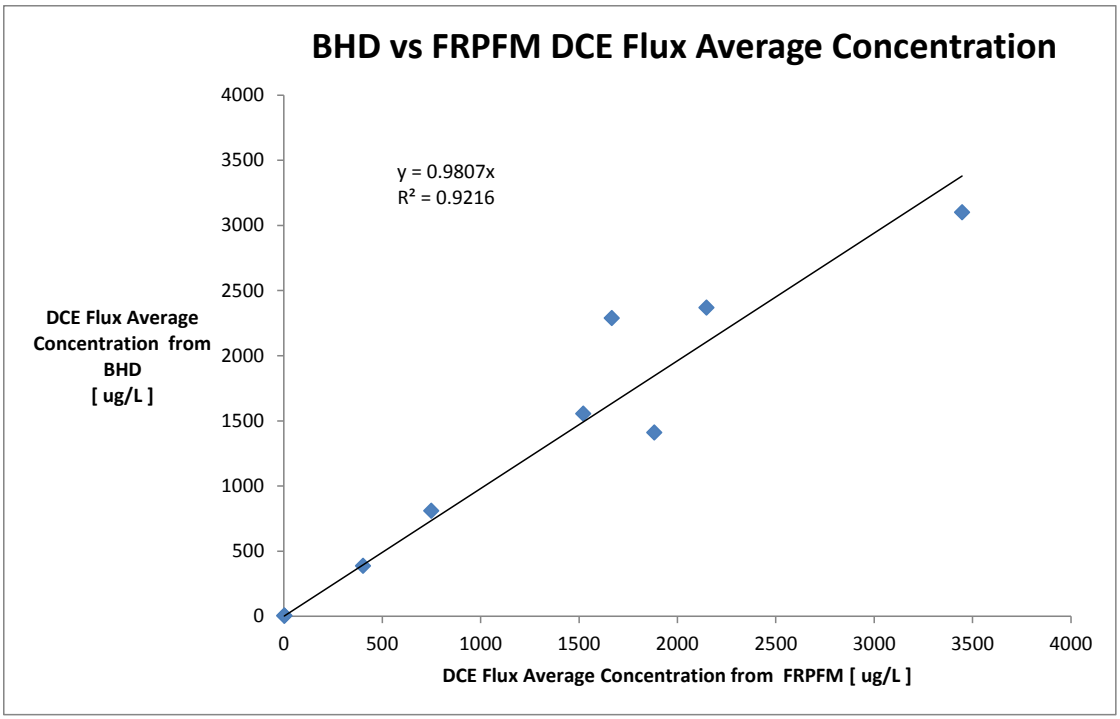

Figure 71. Comparison of results for data type 6B—DCE flux average concentration by BHD and FRPFM.

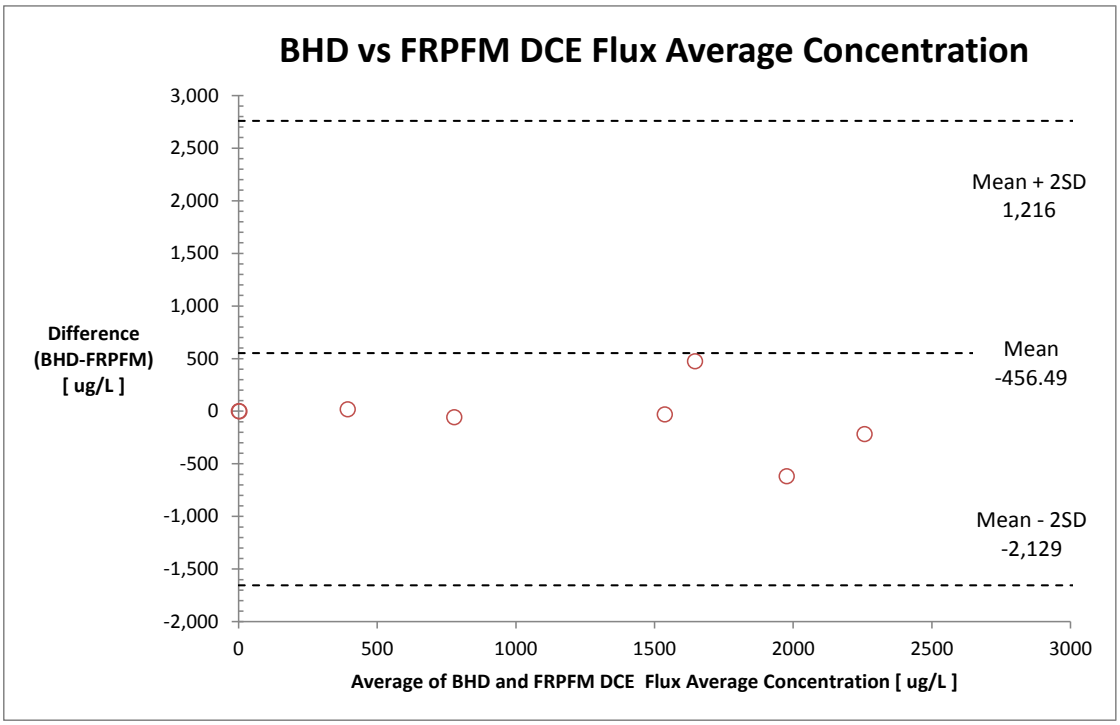

Figure 72. Summary of statistical analysis for data type 6B—DCE flux average concentration by BHD and FRPFM.

Table 22. Summary of Quantitative Performance Objectives with Comparative Results.

Performance Objective		Data Requirements	Success Criteria	Technology Comparison
Quantitative Performance Objectives				**Average Percent Difference**
1	Detection of Flowing Fractures	Measures from visible and non-visible FRPFM tracers and comparative technologies	Detect presence of flowing fractures +/- 10%	-0.42%
2	Fracture location (depth)	Measures from visible and non-visible FRPFM tracers and comparative technologies	Detect fracture location within +/- 10%	-0.04%
3	Fracture orientation	Visible dye measures and measures from comparative technology	Measurement validation to within *+/- 15%*	3.3 %
4	Fracture Flow Direction	Visible dye measures and measures from competing technology	Measurement validation to within *+/- 25%*	19.1%
5	Accuracy of water flux measurements	Measures from FRPFM and comparative technologies	Measurement validation to within *+/- 25%*	6.7%
6	Accuracy of contaminant flux measurements	Measures from FRPFM and comparative technologies	Measurement validation to within *+/- 25%*	2.0%

7.0 COST ASSESSMENT

7.1 COST MODEL

The FRPFM is the only technology that provides simultaneous measurement of 6 data types (Table 22) within fractured rock wells: 1) detection of flowing fractures, 2) fracture location (depth), 3) fracture orientation, 4) fracture flow direction, 5) groundwater flux (specific discharge), and 6) contaminant mass flux. The FRPFM provides high resolution measurements over a specific interrogation zone (currently 1 meter). Due to the high resolution nature of the technology, FRPFM application is meant to be focused on high priority target zones and not intended as tool for screening flow conditions across an entire borehole. In order to select the priority target zones, baseline characterization should include at a minimum standard ATV and OTV logs, and aqueous contaminant concentrations from zones of interest. Ideally, it is beneficial to have preliminary indications of potential flow zones based upon comparative and complementary technologies such as BHD and HRTP/TVP to help identify the priority zones for high resolution FRPM measurements.

The FRPFM technology currently functions through deployment of custom-built prototypes designed with a specified interrogation zone (typically 1 meter). Currently prototypes exist for application in 4-inch and 6-inch fractured rock wells. Determining the price for application is based upon the number of wells to be evaluated, the number of target deployment zones within each well, and the resolution of FRPFM sorbent analysis for water and contaminant flux distributions. The cost of mobilization and demobilization are dependent upon site location. In order to estimate the cost of FRPFM deployment it is assumed that the technology will be used to investigate 1 well with 1 (1-meter) interrogation interval and a sampling resolution of 20 samples (5 cm depth resolution) for flux estimates.

7.2 COST DRIVERS

7.2.1. COST ELEMENT: Mobilization

Mobilization encompasses required personnel and associated labor, planning, contracting, transportation/shipping requirements, permitting to secure regulatory approval for alcohol tracer use, and site preparation. The scale of mobilization will depend on the number of wells to be characterized.

7.2.2. COST ELEMENT: Baseline Characterization

Baseline characterization encompasses required personnel and associated labor, investigation into available site-specific literature, a preliminary site visit, water level measurements, contaminant sampling and analysis, sample shipping, analytical laboratory costs, and residual waste handling. The scale of baseline characterization will depend on the number of wells to be characterized.

7.2.3. COST ELEMENT: FRPFM

Deploying, extracting, and sampling the FRPFM will encompass required personnel and associated labor, capital equipment purchases, operator labor, operator training, raw materials, consumables, supplies, sampling, sample shipping, sample analysis, analytical laboratory costs, and residual waste handling. The scale of the FRPFM cost component will depend on the number interrogation zones to be investigated and the resolution of FRPFM sorbent analysis for water and contaminant flux distributions.

7.2.4. COST ELEMENT: Alternative Technologies

The alternative technologies element encompasses costs of using alternative technologies including: BHD and HRTP/TVP in a FLUTe liner. With the exception of BHD there are existing commercial entities that provide characterization services using the above technologies. For estimating costs of conducing borehole dilution, the following cost parameters will be tracked: transportation of personnel, materials and labor to construct a borehole dilution setup, shipping of equipment, water sampling, water sample analysis, analytical laboratory costs, and residual waste handling and all related labor related costs. The scale of the alternative technologies component will depend on the number of wells to be characterized.

7.2.5. COST ELEMENT: Demobilization

Demobilization encompasses required personnel and associated labor, planning, contracting, transportation/shipping requirements. The scale of demobilization will depend on the number of wells to be characterized.

7.3 COST ANALYSIS

Because the FRPFM is the only device capable of providing high resolution simultaneous measurement of the 6 data types outlined in Table 22, there are no alternative methods available for direct comparison of cost. BHD provides an alternative method for measuring two of the six data types: water and contaminant flux. However, for low flow conditions (<10 cm/day) required BHD test durations can approach 1 week requiring continuous staffing and maintenance (Test R at NAWC required a BHD test of 7 days to obtain stable contaminant flux estimate). HRTP and TVP provides an alternative method for measuring three of the six data types: presence of flowing fractures, fracture location, and flow direction. These methods have the added benefit that they provide characterization of these three measures over the entire depth of lined borehole. The TVP analysis used as basis of comparison in section 6 (Pehme et al., 2014) was performed in a lined borehole, which requires purchase of a FLUTe liner if one is not already in use. As many sites actively use liners, the purchase of a FLUTe liner is considered an optional cost.

In order to provide an accurate estimate for FRPFM cost the following conditions are assumed: all wells for testing are pre-existing (no drilling costs), minimal baseline characterization includes ATV/OTV and aqueous contaminant concentrations obtained within target zones. Table 23 outlines the total cost for FRPFM deployment assuming the technology will be used to investigate 1 well with 1 (1-meter) interrogation interval and a sampling resolution of 20 samples (5 cm depth resolution) for flux estimates. For most FRPFM operations, mobilization and demobilization are symmetric operations with similar costs, and the total mobilization and demobilization costs are combined to include all planning, travel, and salary. The FRPFM cost is broken out to show consumable materials and preparation, sample analysis, and interpretation of results. The total cost for FRPFM deployment, retrieval, sampling and analysis per the conditions outlined in Table 23 is $11,283. Table 24 provides a detailed breakdown of the cost to construct one FRPFM device. Once constructed, the FRPFM device can be used repetitively for approximately 25 deployments before routine maintenance is recommended and possible replacement of packer gum rubber may be required.

To provide an accurate BHD cost estimate for comparison to FRPFM it was assumed that the technology would be used to investigate 1 well with 1 (1-meter) interrogation interval with a total of 20 aqueous samples over the duration of the BHD test. Mobilization and demobilization costs are very similar to FRPFM with the primary difference being the amount of time staff must be on site to monitor BHD testing. It was assumed that a BHD test duration of 5 days would provide a reliable estimate for contaminant flux. Depending on the flow conditions, shorter duration tests (24 hour) will cost less while still provide reliable water flux estimates, but contaminant flux estimates would not be viable. The total cost for BHD testing per the conditions outlined in Table 25 is $11,295.

To provide an HRTP/TVP cost estimate for comparison to FRPFM it was assumed that the technology would be used to characterize flow over the entire depth of a 200-ft well. The cost of mobilization was considered to be comparable to FRPFM with the primary difference being that typical HRTP/TVP testing takes about three days per borehole. As mentioned previously, the purchase of a flute liner for HRTP/TVP testing is included as an optional cost. The total cost for HRTP/TVP testing per the conditions outlined in Table 26 is $6,722 if a FLUTe liner is already available, and $11,722 if the optional cost of a FLUTe liner is included.

Table 23. FRPFM Deployment Cost.

1	Nunber of wells	
1	Number of target intervals per well	
1	Total number of interrogation Intervals	
20	samples per FRPFM	
20	Total Number of Samples	
Costs		
Mobilizaton and Demobilization		
Travel		
2	Number of round trips	
2	days & nights per trip	
$350	Airline ticket per trip	
$70	Rental car per day (minivan)	
$140	Rental car total	
$120	Hotel per night	
$240	Hotel per trip	
$100	Fuel per trip	
$36	Perdiem (per person per day)	
$72	Perdiem per trip	
$902	Travel Total	
$300	shipping of equipment, supplies and samples	
$1,120	Salary and Benefits costs	(2 trips with 2 x 8-hour work days at $35/hour)
$2,322	**Total for mobilization and demobilization**	
FRPFM		
$500	FRPFM AC-felt and visual dye sock preparation	
$4,000	Sample analysis	($300 per sample for 20 samples)
$700	Interpretation of results	(20 hours at $35/hour)
$5,200	**FRPFM Total**	
$7,522	Direct Cost	
$3,761	IDC	
$11,283	**Total Cost**	
Construction Cost of one FRPFM Device (for 6-inch borehole with 1-meter interrogation zone)		
$1,989	Including materials and labor	(detailed cost is provided in Table 24)
Note: Construction cost does not include consumables such as AC-felt and visual dye sock.		

Table 24. FRPFM Construction Cost.

Cost to construct one FRPFM (6-inch diameter with 1-meter interrogation zone)[1]					
	Unit Cost		**Unit**		**Total Cost**
Gum rubber for packers (4" ID, 4.5" OD)[2]	$33.90	per foot	4.5	ft	$152.55
Gum rubber for core (3" ID, 3.5" OD)[2]	$20.00	per foot	3.5	ft	$70.00
PVC stock (rods) for packers (6" OD)	$96.00	per foot	4.5	ft	$432.00
Swageloc fittings	$12.00	each	8		$96.00
Tubing	$0.92	per foot	300	ft	$276.00
Low Profile Clamps	$7.60	each	10		$76.00
Stainless steel shield (material)	$40.60	per foot	10	ft	$406.00
Man hours (machinist)	$20.00	per hour	24	hours	$480.00
					$1,988.55

1 - Construction cost does not include consumables such as AC-felt and visual dye sock.
2 - Once constructed, the FRPFM device can be used repetitively for approximately 25 deployments before routine maintenance is recommended and possible replacement of packer gum rubber may be required.

Table 25. BHD Cost.

1	Number of wells	
1	Number of target intervals per well	
1	Total Number of Interrogation Intervals	
20	Total Number of Samples	
Costs		
Mobilizaton and Demobilization		
Travel		
1	Number of round trips	
5	days & nights per trip	
$350	Airline ticket per trip	
$70	Rental car per day (minivan)	
$350	Rental car total	
$100	Hotel per night	
$500	Hotel per trip	
$100	Fuel per trip	
$36	Perdiem (per person per day)	
$180	Perdiem per trip	
$1,480	Travel Total	
$300	shipping of equipment, supplies and samples	
$1,400	Salary and Benefit costs	(1 trip with 5 x 8-hour work days at $35/hour)
$3,180	**Total for mobilization and demobilization**	
BHD		
$4,000	Sample analysis	($300 per sample for 20 samples)
$350	Interpretation of results	(10 hours at $35/hour)
$4,350	**BHD Total**	
$7,530	Direct Cost	
$3,765	IDC	
$11,295	Total Cost	

Table 26. HRTP/TVP Cost.

HRTP/TVP Pricing			
	1	200-ft well	
	Costs		
	Mobilizaton and Demobilization		
	Travel		
	1	Number of round trips	
	2	days & nights per trip	
	$350	Airline ticket per trip	
	$70	Rental car per day (minivan)	
	$140	Rental car total	
	$100	Hotel per night	
	$200	Hotel per trip	
	$100	Fuel per trip	
	$36	Perdiem (per person per day)	
	$72	Perdiem per trip	
	$862	Travel Total	
	$300	shipping of equipment, supplies and samples	
	$560	Salary and Benefits costs	(1 trip with 3 x 8-hour work days at $35/hour)
	$1,722	**Total for mobilization and demobilization**	
	HRTP/TVP		
	$5,000	**HRTP/TVP without mobilization (typically 3 days work)**	
	$6,722	**Total Cost**	
	$5,000	Optional Cost of Flute liner for 200-ft well with installation	
	$11,722	Total HRTP/TVP optional with liner	
	Rental costs for HRTP/TVP equipment		
	$1,667	**per day**	

8.0 IMPLEMENTATION ISSUES

8.1 Environmental Checklist

Depending on site conditions, permits may be required for permission to release small quantities of food-grade tracers into the aquifer. A standard list of tracers is available, and no issues have been experienced with previous permit requests.

8.2 Other Regulatory Issues

Continuous contact with appropriate sire managers is strongly recommended through the duration of all testing to avoid issues with any site-specific regulations.

8.3 End-User Issues

The FRPFM technology currently functions through deployment of custom-built prototypes designed with a specified interrogation zone (typically 1 meter). Currently prototypes exist for application in 4-inch and 6-inch fractured rock wells. Deployment, retrieval and sampling is straightforward and has been demonstrated to field technicians from the University of Guelph and USGS who experienced minimal issues with methodology transfer.

As technology development continues, refinements will be made and applied to future prototypes (such as expanded interrogation zone). Site specific refinements can be made as needed.

9.0 REFERENCES

Acar, O., H. Klammler, K. Hatfield, M.A. Newman, M.D. Annable, J. Cho, B. Parker, J. Cherry, P. Pehme, P. Quinn, and R. Kroeker. 2013. A stochastic model for estimating groundwater and contaminant discharges from fractured rock passive flux meter measurements. Water Resources Research, 49. http://dx.doi.org/10.1002/wrcr.20109.

Annable, M.D., P.S.C. Rao, K. Hatfield, W.D. Graham, and A.L. Wood. 1998. Use of partitioning tracers for measuring residual NAPL: results from a field-scale test. ASCE Journal of Environmental Engineering, 124(6), 498-503.

Annable, M.D., K. Hatfield, J. Cho, H. Klammler, B. Parker, J. Cherry, and P.S.C. Rao. 2005. Field-scale evaluation of the passive flux meter for simultaneous measurement of groundwater and contaminant fluxes. Environmental Science and Technology, 39 (18), 7194 -7201.

Betz, A. 1964. Konforme Abbildung. Springer.

Cherry, J.A., B.L. Parker and C. Keller, 2007. A new depth-discrete multilevel monitoring approach for fractured rock. Ground Water Monitoring & Remediation, 27(2): 57-70.

CNSR. Feasibility Study: Former Bucks Harbor Air Force Radar Tracking Station, Machiasport, Maine. March, 2007. Report to U.S. Army Corps of Engineers. Concord, MA.

Guitierrez, G.M., Guimera, J., Yllera de Llano, A., Hernandez Benitez, A., Humm, J., Saltink, M., 1977. Tracer test at El Berrocal site. J. Cont. Hydrol. 26 (1997), 179– 188.

Goovaerts, P. 1997. “Geostatistics for natural resources evaluation”. Oxford University Press.

Guilbeault, M.A., B.L. Parker, and J.A. Cherry, 2005. Mass and flux distributions from DNAPL zones in sandy aquifers. Ground Water, 43(1):70-86.

Hatfield, K., M. Annable, J. Cho, P.S.C. Rao, and H. Klammler. 2004. A direct passive method for measuring water and contaminant fluxes in porous media. Journal of Contaminant Hydrology, 75 (3-4), 155-181.

Hatfield, K., M. Annable, J. Cho, P.S.C. Rao, H. Klammler. 2004. "A direct passive method for measuring water and contaminant fluxes in porous media". Journal of Contaminant Hydrology, 75(3-4), 155-181.

Kacimov, A., H. Klammler, N. Ilyinsky, K. Hatfield. 2011. "Constructal design of permeable reactive barriers: groundwater hydraulics criteria". Journal of Engineering Mathematics, 71(4), 319-338.

Keller, C., Cherry, J.A. and B.L. Parker. 2007. A New Method for Fracture Identification and Continuous Hydraulic Conductivity Profiling in Fractured Rock Boreholes, for submittal to Gound Water Monitoring and Review.

Klammler, H. 2004. “Conceptual models for advanced monitoring of subsurface and surface water and contaminant fluxes”, Ph.D Dissertation. Graz University of Technology, Austria.

Klammler, H., K. Hatfield, M. Annable, B. Parker, and J. Cherry. 2006., Device and method for measuring fluid fluxes, solute fluxes and fractured parameters in fractured flow systems, US Patent (SN 11/409,701).

Klammler, H., K. Hatfield, M. D. Annable, E. Agyei, B. Parker, J. Cherry, and P.S.C. Rao. 2007. General analytical treatment of the flow field relevant to the interpretation of passive fluxmeter measurements. Water Resour. Res., 43, W04407, doi:10.1029/2005WR004718.

Klammler, H., K. Hatfield, M. Annable, E. Agyei, B. Parker, J. Cherry, P.S.C. Rao. 2007. "General analytical treatment of the flow field relevant to the interpretation of passive fluxmeter measurements". Water Resources Research, 43(4), W04407.

Klammler, H., K. Hatfield, I. Perminova. 2009. Groundwater and contaminant travel time distributions near permeable reactive barriers. In: Water Resources Management V. C.A. Brebbia, V. Popov, eds. WIT Transactions on Ecology and the Environment, Vol. 125, ISBN 978-1-84564-199-3, 245-256.

Kitanidis, P.K. 1997. “Introduction to geostatistics: applications to hydrogeology”. Cambride University Press.

Lacombe, P.J., 2011. Mass of chlorinated volatile organic compounds removed by Pump-and-Treat, Naval Air Warfare Center, West Trenton, New Jersey, 1996–2010: U.S. Geological Survey Scientific Investigations Report 2011–5003, 48 p.

Lisle, R.J., P.R. Leyshon. 2004. "Stereographic Projection Techniques for Geologists and Civil Engineers", 2nd edition. Cambridge University Press, UK.

Newman, M.A., K. Hatfield, J.S. Hayworth, P.S.C. Rao, T.B. Stauffer. 2005. A hybrid method for inverse characterization of subsurface contaminant flux. Journal of Contaminant Hydrology. 81(1-4), 34-62.

Newman, M., K. Hatfield, J. Hayworth, P.S.C. Rao, and T. Stauffer. 2006. Inverse characterization of NAPL source zones. Environmental Science and Technology, 40(19), 6044-6050.

Novakowski, K., G. Bickerton, P. Lapcevic, J. Voralek, and N. Ross. 2006. Measurements of groundwater velocity in discrete rock fractures. Journal of Contaminant Hydrology. 82(1-2), 44-60.

Pehme, P.E., Parker, B.L., Cherry, J.A., Greenhouse, J.P., 2010. Improved resolution of ambient flow through fractured rock with temperature logs. Ground Water 28 (2), 191–211.

Pehme, P.E., Parker, B.L., Cherry, J.A., Molson, J., Greenhouse, J.P., 2013. Enhanced detection of hydraulically active fractures by temperature profiling in lined heated bedrock boreholes. J. Hydrol. (484), 1–15. http://dx.doi.org/10.1016/j.jhydrol.2012.12.048.

Pehme, P.E., Parker, B.L., Cherry, J.A., Blohm, D., 2014. Detailed measurement of the magnitude and orientation of thermal gradients in lined boreholes for characterizing groundwater flow in fractured rock. J. Hydrol. (484), 1–15. http://dx.doi.org/10.1016/j.jhydrol.2014.03.015.

Plett, J.H., 2006. Metolachlor and TCE plume characteristics in a dolomite aquifer using a transect. M.Sc. thesis, Dept. of Earth Sciences, University of Waterloo, Waterloo, Ontario.

Priest, S.D. 1985. "Hemispherical Projection Methods in Rock Mechanics". George Allen & Unwin (Publishers) Ltd., UK

SERDP/ESTCP 2006. SERDP and ESTCP expert panel workshop on reducing uncertainty of DNAPL source zone remediation, http://docs.serdp-estcp.org/viewfile.cfm?Doc=DNAPLWorkshopReport.pdf.

Sterling, S.N., B.L. Parker, J.A. Cherry, J.H. Williams, J.W. Lane Jr., and F.P. Haeni, 2005. Vertical cross contamination of trichloroethylene in a borehole in fractured sandstone. Ground Water, 43(4): 557-573.

Strack, O.D.L. 1989. Groundwater Mechanics. Prentice Hall.

Tiedeman, C.R., P.J. Laombe, and D.J. Goode. 2010. Multiple well-shutdown tests and site-scale flow simulation in fractured rocks. Ground Water, 48 (3): 401-415.

Willink, R. 2005. “A confidence interval and test for the mean of an asymmetric distribution”. Communications in Statistics – Theory and Methods, 34, 753-766.
Wilson, J.T., W.A. Mandell, F.L. Paillet, E. R. Bayless, R.T. Hanson, P.M. Kearl, W.B. Kerfoot, M.W. Newhouse, and W.H. Pedler. 1999. An Evaluation of Borehole Flowmeters Used to Measure Horizontal Ground-Water Flow in Limestones of Indiana, Kentucky, and Tennessee: U.S. Geological Survey Water-Resources Investigations Report 01-4139, 129 p.
Xu, Y., van Tonder, G., van Wyk, B., van Wyk, E., Aleobua, B., 1997. Borehole dilution experiment in a Karoo aquifer in
Bloemfontein. Water SA 23 (2), 141–145.

APPENDICES

Appendix A: Points of Contact

POINT OF CONTACT Name	ORGANIZATION Name Address	Phone Fax E-mail	Role in Project
Kirk Hatfield	University of Florida	Phone: 352-392-9537 Fax: 352-392-3394 Email: khh@ce.ufl.edu	Laboratory/field/modeling
Michael Annable	University of Florida	Phone: 352-392-3294 Fax: 352-392-3076 Email: annable@ufl.edu	Laboratory/field/analytical
Harald Klammler	University of Florida	Phone: 352-392-9537 Fax: 352-392-3394 Email: haki@gmx.at	Modeling/Statistical Analysis
Mark Newman	University of Florida	Phone: 352-392-9537 Fax: 352-392-3394 Email: markn@ce.ufl.edu	Laboratory/field/analytical
Beth Parker	University of Guelph	Phone: 519-824-4120 Fax: 519-836-0227 Email: bparker@uoguelph.ca	Field/laboratory
John Cherry	University of Guelph	Phone: 519-888-4516 Fax: 519-883-0220 Email: cherryja@rogers.blackberry.net	Field/modeling

Appendix B: Standard Operating Procedure for Analysis of Alcohol Tracers

SCOPE AND APPLICATION

1. This SOP describes the analytical procedures utilized by the University of Florida for analysis of alcohols used as partitioning tracers in both lab and field studies in order to quantify the amount and distribution of residual non-aqueous phase liquids (NAPLs) present in the saturated zone.

2. This SOP was written by R.D. Rhue, Soil and Water Science Department, University of Florida, Gainesville, Fl. It is a modification of SOP-UF-Hill-95-07-0010-v.2, prepared by D.P. Dai, H.K. Kim, and P.S.C. Rao, Soil and Water Science Department, University of Florida. The SOP of Dai, Kim, and Rao was modified from a protocol provided to them by Professor Gary Pope at the University of Texas-Austin.

3. The alcohol tracers used in the UF lab and field studies are ethanol, n-butanol, n-pentanol, n-hexanol, n-heptanol, 2,2-dimethyl-3-pentanol, and 6-methyl-2-heptanol.

4. The method involves gas chromatography (GC) analysis for alcohol concentrations in aqueous samples. A flame-ionization detector (FID) is used to quantify the analyte concentrations in the sample. The method has been found to provide reliable and reproducible quantitation of alcohols for concentrations > 1 ug/mL. This value may be considered the minimum detection level (MDL). The standard calibration curve for FID response has been found to be linear up to 3,000 ug/mL for ethanol.

5. Samples selected for GC-FID analysis may be chosen on the basis of preliminary screening which will provide approximate concentration ranges and appropriate sample injection volumes, standard concentrations, etc.

PURPOSE

The purpose of this SOP is to insure reliable and reproducible analytical results for alcohols in aqueous samples for laboratory-based or on-site (field-based) GC-FID analyses, and to permit tracing sources of error in analytical results.

PROCEDURES

1. Sample Containers, Collection, Transportation and Storage

Sample Containers: Field samples will be collected in 5-mL glass sample vials (Fisher Catalog # 06-406-19F) with teflon-faced septa caps. Glass vials and caps are not reused.

Sample Collection: Each field sample vial will be completely filled with liquid, such that no gas headspace exists, and capped. The vials will not be opened until the time for analysis.

Transportation and Storage: Field samples will be stored in coolers containing "blue ice", and later stored in refrigerators in a trailer located on the site. Samples may be subjected to on-site GC

analysis, and/or shipped back to UF labs; samples will be packed in coolers and shipped via overnight air express (e.g., FedEx). The samples will be stored in the cold storage room or refrigerator at 4C, until GC analysis. After sub-sampling, the samples are returned to cold storage.

For lab studies, samples will be collected directly in 2 mL GC vials whenever possible and stored in a refrigerator if analysis is expected to take more than a day.

2. Sub-sampling and Dilution

Field samples will be sub-sampled into 2-ml vials for automated GC analysis. Disposable, Pasture glass pipets (Fisher Catalog # 13-678-20B) will be used to transfer samples from 5-mL sample vials to the 2-mL GC vials.

For samples needing dilution prior to GC analysis, a dilution of 1:10 should be sufficient. Dilutions will be made using double-distilled, deionized water.

3. Apparatus and Materials

Glassware: Disposable micro-pipets (100 uL; Fisher Catalog # 21-175B; 21-175F) and Class A volumetric pipets (1 or 2 mL) are required for sample dilution.

Disposable Pasteur glass pipets (Fisher Catalog # 13-678-20B) are required for sub-sampling.

GC vials (2-mL) with Teflon-faced caps (Fisher Catalog # 03-375-16A) are required for GC analysis.

Volumetric class A pipets and volumetric class A flasks are required for preparations of the calibration standards.

Gas Chromatograph System: An analytical GC system with a temperature-programmable oven, auto-injector capable of on-column injection, and either an integrator or a PC-based data acquisition/analysis software system are required. Also required are other accessories, including analytical columns and the gases required for GC-FID operation.

A Perkin Elmer Autosystem with an FID and an integrated autosampler will be used for analysis of field and laboratory samples. The Perkin Elmer system will be linked to an IBM-compatible PC loaded with Turbochrom (version 4.01) software.

A J&W Scientific DB-624 capillary column (30m X 0.53mm, 3 □m film thick
Zero-grade air and ultra-high purity hydrogen will be used for the FID. Ultra-high purity nitrogen or helium will be used for carrier gas.

4. Reagents

Deionized, Double-Distilled Water: Deionized, double distilled water is prepared by double distillation of deionized water in a quartz still. This water will be referred to as reagent water.

Alcohols: Certified ACS grade alcohols will be purchased from Fisher Scientific and used as received.

5. Standard Solutions

Stock Standard Solution: Analytical standards will be prepared from reagent chemicals by the laboratory. Stock standards each contain a single alcohol dissolved in reagent water and stored in 20 mL glass vials (Fisher Catalog # 03-393-D) with teflon-lined caps. These stock solutions will be kept in a refrigerator at 4 C. Fresh stock standards will be prepared every six months. The procedure for making stock standard solutions is essentially that given in the Federal Register, Rules and Regulations, Thursday, November 29, 1979, Part III, Appendix C, Section 5.10, "Standard Stock Solutions". The only modification of the procedure for the current study is that reagent water is used as the solvent in place of methanol.

Calibration Standards: Calibration standards will be prepared by diluting the stock standards in reagent water. Each calibration standard will contain each of the alcohols listed above. Five concentrations will be prepared that cover the approximate concentration range utilized in the partitioning tracer experiments.

6. QC blank Spike/Matrix Spike

Two 1 mL aliquots of the sample to be spiked will be transferred to clean vials. To one vial, 1 mL of reagent water will be added. To the second vial, 1 mL of a calibration standard will be added. The spike recovery will be calculated using the difference between the two measured concentrations and the known spike concentration.

7. Quality Control

GC injector septa will be changed every 80 to 100 injections, or sooner if any related problems occur.

Injector liner will be cleaned or changed every 80 to 100 injections or sooner if any related problems occur.

A method blank will be included in every 50 samples

A complete set of calibration standards (5) will be run at the beginning of each day and after every fiftieth sample.

One standard and a blank will be included in every 25 samples.

A sample spike and a blank spike will be included in every 50 samples.

8. Instrumental Procedures

Gas Chromatography: For J&W DB-624 Column:

Injection port temperature 200C
FID detector temperature 225C

Temp Program: Isothermal at 60C for 0 min; Ramp to 120C at 5 C/min.

9. Sample Preparation

Sub-sampling: Field samples will be transferred from the 5 mL sample vials to the 2 mL GC vials and capped with open-top, teflon-lined septa caps.

Dilution: Samples will be diluted if chromatographic peak areas for any of the alcohols exceed those of the highest calibration standard. One mL of sample will be added to an appropriate amount of reagent water to make the dilution.

10. Sample Analysis

Analysis: The samples will be allowed to reach ambient temperature prior to GC analysis.

Sample vials (2 mL) will be loaded onto the Perking Elmer GC auto-injector. A one uL injection volume will be used for both samples and standards.

Analyte Identification: Analyte identification will be based on absolute retention times. The analytes of interest should elute at their characteristic retention times within □0.1 minute f automated GC system.

Analyte Quantitation: When an analyte has been identified, the concentration will be based on the peak area, which is converted to concentration using a standard calibration curve.

11. Interferences
Contamination by carry-over can occur whenever high-level and low-level samples are sequentially analyzed. To reduce carry over, the injector syringe should rinsed with reagent water between samples.

Potential carry-over will be checked by running a highly concentrated sample, but one still within the standard concentration range, followed by a blank. A negligible reading for the blank will insure that carry-over has been minimized.

12. Safety

The main safety issue concerning the use of the GC at a field site relates to the compressed gases. The FID gases (hydrogen and air) form explosive mixtures. It is important to keep this in mind at all times, and be aware of the hazard potential in the event of an undetected hydrogen leak. All gas connections will be properly leak tested at installation.

High-pressure compressed-gas cylinders will be secured to a firm mounting point, whether they are located internally or externally.

Gas cylinders should preferably be located outside the trailer on a flat, level base, and the gas lines run inside through a duct or window opening. If the gases are located outside, then some form of weatherproofing for the gauges will be necessary. As a temporary measure, heavy-duty polyethylene bags, secured with tie-wraps, have been used successfully; this may not be very elegant but it is very effective for short-term use of the GC. A more permanent protective housing must be built if the GC is located at the trailer for an extended time period.

The main operating drawback to locating the gas cylinders externally is that it is not easy to monitor the cylinder contents from inside. The gas which could be used up most quickly is air for the FID, particularly if two instruments are hooked up to the same supply and they are running continuously. A reserve cylinder of air should be available at all times to prevent down time.

If it is not possible to arrange external citing easily, the gas cylinders should be secured to a wall inside the trailer.

It is a good laboratory operating practice to make sure the flame is attended at all times.

When it is necessary to change the injection liner on the GC, the detector gases should be shut off.

The column must be connected to the detector before igniting the flame.

The trailer should be kept well ventilated when using the GC.

Reference to the Materials Safety Data Sheets (MSDS) will be made for information on toxicity, flammability, and other hazard data

Appendix C: Standard Operating Procedure for Analysis of Target Analytes in Groundwater Samples

SCOPE AND APPLICATION

1. This SOP describes the analytical procedures utilized by the Department of Environmental Engineering Sciences, University of Florida, for analysis of target analytes in groundwater samples from both lab and field studies. This analysis provides characterization of existing site and lab column aqueous contamination both before and following flushing technology applications.

2. This SOP was written by M.D. Annable, Department of Environmental Engineering Sciences, University of Florida, Gainesville, FL. It is a modification of SOP-UF-Hill-95-07-0012-v.2, prepared by D.P. Dai and P.S.C. Rao, Soil and Water Science Department, University of Florida.

3. The selected constituents are benzene, toluene, o-xylene, 1,1,1-trichloroethane, 1,3,5,-trimethylbenzene, 1,2-dichlorobenzene, decane, and naphthalene.

4. The method involves gas chromatography (GC) analysis for target analyte concentrations in aqueous samples. Headspace analysis with a flame-ionization detector (FID) is used to quantify the analyte concentrations in the sample. The method has been found to provide reliable and reproducible quantitation of the above constituents for concentrations > 5 ug/L. This value may be considered the method detection level (MDL).

5. Samples selected for GC-FID analysis may be chosen on the basis of preliminary screening which will provide approximate concentration ranges and appropriate sample injection times, and standard concentrations, etc.

PURPOSE

The purpose of this SOP is to insure reliable and reproducible analytical results for soluble NAPL constituents in aqueous samples for laboratory-based GC-FID analyses, and to permit tracing sources of error in analytical results.

PROCEDURES

1. Sample Containers, Collection, Transportation and Storage

Sample Containers: Field samples will be collected in 20-mL glass sample vials (Fisher Catalog # 03-340-121) with teflon-faced rubber backed caps. Glass vials and caps are not reused.

Sample Collection: Each field sample vial will be completely filled with liquid, such that no gas headspace exists, and capped. The vials will not be opened until the time for analysis.

Transportation and Storage: Field samples will be stored in coolers containing "blue ice", and later stored in refrigerators in a trailer located on the site. Samples will be sent to UF labs packed in coolers and shipped via overnight air express (e.g., FedEx). The samples will be stored in the cold storage

room or refrigerator at 4C, until GC analysis. After sub-sampling, the samples are returned to cold storage.

For lab studies, samples will be collected directly in 20 mL Headspace vials whenever possible and stored in a refrigerator if analysis is expected to take more than a day.

2. Sub-sampling and Dilution

Field samples will be sub-sampled placing 10-ml into 20-ml headspace vials containing 2 g of sodium chloride for automated GC analysis. Pipets will be used to transfer samples from 20-mL sample vials to the 20-mL GC headspace vials.

3. Apparatus and Materials

Glassware: Glass pipets are required for sub-sampling.

GC headspace vials (20-mL) with Teflon-faced caps are required for GC analysis.

Volumetric class A pipets and volumetric class A flasks are required for preparations of the calibration standards.

Gas Chromatograph System: An analytical GC system with a temperature-programmable oven, headspace sample injection system, and either an integrator or a PC-based data acquisition/analysis software system are required. Also required are other accessories, including analytical columns and the gases required for GC-FID operation.

A Perkin Elmer Autosystems with an HS40 Auto-headspace sampler and a FID will be used for analysis of field and laboratory samples. The Perkin Elmer system will be linked to an IBM-compatible PC loaded with Turbochrom (version 4.01) software.

A J&W Scientific DB-624 capillary column (50m X 0.53mm, 3 □m film thick
Zero-grade air and high purity hydrogen will be used for the FID. Ultra-high purity nitrogen or helium will be used for carrier gas.

4. Reagents

Deionized, Double-Distilled Water: Deionized, double distilled water is prepared by double distillation of deionized water in a quartz still. This water will be referred to as reagent water.

5. Standard Solutions

Stock Standard Solution: Analytical standards will be prepared from reagent chemicals by the laboratory. Stock standards will each contain a single analyte dissolved in methanol and stored in 20 mL glass vials (Fisher Catalog # 03-393-D) with teflon-lined caps. These stock solutions will be kept in a refrigerator at 4 C. Fresh stock standards will be prepared every six months. The procedure for making stock standard solutions is essentially that given in the Federal Register, Rules and

Regulations, Thursday, November 29, 1979, Part III, Appendix C, Section 5.10, "Standard Stock Solutions".

Calibration Standards: Calibration standards will be prepared by diluting the stock standards in water. Each calibration standard will contain each of the eight analytes listed above. Five concentrations will be prepared that cover the approximate concentration range from 0 to 20 mg/L.

6. QC blank Spike/Matrix Spike

Two 1 mL aliquots of the sample to be spiked will be transferred to clean vials. To one vial, 1 mL of reagent water will be added. To the second vial, 1 mL of a calibration standard will be added. The spike recovery will be calculated using the difference between the two measured concentrations and the known spike concentration.

7. Quality Control

A method blank will be included in every 50 samples

A complete set of calibration standards (5) will be run at the beginning of each day and after every fiftieth sample.

One standard and a blank will be included in every 25 samples.

A sample spike and a blank spike will be included in every 50 samples.

8. Instrumental Procedures

Gas Chromatography: For J&W DB-624 Column:

Headspace sample temperature	90C
Injection needle temperature	100C
Transfer line Temperature	110C
FID detector temperature	225C
Carrier gas pressure	8psi

Temp Program: Isothermal at 50C for 0 min; Ramp to 200C at 5 C/min; hold for 10 min.

9. Sample Preparation

Sub-sampling: Field samples will be transferred from the 20 mL sample vials to the 20 mL GC headspace vials and capped with open-top, teflon-lined septa caps.

Dilution: Samples will be diluted if chromatographic peak areas for any of the analytes exceed those of the highest calibration standard. One mL of sample will be added to an appropriate amount of reagent water to make the dilution.

10. Sample Analysis

Analysis: Sample headspace vials (20 mL) will be loaded onto the Perking Elmer HS40 auto-sampler. Samples will be pressurized for 1 min followed by a 0.1 minute injection time and a withdrawal time of 0.5 minute.

Analyte Identification: Analyte identification will be based on absolute retention times. The analytes of interest should elute at their characteristic retention times within ±0.1 minute for the automated GC system.

Analyte Quantitation: When an analyte has been identified, the concentration will be based on the peak area, which is converted to concentration using a standard calibration curve.

11. Interferences

Contamination by carry-over can occur whenever high-level and low-level samples are sequentially analyzed. To reduce carry over, the injector needle should purged with carrier gas between samples.

Potential carry-over will be checked by running a highly concentrated sample, but one still within the standard concentration range, followed by a blank. A negligible reading for the blank will insure that carry-over has been minimized.

12. Safety

The main safety issue concerning the use of the GC relates to the compressed gases. The FID gases (hydrogen and air) form explosive mixtures. It is important to keep this in mind at all times, and be aware of the hazard potential in the event of an undetected hydrogen leak. All gas connections will be properly leak tested at installation.

High-pressure compressed-gas cylinders will be secured to a firm mounting point, whether they are located internally or externally.

When it is necessary to change the injection liner on the GC, the detector gases should be shut off.

The column must be connected to the detector before igniting the flame.

Reference to the Materials Safety Data Sheets (MSDS) will be made for information on toxicity, flammability, and other hazard data.

Appendix D: Standard Operating Procedure for Extraction of Analytes from Flux Device Sorbents

SCOPE AND APPLICATION

1. This SOP describes the procedures used by the Department of Environmental Engineering Sciences, University of Florida, for extraction of target analytes (including tracers) from sorbents used in flux devices inserted in monitoring wells.

2. This SOP was written by M.D. Annable, Department of Environmental Engineering Sciences, University of Florida, Gainesville, FL.

3. The selected constituents are TCE, PCE, and alcohol tracers:

Methanol
Ethanol
2-propanol (IPA)
2-methyl-1-propanol (IBA)
2-methyl-2-propanol (TBA)
n-propanol
n-butanol
n-pentanol
n-hexanol
n-heptanol
3-heptanol
n-octanol
2-octanol
2,4-dimethyl-3-pentanol
2-ethyl-1-hexanol
3,5,5-trimethyl-1-hexanol
6-methyl-2-heptanol
2,6-dimethyl-2-heptanol
n-decane

Potential Sorbents include:

Liquid (mixed in a sand matrix at a pore volume saturation of 10%)
Tetradecane
Heptadecane
Hexadecane

Solid
Activated Carbon
Surfactant modified zeolytes

4. The method involves liquid extraction in 20 or 40 ml VOA vials using organic solvents.

PURPOSE

The purpose of this SOP is to insure reliable and reproducible analytical results. Extracted constituents will be quantified suing analytical methods described in other SOPs.

PROCEDURES

1. Sample Containers, Collection, Transportation and Storage

Sample Containers: Field samples will be collected in 20-mL or 40-ml glass sample vials (Fisher Catalog # 03-340-121) with teflon-faced rubber backed caps.

Sample Collection: Each field sample vial will be partially filled with the extraction solvent (alcohol IPA, IBA, etc. or Methylenechloride) using a pipet or repeating volume dispenser. Typically 10 or 20-ml of solvent will be used.

Transportation and Storage: Field samples will be stored in coolers containing "blue ice", and later stored in refrigerators in a trailer located on the site. Samples will be sent to UF labs packed in coolers and shipped via overnight air express (e.g., FedEx). The samples will be stored in the cold storage room or refrigerator at 4C, until GC analysis. After sub-sampling, the samples are returned to cold storage.

For lab studies, samples will be collected directly in 20 mL Headspace vials whenever possible and stored in a refrigerator if analysis is expected to take more than a day.

2. In the laboratory, samples will be rotated for a minimum of 8 hours on a rotator (Glas-Col model RD 4512).

3. Sub-sampling and Dilution

Field samples will be sub-sampled into 2 ml GC vials. Pipets will be used to transfer samples from 20-mL sample vials to the 2-mL GC vials.

3. Apparatus and Materials

Glassware: Glass pipets are required for sub-sampling.

Safety

Gloves and eye protection will be worn during all extraction activities.
Reference to the Materials Safety Data Sheets (MSDS) will be made for information on toxicity, flammability, and other hazard data.

Appendix E: Appendix E: Quality Assurance Project Plan (QAPP)

E.1 Purpose and Scope of the Plan

This Quality Assurance plan is written to cover activities associated with testing the Flux Meter at the Canadian Forces Base Borden site. The plan focuses on field installation, sampling and processing of data from the Flux Meters.

E.2 Quality Assurance Responsibilities

The responsibility for QA will be shared by Kirk Hatfield and Mike Annable at the University of Florida. During field activities one of the PI's will be present to oversee QA procedures. Other personnel present during field sampling activities will include graduate students or post-doctoral researchers from the University of Florida, Purdue University, and the University of Waterloo.

E.3 Data Quality Parameters

This section discusses measures to be taken to ensure the representativeness, completeness, comparability, accuracy, and precision of the data.

Accuracy

Accuracy is defined as the closeness of the results to the true value.

The percent recoveries of surrogates, QC check standards, and matrix-spiked analytes are used to evaluate the accuracy of an analysis. The percent recovery represented by X can be calculated using the following equations:

For surrogates and QC check standards:

$$X = \frac{SSR}{SA} x\,100$$

For matrix spikes:

$$X = \frac{SSR - SS}{SA} \times 100$$

where:

SSR = Spiked sample result
SS = Sample result
SA = Spike added from spiking mix

The mean percent recovery (X) is defined by:

$$\overline{X} = \frac{\sum_{i=1}^{N} X_i}{N}$$

where:

X_i	=	The percent recovery value of a spike replicate
N	=	Number of spikes

Precision

Precision is a measure of the mutual agreement among individual measurements of the same parameters under prescribed similar conditions.

The analytical precision is determined using results from duplicate or replicate analyses of samples and from matrix spike results for a given matrix. The Relative Percent Difference (RPD) is used to evaluate the precision of duplicate analyses. Relative Percent Difference is defined in the following equation:

$$\%RPD = \frac{2(X1 - X2)}{\overline{x}} \, x \, 100$$

X1 = First duplicate value
X2 = Second duplicate value

When replicate analyses are performed, precision is measured in terms of the Standard Deviation (SD) which is defined in the following equation:

$$S = \sum_{i=1}^{N} \left[\frac{(X_i - \overline{X})^2}{N - 1} \right]^{\text{‰}}$$

where:

X_i	=	The recovery value of a spike replicate
X	=	Arithmetic average of the replicate values
N	=	Number of spikes

Completeness

Completeness is defined as the percent of parameters falling within acceptance criteria and the results subsequently reported. A goal of 95 percent completeness has been set for all samples.

The general requirement of this quality assurance program is to analyze a sufficient number of standards, replicates, blanks, and spike samples to evaluate results adequately against numerical QA objectives.

E.4 Calibration Procedures, Quality Control Checks, and Corrective Action

The focus of the following section is to describe initial and continuing calibration procedures for analytical instrumentation, duplicate and control testing and data reduction, validation, and reporting.

Supplies and Quality Control Materials

All supplies (i.e., glassware, chemicals, reagents) used will be of the best possible quality to ensure proper instrument calibration and avoid contamination. All reagents used are prepared from Analytical Reagent Grade (AR) chemicals or higher purity grades, unless such purity is not available. The preparation of all reagents will be documented, including source, mass, and dilutions. Each reagent will be clearly labeled with the composition, concentration, date prepared, initials of preparer, expiration date, and special storage requirements, if any.

Reagents

Reagent solutions are stored in appropriate glass, plastic, or metal containers. Reagents are stored under conditions designed to maintain their integrity (refrigerated, dark, etc.). Shelf life is listed on the label and the reagent is discarded after it has expired. Dry reagents such as sodium sulfate, silica gel, alumina, and glass wool are either muffled at 400°C or extracted with solvent before use for organic chemical analyses. Water used in the laboratory is glass distilled or deionized, and periodically checked for purity. In addition, water used in the organics area is carbon-filtered or purchased as HPLC grade. All organic solvents used are either glass-distilled or pesticide grade. Solvents and reagent solutions are checked for contamination by employing reagent blanks, before use in any analysis.

Quality Control Reference Materials

All Quality Control Reference Materials are acquired only from authorized vendors or sources commonly used by U.S. EPA Regional Laboratories.

Standards Traceability

When standard reference materials arrive at the laboratory, they are registered in a bound log book, "Standards Notebook for Neat Materials and Primary Solutions." An example of a logging sequence is used to illustrate this process.

(1-S-XXX-12-4) (label and log sequence)

Where:

1 = Notebook log number
S = Standard Notebook--"Neat and Primary Standards"
XXX = Receiving analyst's initials
12 = Notebook page
4 = Entry number on notebook page

All working standards prepared at the site lab are logged in the "Standards Notebook for Intermediate and Working Standards." A similar labeling convention has been adopted for classifying these working standard materials. An example is given below.

1-W-XXX-6-5 (label and log)
Where:
1 = Number of notebook
W = Standards notebook - "Intermediate and Working" Standard
XXX = Analyst's initial
6 = Page Number
5 = Page entry number in sequence

Instrument Calibration

Every instrument used to analyze samples must pass the calibration criteria established in the appropriate SOP. Initial calibration criteria for instrument linearity, sensitivity, resolution, and deactivation must be met before samples can be analyzed. Sustained performance is monitored periodically during sample analyses by the use of continuing calibration check standards.

GC Section

Initial Calibration

The linear calibration range of the instrument must be determined before the analysis of any samples. Gas chromatographic conditions used for sample analyses are used during calibration.

The calibration is performed in accordance with the SOP derived from the methods used. For most GC analyses, a 5-level calibration is run. The concentrations of the standards must bracket the linear range of the instrument. Calibration using fewer than 5-levels is done only when specifically allowed by the method.

Relative Retention Times and Relative Response Factors

Instrument calibration and sample analysis must be performed using appropriate internal standards to establish relative retention times (RRT) and relative response factors (RRF) where required. Internal standards appearing in a chromatogram will establish primary search windows for those target compounds nearby in the chromatogram. RRT are calculated using this equation:

$$RRT = \frac{RT^{target}}{RT^{is}}$$

The RRF may be calculated as follows:

$$\text{Absolute Response Factor} = RF = \frac{\text{Area}}{\text{Amount}}$$

Note: Amount in this equation refers to the mass (e.g. ug) of compound mixed into the solution injected.

Each calibration standard is analyzed and the RRF is calculated for each analyte according to the following equation:

$$RRF = \frac{A_s \, x \, C_{is}}{A_{is} \, x \, C_s}$$

A_s = Area of analyte
A_{is} = Area of internal standard
C_{is} = Concentration of internal standard
C_s = Concentration of analyte

Note: Certain data processors may calculate the RRF differently.

The standard deviation (SD) and the % coefficient of variation (CV) of RRFs for the compounds are calculated using the following equations:

$$S = \sum_{i=1}^{N} \left[\frac{(RRF_i - RRF_m)^2}{N - 1} \right]^{‰}$$

Where:

RRF_i = Individual RRF
RRF_m = Mean RRF
N = Number of RRFs

and

$$\%CV = \frac{S \times 100}{RRF_m}$$

Coefficient of Variation

The %CV of each compound must be less than 30 percent. This criterion must be achieved for the calibration to be valid.

If the %CV is less than 20 percent, the RRF of the compound can be assumed to be invariant, and the average RRF can be used for calculations.

If the %CV is between 20 percent and 30 percent, calculations must be made from the calibration curve. Both the slope and the intercept of the curve must be used to perform calculations.

Initial Calibration Verification

The calibration curve must be validated further by analyzing a QC check sample. The QC check sample must be obtained from EPA, another vendor, or it must be from another lot number. The QC check sample verifies the validity of the concentrations of the standards used to obtain the initial calibration.

All analytes in the QC check standard must be recovered within 80 to 100 percent. If any analyte exceeds this criterion, then a new calibration curve must be established. All sample results for a target analyte can be reported only from valid initial calibrations.

Continuing Calibration

The working calibration curve or RRF for each analyte must be verified daily by the analysis of a continuing calibration standard. The ongoing daily continuing calibration must be compared to the initial calibration curve to verify that the operation of the measurement system is in control.

The continuing calibration check must be performed during each day of analysis to verify the continuing calibration of the instrument. A day is defined as 24 hours from the start run time of the last valid continuing calibration. Generally, a continuing calibration check sample is injected every 10 samples.

Verification of continuing calibration is performed by the analysis of a midpoint standard containing all of the analytes of interest. Verification of continuing calibration of the measurement system is done by calculating the percent difference (%D) of the continuing calibration RRF from the mean RRF from the initial calibration curve using the following equation:

$$\%D = \frac{(RRF_m - RRF) \times 100}{RRF_m}$$

Where:

RRF_m = The mean relative response factor from the initial calibration curve

RRF = The relative response factor from the continuing calibration standard

The %D must meet the acceptance criteria established in the appropriate SOP. If these criteria are exceeded, a new calibration curve must be established.

Other Calibrations

Weekly calibrations are performed for equipment such as balances, thermometers, ovens, incubators, and dissolved oxygen (D.O.) meters that are required in analytical methods, but which are not recorded in a dedicated QA instrument log.

Balances

Balances are checked with Class S weights on a daily basis. Before a weighing session, the analyst is required to perform at least one calibration check in the range of the material to be weighed. This value is also recorded on the specific balance control chart and must be within the control limit. The criteria for calibration checks are given in Table E.1.

Table E.1
CRITERIA FOR BALANCE CALIBRATION CHECKS

Class S Weight (grams)	Warning Level (grams)	Control Level (grams)
Analytical Balances		
0.0100	0.0098-0.0102	0.0097-0.0103
0.1000	0.098-0.102	0.097-0.103
1.000	0.995-1.005	0.990-1.010
10.000	9.995-10.005	9.990-10.010
50.00	49.98-50.02	49.95-50.05
Top Loading Balances		
1.00	0.95-1.05	0.90-1.10
10.0	9.9-10.1	9.8-10.2
50.0	49.7-50.3	49.5-50.5

Incubators, ovens, and waterbaths

Temperatures are checked daily with an NBS grade thermometer and necessary adjustments made as required. All temperature readings are recorded and posted on the appropriate equipment.

DO meters

DO meter is calculated daily using a modified Winkler technique. The Winkler solution is titrated against 0.025N sodium thiosulfate.

Conductivity bridges

Conductivity meter is standardized daily against a solution of KCl to obtain a new cell constant.

pH meters

The pH meter is standardized daily using buffers at pH of 4, 7, and 10.

Refrigerators

Refrigerators are maintained at 4°C, with control levels ranging from 1°C to 10°C. A temperature reading is taken each workday morning immediately after unlocking the refrigerator. The temperature reading is recorded and entered on the control chart posted on the door of the refrigerator. If a trend is apparent or if the temperature is outside the acceptable range, the Lab Manager is notified so that corrective action can be initiated if required.

Freezers

Freezers are maintained at -10°C, with control levels ranging from 0°C to -35°C. A temperature reading is taken each workday morning immediately after unlocking the freezer. The temperature reading is recorded and entered on the control chart posted on the door of the freezer. If a trend is apparent, or if the temperature is outside the acceptable range, the Lab Manager is notified so that corrective action can be initiated if required.

Calibration Standards

All calibration standards, including internal standards used in LMG, are obtained from chemical suppliers with certificates of high purity and concentration.

Traceability

All standards are traceable to the National Institue of Standards and Testing (NITS) Standard Reference Materials (SRM) or to the U.S. EPA Reference Standards.

Working Standards

The commercial standards are used as stock standards. Working standards are made from the stock standards at appropriate concentrations to cover the linear range of the calibration curve. The working standards are used for initial calibration curves, continuing calibration checks, and preparation of analyte spiking solutions as appropriate for a particular analysis. All stock and working solutions are uniquely identified, dated, labeled, and initialed.

Standards Logbook

All stock solutions are given a unique code number and are entered into a bound "Primary Standards" logbook. The name of the compound and other pertinent information, including concentration, date of receipt, and analyst's name, are also entered.

Working standards are given a unique code number that allows them to be traced to a specific stock solution. The working standard is entered in a "Working Standards" logbook with analyst's name, date and method of preparation, and other pertinent information.

CORRECTIVE ACTIONS

Laboratory Imposed

Corrective actions will be initiated if the quality control criteria indicate an analysis is out of control.

- Check calculations for accuracy
- Check instrumentation to ensure it is operating properly. Recalibrate if necessary.
- Remake standards and reagents and reanalyze samples.
- Re-prep and re-analyze samples.

The analyst is responsible for initiating corrective actions for analytical problems encountered during analysis of samples. Most problems which occur and are corrected during the analytical run will be explained in the run log or analytical bench sheet for that run. A corrective action report (CAR) may be necessary for some problems encountered, such as complete system failure, chronic calibration failure, or severe matrix interferences.

During data review, the reviewer may initiate corrective actions based on problems or questions arising from the review. A CAR will be initiated.

The Laboratory Manager may initiate corrective actions if a problem is noticed during a QC review of data, a system audit, or a performance audit. A CAR will be initiated.

CARs are signed and dated by Project Manager, and by the Laboratory Manager. CARs will be filed in appropriate department files and in the Lab Manger's files.

Agency Imposed

Any actions deemed necessary by regulatory agencies, such as EPA, will be taken. These actions are most likely to arise from a systems or performance audit, or from data review conducted by the agency.

Corrective Action Reports

Corrective Action Reports

The field laboratory will have a Corrective Action System that ensures the proper documentation and dispositions of conditions requiring corrective action. The system will also ensure that the proper corrective action is implemented to prevent recurrence of the condition.

Situations Requiring Corrective Action Reports

The Corrective Action System applies to all situations that affect data quality. These situations include, but are not limited to, quality control criteria being exceeded, statistically out-of-control events, deviations from normally expected results, suspect data, deviations from the standard operating procedure, and special sample handling requirements. Corrective actions may also be initiated as a result of other QA activities, such as performance audits, systems audits, laboratory/interfield comparison studies, and QA project-related requirements of certifying agencies such as EPA.

Corrective Action Procedures

The procedure requires documenting the condition requiring corrective action on a Corrective Action Report and implementing corrective action based on the results of the investigation performed to determine the cause of the condition (Table E.2).

When a condition requiring corrective action arises, the Corrective Action Report is initiated. The initiator describes the condition requiring corrective action. An investigation, if necessary, is conducted to determine the cause of the condition. A corrective action is recommended based on the results of the investigation. The Corrective Action Report is reviewed by the Project Manager and the Field Site Manager who either approve the recommended corrective action or indicate a different corrective action. The originator has the responsibility of following up to be sure that the corrective action is implemented. Implementation of the corrective action is documented by the Corrective Action Report being signed and dated by the person who implemented the corrective action.

Table E.2
Corrective Actions

QC Activity	Acceptance Criteria	Recommended Corrective Action
Initial instrument blank	Instrument response <MDL response	Prepare another blank, if same response, determine cause of contamination: reagents, environment, instrument equipment failure, etc.
Initial calibration standards	Coefficient of variation >0.99995 or standard concentration value ± 10% of expected value	Reanalyze standards. If still unacceptable, then remake standards
QC Check Standard	± 10% of expected value	Reanalyze standard. if still unacceptable, then remake standards, or use new primary standards if necessary
Continuing calibration Standards	± of expected value	Reanalyze standard. If still unacceptable, then recalibrate and rerun samples from the last cc stnd. Check
Method blank	<MDL	Reanalyze blank. If still positive, determine source of contamination. If necessary, reprocess (i.e., digest or extract) sample set
Initial calibration Standards (GC/MS)	RRF <30%	Reanalyze standards. If still unacceptable, prepare new standards.
Surrogate recovery (GC/MS Semivolatiles)	0 or 1 outside CLP criteria	Re-extract and/or re-analyze
Surrogate recovery (GC/MS volatiles)	0 outside criteria	Re-analyze

Table E.3
Corrective Action Report Criteria for Control Charts

Criteria	Corrective Action
A point outside ±3 standard deviations	Attempt to determine the source of the problem. Verbally report the deviation and results of preliminary investigation to the Field Site Manager, who will decide jointly what action to take. After implementing corrective action, complete the Corrective Action Report and submit it to the Project Manager and the Field Site Manager for approval.
Three consecutive points accuracy outside ± standard deviation	Conduct investigation. Check accuracy of data input, calculations, instrument, standards, etc., to locate the source of the problem. Document results in a Corrective Action Report. Have the report approved by the supervisor. No results can be reported until the Corrective Action Report has been approved. Send a copy of the Corrective Action Report and a copy of the QC chart to the Field Site Manager.
Obvious outlier.	Conduct investigation. Check accuracy of data input, calculations, dilutions, instrument, standard, etc.. present initial findings to the Field Site Manager. They will jointly decide what actions need to be taken. Document the results in a Corrective Action Report and have it approved by the Field Site Manager. No results can be reported until the Corrective Action Report is approved. Send a copy of the Corrective Action report and a copy of the control chart to the Field Site Manager.
Obvious shift in the mean.	Conduct investigation. Check calculations, data entry, standards, instrument, calibrations, etc. Document results in a Corrective Action Report. Have the Corrective Action Report approved by the Field Site Manager. No results can be reported until the report is approved. Send a copy of the Corrective Action Report and a copy of the QC chart to the Field Site Manager.

E.5 Demonstration Procedures

Initiating the flux meter experiments will involve limited field effort. All of the components of the device can be prepared prior to field activities. In the field, the primary activity will be assembly of the flux meters which can be completed with two people in a mater of minutes. Extraction and sub-sampling also required fairly minimal time and personnel. Only the controlled flow flume experiments will require establishing steady flow from one end of the flume using peristaltic pumps. These pumps will be calibrated in the field using simple time and volume measurements. Periodic flow measurements will be made to determine total average flow.

Samples collected at the Borden site will be sent to the University of Florida for analysis. In the laboratory, instrument maintenance will include the following.

Maintenance Schedule

Preventive maintenance, such as lubrication, source cleaning, and detector cleaning, is performed according to the procedures delineated in the manufacturer's instrument manuals.

The frequency of preventive maintenance varies with different instruments. Routine maintenance performed includes cleaning and/or replacement of various instrument components. In general, the frequency recommended by the manufacturer is followed. In addition to the regular schedule, maintenance is performed as needed. Precision and accuracy data are examined for trends and excursions beyond control limits to determine evidence of instrument malfunction. Maintenance is performed when an instrument begins to degrade as evidenced by the degradation of peak resolution, shift in calibration curves, decreased ion sensitivity, or failure to meet one or another of the quality control criteria. Table E.4 lists routine equipment maintenance procedures and frequency.

Instrument maintenance logbooks are maintained in the laboratory at all times. The logbook contains a complete history of past maintenance, both routine and nonroutine. The nature of work performed, the date, and the signature of the person who performed the work are recorded in the logbook. Preventive maintenance is scheduled according to each manufacturer's recommendation. Instrument downtime is minimized by keeping adequate supplies of all expendable items on hand. Expendable items are those with an expected lifetime of less than one year. Routine instrument preventive maintenance is handled by the instrument operator. Repair maintenance is performed by a full-time electronics technician, or by the manufacturer's service personnel.

Table E.4
PREVENTIVE MAINTENANCE

Instrument	Activity	Frequency
Gas Chromatograph	Change septum Check carrier gas Change carrier gas Change in-line filters Perform ECD wipe test Clean ECO Check system for leaks Clean/replace injection point liner Clean/replace jet tip Service flame photomeric detector	As needed Daily As needed As needed As license requires Return to vendor as needed As needed As needed As needed As needed
IR	Change desiccant Electronics maintenance	Every six months Every six months
UV	Clean and align optics Replace lamp Calibrate	Annually As needed Weekly
pH Meter	Calibrate Check fluid in probe	Daily Daily
D.O. Meter	Clean and replace membrane and HCl solution Calibrate	Daily Daily
Balance	Calibrate Maintenance	Daily Annually
Ovens	Temperature checks	Daily
Refrigerators and Freezers	Temperature checks	Daily
COD Heating Block	Check temperature with NBS thermometer	As needed
Conductivity Meter	Standardize with KCl Check probe visually	Daily Daily

E.6 Calculation of Data Quality Indicators

The focus of this section is to present methods of calculating data quality that will be used for this project.

Control Samples

The laboratory will employ control samples to assess the validity of the analytical results of the field samples. Determination of the validity of field sample results is based on the acceptance criteria being met by the control sample. The acceptance criteria for each type of control sample are delineated in the appropriate SOP. These acceptance criteria are based on the laboratory's statistical process capabilities determined from historical data, and meet the EPA CLP acceptance criteria as a minimum. Often, in-house criteria are more stringent than required by CLP. The control samples are analyzed in the same manner as the field samples. They are interspersed with the field samples at frequencies that are specified by the appropriate SOP.

Method Blank Analyses

A method blank is a "clean" sample (i.e., containing no analyte of concern), most often deionized water, to which all reagents are added and analytical procedures are performed. Method blanks are analyzed at a rate of one per sample lot or at least every 20 samples. The blank is analyzed in order to assess possible contamination from the laboratory or the procedure. If the analyte of interest is found in the blank at above reporting levels, inorganic analysis is suspended until the source of contamination is found and corrective action is taken. The Laboratory Manager is notified when blank results are unacceptably high, and may assist in the investigation.

Surrogate Spike Analyses

For certain analyses such as those performed by GC/MS, each sample and blank is spiked with one or more surrogate compounds before preparatory operations such as purging or extraction. These surrogate standards are chosen for properties similar to sample analytes of interest, but are usually absent from the natural sample.

Surrogate spikes evaluate the efficiency of the analytical procedure in recovering the true amount of a known compound.

The results of surrogate standard determinations are compared with the true values spiked into the sample matrix prior to extraction and analysis, and the percent recoveries of the surrogate standards are determined. Recoveries should meet the upper and lower control limits as specified for each compound. If control limits are exceeded for surrogate standards, the following sequence of actions is taken:

a. The sample is re-injected.

b. Raw data and calculations are checked for errors.

c. Internal standards and surrogate spiking solutions are checked for degradation, contamination, or solvent evaporation.

d. Instrument performance is checked.

e. If a, b, and c fail to reveal the cause of the noncompliance surrogate recoveries, the sample is re-purged or re-extracted.

f. If all the measures listed above fail to correct the problem for laboratory blank surrogate analyses, the analytical system is considered out of control, and the instrument must be recalibrated and examined for mechanical faults.

g. If all the measures listed above fail to correct the problem for field sample surrogate analyses, the deficiency probably is due to sample interferences, and not due to any procedural or mechanical problems in the laboratory. The surrogate spike recovery data and the sample data from both extractions are reported and are flagged. The Laboratory Manager is notified with an exceptions report and the corrective actions taken.

Matrix Spike/Matrix Spike Duplicate Analyses

To evaluate the effect of the sample matrix on the analytical methodology, two separate aliquot samples may be spiked with a standard mix of compounds appropriate to a given analysis. The matrix spike and the matrix spike duplicate (MS/MSD) are analyzed at a frequency of one per lot or one per 20 samples, whichever is more frequent. The percent recovery for each of the spiking compounds is calculated. The relative percent difference (RPD) between the MS/MSD is also calculated.

The observed percent recoveries (%R) and relative percent differences (RPD) between the MS/MSD are used to determine the accuracy and the precision of the analytical method for the sample matrix. If the percent recovery and RPD results exceed the control limits as specified for each spiking compound, the sample is not reanalyzed. Poor recovery in matrix spiked samples does not necessarily represent an analytical system out of control. It is possible that unavoidable interferences and matrix effects from the sample itself preclude efficient recoveries. The poor recovery is documented for the Project Manager.

Internal Standards Analysis

Once an instrument has been calibrated, it is necessary to confirm periodically that the analytical system remains in calibration. The continuing calibration and precision of the organics analytical system are checked for each sample analysis by monitoring the instrument response to internal standards. When internal standard addition is not appropriate to a particular method, other means of accuracy checks, such as standard addition, are used. Results from internal standard analyses are compared to the mean calibrated value. Deviation from this mean beyond

a predetermined magnitude, depending on the type of analysis, defines an out-of-control condition. The system must then be brought back into control by:

- Checking the quality of the internal standards and reanalyzing the sample
- Recalibrating the system
- Correcting the malfunctions causing the instrument to fall out of calibration

Duplicate Sample Analyses

Duplicate analyses are performed for cations analyses and upon special request for selected other parameters to evaluate the reproducibility of the method. Results of the duplicate analyses are used to determine the RPD between replicate samples. For each parameter analyzed, at least one duplicate sample is run per group of 20 samples.

The precision value, RPD, is reviewed by the section supervisor and the division manager. If the precision value exceeds the control limit or the established protocol criteria for the given parameter, the sample set is reanalyzed for the parameter in question unless it is determined that heterogeneity of the sample has caused the high RPD.

QC Check Standard Analyses

Analysis of QC check standards is used to verify the preparation process or the standard curve, and is performed with each group of samples. Results of these data are summarized, evaluated, and presented to the section supervisor and the division manager for review.

The results of the QC check standard analysis are compared with the true values, and the percent recovery of the check standard is calculated. If correction of a procedure or instrument repair is done, the check standard is reanalyzed to demonstrate that the corrective action has been successful.

At least twice a year, a QC check standard for each parameter group is analyzed as a double-blind sample. Samples are prepared, submitted, and evaluated by the Laboratory Manager.

Other Quality Control Samples

Under some sampling analysis, additional quality control samples may be required. These may include:

a. **Blank/Spike--**Analyte of interest or surrogate is spiked into blank water rather than into a sample. The blank/spike goes through the entire analytical procedure, and percent recovery is calculated with no likelihood of matrix effect. For many contracts, an externally provided LCS sample (EPA) serves as a blank/spike sample.

b. **Trip Blank**--A sample bottle filled with laboratory blank water travels with the sample kit to the sampling site, and is sent back to the laboratory packed in the same container as any volatile samples collected. Trip blank analyses check for possible volatile contamination during shipping or sampling.

c. **Field Blank**--A field blank can be a sample container filled with laboratory blank water and sent to the sampling site, or it may be filled at the site with purchased distilled water or decontamination water. The field blank analysis checks for possible contamination by the sampling team.

d. **Equipment Rinsates**--After equipment has been cleaned in the field, many contracts require that the equipment be rinsed and the rinsate analyzed for the same parameters requested on the samples. The rinsate analysis proves the equipment has been cleaned properly and will not contaminate the next samples taken.

Control Charts

The laboratory will use control charts to monitor for out-of-control conditions.

Control Charting Process

The control chart program uses a series of Lotus (or equivalent) macros to perform data processing and control charting. These macros also perform statistical decisions on the acceptability of the data.

The control chart used is a variation of the Shewart control chart of averages. The chart plots individual quantitative results against the order of time measurement. The plotted values are compared with control limits determined by the variability about the mean of the standard "in control" process. The control chart estimates the process mean and the variability from a moving window of 50 to 200 samples, depending upon the analytical parameters involved. The mean is estimated from the arithmetic average of the samples in the current window. The variability is estimated as the sample SD of the sample values in the current window. The program calculates the -statistic and uses 3 SD limits and displays estimate the 99.7 percent tolerance limits for the degrees of freedom in the current window. Values outside the t-statistic limits are unconditionally rejected from inclusion in the sample window and automatically documented in a Corrective Action Report (CAR). The CAR prompts the analyst to initiate investigation and corrective action.

When the maximum number of samples has accumulated in the current window, the summary statistics of the mean and SD are written to the long-term data base. The last 20 samples in the old window are then transferred to a new window for continued use in the charting process.

The long-term data base charts the mean 1 SD error bars.

Instrument Detection Limits, Method Detection Limits, and Reporting Limits

Instrument Detection Limits (IDL)

Instrument Detection Limit (IDL) studies are performed for inorganic parameters when an instrument is installed, when major maintenance or repair work has been done, and routinely once per calendar quarter.

To determine IDL, seven consecutive measurements per day are made on a prepared standard solution (in reagent water) of an analyte at a concentration 3 to 5 times the instrument manufacturer's suggested IDL. Each measurement is performed as though it were a separate analytical sample. This procedure is repeated on three nonconsecutive days. The standard deviation is calculated for each set of seven replicates and the average of the standard deviations is obtained. This average is multiplied by 3 to give the instrument detection limit (IDL).

Method Detection Limits (MDL)

The Method Detection Limit (MDL) is the minimum concentration of a substance that can be measured and reported with 99 percent confidence that the value is above zero. The sample must be carried through the entire method under ideal conditions. MDL is determined according to the method outlined in 40 CFR 136, Appendix B. MDLs are determined at least annually for all parameters. MDL studies are also conducted for new methods introduced in the lab, after major maintenance or modification to an instrument, and as part of the training of new analysts.

To determine MDL, seven replicate analyses are made of analytes spiked into blank water at 1 to 5 times the estimated method detection limit. The spiked samples must be carried through the entire analytical procedure, including any extraction, digestion, or distillation process, for MDL calculation. The SD of these replicates is calculated. Where:t = The student t value for a 99% confidence interval

$$MDL = t \times S$$

S = Standard deviation of the replicate analyses

Reporting Limits

In most cases, final report forms list reporting limits rather than either IDL or MDL. Reporting limits are taken from EPA SW846 published limits or from historical data. Matrixes or analyte concentrations which require dilution will change the detection limits for that sample.

E.7 Performance and System Audits

In this section information is provided on performance audits and onsite system audits.

Performance Evaluation Samples

Performance evaluation samples are analyzed throughout the project for all parameters, as a constant check on accuracy and precision for all analyses.

Audits

Internal audits of the laboratory are conducted in two phases. The first phase is conducted by the Laboratory Quality Assurance Coordinator during the fourth quarter of the year. This is usually a 2-day systems audit which covers all sections of the laboratory. An audit report is issued within 2 weeks of completion. The Field Site Manager has the responsibility for coordinating all responses to the audit finding and for following up on the required corrective action. A followup audit is made when deemed necessary by the by the Field Site Manager or the Laboratory Manager. A quality assurance review questionnaire is provided in the Appendix.

The second phase consists of quarterly audits performed by the Field Site Manager. These are half-day or day-long audits, and are concentrated on specific areas that are deemed problem areas by the Field Site Manager. An audit report is issued at the completion of the audit. Responses and followup corrective action to the audit findings are required, and are monitored by the Field Site Manager.

All audit reports are issued to management and circulated to all staff. Copies are filed with the Field Site Manager and the Laboratory Manager.

E.8 Quality Assurance Reports

The performance of the field laboratory as assessed by the quality monitoring systems in place is reported by the Field Site Manager to management quarterly and as needed. Copies of all quality reports are maintained in the Field Site Manager and Laboratory Manager files.

Quality assurance reports to management include, but are not limited to, the following:

- Results of performance and systems audits
- Status of corrective actions
- Periodic assessment of data accuracy, precision, and completeness
- Significant QA problems and recommended solutions

In addition to the quarterly reports, a final report summarizing items covered in the quarterly reports is provided by the Field Site Manager to the Project Manager.

E.9 Data Format

Introduction

In order to provide analytical data which is technically sound and defensible, a system of data management will be implemented in the laboratory. All activities which pertain to a sample are documented.

All data generated during the demonstration, except those that are generated by automated data collection systems, will be recorded directly, promptly, and legibly in ink. All data entries will be dated on the day of entry and signed or initialed by the person entering the data. Any change in entries will not obscure the original entry, will indicate the reason for such change, and will be dated and signed or identified at the time of the change.

In automated data collection systems, the individual responsible for direct data input will be identified at the time of data input. Any change in automated data entries will not obscure the original entry. Updated entries will indicate the reason for the change, the date, and the person responsible for making the change.

Data Tracking in the Laboratory

The Field Site Manager is responsible for developing a system for tracking and maintaining sample identity between the collection point, analysis and reporting. This process will be periodically reviewed by the Project Manager.

Analyses and Data Reduction

The Field Site Manager is responsible for the reduction of raw data when such steps are required to produce the correct data format for reporting. Data reduction may be done manually or through one of a number of computer programs used in the laboratory.

Chromatogram Identification

In the GC section computer software is used to identify chromatograms. A system-supplied file name (a hexadecimal date-time) and a user-supplied file name (related to an entry in the injection log) identify each acquisition.

Data Reduction Formulas

Linear regression formulas are used in a computer software system to calculate samples values for many general inorganic parameters and metals analyses. These programs use the general formula for linear regression:

$$Y' = a + bx$$

where:

Y'	=	The predicted value of y for a selected value of x
a	=	The value of y when x = 0
b	=	The slope of the straight line
x	=	Any value of x selected

Sample values for GC/MS parameters are calculated by systems software using the general formula:

$$\frac{Area_{Target} \ x \ Amount_{IS}}{Area_{IS} \ x \ Response \ Factor}$$

GC data is calculated using either an internal or an external standard. For internal standards:

$$Concentration = \left(\frac{A_x^{sample}}{A_x^{standard}}\right)\left(\frac{A_{IS}^{standard}}{A_{IS}^{sample}}\right)\left(amt_x^{standard}\right)\left(\frac{P}{T}\right)\left(\frac{amt_{IS}^{Sample}}{Amt_{IS}^{standard}}\right)$$

where: P = 1/fraction of extract to which IS is added

For calculations using an external standard:

$$Concentration = \left(\frac{A_x^{sample}}{A_x^{standard}}\right)\left(C_x^{standard}\right)\left(\frac{V}{T}\right)$$

where: C = concentration of x in standard
V = volume of final extract
T = total sample extracted

E.10 Data Storage and Archiving Procedures

Data from GC's will be saved and archived in P&E Turbochrom format. All data will be backed-up on ZIP disks. This data will be batch processed into an Excel .csv file that can be easily converted to an Excel Worksheet. These files will be backed-up and transferred to individuals responsible for calculating flux results. All data related to the project will be organized for rapid retrieval and transfer to other interested parties.